The rheology and strength of hot melt adhesives

Doody, Paul David

Award date:
1997

Awarding institution:
Coventry University

The Rheology and Strength of Hot Melt Adhesives

Paul David Doody

A thesis submitted in partial fulfilment of the
University's requirements for the degree of
Doctor of Philosophy.

Coventry University
January 1997

Abstract

This thesis is concerned with the scientific basis of the industrial practice in the use and development of hot melt adhesives. A key feature of this work is the systematic formulation and detailed characterisation of the polymeric components and adhesives. Fourteen commercially available poly(ethylene-*co*-vinyl acetate) (EVA) copolymer samples were selected in which there was a systematic change in the melt index, amount of vinyl acetate, and degree of crystallinity. Various hot melt adhesives were made using these copolymers and a standard amount of wax and resin. The materials were examined using differential scanning calorimetry (DSC), oscillatory rheometry (both controlled strain and controlled stress), and transient (creep) rheometry. The adhesives were also investigated using a variety of industrial tests which included peel adhesion and tensile testing at four different rates, open and setting time, shear and peel stress resistance at elevated temperatures, and viscosity determination over a wide range of temperatures. Detailed thermal analysis and characterisation have provided a range of accurate and systematic data on all of the materials and in particular showed that the components of the adhesive did not merely act as a mechanical mixture but had a distinct compatibility.

The controlled stress technique was found to more discriminatory than the controlled strain, due to the more precisely controlled heating and cooling of the sample during loading and evaluation. Other key differences between the techniques are attributable to the different thermal histories imposed upon the semi-crystalline adhesive components. Detailed analysis of the complex rheological curves showed several key factors. One of the most important was the modulus crossover temperature T_X which was shown to correlate well with the softening point of the adhesive, its open time, and the heat resistance under shear as determined by the shear adhesion failure temperature (SAFT). It was possible to construct a linear relationship between T_X and SAFT which allowed prediction of this key adhesive parameter. There was no significant relationship established between the softening point of an adhesive and its heat resistance, open time, or critical thermal characteristics, and the use of the softening point as a useful indicator of adhesive performance is contested. The open time was shown to be clearly influenced by the properties of the copolymer. The relationship between open time and melt index is complex and two competing mechanisms are thought responsible. These are the inability to fully wet the substrate for high molecular weights and resistance to complete substrate penetration by capillary effects for adhesives formulated with low molecular weight polymers. Both of these effects cause a reduction in open time. The cloud points of the adhesives were independent of the molecular weight but strongly affected by composition. Degree of crystallinity was also an influence at higher molecular weights. Cloud point correlated slightly with the onset of crystallisation as determined by DSC however differences are extremely small and the method was not deemed robust enough for widespread industrial application.

Various properties of the components and adhesives were modelled. The compatibility of the components were successfully incorporated into an extended Fox equation to predict the glass transition temperature. The peel strength of the adhesive was modelled in terms of the rheological properties of elastic moduli and loss tangent values at different temperatures. A second model based upon the value of the loss tangent at room temperature was also broadly successful but deviations from predicted behaviour were observed which were attributable to failure of the adhesive joints by a mode not included in the model. The modulus of the adhesive was modelled on the basis of an extended mixture rule in which the extent of compatibility was identified by a parameter n. The value of n varied as a function of adhesive composition and temperature, indicating that the behaviour of the adhesives changed subtly as the compatibility of the phases changed. The value of the parameter could not be directly related to the morphology of the adhesive phases.

Contents

Chapter 1 - Introduction

CHAPTER ONE

INTRODUCTION

1.1 Hot melt adhesives

There are many ways that materials may be joined together. These include such processes as welding, soldering, diffusion bonding, riveting, and other mechanical fastening processes. However, one of the most versatile, and inexpensive processes, is to use adhesives to bond the materials together. In addition to actually forming a strong bond with the substrate, the adhesive must also have the properties by which the integrity of the assembly may be maintained in service. To provide the optimum performance for a wide range of materials, operating under a wide range of service conditions, there has been developed an enormous number of adhesives, and the search for new adhesives, and the improvement of existing ones, continues.

Hot melt adhesives (HMAs) represent a very large proportion of the total volume of industrial adhesives sold. The European market alone consumed nearly 202 000 tonnes in 1994. This has grown over 20% in the last five years and it is expected that this will grow a further 4% by the end of 1996 [1]. HMAs are almost completely non-volatile thermoplastic materials which are typically solid at room temperature. They are usually applied to an adherend as a hot fluid which, upon cooling, sets or crystallises thereby producing a durable bond. HMAs differ from other liquid adhesives because they set by cooling rather than by the absorption or evaporation of a liquid carrier (typically water or an organic solvent). This confers two principal advantages; it eliminates the possibility of potentially injurious solvent vapour emissions, and it reduces the amount of time required to form a bond that will withstand mechanical handling.

Hot melt adhesives can be placed into two categories dependent upon them solidifying into either hard materials, with little or no surface tack, or materials that remain soft and tacky, even at room temperature (called pressure

sensitive HMAs). Tack is defined as the ability of an adhesive to form an instantaneous bond, of measurable strength, with little, or no, pressure applied to the adherend [2]. Hard setting HMAs typically find use in applications such as bookbinding, sealing of cardboard cases and cartons, and labelling of cans and jars; whilst pressure sensitive HMAs are used for tapes, self-adhesive labels, and other contact applications.

As a hard setting HMA loses heat its properties change and its behaviour may be classified into different stages as show in Fig 1. The initial, fluid, stage (A), at the point at which the adhesive is applied, is categorised by the HMA being well above its softening point and acting in a manner of a viscous fluid, able to thoroughly wet the surface of the adherends to which it is applied. As the adhesive cools, its viscosity increases, partial solidification may occur and the adhesives strength starts to increase. Instantaneous measurable bond formation is now possible and the HMA is said to possess hot tack (B in Fig 1). As cooling continues, the adhesive loses the ability to wet surfaces as it has become too highly viscous, due to further solidification; however it will still easily deform under applied pressure (C). Further heat loss results in increased cohesive strength until the material starts acting more solid-like (D) and shows flexible behaviour rather than flow. If the adhesive is cooled further, typically below room temperature, the strength increases. However, it becomes increasingly likely that it may become brittle (E). Pressure sensitive HMAs, in contrast, remain permanently tacky upon cooling and are capable of forming bonds at any stage until the final brittle region (E).

The rate at which a HMA loses its heat is dependent upon many factors *e.g.* composition, amount of adhesive, surface area, temperature of both adhesive and adherend, and amount of compression applied to the bond. The cooling rate is of critical importance in industrial applications as it influences such factors as production rates and machine design. Figure 2 shows the setting characteristics of a hard setting HMA. The line ABCD represents the cooling curve under conditions of no compression however, in practice, some compression is always present with bond formation and the effect on the curve is shown AEFGH where E represents the point at which the compression is

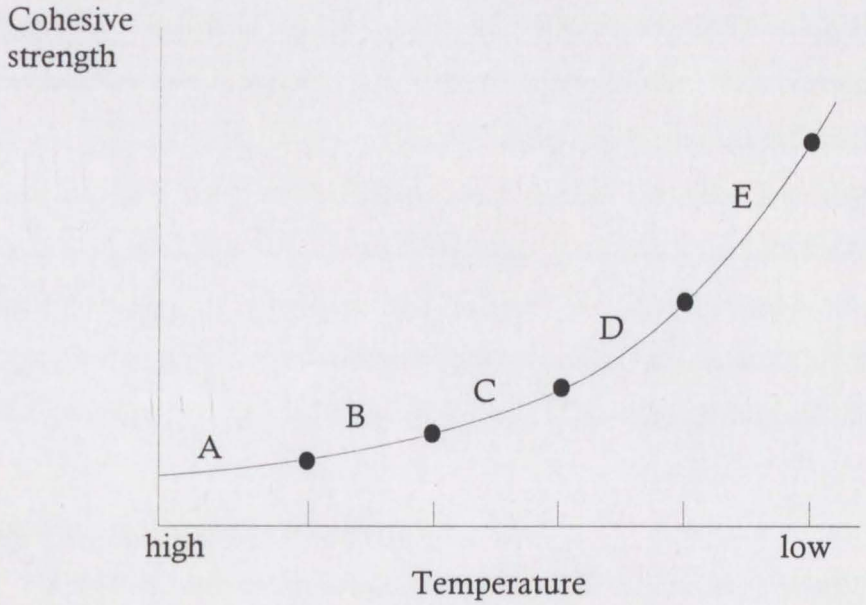

Fig 1. Schematic showing cohesive strength development during the cooling of a hot melt adhesive. A = fluid stage, B = tacky stage, C = deformable stage, D = flexible stage, E = brittle stage. See text for details.

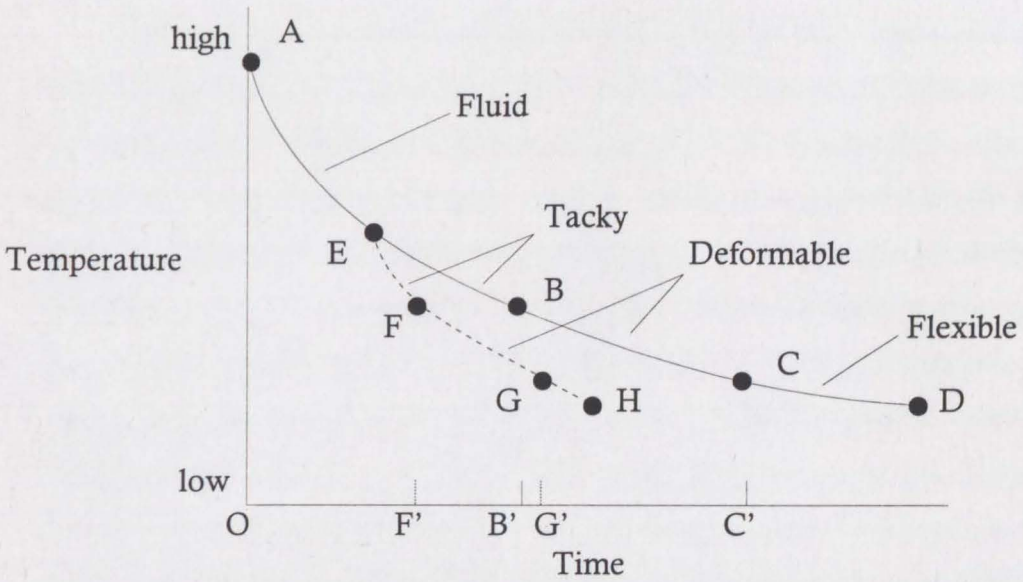

Fig 2. Schematic showing the cooling characteristics of a hard setting hot melt adhesive for a) an uncompressed application ABCD (———) and b) a compressed application AEFGH (--------). A = adhesive applied, OB' = open time (uncompressed), OC' = setting time (uncompressed), D = fully set adhesive, E = compression applied, OF' = open time (compressed), OG' = setting time (compressed), H = fully set adhesive. See text for details.

applied. The HMA is applied at A. If left uncompressed, point B signifies the point at which the adhesive shifts from the tacky to the deformable stage, after which point further wetting of adherends is not possible. The time taken to reach B is called the open time of the adhesive. If, however, pressure is applied at E, the cooling rate is faster and the open time (F) is correspondingly shorter. Compression pressure should not be released until the joint has sufficient strength to withstand any stresses placed upon it. This is usually associated with point G, the transition from deformable to flexible behaviour. The time taken to develop a strong enough bond is called the setting time of the adhesive.

1.2 Components of hot melt adhesives

The simplest HMAs are blends of three components, a single thermoplastic polymer which gives the adhesive mechanical strength and flexibility, a tackifying resin which imparts hot tack and contributes to specific, chemical bonding and a diluent which, for hard setting HMAs, is typically a petroleum wax.

Poly(ethylene-*co*-vinyl acetate) (EVA) copolymers are one of the most common thermoplastics used in HMAs. Adhesives containing these polymers account for almost 60% of the total trade [3]. EVA is available from a large number of manufacturers in a wide range of compositions (based on the ratio of acetal to ethylene mers), molecular weights, and number and length of side branches [4 - 7]. EVA is a semi-crystalline polymer based upon poly(ethylene). It is widely reported *e.g.* [8] that poly(ethylene) has a melting (alpha transition) temperature of approximately 137°C and a glass transition (gamma transition) temperature of -125°C. In addition there may be sometimes be seen a small (beta) transition between -35 and 0°C. This beta transition is dependant upon the composition and density of the poly(ethylene) and is more pronounced with EVA polymers. This is what is often quoted as the glass transition temperature for EVA copolymers and, whilst this is strictly untrue, the present author will keep to the same convention. The crystallinity of an EVA polymer may vary from about 5 to 40% depending on the extent of the factors given above. In some polymers, *e.g.* poly(ethylene), the degree of crystallinity can be calculated

from density considerations using a simple rule of mixtures. For example, high density poly(ethylene) has a density approximately equal to 0.96 g cm^{-3} and a crystallinity of 80%, whereas low density poly(ethylene) has a density of 0.92 g cm^{-3} and a crystallinity of 50%. This can be explained by considering the degree of side chain branching; high density poly(ethylene) has few side chains which allows the polymer molecules to fold into regular crystals with few inter-crystalline amorphous regions, whereas low density poly(ethylene) has a high degree of side chain branching which disrupts the regular crystalline structure and causes a reduction in density. However, in the case of copolymers such as EVA the situation is not as simple. Addition of vinyl acetate (VA) monomers reduces the overall crystallinity of the copolymer by increasing the amount of inter-crystalline amorphous regions and by reducing the amount of crystallinity within a crystalline region due to stearic hindrance of the chain folding process. This would lead to an expected overall drop in density as VA concentration increases, however VA monomers have a higher molecular weight than ethylene monomers and so increase the density of the copolymer. These two effects give a non-linear relationship between the density and the amount of crystallinity. In practice the density varies from 0.93 g cm^{-3} for a 6% VA copolymer with approximately 40% crystallinity, to 0.97 g cm^{-3} for zero crystallinity copolymer with 40% VA [9]. EVA is a random copolymer with VA monomers distributed along the main poly(ethylene) chain and side chains. This is in contrast to styrenic block copolymers, which are widely used in pressure sensitive HMAs, in which the styrene molecules are added to the ends of a rubbery midblock molecule such as isoprene or butadiene. The block nature of the styrene addition allows for the formation of styrene domains [10], a phenomenon which is not observed with VA in EVA copolymers. The random nature of the VA distribution tends to give EVAs with different polymeric structures dependent upon VA concentration. Studies with carbon-13 nuclear magnetic resonance [11,12] have shown that as the VA concentration increases, the degree and nature of chain branching changes, with an overall reduction in branching, particularly with short (less than 6 carbon atoms) chain branches. This reduction, which will vary from manufacturer to manufacturer depending upon

reaction vessels, process times and other factors, results in a large number of commercial grades, each with slightly different properties, which can be used in the HMA industry. The addition of VA to an EVA copolymer also increases its polarity which helps promote specific adhesion by inducing increased van der Waals forces between the adhesive and the adherend [13].

Tackifying resins are low molecular weight species (~900 - 1 500) derived either from natural sources *e.g.* rosin, or from the distillation and modification of crude oil [14]. Rosin is a mixture of resin acids which have the empirical formula $C_{20}H_{30}O_2$. They exist as isomers of a three ring fused structure, the most abundant of which, the abietic and pimaric acid types, are commonly used as the bases for commercial tackifying resins. The acids can be modified to give resins with a wide range of softening points (typically 80 - 120°C, although liquid rosin resins are available), improved oxidation resistance and thermal stability and differing degrees of chemical functionality. There are four basic reaction mechanisms that can be used to modify rosin, these are disproportionation, polymerisation, hydrogenation and esterification [15]. The latter is most popular, with a large number of rosin ester resins based upon glycerol and pentaerithritol which give excellent stability, hydrolysis resistance and light colour. Rosin based resins show excellent compatibility with most polymers used in HMAs due to their polar, acidic and cyclic/aromatic nature. Hydrocarbon tackifying resins are true polymers obtained from the fractional distillation of petroleum or naphtha. The principal petroleum fractions used give resins with predominantly aliphatic, aromatic or mixed aliphatic/aromatic characters. Aliphatic resins are manufactured from monomers obtained from the C_5 fractions. These consist primarily of piperylene (*cis*- and *trans*-1, 3-pentadiene), isoprene (2-methyl-butadiene), 2-methyl butene-2 and, in some instances, cyclo- and dicyclo-pentadiene [16]. They are typically compatible with petroleum waxes, particularly paraffin waxes, and tackify natural rubber, polyisoprene, and styrene-isoprene block copolymers [17]. The resins produced also tend to have softening points in the range 80°C to 120°C which may be accurately controlled by the adjustment of the composition of the diluent or monomers used during manufacture [18]. Aromatic hydrocarbon resins are

produced from feed streams primarily containing indene with minor amounts of styrene, methyl indene and methyl styrene. They tend to be darker in colour than the aliphatic hydrocarbons but show excellent compatibility with most of the thermoplastic polymers used in HMAs. They also show particular utility as reinforcing agents for the styrenic domains in styrenic block copolymers [14]. Mixed aliphatic/aromatic resins have characteristics that are somewhere between the two extremes. Formed by blending of the C_5 and C_9 streams, followed by polymerisation, this class of resin can be uniquely tailored in terms of chemical nature, softening point and compatibility to suit a variety of applications and polymer types.

Both rosin based and hydrocarbon resins can be used in EVA based HMAs, the choice often being made in terms of a trade-off between stability, level of hot tack, specific adhesion (particularly to polar substrates) and cost. Rosin based resins are commonly used where they are the sole, or principle, tackifying resin whereas hydrocarbon resins are often used in combination with other types, usually to provide specific modification of an adhesives properties, by mid-block or end-block reinforcement of styrenic block copolymers, for example.

Waxes are ill-defined, thermoplastic, organic materials that show certain characteristics and as such there is no simple definition based upon chemical or physical properties. However, a description adopted for trade purposes is that wax is a technologically collective term for a range of naturally or synthetically derived substances which have the following properties: they are solid at 20°C and vary from being soft and plastic to hard and brittle at that temperature; form solids that may be coarsely, or finely, crystalline, transparent or opaque, but not glass-like; melt without decomposition above 40°C; are of relatively low viscosity at temperatures slightly above the melting point; vary in consistency and solubility with changes in temperature; and they may be polished by rubbing using light pressures [19]. This is an extremely broad definition that serves little purpose for the adhesives chemist, but is useful in emphasising the physical form, melting behaviour and low viscosity. Only mineral (produced from distillates of petroleum or crude oil) and synthetic (poly(ethylene) or Fischer-

Tropsch process) waxes are widely used in HMAs due, in part, to their low odour, superior stability and consistent properties. All petroleum waxes can be considered as a mixture of saturated hydrocarbon molecules (alkanes). Paraffin waxes consist primarily (70 - 90%) of unbranched *n*-alkanes with a carbon chain length distribution between 18 to 40, although the proportions of branched *iso*-alkanes (typically 5 - 20%) and cycloalkanes (5 - 10%) tends to increase as the average molecular weight of the wax increases [20]. Paraffin waxes have a coarse crystalline structure that is either orthorhombic (at ambient temperatures) or hexagonal, the exact temperature of the solid state transition depending upon the composition of the wax [21]. The orthogonal form is hard and brittle whilst the hexagonal structure imparts flexibility to the wax. The crystalline portions of a solid wax are reported to be inter-dispersed within a gel-like amorphous matrix [22] which contains the lower molecular weight and highly branched *iso*-alkane species. The presence of these species in other petroleum based waxes has been shown to contribute to poor high temperature performance, reduced tensile strength, and increased flexibility of HMA formulations [23]. The lower molecular weight species may be observed to cause a broadening of the melting peak (as determined by differential scanning calorimetry) and it has been suggested that this may be used to identify any reduction in the high temperature performance of an adhesive formulation [24]. This hypothesis was conclusively demonstrated for a wide variety of waxes including paraffin and synthetic waxes [25].

1.3 Introduction to the aims of this thesis

Much of the testing and use of adhesives has been of an empirical nature, and the few more scientific studies have generally been more concerned with a limited range of materials or properties. The aim of the present work is to systematically and comprehensively investigate the rheological properties of a range of hot melt adhesives so as to understand the rôles of the individual components and thereby aid the development of adhesives with superior properties. In this chapter we have introduced mainly the industrial aspects of hot melt adhesives. In chapter two, after concise reviews of those aspects of

polymers important in hot melt adhesives and of rheology and adhesive principles, the type of adhesive joints and the nature of hot melt adhesives are critically assessed, and from these the major objectives of the present work are formulated. Chapter three describes experimental techniques, chapter four the results and chapter five contains the discussion, conclusions, and the suggestions for future work arising from this thesis.

Chapter 2 - Literature Survey

CHAPTER TWO

LITERATURE SURVEY

After a concise review of the general structure of polymers important in the present work, the principles of rheology, of adhesion, and details of the many types of adhesive joints are given. The literature on the structure and properties of hot melt adhesives is then critically assessed and from this the major objectives of the present work are formulated.

2.1 Phase transformations and microstructures in polymeric materials

The industrial use of polymers is governed by the properties of the polymer under service conditions. Depending upon such factors as temperature, magnitude of and rate of stress application, and method of manufacture, together with other external factors such as pressure, the polymer may be in one of several states each with its characteristic microstructure and properties. Polymer melts flow readily, whilst cooling typically induces the glassy state wherein the essentially amorphous structure of the melt is retained as a rigid solid. Alternatively, in crystalline polymers, the reduction in thermal energy causes crystallisation which has a significant effect on the polymer's mechanical behaviour. In polymers that can crystallise, it is rare for complete crystallisation to occur. Two states can exist: the part that has crystallised; and the part that has not crystallised and has transformed into a glass. The presence of the two states in the solid polymer has a profound effect on the microstructure and properties of the material.

Poly(ethylene), and other commercial polymers which are derived from it, are complex materials and their behaviour in the molten state is of tremendous scientific, and technological, importance. To this extent they have been extensively studied *e.g.* [26 - 28], and there are many theories proposed to explain their behaviours. It is generally observed that at low shear rates or stresses, Newtonian behaviour is observed and the melt possesses a so-called

zero shear viscosity η_0. At intermediate shear rates the melt is pseudoplastic; and at higher shear rates a second Newtonian region is observed (upper Newtonian region) and the melt possesses a viscosity η_∞. It has been suggested that [29] at low rates of shear, the natural thermal motions of the chain segments will tend to give a random and entangled state that resists the alignment due to the applied shear field. This gives the greatest resistance to untangling and hence the slippage that is characterised as flow. As the shear field increases in magnitude, the molecules will have enough energy imparted to them to overcome the random thermal motions and disentanglement will start to occur. This reduces the resistance to slippage and hence the viscosity will reduce. When the shear field exceeds a critical value, most of the molecules will be untangled and the viscosity of the melt becomes constant and representative of the friction between the unentangled and elongated chains. This is illustrated in Fig 3. In practice, excessive shearing may lead to polymer degradation (main chain scission) which will cause a decrease in η_∞ with time. Viscous heating is also great as the rate of viscous energy dissipation per unit volume is equivalent to the product of the applied shear stress and the shear rate. It is, therefore, often extremely difficult to obtain η_∞ data for polymeric melts [30].

The detailed supramolecular structure of polymer melts has been described by means of many models; essentially these consist of the statistically-coiled, interpenetrating, and entangled model which shows minimal short range order (~5 nm) proposed by Rouse [31] and others [32 - 38] and more recent meander models such as those proposed by Pechhold [39 - 43] which postulates the existence of superfolded bunches of molecules in energetically-favourable states. These bundles in turn form superstructures which fill the available volume in the melt (Fig 4). The two models are said to be mutually exclusive [44]. The coil models have a considerable following but suffer from being unable to deal with spatial packing, particularly with stiff chains. In contrast, the meander model copes well with packing behaviour and also, most importantly, is able to deal quantitatively with the total spectrum of relaxation phenomena in polymer melts and solids.

Relaxation processes in polymeric materials are widely interpreted in

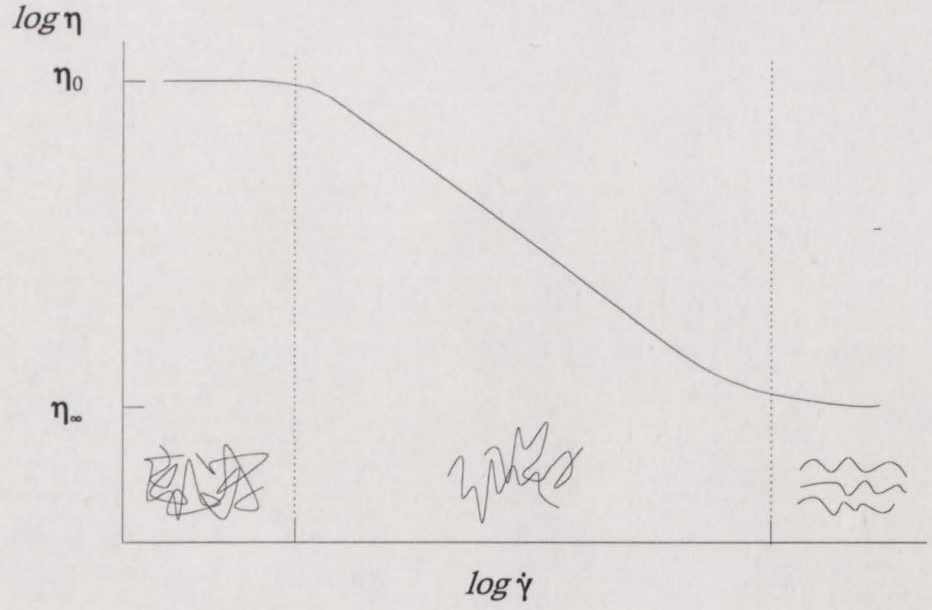

Fig 3. Diagram showing variation of viscosity η as a function of shear rate $\dot{\gamma}$ (logarithmic scales) together with sketches showing the associated arrangements or entanglements of the polymer chains. η_0, η_∞ are zero shear and infinite shear viscosities respectively.

Figure 4 has been removed due to third party copyright. The unabridged version of the thesis can be viewed at the Lanchester library, Coventry University.

Fig 4. The meander model of polymer melts e.g. [39]. The theory can apply equally to polymeric solids and can be used to illustrate and explain many viscoelastic properties. (a) the gross arrangement of chains in a polymer melt, (b) folding of a single molecule into a melt bundle which can be considered essentially one-dimensional; (c) superfolding of melt bundles into a space filling meander block, and (d) agglomeration of meander blocks into a coarse, grain-like melt structure.

terms of reptation in which the wriggling, snake-like motion of a polymer molecule is visualised as being contained in a virtual tube caused by neighbouring molecules (Fig 5) [45]. There are many texts on the treatment of reptation [46] and its applicability to various rheological phenomena and these are well documented *e.g.* [47]. The various characteristic response times of polymer melts are thought to be representative of different times of repose in, or exit from the virtual tube, however it is evident from the most recent work that much research is still required to fully characterise and understand this model. Indeed it seems to the present author that as the models become more complex, they become less useful to the non-specialist since vast computing power is often necessary. Nevertheless, the concept is of continuing use in interpreting the relaxation process in complex polymer materials.

In any thermoplastic polymer there will exist, on cooling beneath a certain (small) temperature range, a solid glass. The extent of this phase will depend on the amount of crystallinity present, but in even highly crystalline polymers there will always be some material of an amorphous nature [48]. The precise nature of the glass transition is still under debate, see for example [49], but there is general acceptance that there is a change in the internal free volume of the polymer which restricts the molecular mobility and hence does not allow the reorganisation of molecular chains into close-packed structures and configurations of zero configurational entropy over a practicably measurable timescale. The time dependent effect in the determination of the glass transition temperature T_g and the frequency or speed of heating or cooling at which a T_g is determined clearly then affects the transformation. Some key factors are given in Table 1. In the present work it is particularly important to note that the presence in the adhesive formulation of both low molecular weight amorphous polymers (tackifying resins) and crystalline entities (waxes) will give rise to complex structures in which there will be competing effects on the temperature of the glass transition. Simple attempts to model the T_g based upon the Fox equation (see later) will not always be successful due to the nature of the solubility parameters between the components, co-crystallisation of the components, and the effects of reduction in molecular weight and broadening of the polydispersity

Figure 5 has been removed due to third party copyright. The unabridged version of the thesis can be viewed at the Lanchester library, Coventry University.

Fig 5. The reptation model of polymeric relaxation processes. Neighbouring molecules, which are perpendicular to the plane of the paper, constrain molecule A, which can then only move as if it was contained within the tube B [45].

Table 1 Intrinsic and external factors affecting the glass transition temperature, T_g. Adapted from refs. [49 - 53].

Factor	Rationale	Experimental observation
INTRINSIC		
Free volume, v_f	$v_f = v - v_s$ where v_s is the molecular volume of the substance and v is the specific volume. As v_f decreases, the necessary room required for configurational rearrangement reduces. At T_g, the free volume reduces to a level which cannot support co-operative chain rearrangement. $v_f/v \approx 0.025$ at T_g for most polymers.	At high pressures (>10 000 N m^{-2}), T_g is observed to increase as v decreases. As v_s is constant, v_f is reduced and chain motion is restricted.
Intermolecular forces	Strong attractive forces between molecules (H bonding or polar groups) require greater thermal activation energies to initiate the co-operative motion required for crystallisation or elasticity.	Solubility parameters indicate intermolecular forces; T_g increases with increasing solubility.
Chain mobility	Bond rotation around ether linkages or C-C bonds permits low energy conformations and reduces the energy required for co-operative chain rotation. Double C=C bonds reduce chain mobility and T_gs rise. Stearic hindrance acts against ease of bond rotation and hence also increases T_g.	Poly(styrene) has a T_g of +100°C whilst poly(*iso*-butylene) has a T_g of -70°C.
Chain stiffness	Similar to above	
Molecular weight	Smaller chains have lower activation energies for movement, hence T_gs are lower. The empirical $T_g = T_g^{\infty} - C/x$ where x is chain length, C is a polymeric constant and T_g^{∞} is the asymptotic T_g at infinite chain length has been proposed.	Most commercial polymers are high enough in molecular weight for $T_g \approx T_g^{\infty}$.

continued

Table 1 continued

EXTERNAL		
Filler content	Fillers are usually incompatible with the polymer and form separate phases. They have little impact on T_g but will increase modulus significantly.	Adhesives with silicon microspheres show increased modulus however the T_g is identical to that of the unfilled system.
Plasticiser content	Low molecular weight species (solid or liquid) appreciably lower the T_g by separating polymer chains and thereby increasing v_f and/or reduce intramoleculer bonding forces by either stearic hindrance or preferential bonding to the chain.	PVC is typically a hard rigid material (T_g = 74°C) however plasticisation with dioctylphthalate gives a T_g reduction of 40 - 60°C. To a first approximation $1/T_g = W_1/T_{g1} + W_2/T_{g2}$ where 1, 2 refer to polymer and plasticiser respectively.
Copolymer content	Non-crystallisable random comonomers will also reduce T_g by the same empirical equation as given above however T_m will also drop, as will crystallinity. Mutually soluble comonomers give single T_gs; incompatible comonomers give separate T_gs (albeit shifted toward each other).	Random copolymerisation can give a broadening of the T_g range due to the distribution of comonomer molecules in the material. This gives a material with spread of T_gs.
Frequency of measurements	Molecular rearrangement occurs in a finite time. If the frequency of measurement is greater than the relaxation time of the rearrangement, the material will appear to have gone through its T_g. T_g increases with increasing frequency.	Poly(*iso*-butylene) for frequency ω ω = 0.01 Hz $T_g \approx$ -60°C ω = 100 Hz $T_g \approx$ -15°C ω = 10 kHz $T_g \approx$ +20°C
Heating /cooling rate	As above, cooling/heating rate after measured value of T_g. If cooling is rapid, a greater proportion of rearrangements cannot occur and hence the T_g is raised.	Poly(styrene) for cooling rates r r = 1 K hr^{-1} $T_g \approx$ 92°C r = 1 K s^{-1} $T_g \approx$ 107°C

ratio (of the adhesive as a whole) by virtue of addition of low molecular weight species to a high molecular weight polymer such as EVA.

Random copolymers of amorphous materials have the type of generalised phase diagram shown in Fig 6. It is possible to expand the diagram by the consideration of meso-phases with changes in properties being attributed to each phase change but this more complete picture does not appear to have universal applicability [53].

Poly(ethylene), and other commercial polymers which are derived from it, are complex materials which have varied morphologies dependant upon their composition, method of synthesis, the nature and quantity of the feedstocks used and the rate at which polymerisation occurs [54]. Poly(ethylene) is regarded as a crystalline polymer in that there is evidence of medium range ordering of polymer molecules in the solid state. Single crystals grown both from solution and from the melt have been extensively studied using analytical techniques such as electron microscopy, *e.g.* [55 - 57], X-ray diffraction [58 - 60] and neutron scattering [61].

Crystallinity implies the formation of a lattice structure with periodicity of composition. Simple polymeric materials such as poly(ethylene) provide the compositional periodicity along the chain length and hence, expanding this to three dimensions, compositional periodicity maybe readily achieved by parallel chain alignment. There have been many models proposed to account for this parallel chain alignment in both simple macromolecules and more complex biological macromolecules. Parallel chain alignment can occur in a number of ways. Initially it was thought that polymer crystallisation was around the basis of extended polymer chains aligning in crystals whose dimensions corresponded to the length of the molecule [62]. An alternative early theory for semi-crystalline polymers was that of the fringed micelle (Fig 7) [63] in which polymer molecules meandered from one aligned micelle to another, traversing regions of amorphous material in between. This theory for many years neglected the possibility of chain folding *e.g.* [64] however evidence that micellar structures exist was obtained for certain natural polymers [65]. The concept of chain folding was first introduced [66] as a result of work performed

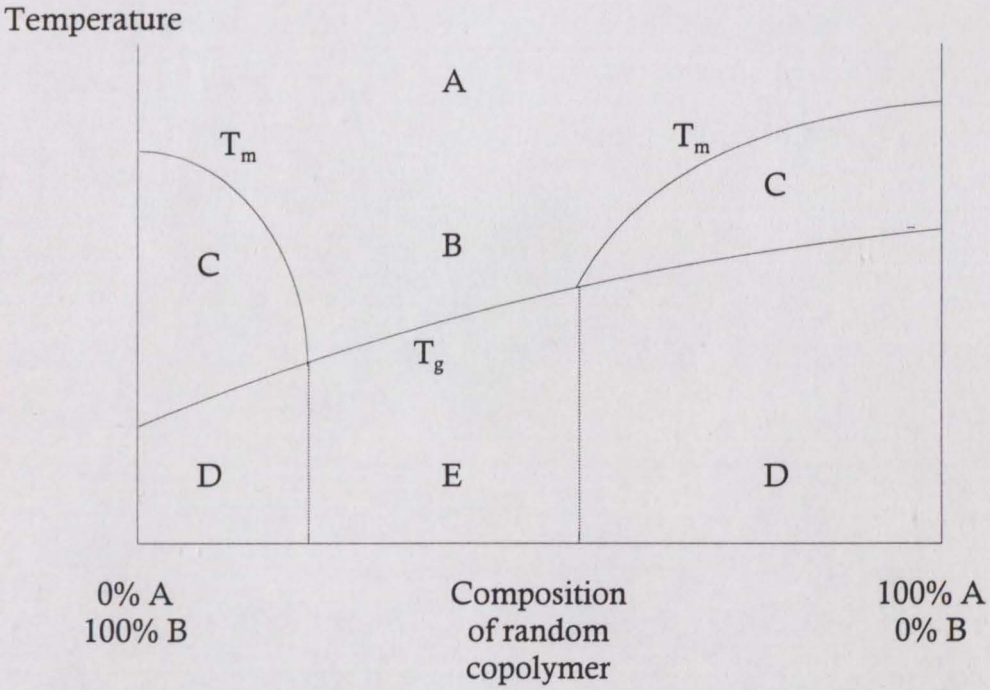

Fig 6. Schematic phase diagram for a random copolymer system. T_m, T_g are the melting point and glass transition temperature of the composition. A = melt, B = rubbery, C = rubbery and crystalline, D = glassy and crystalline, and E = glass. Adapted from reference [53].

Fig 7. Fringed micelle model of partially crystalline polymer solids [63].

on gutta percha (*trans*-1,4-poly(2-methyl butadiene)) and expanded upon by several workers [67, 68] however it was largely neglected until direct evidence by electron microscopic observation and electron diffraction [57] on single crystals of, for example, poly(ethylene) and polyamides. If a simple polymeric material such as poly(ethylene) is considered then three simple mechanisms of chain folding can be represented (Fig 8). The adjacent re-entry model is considered the ideal case but the loose folding (switchboard model) and meander model (or indeed a combination) are suggested as being more realistic [69]. It is likely in a real polymer system that all of the above molecular conformations are present as is illustrated in Fig 9 [70].

The consideration that chain folding can occur is linked closely in with the concept of crystalline lamellae consisting of regularly packed sequences of polymeric chains. The lamellae form as a result of chain folding within a single molecule and also through the incorporation of segments of adjacent molecules into the regular folded structure as previously described. These so-called tie-molecules (Fig 10a) [71, 72] may be contained within more than one lamellae and play a crucial role in the ability of a polymeric material to withstand stress and undergo deformation. Tie-molecules are responsible for cohesion between the lamellae and for the transfer of stress through the material [73].

Even crystalline polymers however are not fully crystalline but are composed of complex morphological features (Fig 10b) dependant again upon the conformations of the polymer molecule. Spherulites are supra-molecular morphological structures consisting of crystalline lamellae arranged around a nucleus, *e.g.* [68, 74, 75]. Amorphous, unstructured molecules surround the regular lamellae within the spherulite (intra-spherulitic amorphous regions) and spherulitic growth occurs radially in three dimensions such that the growth direction is perpendicular to the ordered molecules within the lamellae. Spherulite growth continues until the spherulite impinges on the border of a neighbouring spherulite and hence a second inter-spherulitic amorphous region is formed. Simple polymers such as poly(ethylene) have been shown to exhibit the spherulite microstructure clearly [76], whilst more complex polymers show considerable deviation from the models illustrated.

Figure 8 has been removed due to third party copyright. The unabridged version of the thesis can be viewed at the Lanchester library, Coventry University.

Fig 8. Alternative models of crystal lamellae [69]. (a) acute folds, (b) loose folding (switchboard model), and (c) meander model.

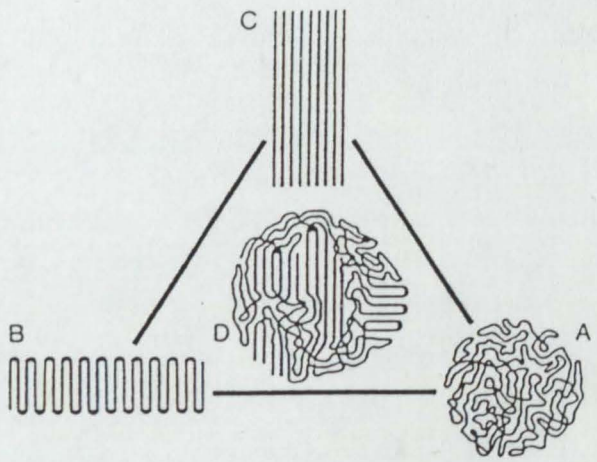

Fig 9. Macroconformations in a polymeric solid. Three possible arrangements are A, B, and C. D illustrates crystalline lamellae surrounded by a disordered region.

Fig 10. Spherulitic microstructure of partially crystalline polymeric solids. (a) ordering of the lamellae in the region around the core of a spherulite, and (b) a sketch showing the ordering of lamellae in a spherulite and the resulting microstructures e.g. [68].

Spherulite formation is by a process of nucleation and it has been shown that the factors affecting nucleation not only affect the rate of spherulite formation, but also the conformation of the lamellae within the spherulite. EVA has been shown to possess a spherulitic morphology whose shape varies with the temperature of crystallisation [77]. At higher temperatures, the spherulites become more feathery. The spherulite shape also varies as a result of comonomer composition, with high VA copolymers being considerably non-spherical [78]. The concentration of nuclei also affects the spherulitic morphology. High concentrations of nuclei tend to give fine crystalline structures whilst low nuclei concentration will give coarse grain structures. Spherulitic growth continues by secondary and tertiary nucleation in processes governed by the Avrami equation (see, for example, [79]):

$$\alpha(t) = 1 - exp(-kt^n) \qquad \ldots (1)$$

where $\alpha(t)$ is the degree of crystallisation, n is the Avrami exponent and k is a constant of proportionality dependant upon the number of nuclei per unit volume and the rate at which the nuclei are forming. Other crystalline morphologies are present if polymer melts are subjected to stresses and strains (such as melt processing) and there are numerous examples of different proposed structures in the literature *e.g.* [69, 80, 81].

As a crystalline polymer melts it undergoes a transformation involving the dissolution of the crystalline portions of the spherulite into the amorphous material surrounding them. However, unlike the case with lower molecular weight organic compounds, it is not usually possible to determine the unique melting point of a polymeric material, since the melting point is dependant, amongst other things, upon molecular weight distribution, rate of heating, degree of chain branching, and amount of crystallinity. Highly crystalline polymers generally show much narrower melting ranges and have higher enthalpies of melting or freezing due to the regularity of their structure. The measurements however must be carefully controlled when comparing different polymeric materials so that other thermodynamic effects (such as post-crystallisation or cold crystallisation) do not occur and lead to erroneous comparisons. If mixtures of melt-compatible polymers are made such that co-

crystallisation cannot occur, then the melting point is depressed according to equation (2):

$$1/T_m - 1/T_m^0 = -(R/\Delta H_2)(v_2/v_1)\chi(1-\phi_2)^2 \quad \ldots (2)$$

where the subscripts 1 and 2 refer to the non-crystallisable and crystallisable polymers respectively, v represents the molar volumes, ΔH_2 is the molar enthalpy of melting per monomer unit, ϕ_2 is the volume fraction of polymer 2, and χ is an interaction parameter. T_m and T_m^0 refer to the observed and equilibrium melting points respectively [82].

2.2 Rheology

The deformation and flow of adhesives and adhesive joints are of vital concern for three main reasons: firstly, the adhesive must flow to form the joint, secondly, the joint in service will be subject to creep and stress relaxation, and thirdly, analysis of the dynamic behaviour provides a valuable insight into the mechanisms responsible for the molecular and mechanical behaviour. Thus information on the rheological properties of the adhesive and the joints are central to the successful application and use of adhesives.

Simple deformation behaviour is summarised in Figs 11 and 12. Plastic flow and other non-Hookean behaviour (Fig 11) are of particular interest in the service performance of real joints and these are considered in more detail in the next section.

Viscous deformation (Fig 12) is of crucial importance in understanding the mechanical properties of adhesives. Viscosity is a thermally activated process, and may be modelled at a simple molecular level. There are two fundamental aspects of the model. The first is that simple molecules are thermally activated and jump to an adjacent site. This involves thermal energy needed to enable the molecule to jump (the Boltzmann factor), and thermal energy to create a vacancy or hole for the molecule to jump into. Put another way, the probability of jumping, P, is given by

$$P = P_V P_E \quad \ldots (3)$$

where P_E is the probability the molecule has sufficient energy to scale the energy barrier E, and P_V is the probability that there is a suitable hole next to the

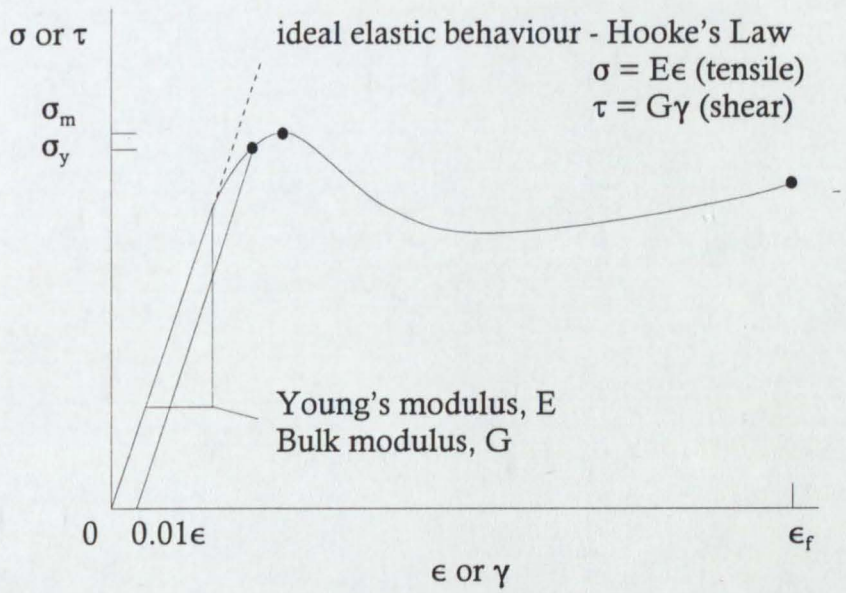

Fig 11. Typical curve showing the deformation of a real material with elastic, plastic and fracture behaviour. σ, ϵ = tensile stress, strain, τ, γ = shear stress, strain, E, G = tensile (Young's) modulus, shear (bulk) modulus, σ_m = maximum tensile stress, σ_y = tensile yield stress at $\epsilon = 0.01$, ϵ_f = tensile strain at fracture.

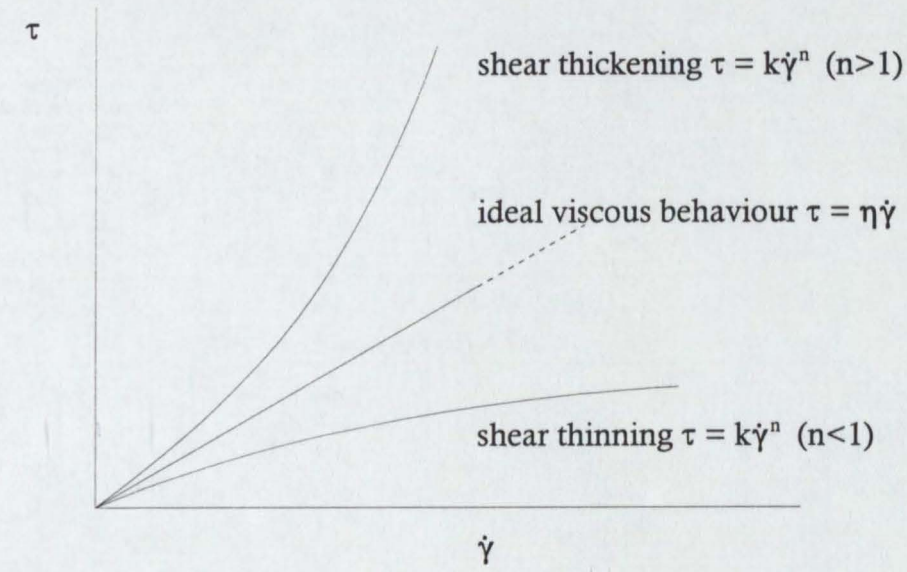

(a)

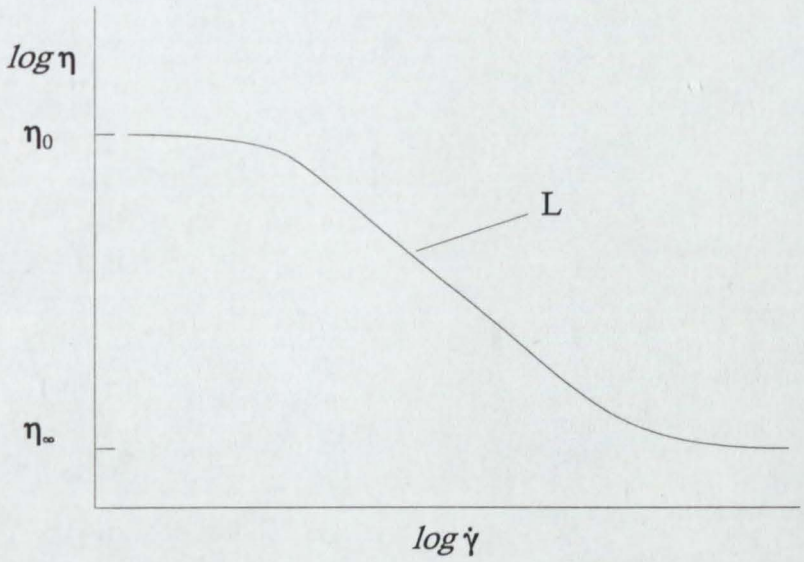

(b)

Fig 12. Typical curves showing (a) ideal and non-linear viscous behaviour and (b) generalised flow curve for non-Newtonian fluids. τ, γ = shear stress, strain, $\dot{\gamma}$ = shear strain rate, η = viscosity, η_0 = zero shear viscosity, η_∞ = infinite shear viscosity, L = linear region of generalised flow curve corresponding to power law region. See text for details.

jumping molecule. The second fundamental aspect of the model is that a shear stress biases the inherently random jumps in the direction of the stress. The result is that the viscosity, is given by

$$\eta = f_0 \, exp\,(v^*/v_f) \, exp\,(E/RT) \qquad \ldots (4)$$

where v^* is the volume of the molecule, and v_f is the average free volume per molecule, f_0 is the frequency of vibration of the molecule, E is the activation energy for jumping per mole, R is the gas constant and T is the temperature [83]. Alternatively

$$\eta = f_0 \, exp\,(V_m/(V-V_m) + E/RT) \qquad \ldots (5)$$

where V is the total volume and V_m is the molecular volume. Other models have been developed that differ in the pre-experimental factor. The above theory is based on the movement of small molecules. Very large polymer molecules do not diffuse by the jumping of the whole molecule, rather small segments containing about five to ten monomer units move by a process of segmental motion. Essentially the centre of the mass effectively moves as the segment of chain rotates [45, 84]. A number of other models of flow in polymer melts have been proposed. For example, using the meander model [44]

$$\eta = 2\tau_F/\Delta J_F^0 \qquad \ldots (6)$$

where τ_F is the characteristic flow time, and $\Delta J_F^0 \approx (M/M_0)^{0.5}$ where M is the molar mass, and M_0 is the molar mass of a monomer unit.

Most fluids do not show simple Newtonian behaviour [30] and the viscosity η is a complex function of the strain rate $\dot{\gamma}$, temperature, time of shearing, and pressure. The deviation takes many forms (Fig 12a). The most common in polymer melt systems being an observable decrease in η with an increase in $\dot{\gamma}$ (shear thinning behaviour, often called pseudoplasticity). If η is plotted *vs* $\dot{\gamma}$ the characteristic sigmoidal shape of the generalised flow curve is often seen (Fig 12b). There are three main regions of interest, the areas of Newtonian behaviour at low and high values of $\dot{\gamma}$ and the steeply sloping central portion of the graph. The constant values of η obtained at low and high $\dot{\gamma}$ are called the zero-shear (η_0) and infinite shear (η_∞) viscosities respectively. Many workers have introduced factors (often empirically) to explain experimental observations.

Of these, the most widely utilised for general description of the shape of the flow curve is the model due to Cross. Four parameters completely describe the rheological behaviour [85] where K_1 is a constant with dimensions of time and m is a dimensionless constant:

$$(\eta - \eta_0)/(\eta_0 - \eta_\infty) = 1/ (1+(K_1\dot{\gamma})^m) \quad \ldots (7)$$

If $\eta \ll \eta_0$ and $\eta \gg \eta_\infty$ then the Cross model reduces to a power law which can successfully describe the change of η over the middle decades of $\dot{\gamma}$

$$\eta = K_2\dot{\gamma}^{n-1} \quad \ldots (8)$$

where n is the power law index and K_2 is a constant with units of Pa s^n. These equations can be successfully used to determine the behaviour of a material at different rates of shear. However, great care must be taken when extrapolating data to ranges far from the region of study.

Application of a cyclic stress (or strain) and measuring the resulting strain (or stress) provides considerable information on the viscoelastic properties of materials [86]. When a cyclic stress is applied to a material

$$\sigma = \sigma_0 \cos(\omega t) \quad \ldots (9)$$

where σ is the stress at any time t, σ_0 is the maximum stress, and ω is the angular frequency of stress cycling (Fig 13). For an elastic solid, the strain ϵ is in phase with the stress and

$$\epsilon = \epsilon_0 \cos(\omega t) \quad \ldots (10)$$

However, if there is a viscous component, then there is a delay in the response since the strain is now dependent on the time, and now

$$\epsilon = \epsilon_0 \cos(\omega t - \delta) \quad \ldots (11)$$

the term δ is the phase angle or lag (Fig 13b). The case for an ideally viscous fluid is also shown (Fig 13c), here the maximum stress and the maximum strain are not coincident. Further development and analysis is facilitated by defining a complex stress σ^* and complex strain ϵ^*

$$\sigma^* = \sigma_0 \exp(i\omega t) \quad \ldots (12)$$

$$\epsilon^* = \epsilon_0 \exp(i(\omega t - \delta)) \quad \ldots (13)$$

where $i^2 = -1$. From these the real stress and real strain are determined as the real parts of the complex function

$$\sigma = \mathrm{Re}(\sigma^*) \quad \ldots (14)$$

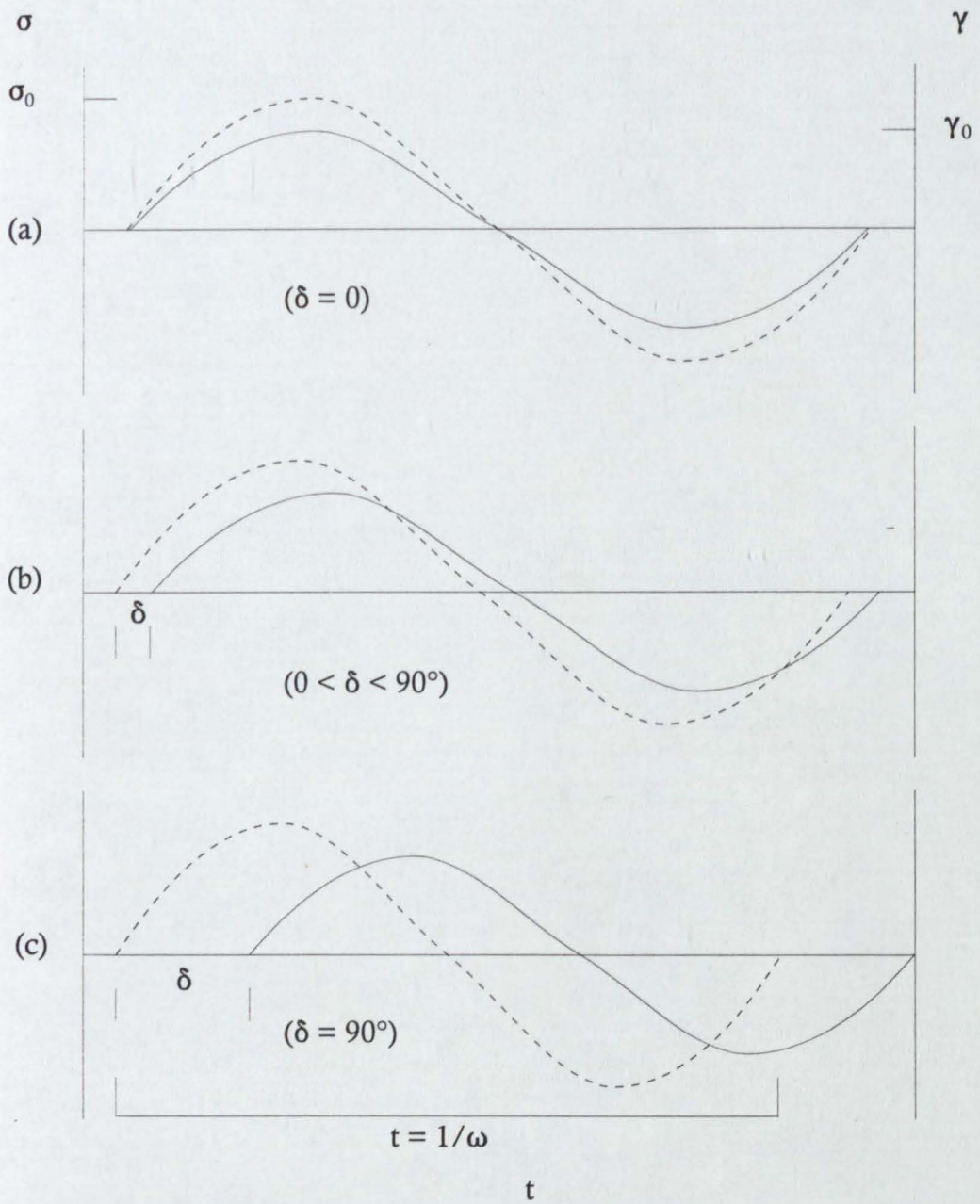

Fig 13. Schematic of applied stress σ, and resultant strain ϵ, curves *vs* time t in a dynamic experiment for (a) an elastic solid, (b) a viscoelastic material and (c) a viscous fluid. (--------) = applied stress, (———) = resultant strain, σ_0 = stress amplitude, ϵ_0 = strain amplitude, δ = phase angle, ω = frequency of oscillation. Adapted from reference [86].

$$\epsilon = Re(\epsilon^*) \quad \ldots (15)$$

A complex modulus $G^*(\omega)$ may also be defined

$$G^*(\omega) = (\sigma^*/\epsilon^*) = G'(\omega) + iG''(\omega) \quad \ldots (16)$$

where G' and G" are the storage and loss moduli respectively (Fig 14). The important point of cyclic (or oscillatory) rheology is that, within the region where linear viscoelasticity is valid, the phase angle δ and σ_0/ϵ_0 are properties of the material for any given ω, and they give valuable information on the viscoelastic behaviour of the material.

The relationship between modulus and temperature is strongly dependent upon polymer morphology, at higher temperatures polymer molecules possess higher energies and can change conformations easily as different bond rotations become possible. Amorphous polymers show distinct regions of viscoelastic behaviour (Fig 15) with differences dependent upon molecular weight, composition, and degree of cross-linking [29]. Semi-crystalline polymers tend to have less clearly defined zones, shifting from glassy to flexible, or leathery, behaviour before showing a distinct transition attributable to melting of any crystalline regions that are present [87]. A schematic curve representing the viscoelastic behaviour of a semi-crystalline polymer, or adhesive, with temperature is annotated with points of interest (Fig 16). The point at which *tan* δ has a local maximum, P_L, corresponds with a transition representing a large increase in modulus, referred to as a glass transition temperature. A second transition point, P_X, is the point of modulus crossover, where G" becomes greater than G'. This point represents the alteration in behaviour of the polymer or adhesive from viscoelastic solid to viscoelastic liquid [88].

Adhesives are typically viscoelastic and contain both elastic and viscous components. These may be represented by a spring of modulus G and a dashpot a viscosity η (Fig 17), and the phenomenological behaviour of a complex viscoelastic body may then be modelled by combining any number of such springs and dashpots (of any G and η) in any parallel and/or series combination. The two simplest models are the Voigt/Kelvin and Maxwell models. For example, with the Voigt/Kelvin model the variation of shear with time is given by summing the terms of the spring and dashpot equations:

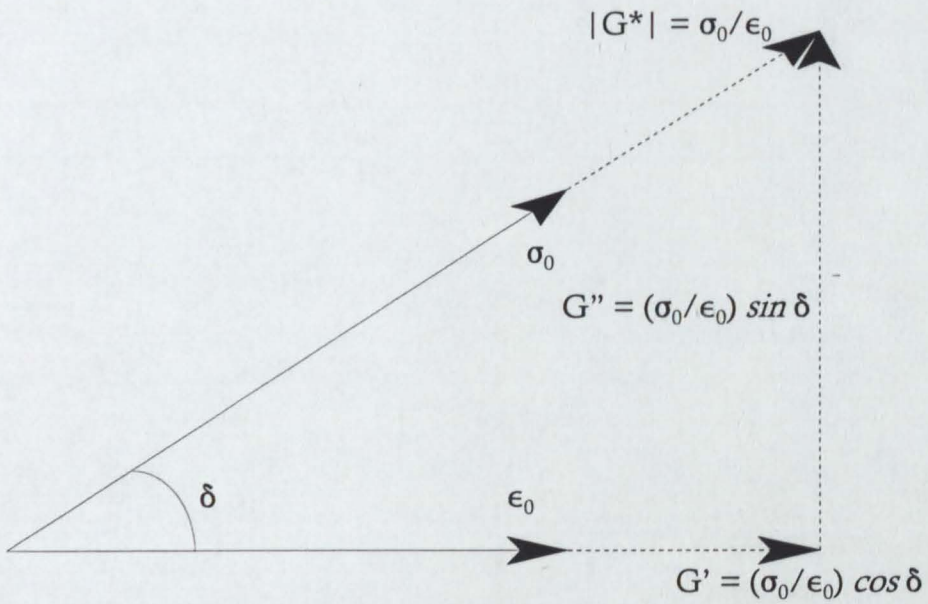

Fig 14. Vector diagram of the complex modulus G* and its resolution into the storage and loss moduli G', G". σ_0, ϵ_0 = stress, strain amplitude, δ = phase angle.

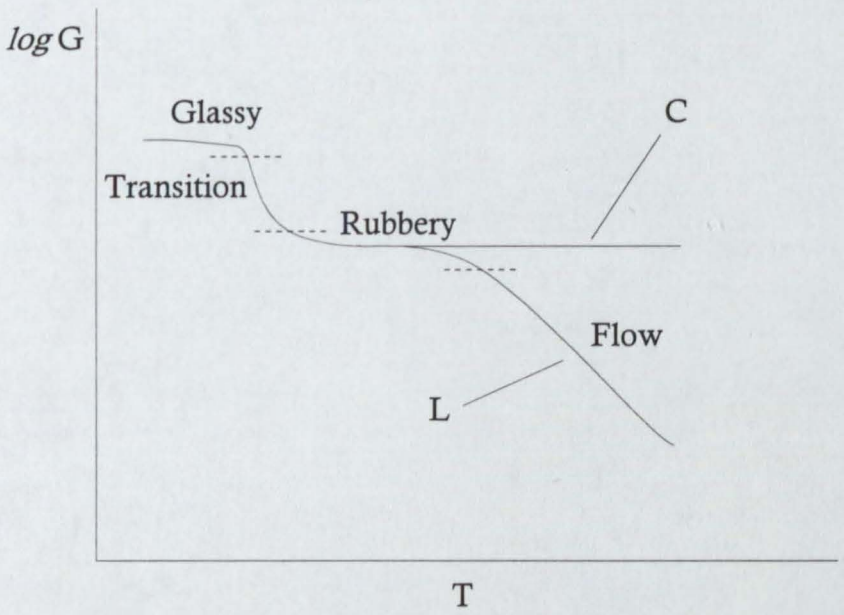

Fig 15. Idealised modulus G as a function of temperature T curve showing regions of viscoelastic behaviour. L = flow region for linear, amorphous polymers, C = extension of rubbery plateau for lightly crosslinked networks.

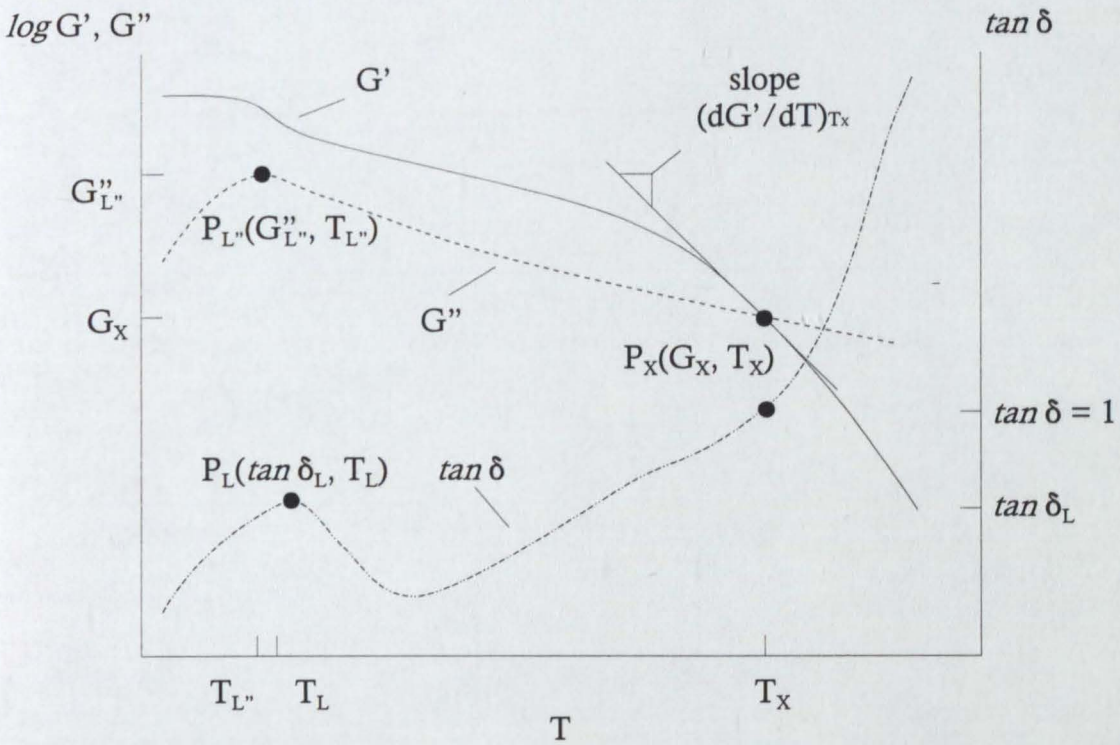

Fig 16. Schematic of controlled strain and controlled stress oscillation rheogram for a fixed frequency showing the storage and loss moduli G', G", and loss tangent *tan* δ, as a function of temperature T. Note the points P_L (*tan* δ_L, T_L) where *tan* δ has a local maximum, $P_{L"}$ ($G"_{L"}$, $T_{L"}$) where G" has a local maximum, and P_X (G_X, T_X) where the modulus curves cross and G' = G" = G_X (say) and by definition *tan* δ = 1.

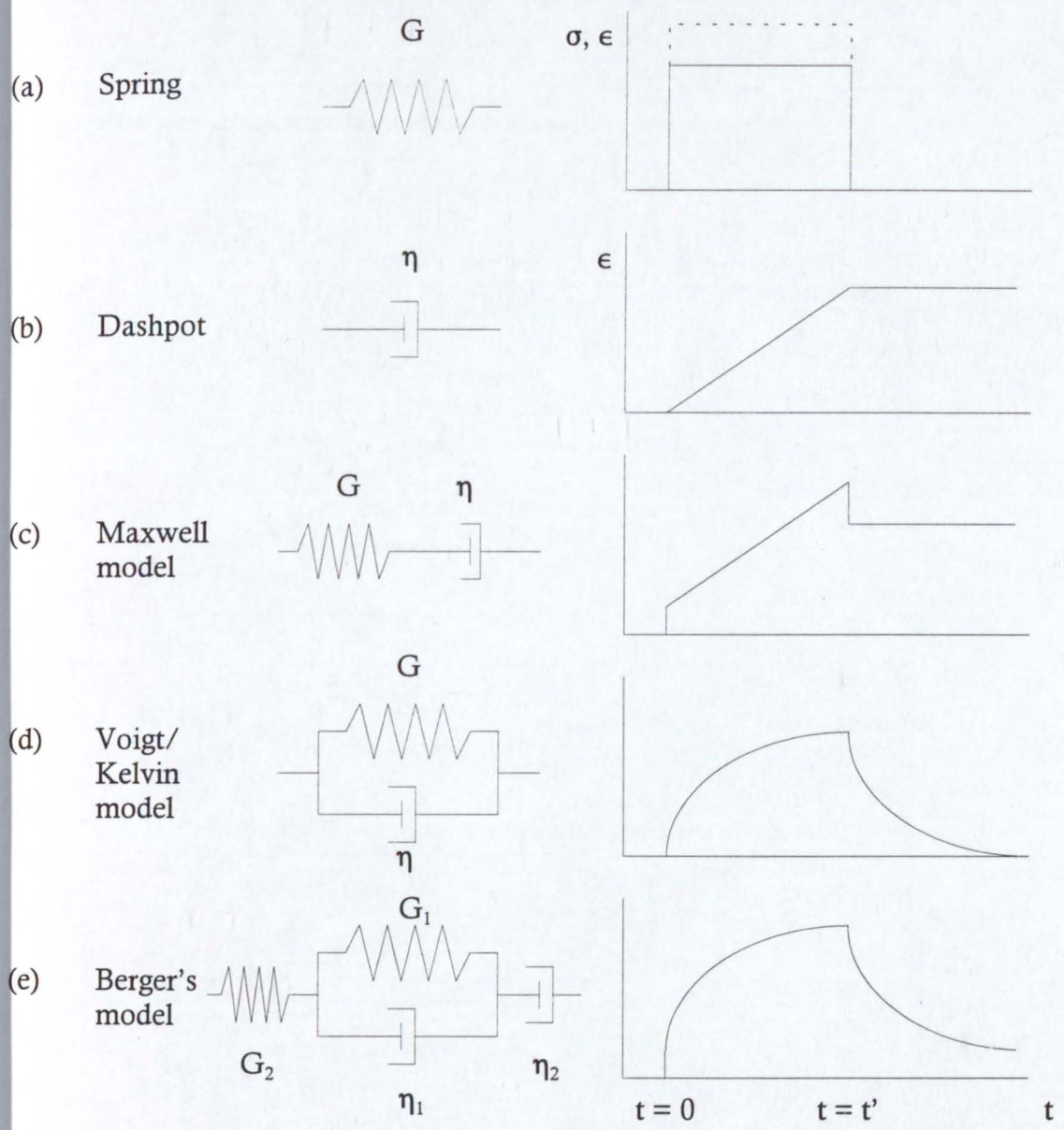

Fig 17. Viscoelastic elements, behaviour and simple viscoelastic models. (a) Hookean spring of modulus G (deformation and energy recovery), (b) Newtonian dashpot of viscosity η (permanent deformation and energy dissipation), (c) parallel spring and dashpot (recoverable deformation), (d) series spring and dashpot (permanent deformation), and (e) series/parallel spring and dashpot (recoverable and permanent deformation). σ = stress (---------); ϵ = strain (————); t = 0, time at which load is applied; t = t', time at which load is released.

$$\sigma(t) = \epsilon(t)G_1 + \eta_1 \, d\epsilon(t)/dt \qquad \ldots (17)$$

As the stress is constant

$$d\epsilon(t)/dt + \epsilon(t)/\tau = \sigma_0/\eta \qquad \ldots (18)$$

where τ is defined as the characteristic time of the element, being equivalent to the time required for the Voigt/Kelvin unit to fully extend and reach equilibrium under the applied stress σ_0. If the above is integrated using the factor $exp\,(t/\tau)$ between limits of $\epsilon(0)=0$ and $\epsilon(t) = \epsilon(t)$ then

$$\epsilon(t)\, exp\,(t/\tau) = (\sigma_0/G_1)\, exp\,((t/\tau) - 1) \qquad \ldots (19)$$

or

$$\epsilon(t)/\sigma_0 = J(t) = J(1 - exp\,(t/\tau)) \qquad \ldots (20)$$

where J(t) is the creep compliance. More complex models, such as Berger's Model (Fig 17e) can be introduced which attempt to model real data with greater degrees of accuracy. This is a four component model that models permanent and recoverable deformation. Real materials however can show even more complex behaviour and further Voigt/Kelvin or Maxwell units can be added to ensure better data fitting.

The Boltzmann Superposition Principle *e.g.* [89, 90] can be used to effectively model the creep response of real materials by formalising that (a) the creep in a specimen is a function of the entire loading history, (b) that each loading step makes an independent contribution to the final deformation, and (c) that the final deformation can be obtained by summing each contribution. This is illustrated in Fig 18. The time-dependant strain in the sample, $\epsilon(t)$, can be shown to be [90]

$$\epsilon(t) = \sigma_0 J(t) + \sigma_1 J(t - t_1) + \sigma_2 J(t - t_2) \qquad \ldots (21)$$

where σ_1, σ_2 are discrete stresses applied at t_1, t_2. The stress on a sample undergoing a continuous application of stress σ_t, *i.e.* a creep experiment, can thus be regarded as a derivative of the total stress. The individual compliancies associated with each applied stress, or time period, can now be associated with individual Voigt/Kelvin or Maxwell units if the mechanical analogue is again considered. Ultimately, for the case of an infinite number of mechanical units, a creep spectrum can be considered

$$J(t) = J_0 + \int_{-\infty}^{\infty} L\,(1 - exp\,(-t/\tau))\, d\, ln\, \tau + t/\eta_0 \qquad \ldots (22)$$

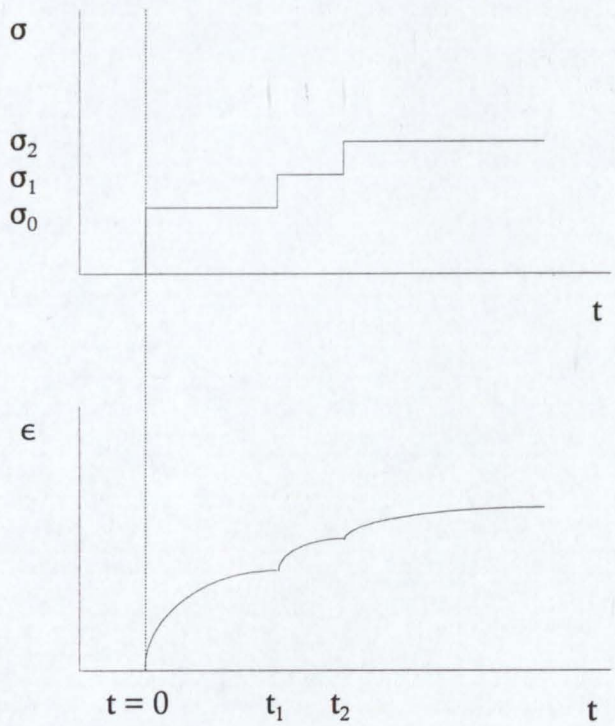

Fig 18. Relationship between stress σ and resultant strain ϵ for a creep experiment illustrating the Boltzmann Superposition Principle where σ_1, σ_2 represent additional stresses applied at t_1, t_2 after the original stress application σ_0 at t = 0. See text for details. Adapted from reference [90].

where J_0 is the instantaneous compliance, η_0 is the zero shear viscosity, and L is the continuous spectrum of creep times τ corresponding to the characteristic time of each Voigt/Kelvin element. L will diminish at long time scales and t/η_0 will become the dominant factor, representing the contribution of viscous flow to the overall deformation [91].

The two approaches, phenomenological (mechanical) analogues and statistical mechanics provide alternative descriptions with differing degrees of insight into viscoelastic behaviour. However, the statistical models tend to be more complex and apply more readily to simpler systems. There is considerable evidence that the two approaches (phenomenological and statistical) are equivalent *e.g.* [90, 92 - 94]. The advantage of the phenomenological approach is that it is a simple and useful means to visualise and extract numerical information from experimental data.

The exact inter-relations between the functions derived from creep, stress relaxation and oscillatory rheometry can be calculated by means of Fourier and Laplacian transformations in a manner analogous to the analysis of electronic circuits [90]. However these relationships tend to be complex. It is now more usual to present rheological data as graphs of the resolved components of dynamic parameters and these are rarely transformed into relaxation spectra [92].

2.3 Principles of adhesion

Adhesion requires the fulfilment of three basic requirements, namely; (a) the establishment of intimate contact between adhesive and adherend, (b) the absence of weak boundary layers within the joint, and (c) the minimisation of stress concentrations which can lead to debonding.

The initial step in bond formation must be the formation of a degree of intimate contact between the adhesive and adherend. The adhesive must therefore wet the surface of the adherend in order to achieve the necessary contact and, during spreading, it must remove surface contaminants, either by displacing or dissolving them.

When a hot melt adhesive (HMA) makes contact with the surface of an

ideally smooth adherend, a drop is formed which usually takes the form of a hemispherical cap (Fig 19a). The critical feature in wetting is the contact angle θ which the liquid was at the periphery of the drop. At equilibrium

$$\gamma_{SV} = \gamma_{SL} + \gamma_{LV} \cos\theta \quad \ldots (23)$$

where the surface energies of the solid/vapour, solid/liquid and liquid/vapour interfaces are given by γ_{SV}, γ_{SL} and γ_{LV} respectively [95]. When $\theta < 90°$ wetting occurs and the adhesive will spread over the adherend. If, however, γ_{SV} is less than γ_{SL} then $\theta > 90°$ and spontaneous wetting will not occur. If the surface to which the HMA is applied is not smooth, *e.g.* the adhesive is applied to paper or board, then a situation such as that given in Fig 19b may occur and pockets of air or moisture may be entrapped on the interface. Surface roughness was originally believed to aid wetting [96] however this is shown to be true only in cases where systems already have low contact angles or adhesives are applied to very rough surfaces [97]. The rate at which wetting occurs on a rough surface may be estimated by considering flow in capillaries where the time t required to move a distance x in a capillary of radius r is given by

$$t = (2\eta/\gamma_W \cos\theta)(x^2/r) \quad \ldots (24)$$

where η and γ_W are the viscosity and surface tension of the adhesive respectively [98]. This equation, however assumes equilibrium condition and spontaneous wetting (*i.e.* $\theta < 90°$). This is not always the case and HMAs typically have contact angles greater than 90°. Pressure must therefore be applied in order that wetting of the rough surface may occur. This pressure is usually applied by the application of the second adherend whilst the adhesive is still molten. This pressure leads to an apparent dynamic contact angle θ_D which can be related to the viscosity of the adhesive [99] by

$$\tan\theta_D = m(\eta v_S/\gamma_{LV})^n \quad \ldots (25)$$

where m and n are constants and v_S is the spreading velocity of the adhesive. It can be seen that the lower an adhesive's viscosity, the smaller the contact angle and hence the easier wetting will be, however the reduction in viscosity is usually accompanied by a reduction in the mechanical properties of the adhesive and may therefore be undesirable.

The presence of discrete weak boundary layers in adhesive joints has been

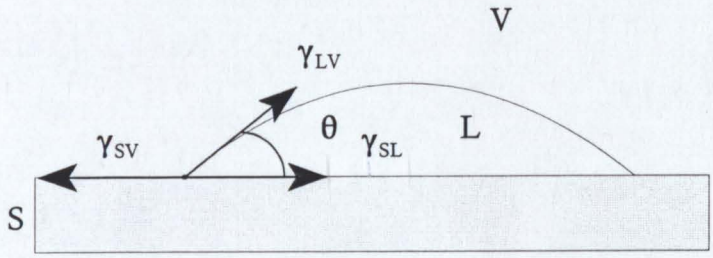

(a)

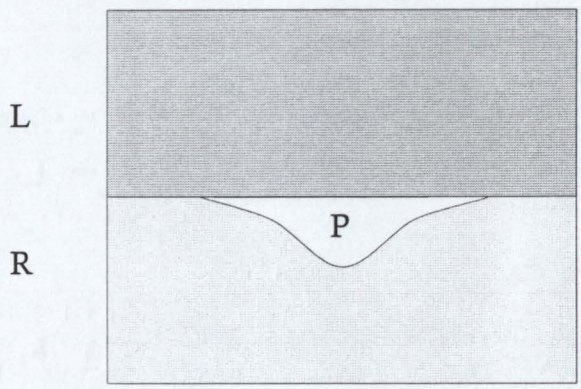

(b)

Fig 19. Schematic diagrams showing a liquid adhesive resting on: (a) a perfectly smooth surface and (b) a rough surface illustrating entrapment of air or moisture, P, on the interface. L = liquid adhesive, S, R = smooth, rough surfaces, V = vapour phase, γ_{SV}, γ_{SL}, γ_{LV} = surface energies of the solid/vapour, solid/liquid and liquid/vapour interfaces, θ = contact angle. See text for details.

proposed [100, 101] and experimental evidence of their existence has been shown in some systems, usually paint/metal adhesion [102]. More recently, in certain wax-bearing HMAs in contact with poly(propylene) substrates, X-ray photoelectron spectroscopy studies of fracture surfaces have identified the presence and composition of what was thought to be a wax weak boundary layer and appropriate advice on formulation strategies to overcome its occurrence were offered [103]. Further work on other polyolefinic substrates, with and without surface treatments such as corona discharge, offer alternative theories for the reduction in surface oxygen/carbon ratios such as polar group redistribution due to localised packing of the surface during bonding [104]. It was also claimed that compatibility effects between untreated poly(ethylene) and the low molecular weight paraffinic wax component may cause redistribution of the incompatible wax component so as to give a variation in composition throughout the joint. Weak boundary layers must therefore be considered in adhesive bonding, although the likelihood of their formation, and indeed the form they may take cannot be explained easily for all systems and careful study is required in critical applications.

Bond strength develops by the interaction between adhesive and adherend and there are many theories of adhesion. The main mechanisms are the formation of chemical and/or physical bonds at the interface, and hence the surface must be sufficiently clean or the adhesive pressed on the surface to aid contact and/or spreading if the contact angle is unfavourable. It is important to realise that wettability, *i.e.* spreading of the adhesive, does not necessarily imply a strong bond is formed. This depends entirely upon the mechanical, chemical, and physical properties of the adhesive and adherend. The main theories associated with adhesion of HMAs are summarised in Table 2. Also included in the Table are the limitations of the theories and comments on their applicability. It is important to realise that the theories are limiting cases. In practice, various processes may contribute to the formation of a bond and it is not possible to precisely separate the contribution made by each mechanism.

It is important to be aware that the theories presented in Table 2 represent bond formation and adhesion development and they often cannot be used to

Table 2 Principal theories of adhesion in hot melt adhesives [105]

Mechanism	Examples	Limitations	Conclusions
(a) Adsorption, *e.g.* refs. [106, 107]			
Chemical and/or physical bonds; Van der Waals, Hydrogen bonds.	Much experimental work on polymers, metals, and ceramics.	No major disadvantages although autohesion between chemically similar substrates is not particularly well explained by this theory alone.	Most representative and dominant theory. General applicability in most adhesive systems.
(b) Mechanical, *e.g.* refs. [108 - 112]			
Rough surfaces aid keying/interlocking by adhesive.	Hot melt adhesives to card/paper, plastics/metal.	Ignores viscoelastic energy dissipation. Cannot solely account for adhesion in many systems.	Frequently important in conjunction with other factors.
(c) Diffusion, *e.g.* refs. [113 - 119]			
Interdiffusion across the interface.	Autohesion of polymers, solvent welding of glassy polymers.	Polymers are required to have similar solubility parameters. Ignores viscoelastic energy dissipation on debonding.	Applicable in certain polymer systems. May promote adhesion between polymers and metals due to effective increase of surface areas.

fully predict the behaviour of real joints. The thermodynamic work of adhesion W_A may be calculated from

$$W_A = \gamma_S + \gamma_{LV} - \gamma_{SL} \quad \ldots (26)$$

where γ_S is the interfacial surface energy of the solid in an inert medium (as compared with γ_{SL} in equation 23 [95]). However numerous attempts by several workers to relate W_A to surface free energy γ_S have been made, and whilst some have been successful [120], others have failed to see a significant correlation [121]. It has been observed, however, that adhesive joints typically fail by initiation and propagation of cracks and flaws present within the joint. A considerable amount of theoretical and practical work on the application of fracture mechanics to adhesive joints has been undertaken [122] and it is clear that the application of these techniques has allowed the consideration of other adhesive properties, such as viscoelastic behaviour, morphology and fatigue behaviour, to be included in consideration of bonds and bond strengths.

Both energy balance and stress intensity factor approaches to fracture mechanics of adhesive joints have been studied extensively, although the energy balance approach is more easily determined and seems to have gained wider acceptance. The energy balance approach supposes that fracture occurs in a homogenous, linearly elastic material when sufficient elastic energy is release from the stress field (dW) to supply the energy requirements of the new fracture surfaces. Consider a crack growing by length da, this will cause an incremental increase in the fracture surface area dA. This implies

$$-dW/da \geq S\, dA/da \quad \ldots (27)$$

where S is the specific surface free energy of the material. If the crack is in a lamina of thickness b then the criteria for fracture becomes

$$(1/b)(dW/da) \geq 2S \quad \ldots (28)$$

where 2S can be replaced by the symbol G_C signifying fracture energy (if simplifying assumptions about energy dissipation about the crack tip can be made). G_C encompasses all the energy losses incurred around the crack tip and may be considered as the energy required to increase the crack by unit length in a specimen of unit width.

It has been shown that equation (27) can also be utilised in non-linearly

elastic materials such as crosslinked rubber [123] and in adhesive fracture between rubbery adhesives and poly(ethylene terephthalate) adherends [124]. For non-linearly elastic materials G_C can be related to an intrinsic fracture energy (related to rupture of primary and secondary adhesive bonds) and a viscoelastic loss function Φ_V which is dependent upon crack growth rate, level of strain and temperature although additional care must now be taken in identifying loci of failure (interfacial, adhesive-in-adhesive, or cohesive-in-substrate) and the type of deformation about the crack tip (viscoelastic or plastic).

2.4 Adhesive joints

Adhesives in service are part of a joint. The behaviour of the joint is a complex function of, for example, the adhesive, bonding conditions, adherends, joint geometry, applied stress, and testing conditions. To obtain meaningful and useful data, precisely defined tests are necessary. There are four basic types of stress that can be applied to a joint (Fig 20) and we consider here the basis of the tests that are used in the present work; the peel test (Fig 20a) and the static shear test (Fig 20b). In addition, the importance of surface pre-treatment, and the methods of determining open times and setting times are discussed, with particular reference to industrial, automated tests.

It is essential that with any adhesive bonding process that the surfaces of the adherends to be joined are clean and suitable for adhesive application *e.g.* [125]. In the case of metallic adherends, such as aluminium or steel, this may require pre-treatment of the surfaces with an etchant so as to remove traces of oxide layers and filmic process additives. These latter surface contaminants may be particularly deleterious to the performance of hot melt adhesives as lubricants used in sheet rolling processes can migrate into the adhesive where they act as efficient plasticisers, causing loss of adhesive strength and increasing the likelihood of failure processes such as creep. When non-metallic adherends are considered (as is often the case for EVA-based hot melt adhesives) it is essential that they also are conditioned prior to bonding. In the case of non-polar polymeric adherends (such as poly(ethylene)), corona discharge or flame treating is an efficient continuous method. With card and paper substrates,

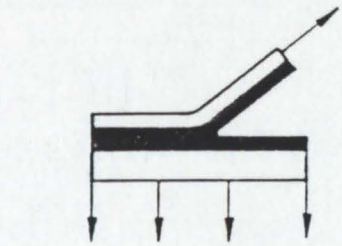

(a)

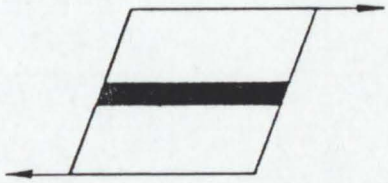

(b)

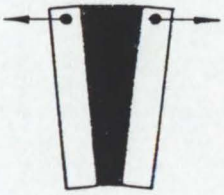

(c)

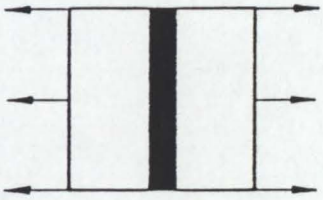

(d)

Fig 20. Types of stresses that can be applied to adhesive joints. (a) peel stress, (b) shear stress, (c) cleavage stress and (d) normal (direct) stress. Adapted from reference [126].

being naturally variable surfaces, it is necessary to ensure that such external factors as relative humidity and ambient temperature are considered and controlled wherever possible. It is often necessary in such cases to perform comparative testing against a known standard board in order to obtain a degree of confidence in the results obtained. The nature of testing hot melt adhesives is such that the tests employed are often comparative and must be performed under standard conditions wherever possible.

There has been a great deal of research on the mechanics of the peel test [127 - 130] and the complex relationships between peel rate, temperature, and adhesive properties can be interpreted in many ways. The simplest analysis (Fig 21) considers the adhesive and adherend to behave in a linearly elastic fashion and does not attempt to describe the additional work that may be required during debonding in order to overcome viscoelastic dissipation in the adhesive. The peel force P is related to the different components of stress experienced by the adhesive during peeling (cleavage σ_0 or shear τ_0 depending upon angle of peeling (ω), the joint geometry (width b, adhesive thickness a) and the moduli of the adhesive in tension E and shear G, *i.e.*

$$P = ab[(K\sigma_0)/((2E)^{½}) + (\tau_0 \cos\omega)/((2G/3)^{½})]^2 (1 - \cos\omega)^{-1} \quad \ldots (29)$$

where K is a complicated function of cleavage stress intensification. In joints where the angle of the peel is 180° then $\sigma_0 >> \tau_0$, K is unity and

$$P = (ab\sigma_0^2)/4E = abW_C/2 \quad \ldots (30)$$

where W_C is the work of deformation per unit volume of adhesive (cleavage stress dominating). Although this simple model may describe peel behaviour adequately for certain systems at fixed rates of peel performed at a constant temperature, it has been widely reported that changes in peel behaviour occur with changes in peel rate or temperature. Generally, there is a rise in peel strength, with peel rate and/or temperature until a maximum value is attained, after which point the peel strength diminishes continuously. This behaviour is similar to the viscoelastic responses shown by polymeric materials and there have been several papers [121, 131, 132] which show that, for certain systems, the time temperature superposition principles involving reduced variables are applicable to peel joints [133]. There is clearly then a strong dependence of the

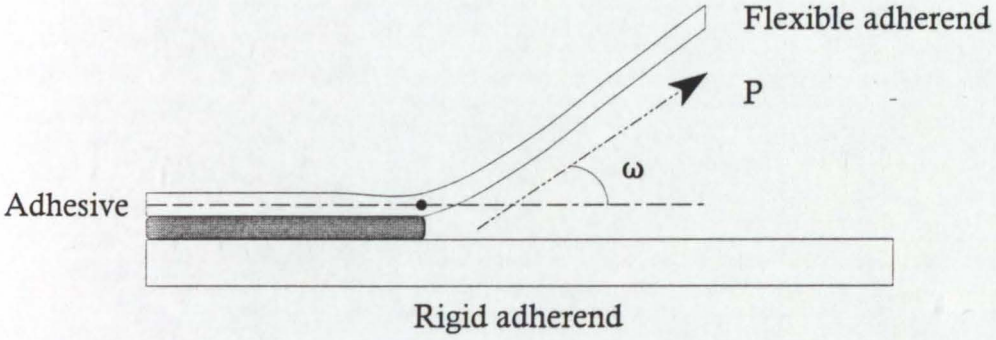

Fig 21. Schematic diagram of a peel test showing the key features required for a simple analysis (adapted from ref. [130]). P = peel force, ω = angle of peel. See text for details.

peel force to the viscoelastic properties of the adhesive.

In addition to the stress analysis approach to peel adhesion, fracture mechanics solutions have also been obtained and it has been reported that the adhesive fracture energy, G_C, is related to peel strength [134 - 138]. Furthermore, the effect on bond strength that the thickness of the adhesive layer has is emphasised. At small values of a, G_C (and hence P) increase rapidly with increasing adhesive thickness, however in thick joints G_C reaches a plateau value and is independent of a. This arrives back at equation (30) with G_C equivalent to W_C. This equivalence has led to the fracture mechanics approach being more widely used [122]. Recent workers [139] have performed detailed linear viscoelastic analyses of peel joints and confirm the influence of crack growth dynamics in peeling. Additional research efforts currently involve finite element analysis and the application of elastico-plastic models to peeling joints, in connection with stress analysis and fracture mechanics approaches.

In considering the viscoelastic nature of an adhesive within a joint, a crude mechanical analogue may be considered [140]. This is illustrated in Fig 22. The symbols represent the phenomenological models associated with different aspects of peeling, OE is original extension of adhesive and backing, HE is the high extension experienced by the adhesive during peeling, F represents irrecoverable fluid flow whilst Ret corresponds with the viscous retardation associated with HE. Although the mathematics were originally presented for 90° peel it has been shown [141] that the analysis may be extended to peel of any angle. The variation of peel force with the rate of peeling was measured and curves were obtained which detailed the transition of bond failure from viscous to glassy (Fig 23). In the force-rate curve there are four distinctive modes of peeling. In region A, separation occurs within the adhesive layer and there is much viscous flow of the adhesive, *i.e.* cohesive failure. Separation at the interface does not occur as there is insufficient stress. Applying the mechanical analogy, this region is equivalent to movement within the dashpot F in Fig 22. As the rate increases the separation becomes adhesive, the failure occurring between the adherend (substrate) and adhesive. The viscoelastic response of the adhesive is now rubbery and the Voigt/Kelvin element of the

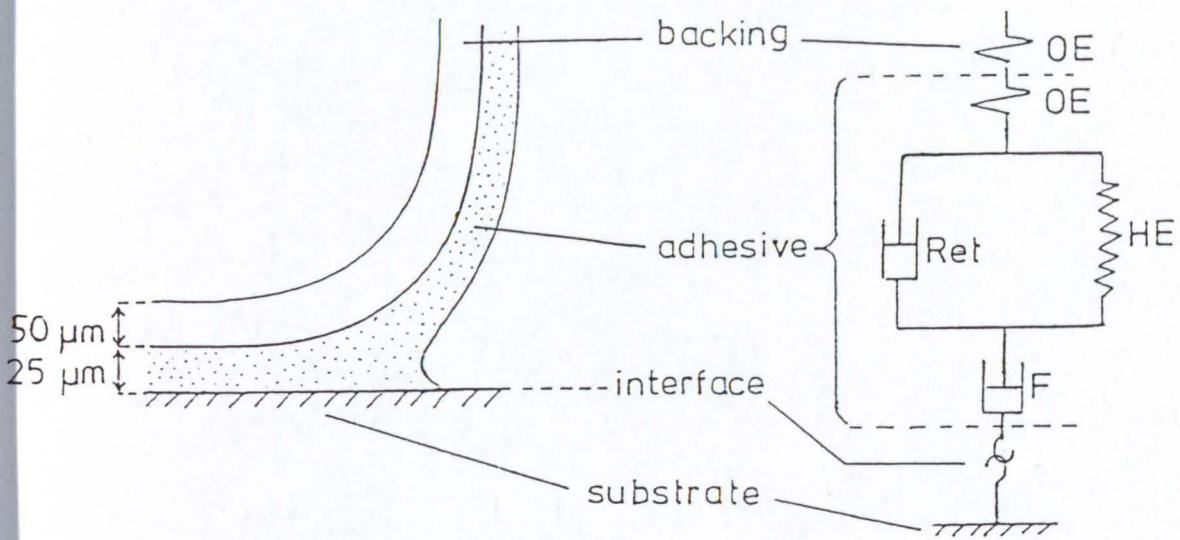

Fig 22. Peeling joint and assumed mechanical analogue (adapted from reference [140]). OE = high modulus spring showing small extensions under load, HE =low modulus spring showing large extensions under load, F = dashpot containing fluid with Newtonian properties, Ret = dashpot containing fluid with Newtonian properties. See text for details.

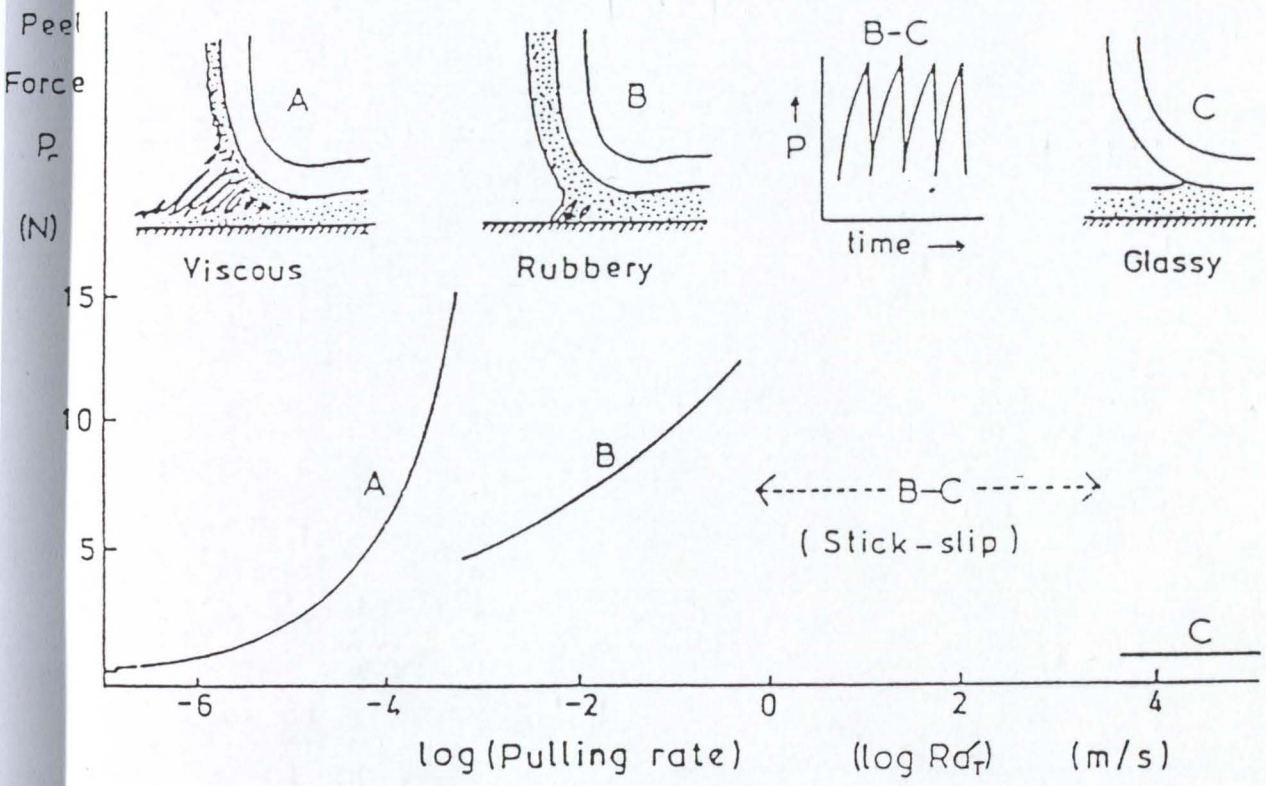

Fig 23. Graph showing dependence of peel force on rate of pulling (adapted from reference [140]). Drawings illustrate the adhesive behaviour of each region: (A) viscous, (B) rubbery, (B/C) "slip-stick", (C) glassy. See text for details.

model (spring and dashpot in parallel) is stretched giving a more shallow slope (region B). Region C represents the situation of a glassy adhesive *i.e.* response at very rapid rates. Here the springs, representing the responses of both backing and polymer, are the only elements of the analogue to respond, the response time of both dashpots being too long. At high rates of peeling thus, the peel force appears to be independent of the peel rate.

The transitory stages between regions A/B and B/C represent shifts from viscous to rubbery, and rubbery to glassy behaviour respectively. In both cases an oscillatory mode of peeling is observed. The response shown in B/C is known as "slip-stick". The mechanism by which slip-stick occurs can be explained by considering energy storage/dissipation [142]. The rate of pulling is assumed constant at an intermediate rate at which slip-stick peeling is occurring. It is assumed that the force of peel has momentarily attained the value for "fast" peeling although the peel mechanism at that instant is "slow", point A, at a rate represented by A' (Fig 24). However, if the tape is pulled faster than this, the force will rise through point B. At this point the elastic energy stored in the unattached backing tape will exceed the value for fast pulling at a steady rate. This excess energy would be sufficient to briefly maintain a rate of peel greater than that of the rate of pulling should the rate of pulling drop below that of B. The corresponding fall in force would drop the peel strength to that obtained with fast peeling *i.e.* Point A. This proceeds until point C, at which time the system is so unstable that the mechanism changes to that of fast peeling. This change will only last until the excess energy stored in the backing is lost. The steady rate of pulling at that point is then unable to sustain the fast mechanism thereby it must revert back to the slow. This continues until the joint is fully broken.

The shear joint is also used extensively in adhesive testing, often as a complement to tests of peel performance. Whereas peel tests tend to yield information on short timescale work functions, such as debonding during unwinding of pressure sensitive tape, shear tests can be performed in order to determine the long timescale behaviour of an adhesive, *e.g.* creep. Shear tests are usually performed at the service temperature of the joint however tests at

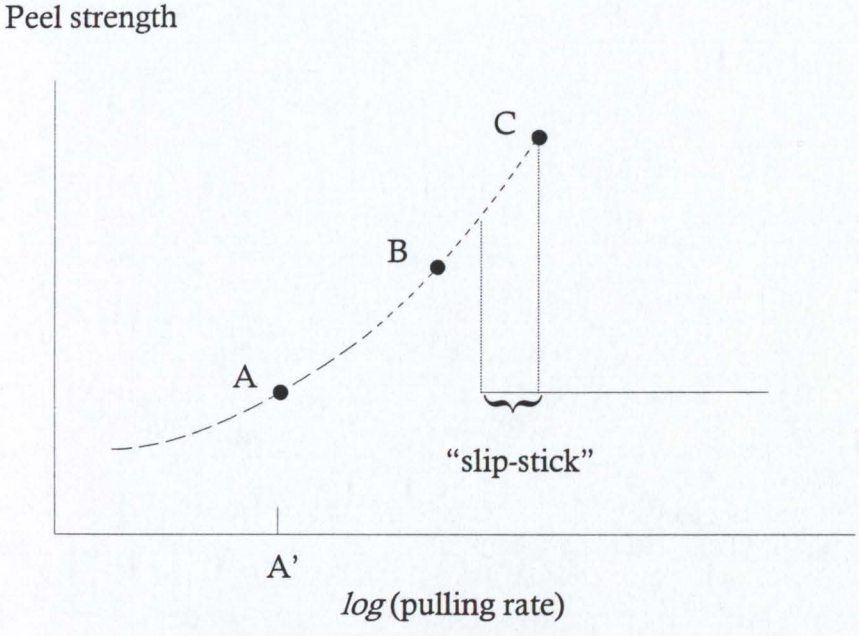

Fig 24. Illustration of the dependence of peel strength and mode of failure on rate of pulling (adapted from reference [142]). Failure mode: viscous (region A) — — — — ; rubbery (region B) ---------- ; "slip-stick" (region B/C); and glassy (region C) ————. See text for details.

elevated temperatures can, in some cases, be used in an attempt to accelerate testing. Similar to the situation with peel tests, there are a large number of commonly used joint geometries that may be employed [143], however for non-structural types of adhesive (such as pressure sensitive or EVA-based hot melt adhesives) lap shear joints (as illustrated in Fig 20b) are usually the preferred arrangement. There are a number of international standards, for example [144], describing methods of test for static lap shear arrangements however all stress the importance of precise bond formation so that the accuracy of any numerical analyses that may be performed is not compromised.

The results of dynamic or static shear tests, of which the latter can take several days to perform, can be expressed in terms of the holding power t of the adhesive which gives an indication of the amount of time elapsed between commencement of the test and bond failure [145]. It can be shown that, for static lap shear joints,

$$t = (L^2 W \eta_0)/2Mga \qquad \ldots (31)$$

where L, W, and a refer to the length, width, and thickness of the adhesive overlap, and Mg is the product of the applied load and the acceleration due to gravity. This term is replaced by F (shear force) in a dynamic shear test. It is seen that t is directly proportional to η_0 which represents a steady flow viscosity of the adhesive under the conditions of the test. It follows that the shear test may, at least to the first approximation, be considered to yield information on the long term rheological properties of the adhesive. This approximation however only holds if certain broad assumptions are made concerning the initial response of the joint to the applied stress (namely that the initial strain is low compared with the ultimate strain at failure) and that equilibrium, steady flow processes do, in fact, occur. Typical behaviours of pressure sensitive adhesives (tested in a dynamic shear test) as described are shown in Fig 25. Figure 25a illustrates an adhesive whose behaviour is described by equation (31) whilst Fig 25b shows a situation where non-Newtonian flow occurs. The rapid drop in force (B) after the initial elastic deformation (E) is indicative of shear breakdown and if this occurs then the holding power is dramatically reduced compared with values predicted by using the above equation.

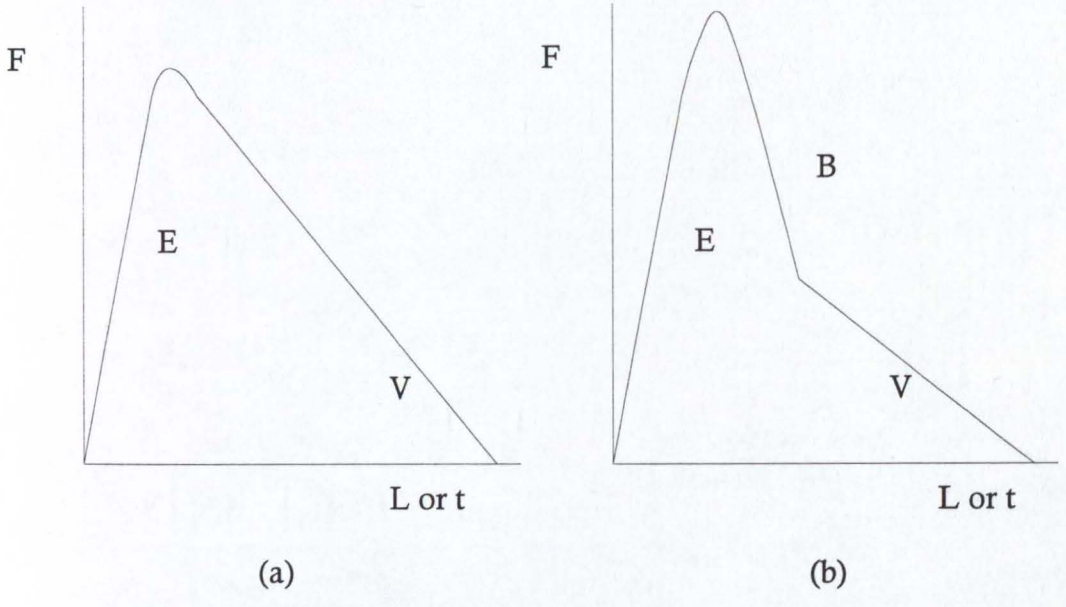

Fig 25. Graphs showing the dependence of shear force F on the length of overlap L, or elapsed time t, for pressure sensitive adhesives in a steady rate of pull (dynamic) lap shear test. (a) no shear breakdown, (b) shear breakdown occurring after initial elastic deformation. E = initial elastic deformation, V = viscous slip, B = rapid drop in force attributable to shear breakdown (adapted from reference [145]). See text for details.

There have been many detailed analyses of shear joints [126]. Superficially they appear much simpler to analyse than complex peel geometries and this is true for certain well defined shear joints (such as torsional shear "napkin ring" joints [146]), however additional complications may arise in lap shear joints due to the development of complex transverse and axial stress distributions attributable to stress concentrations at joint edges, elastic/plastic deformation of the adherends and the development of bending moments within the joint due to the eccentric, off-axis nature of the loading configuration. This last point may manifest itself by deformation of the substrates as shown in Fig 26.

Although the above analyses are useful for structural adhesive applications they cannot fully describe the behaviour of systems comprising EVA-based hot melt adhesives. Hot melt adhesives are typically used in bookbinding or case sealing applications where they may undergo very complex cycles of stress loading and unloading when being transported, stored, and handled. Although shear and peel tests can give an insight into the joints likely strength and mode of failure under certain well-defined states of stress they cannot mimic or reproduce entirely the end use performance of the joints. This is particularly the case with thermoplastic hot melt adhesives whose properties may dramatically vary with changes in service temperature.

Various attempts at developing more relevant tests have been presented, some of which seek not to measure the strength of an adhesive joint but rather the temperature at which the joint can no longer withstand the forces acting upon it. Two of the most common tests are based upon simple shear and peel joints and they measure the shear adhesion failure temperature (SAFT) and peel adhesion failure temperature (PAFT) respectively. Shear and peel joints of closely defined dimensions, utilising suitable substrates, are prepared and loaded. The joints are then heated under controlled heating regimes until the bonds ultimately fail, the temperature of debonding being referred to as the SAFT or PAFT depending upon the geometry being used. Standard methods of testing SAFT and PAFT are available [147, 148] which detail suitable substrates and heating rates. Although these tests again enjoy the benefit of simple analysis, the

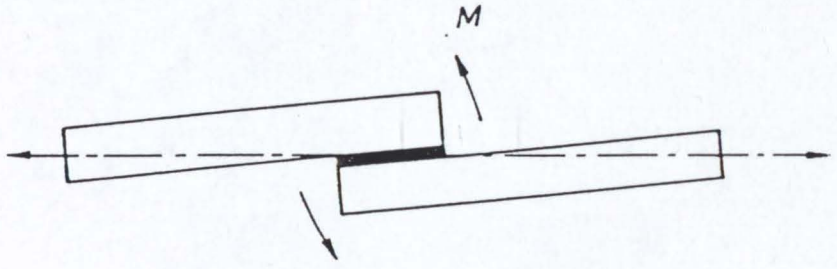

(a)

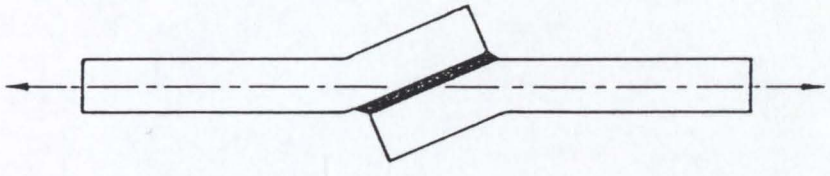

(b)

Fig 26. Schematic representation of (a) undeformed joint showing how eccentricity of the loading path in a single lap joint gives rise to bending moments M in a single lap joint, and (b) deformed joint showing how deformation of the adherends upon loading may reduce the bending moments. Adapted from reference [126].

limitations described above apply equally well when application of the laboratory test results to practical situations is required. These tests give an indication of the adhesives elevated temperature performance (usually called heat resistance or heat fail temperature [2]) and are widely quoted as such (typically by suppliers presenting standardised data on the effect of new adhesive raw materials *e.g.* [149]) although they do not always predict the behaviour of adhesives. For example, the spine of a paperback (called perfect-bound) book may undergo flexural, tensile, torsional, shear and peel-like stress applications during use in conditions which may vary from sub-zero temperatures to very high levels of relative humidity. Standard test methods often fail to account for such differences unless they are extensively modified.

Adhesive manufacturers and their customers usually have non-standard tests, relevant to particular applications, which are used to screen and develop adhesive formulations. The box-flap test [150] for example attempts to mimic the stress situation that exists in a sealed case and there are other published tests which mimic the handling of books and other items. Other test methods are often proprietary and are never published or discussed outside of the organisation that developed the test. The author has experience of several such test methods within his organisation. Although these test methods may be sophisticated and reproducible, the geometries which they employ tend to be complex and do not lend themselves to non-trivial analysis of the scientific principles involved and hence they can only be used on an *ad hoc* basis with little further understanding of the fundamental processes which lead to bond failure.

The open time and setting time of hot melt adhesives are perhaps the most important properties, after ascertaining whether or not the adhesives will adhere to a particular substrate. The open time of an adhesive may be described in many ways but the definition used in the present work is the time from application to the point at which a bond cannot be formed due it becoming non-tacky and thereby unable to wet out a substrate. Similarly, the setting time of an adhesive is hereby defined as the time from application of a second substrate to the adhesive until the point at which the bond can withstand stresses placed

upon it. These need to be considered carefully when formulating new adhesives as these will effectively define the operating window in which the adhesive will run. If the properties of the adhesive do not overlap with the characteristics of the machine on which it is designed to run then it is likely that successful bonding will not be achieved. The determination of these fundamental properties is, however, complicated by the enormous number of factors which can affect them, *e.g.* type, amount and surface area of adhesive, method of application, application temperature, machine speed, ambient conditions, substrate type and conditions, and compression pressure. Although standardised test methods exist, *e.g.* [151], there is still a sufficient lack of correlation between laboratory-determined results and those achieved in practice that they can only be used as a preliminary guide rather than as a reliable index of the adhesives performance. There have been several attempts to overcome the problems experienced with this lack of agreement, many of which require the use of specially designed mechanical bond-testers (of which there are many with differing degrees of sophistication). The simplest designs consist of a means of moving a standard substrate beneath an adhesive dispensing head and then clamping a second substrate onto the first after a preset period [152]. More sophisticated designs can pull bonds apart, determine bond strengths and precisely control adhesive applications at different temperatures onto substrates moving at different speeds [153]. A study using such a mechanical bond-tester [154] demonstrated the degree to which the factors above affect the open and setting times of various adhesives. Although only one factor was changed at a time, and it was acknowledged that a change in application temperature will cause a change in the amount of adhesive deposited (due to the change in viscosity), it was concluded that manual methods of open time and setting time determination are inadequate where relatively small changes in adhesive performance are obtained or expected.

The concept of open time and setting time windows has been explored to some extent using different techniques of open time measuring. It has been reported [155] that the open time can be correlated to a flow index determined by considering flow rates of an adhesive from different diameter nozzles at

different temperatures and pressures, again determined with the use of a mechanical bond-tester. The theory proposed was supported to some extent by a limited number of results, however a fundamental scientific explanation for the concept of an open time was left unexplored. A different approach using dynamic mechanical analysis proposed [156] that certain rheological features may be used to indicate the point at which bonding will not occur. The point initially selected was a combination of factors, namely where the storage modulus G' attains a value of 1×10^5 Pa and the *tan* δ value is at least one. This was thought to represent the point at which the behaviour of the adhesive changes (upon cooling) from that of a viscoelastic liquid to that of a viscoelastic solid.

2.5 Hot melt adhesives

The study of the rheological behaviour of adhesives has been extensive over the past 10 - 15 years, particularly with the advent of sophisticated rheometers and literature is available with particular regard to the rheological measurement of the polymers previously described as being of utility in hot melt adhesive systems.

Hot melt adhesives can be fundamentally divided into those that remain permanently tacky when cool (pressure sensitive adhesives or PSAs) and those that do not. There has been a maintained interest in the morphology, constituents, and viscoelastic properties of the former, but very little fundamental research has been published about the properties of the latter type of adhesive. Both types of hot melt adhesive tend to utilise the same tackifying resins. The primary differences are polymer type, with thermoplastic rubber for PSAs *vs* poly(ethylene-*co*-vinyl acetate) (EVA), and nature of the diluent (paraffinic oil *vs* paraffinic wax, respectively). The fundamental differences between the polymers used in pressure sensitive adhesives, such as styrenic block copolymers, and those in hard setting hot melts, *e.g.* EVA, lies in the former's ability to form physical crosslinks upon cooling due to the coalescence of the styrene endblocks into domains (Fig 27), an effect not seen with the vinyl acetate functional groups in EVA.

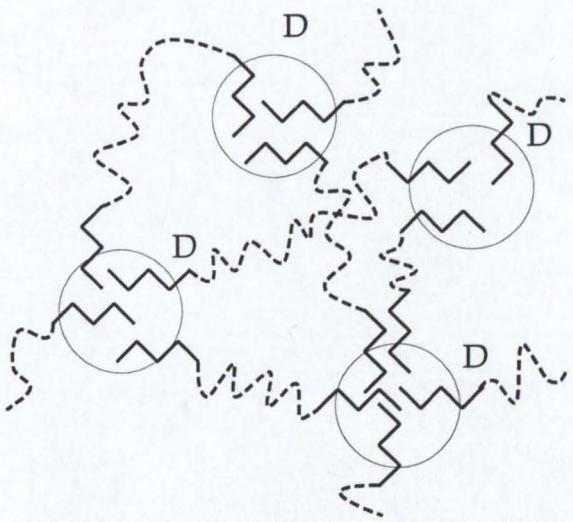

Fig 27. The formation of physical crosslinks in styrenic block copolymer rubbers due to the coalescence of polystyrene into domains D. Key: Styrene endblocks ———— , poly(butadiene) or poly(isoprene) rubber midblocks ---------- .

The viscoelastic properties of hot melt adhesives based upon styrenic block copolymers have been widely studied (Table 3) and there have been many attempts to relate these properties to adhesive characteristics such as tack and, to some extent, adhesive morphology. The latter point was originally thought [157 - 159] to be due to the development of separate phases within a mixture of rubber and resin. The tack of natural and synthetic rubber systems was found to increase to a maximum with increased amounts of tackifying resin which was attributed to the development of a two-phase system in which the mutual solubility of rubber and resin alter with resin concentration. It was proposed that up to resin concentrations of approximately 40%, that the resin was completely soluble in the rubber thereby only raising the tack of the system slightly. As the resin concentration exceeded 40% the tack rose rapidly to a maximum due to saturation of the rubber with resin and the formation of a disperse second phase consisting of resin with low molecular weight rubber dissolved into it. This phase had a lower viscosity than the saturated rubber/resin phase and therefore contributed to a greater efficiency at wetting the substrate *i.e.* it gave a greater bond area for a given bond application time. The tack rose rapidly with concentration until it reached a maximum, which corresponded to the maximum amount of low molecular weight rubber that could be dissolved. Further additions of resin resulted in a change of phase morphology, with the resinous phase becoming continuous and the original rubber/resin phase becoming dispersed. This led to a very dramatic fall in tack as the adhesive was now brittle and glass-like. The presence of two phases was confirmed by electron microscopy [160, 161].

The limited compatibility theory has flaws however, and it is impossible to reconcile the variation in tack levels that are observed when adhesive systems are tested at different speeds by considering this theory alone. Work performed on rubber/resin blends [132, 162, 163], in which it was demonstrated that changes in tack levels and the strength and failure mode in peel tests were related to the viscoelastic properties of the adhesive system, was utilised [164] to show that the effect of the tackifying resin is to bring the viscoelastic properties of the rubber to a state that is more suitable for the bonding and debonding processes

Table 3 Key systems investigated in relation to pressure sensitive hot melt adhesives

Polymer system	Other components	Key points	Ref.
Natural & synthetic rubber	Rosin ester	Mutual solubility of rubber and resin. Two phases postulated	157 - 159
Natural rubber	Rosin ester	Electron microscopy. Two phase morphology observed	160, 161
Natural rubber	Rosin ester, polyterpenes, C_5 hydrocarbon resins	Challenges limited compatibility theory. Concept of resin modifying rubber properties so as to favour bonding/debonding	164
Natural rubber, styrene butadiene rubber	poly(styrene), poly(vinyl cyclohexane), poly (*tert*-butylstyrene)	Resin compatibility has very strong effect on pressure sensitive performance. Similar polarities between resin and rubber aid compatibility	165
Natural rubber, styrene butadiene rubber	poly(styrene), poly(vinyl cyclohexane), poly (*tert*-butylstyrene)	M_w affects compatibility, even with resins with similar polarities to rubber	166
Natural rubber, styrene butadiene rubber	Rosin ester, polyterpenes, C_5 hydrocarbon resins, pure monomer resins	Relationships between plateau G' values of adhesive and resin aid simple property prediction for differing rubber/resin ratios	167

that occur during tack and peeling experiments. It was concluded that this effect was independent of the compatibility of the resin in the rubber as long as it was not completely incompatible. Furthermore it was stated that the T_g of the resin had also a critical effect on the viscoelastic properties.

A later systematic study into the viscoelastic properties of rubber-based blends looked into the effects of resin structure, molecular weight, and concentration. In the first paper [165] it was demonstrated that the degree of resin compatibility can be determined by the measurement of viscoelastic properties. Compatible resins cause a definite shift of the *tan* δ peak temperature together with a lowering of the storage modulus G' within the rubbery plateau whilst an incompatible resin has little effect on the *tan* δ peak and acts to increase the plateau storage modulus. A second *tan* δ peak associated with the resin was observed in some cases. It was also theorised that for a resin/rubber system to be compatible then there must be similar degrees of polarity between the adhesive constituents, even for low molecular weight resins. In conclusion the effects of compatibility (reduced plateau G' and shifted *tan* δ) can be related to the requirements for pressure sensitive adhesive behaviour such that compatible resins give pressure sensitives whilst incompatible resins do not. The second paper [166] explores the effects of resin molecular weight in more depth. It was concluded that, for low molecular weight resins, the compatibility depends upon the molecular weight. Evidence is given which suggests that resins with Mw greater than 1 000 show signs of incompatibility even if the polarity of the resins suggest that they should be compatible. Higher molecular weight resins do not depress the rubbery plateau G', nor do they significantly shift the *tan* δ peak temperature. This is consistent with the formation of an amorphous dispersed phase of the incompatible resin. It was concluded that there is a molecular weight above which the compatibility of any resin is not evident, whilst below this weight, compatible behaviour is manifested if polarity considerations are observed. In the final paper of the series [167] the effects of resin concentration on the viscoelastic properties of the rubber/resin system were investigated. A larger number of resin types, compared with the earlier papers (including C_5 hydrocarbon, terpene and rosin esters), were evaluated and it was

shown that the *tan* δ peak temperature (T_g) for compatible systems can be successfully predicted by application of the empirical Fox equation [168]

$$1/T_g = w_1/T_{g1} + w_2/T_{g2} \quad \ldots (32)$$

where w_1, w_2 are the weight fractions of the resin and rubber respectively and the T_gs are the *tan* δ peak temperatures in kelvin. Critical values of the rubbery plateau modulus G_N^0 were identified as the value of G' obtained as *tan* δ reached a minimum. This is significant as it allows the rubbery plateau modulus of the adhesive to be related back to the plateau modulus of the rubber, G_N^{00}, by means of an empirical volume factor expression, thereby allowing prediction of both *tan* δ peak position and G' values in a pressure sensitive adhesive formulation.

The effects of tackifier compatibility on the overall thermo-mechanical properties of the adhesive were incorporated into the concept of a "viscoelastic window" into which it was shown that certain mechanical properties of the adhesive had to fall in order for it to be truly pressure sensitive . The original concept defined the viscoelastic window in terms of the 1-second creep compliance: good pressure sensitive adhesives had to have a compliance greater than 1×10^{-6} cm^2 $dyne^{-1}$ (1×10^{-5} Pa^{-1}). This criterion is named after Dahlquist (see ref. [163]). These ideas were developed further by several authors *e.g.* [169] to encompass a wider range of polymer and resin systems. Analysis of a wide range of commercial adhesive formulations led to an extension of the original viscoelastic window concept so as to include the values of *tan* δ peak temperature, *tan* δ peak value, and G' value at 25°C and/or the temperature at which the adhesive is to be used. Figure 28a illustrates the development of the viscoelastic window concept for pressure sensitive adhesives used for different applications. It should be noted that this information has typically been obtained by analysis of commercial products rather than by fundamental and systematic research into adhesive formulations although there are several papers *e.g.* [170] in a which systematic study was undertaken. This work successfully explored the viscoelastic properties of different polymer/resin combinations and the morphological and adhesive characteristics of formulations made using these techniques as formulation guides albeit only for pressure sensitive HMAs. This in turn allowed simple predictions to be made when formulating so that by

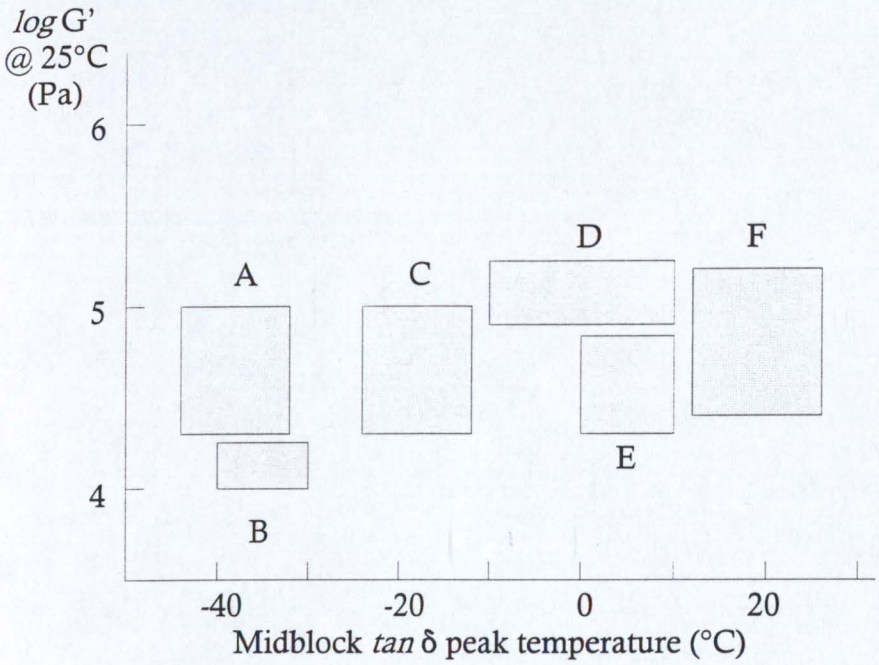

(a)

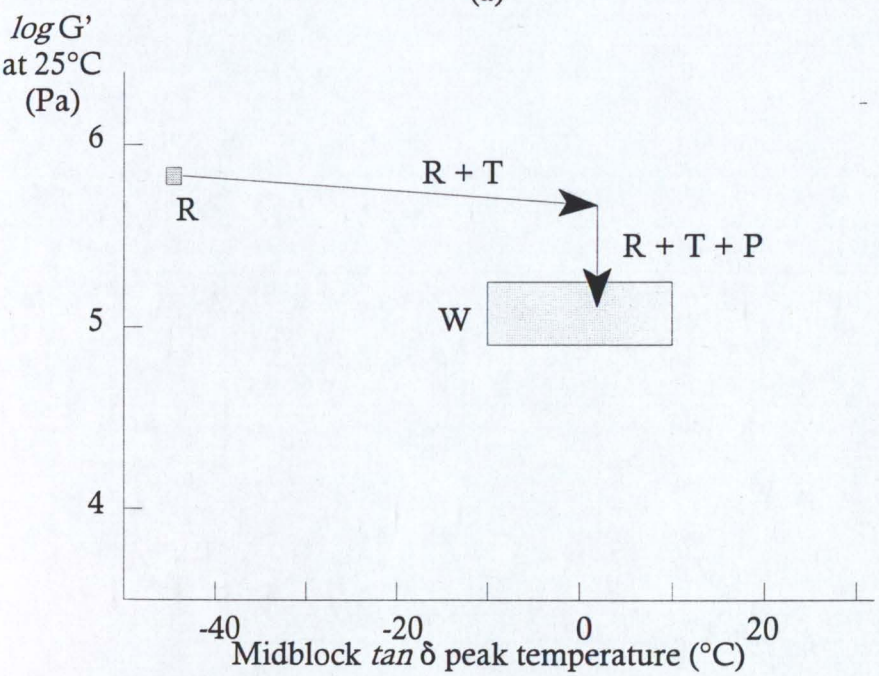

(b)

Fig 28. Viscoelastic windows for pressure sensitive adhesives (adapted from reference [169]). (a) The variation of the viscoelastic window depending upon different end uses for the adhesive. A low peel strength label, B freezer label, C cold temperature label, D general purpose tape, E high peel strength label, and F disposables applications. (b) the effect on the storage modulus of a rubber R when blended with a compatible tackifying resin T and a plasticiser P is to bring the formulation into the viscoelastic window W. See text for details.

judicious addition of tackifying resin and plasticiser (usually mineral oil), adhesives with the desired pressure sensitive properties could be obtained. Figure 28b shows a viscoelastic window for a simple pressure sensitive adhesive, together with the resultant effects on the storage modulus G' caused by the addition of tackifier and plasticiser. The behaviour of the tackifying resin is very much dependant upon its compatibility with the polymer system in question (as seen above). If the resin is compatible then it acts in an anti-plasticising manner such that it raises the glass transition temperature, T_g, of the polymer system, or that part thereof that it is compatible with. If, however the resin is not compatible then it has very little, if any, effect on the T_g but rather acts as an inert filler (albeit a very expensive one).

In a hot melt adhesive, the principle rôles of a wax are to control the viscosity and open/setting time of the formulation [171]. The wax acts as a solvent to the resin/EVA phase and thus reduces the viscosity to manageable levels. Above the melting point of the wax the hot melt adhesive components are mutually soluble in each other [156] and form a continuous phase solution however below the cloudpoint of the adhesive then phase separation of the different components begins to occur. Dependant upon the mutual compatibilities of the adhesive components, four different compositional régimes may exist. Three of these are indicated (Fig 29) for the different types of resin that were examined, however it would be reasonable to expect that there will be cases where compatibilities between the components gives rise to regions of varying concentration. An excellent account of the effects of wax compatibility on the properties of an adhesive formulation [25] provides data to support the claim that crystalline waxes are only compatible with the crystalline portions of the EVA copolymer. As the amount of vinyl acetate concentration increases the amorphous content of the copolymer decreases and therefore a decrease in compatibility is recorded. It should be noted though, that from the results presented in the literature, the change in cloudpoint due to VA content for a paraffin wax is very small and it is of question whether a change of this magnitude would be reproducibly and significantly detected in a routine cloud point test which is based upon the visual examination of the first observable

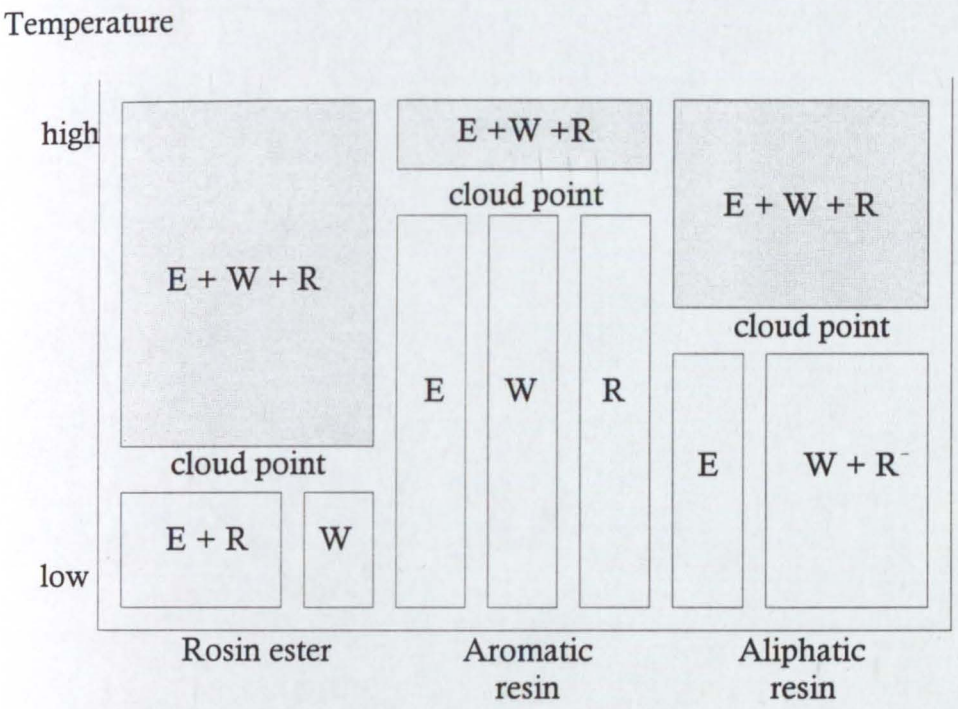

Fig 29. The different phases that can exist in a hard setting hot melt adhesive depending upon the mutual compatibilities of the EVA copolymer E, resin R, and wax W constituents (adapted from reference [156]). See text for details.

turbidity in an adhesive formulation.

The impact of the wax upon the properties of a hot melt adhesive has been discussed in detail by other authors [23] both in terms of molecular weight and structure. Data has been generated to support the arguments that both Mw and degree of branching strongly influence adhesive heat resistance, with increased branching of the wax, at a given molecular weight, leading to reduced high temperature shear performance. Similarly, an increase in molecular weight was found to give an increase in shear until a limiting value of Mw was reached (approximately 800) whereupon the wax showed extensive signs of incompatibility with the EVA/resin solution and the shear strength dropped rapidly. A similar effect was observed with room temperature tensile properties, *i.e.* a gradual increase in tensile strength with increasing molecular weight until incompatibility is observed, followed by a rapid drop in performance. Increasing the amount of branching in the wax reduces the tensile strength and yield strength of the adhesive. The rôle of compatibility of the wax to the thermal properties of the adhesive as determined by DSC analysis was also discussed, with compatible waxes showing a large difference between the onset temperature of adhesive fusion (the point at which the adhesive initially starts to solidify) and the onset of fusion of the wax alone.

There are few papers that utilise a similar approach for the analysis of hard setting, *i.e.* non-pressure sensitive, adhesives. The key papers are shown in Table 4. The first paper to attempt to characterise and predict the properties of hard setting adhesives using rheological techniques [156] was based upon an analysis of commercial formulations used for perfect binding of paperback books and magazines. Although the work served to illustrate the rheological ideas that were proposed, there is little evidence of a far reaching, systematic study on the effects of the constituents contained within the adhesive formulations (which, being commercially sensitive, were not disclosed). Nevertheless, the theories presented on the effects of the compatibilities between the various components of a model system, the physical significance and relationship of certain rheological properties and the simple attempt at pass/fail modelling under a comparative regime are useful and this paper is often quoted in the literature as an initial

Table 4 Key systems investigated in relation to hard setting hot melt adhesives

Polymer system	Other components	Key points	Ref.
EVA	Rosin ester, hydrocarbon resins, pure monomer resins, waxes	Empirical relationships between rheological parameters and commercial formulations	156
EVA	Rosin ester, hydrocarbon resins, synthetic wax	Influence of wax compatibility on adhesive performance - synthetic waxes	25
EVA	Polyterpenes, hydrocarbon resins, waxes	Influence of wax compatibility on adhesive performance - paraffinic waxes	23
EVA	Terpene phenolic resin	Viscoelastic model describing the variation of plateau G' with composition and temperature	172
EVA	Terpene phenolic resin, synthetic wax	Relationship of peel behaviour to viscoelastic properties of the adhesive	88
EVA, ethylene *n*-butyl acrylate (EnBA)	Terpene phenolic resin, liquid rosin ester, microcrystalline wax	Physical model allowing limited prediction of thermomechanical properties	176
EVA	Terpene phenolic resin, synthetic wax	Computation tools to calculate T_g, shear adhesion failure temperature and viscosity from polymer/resin/wax parameters	178
EVA, EnBA	Hydrocarbon resin, liquid hydrocarbon resin,synthetic wax, paraffin wax	Formulation of hot melt adhesives for low temperature applications and the use of statistically designed experiments	179

justification for subsequent analysis.

An attempt to describe the effects of resin concentration on the rheological and adhesive characteristics of simple polymer/resin binary blends [172] related such features as processability and tack to three parameters which were the zero shear viscosity η_0, the limiting instantaneous creep compliance J_E^0, and the terminal relaxation time of the melt τ_0 such that

$$\eta_0 = \lim_{\omega \to 0} G''(\omega)/\omega \qquad \ldots (33)$$

and

$$J_E^0 = \lim_{\omega \to 0} G'(\omega)/(G''(\omega))^2 \qquad \ldots (34)$$

and

$$\tau_0 = \eta_0 J_E^0 \qquad \ldots (35)$$

where ω is the angular frequency at which the rheological properties are determined and $G'(\omega)$, $G''(\omega)$ are frequency dependant shear storage and loss moduli respectively. Elastic properties were determined for the various blends and it was shown that, for the sample of EVA that was used, that the approximation G_X (being the value of the shear modulus when $G' = G''$) can be correlated to a theoretical rubbery plateau modulus (adhesive) G_N^0 by means of

$$G_X = G_N^0 f(P) \qquad \ldots (36)$$

where f(P) is a function of the polydispersity ratio of the EVA.

This paper also made use of time-temperature superposition as represented by the Williams-Landel-Ferry (WLF) equation [173]. The WLF equation facilitates the construction of master curves whereby frequency scans at different temperatures (or *vice versa*) can be reduced by means of a shift factor a_T to a reference temperature T_R. The factor a_T can be taken as the ratio between the viscosity $\eta(T)$ at any temperature and the viscosity $\eta(T_R)$ at the reference temperature. This leads to the WLF equation in the form

$$log\,[\eta(T)/\eta(T_R)] = log\,a_T = (-C_1(T - T_R))/(C_2 + (T - T_R)) \qquad \ldots (37)$$

where C_1, C_2 are constants whose value is dependant upon the polymer system under consideration. The reference temperature for an amorphous polymer is usually taken to be the glass transition temperature T_g however any suitable reference temperature may be chosen. The WLF equation was developed around a consideration of free volume changes in amorphous materials (which

can be defined as being rheologically simple) and hence, the application of time-temperature superposition principles to crystalline or semi-crystalline polymers (thermorheologically complex materials) where changes in free volume may be affected by other factors, such as crystallisation, cannot easily be undertaken. The transform may be compromised to a degree by the need to include other shift factors to compensate for non-linear changes, *e.g.* in density, whose physical significance is not immediately apparent [50]. If crystalline materials are to be transformed, careful thought must be given to the selection of a reference temperature. In the study considered above, a reference temperature in the melt region was selected (110°C) and the master curve was constructed primarily from data in the melt, or terminal, region. Data from the transition region between rubbery and glassy behaviour (see Fig 15) was also included as it was stated that the small amount of crystallinity present in the EVA sample that they studied (approximately 20%) had little effect on the properties of the polymer/resin blend's transition behaviour. This may be true for the particular system studied but other sources using EVAs from different manufacturers show different levels of crystallinity. For example, earlier work characterising the nature of EVA copolymers [174] showed that the crystallinity is critically dependant upon the mole fraction of the VA in the copolymer. The reference gives values of 12% crystallinity for a 28%VA EVA which rises to approximately 25% with a 14%VA EVA. The assumption that 20% crystallinity is not significant in time-temperature superposition exercises also illustrates the lack of critical analysis of the effect of the thermal history on the sample. Semi-crystalline polymers are extremely sensitive to factors which may effect the rate and degree of crystallisation, *e.g.* temperature, length of time at a given temperature, rate of heating or cooling, and to assume that the rheological data for time-temperature superposition is unaffected by this is flawed. In addition to the concerns about applying such tranformations to semi-crystalline polymers, there is even greater uncertainty about the technique if applied to a formulated adhesive which contains a crystalline wax. Indeed it is well recorded that WLF transforms are not meaningful for crystalline polymer systems due to the necessity of vertically shifting curves on to the master curve as a result of the

density changes that occur as a result of the change in degree of crystallinity [175]. Modelling of the relationship between various moduli and resin concentration was also performed and data was presented that seemed to support the model. A key feature of this work was that the elastic properties studied, *e.g.* creep compliance and plateau modulus, depended solely upon the polymer/resin ratio, in those samples of high resin concentration, and the effects of the ratio on molecular mobility in the blend, whilst viscous parameters, *e.g.* viscosity and relaxation times, were primarily affected by the alteration of the blend's T_g due to the antiplasticisation caused by the compatible resin. These findings are similar to those reported earlier for pressure sensitive adhesives [165 - 167] indicating that the methods of analysis applied extensively to pressure sensitive adhesive formulations may have some applicability to the polymer systems used in hard setting adhesives.

An extension of this work used simple ternary blends of polymer, resin and increasing amounts of a crystalline synthetic wax [88]. The thermal (measured by differential scanning calorimetry) and rheological properties of the adhesive were determined and a successful but limited attempt to relate these to the peel behaviour of adhesive joints was made. The primary conclusions were: (a) that the T_g of the blend was affected only by the resin concentration, and not the wax content;(b) that addition of the resin inhibited the crystallisation of the EVA but addition of the wax promotes it, at a higher temperature; (c) the wax substantially modifies the rheological behaviour of the blend, in particular it causes a shift of G_X to higher temperatures; and (d) the addition of the wax causes a shift in the adhesive behaviour of the formulation from that of a viscoelastic liquid, with no wax present, to that of a viscoelastic solid. The earlier points are consistent with some theories on the compatibility of adhesive components whilst the last point was deduced from measurements of the creep performance of the blends and is used to link wax content to peel strength. As the wax content increases, the peel strength diminishes. It was proposed that viscoelastic liquid-like behaviour at room temperature corresponds quite well to cohesive type failure in a peel test and that the addition of wax causes a tendency to interfacial, *i.e.* predominantly elastic, failure. The observation that peel

strengths generally decrease with addition of the wax was briefly attributed to this increased elastic behaviour (the volume of the adhesive involved in the peel increases thereby reducing the amount of overall work required per unit of adhesive), however morphological and/or concentration gradient effects were not considered.

It has been proposed that the rheological phenomena discussed can be incorporated into a single physical model that can be used to describe the general thermomechanical behaviour of hard setting hot melt adhesives [176]. The shear moduli as functions of temperature and frequency, G(T) and G(ω) respectively, are presented as being linked to the molecular weight and polydispersity of the polymer, the glass transition temperatures of the polymer and resin and a function incorporating the effects of the crystallinity of the wax. Using a range of simple formulations in which the volume fraction of the polymer is varied, the complex modulus G*(ω) and complex creep compliance J*(ω) were calculated and modelled using first monodisperse and then polydisperse polymer analogies [177], initially ignoring the effects of crystallinity. These were broadly successful for binary (polymer/resin) blends but had to be adapted for the cases where the crystalline wax was introduced into the formulation. Some success is claimed with the modelling techniques presented although it is pointed out that, at least for the case where crystallinity is involved, the approach is a phenomenological one due to the rheologically complex nature of the induced crystallinity. The prediction of adhesion and other key adhesive parameters were not included in the model although discussions regarding shear adhesion failure temperature and melt viscosity are briefly mentioned elsewhere [178].

Although the model is shown to have general applicability for a few polymer and resin systems, it is acknowledged that the model can be quite sensitive to small errors in the calculation of the adhesive's T_g and that this can affect the viscoelastic curves that are created by the model. In addition, the influence of different wax types and the effect of the polymer composition are not fully explored. Differences in polymer molecular weight and degree of chain branching are not considered fully and the effects of greater degrees of polymer crystallinity are not mentioned. The understanding and modelling of hard

setting hot melt adhesives is thus at an early stage, and fundamental questions remain unanswered.

2.6 Introduction to the present work and objectives

It is seen from the literature and in many cases from detailed examination of industrial practice that there are several factors that are important in the use of hot melt adhesives: (1) In many cases the properties of the adhesive and also of the hot melt adhesive joints are poorly characterised and frequently standardised simulated tests are used as indices of performance. However these tests, whilst generally of use to industry, are difficult to assess and relate, on a fundamental basis, to the adhesive's properties; (2) There has been considerable interest and need to increase the rate at which hot melt adhesives with enhanced properties and performance characteristics can be developed and introduced; (3) Various sophisticated techniques have recently been introduced which have the potential for the rapid determination of the adhesives fundamental properties, in particular, the viscoelastic properties obtained under various conditions; (4) Limited attempts have been made to identify and relate the complex properties of an adhesive, and an adhesive joint, to the fundamental properties of the adhesive; (5) There are relatively few accurate and systematic determinations of the true properties of hot melt adhesives in terms of their composition and there appears to be no information at all on their relationship to the phase stability, microstructure and properties of the joints; (6) There have been only limited investigations into the structure and fundamental property relationships of dual polymer hot melt adhesive systems, particularly for those that may have industrial relevance; and (7) There is a further need for models of the properties and behaviour of the adhesives and joints in terms of their composition as an aid to predictive design.

Therefore, the major objectives of this work are to: (a) Consider in detail the important factors in the properties of hot melt adhesive compositions and formulate a systematic range of compositions that include present day formulations; (b) Establish, critically, the applicability and reproducibility of methods of assessment of the currently accepted vague industrial test methods;

(c) Determine the thermal and rheological properties of the adhesive formulations over a wide range, using differential scanning calorimetry and the systematic application of controlled stress and controlled strain rheometrical techniques; (d) Determine the properties of adhesive joints by measuring the peel strengths of joints prepared and tested under a controlled and systematic programme of study; and (e) Explore systems of predictive design based upon models of behaviour.

Chapter 3 - Experimental

CHAPTER THREE

EXPERIMENTAL

The chemical composition and properties of the poly(ethylene-*co*-vinyl acetate) copolymers, resin, and wax are first given together with the manufacture of the test specimens. This is followed by a detailed description of the techniques to determine the thermal properties using differential scanning calorimetry, softening point and cloud point, tensile properties, open and setting times, and the rheological properties.

3.1 Materials

A hot melt adhesive containing 45% poly(ethylene-*co*-vinyl acetate) (EVA) copolymer, 45% tackifying resin, 9.5% wax, and 0.5% antioxidant, was used as a standard. Although it is not a commercial formulation, it nevertheless is representative of a composition within the normal range of hot melt adhesives [171]. Copolymers were selected so that the influence of composition, melt flow index, and crystallinity, could be studied. Details of the components are given in Tables 5 - 7 and in Fig 30. It was not possible to obtain copolymers with the full range of properties from one manufacturer. Investigation of the main properties of the polymers from a second manufacturer (Elf Atochem UK Limited, Newbury, Berkshire) compared with those from the first (Exxon Chemical Limited, Fareham, Hampshire), however showed slight differences. These will be considered later in section 4 (Results). The resin (Table 6) is a stabilised glycerol ester of gum rosin acids. It was chosen on the basis of the compatibility that it shows with a broad range of EVA copolymers [17]. The wax had a congealing point (determined by ASTM D938) in the range 65 - 68°C (Table 7).

Analysis of the wax by the present author using a differential scanning calorimeter (DSC) determined the solidification peak of the wax to be at 56.8°C (Fig 30a). Molecular weight distribution data for waxes are usually not

Table 5 Composition and typical properties of poly(ethylene-*co*-vinyl acetate) copolymers[a]

Material designation[b]	Vinyl acetate concentration[c] (%)	Melt flow index (g 10min^{-1})	Tensile strength (MPa)	Elongation (%)	1% secant modulus (MPa)	Shore hardness A	Softening point (°C)	Density at 23°C (g cm^{-3})	Molecular weight (g mol^{-1})			Supplier and grade[d]
									M_n	M_w	M_z	
14/2500NC	14.0 ± 2.0	2 500	0.30	85	-	85	85	-	-	-	-	ExUL
19/150NC	19.0 ± 1.5	155 ± 25	5.15	680	-	86	102	0.90	-	-	-	ExUL
28/7NC	27.0 ± 2.0	7 ± 2	> 20.0	>750	-	82	136	0.90	15 700	51 000	96 900	ExUL
28/25NC	27.5 ± 2.0	25 ± 4	8.25	750	11.70	75	127	0.95	13 600	38 600	70 600	ExUL
28/40NC	27.5 ± 2.0	41 ± 7	5.90	750	11.35	76	110	0.95	11 700	32 500	58 600	ExUL
28/145NC	27.5 ± 2.0	145 ± 20	2.95	500	9.00	69	89	0.95	10 200	26 400	44 900	ExUL
28/400NC	28.0 ± 2.0	400 ± 50	1.95	320	8.15	68	82	0.95	7 670	21 700	37 300	ExUL
28/2500NC	28.0 ± 3.0	2 500	1.35	130	-	50	76	-	6 200	18 300	26 000	ExUL
28/40NC*	28.0 ± 1.0	40 ± 5	11.0	850	-	76	110	0.95	-	-	-	AtEV
28/420NC*	28.0 ± 1.0	420 ± 50	2.50	750	-	62	82	0.95	-	-	-	AtEV
33/400NC*	33.0 ± 1.0	400 ± 50	2.5	900	-	45	80	0.96	-	-	-	AtEV
28/400XL	27.5 ± 2.0	400 ± 50	4.55	870	15.20	-	89	0.96	-	-	-	ExAD
28/2500XL	28.0 ± 3.0	2 500	1.40	90	9.30	-	82	0.95	-	-	-	ExAD
33/400XL	33.0 ± 2.0	400 ± 50	2.25	920	6.90	-	80	0.96	-	-	-	ExAD

(a) Typical properties taken from the manufacturers' literature. VA concentrations determined by IR analysis. Melt flow index, tensile properties, hardness, softening point and density, tested according to ASTM D1238 (190°C, 2.16kg, 20 min), D638, D2240, E28, and D1505 respectively. Molecular weight determined by gas phase chromatography (GPC).
(b) Present coding NC = Non-crystalline, XL = crystalline. Note asterisk (*) indicates supplier is Elf Atochem (see note (d)).
(c) All compositions are in weight percent unless given otherwise.
(d) ExUL, ExAD are from Exxon Chemical Escorene Ultra and Adeva ranges respectively. AtEV is from the Elf Atochem Evatane range.

Table 6 Properties of the resin[a]

Property		Typical values[b]
Softening point, °C (Hercules drop method)		91
		(specification 88-96)
Softening point, °C (Ring and Ball, ASTM E28)		85
Colour (50% resin : toluene), Gardner (ASTM D1544)		3
		(specification 5 max)
Acid number, mg KOH g^{-1}		6
		(specification 10 max)
Density, g cm^{-3}		1.08
Melt viscosity (ASTM D3236), mPa s at	120°C	3 700
	140°C	620
	160°C	170
Relative molecular mass distribution[c],	M_n	690
	M_w	810
	M_z	920

(a) A stabilised glycerol ester of gum rosin acids, supplied by Hercules BV, Middelburg, The Netherlands under the tradename Permalyn 5095.
(b) Supplied by manufacturer.
(c) Determined by size exclusion chromatography.

Table 7 Properties of the wax[a]

Property[b]	Specification	Typical values
Congealing point, °C (ASTM D938)	65-68	67
Penetration (25°C), $^1/_{10}$ mm (ASTM D1321)	13-18	13
Viscosity at 100°C, cS (ASTM D445)	5- 7	6.2
Relative molecular mass[c], M_n (approximate)	-	475

(a) A fully refined paraffinic wax blend, supplied by Astor Stag Ltd, Middlesex under the tradename Okerin 236H.
(b) Supplied by manufacturer. See also Fig 30.
(c) Determined by gas phase chromatography.

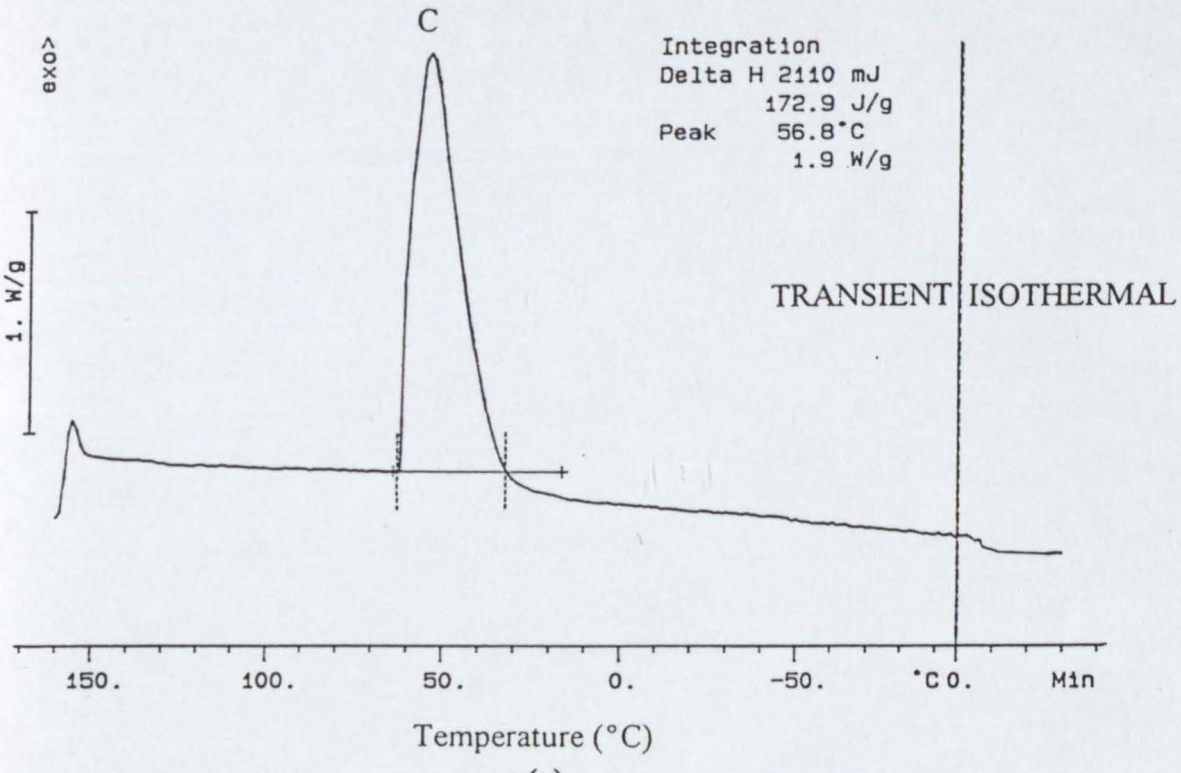

(a)

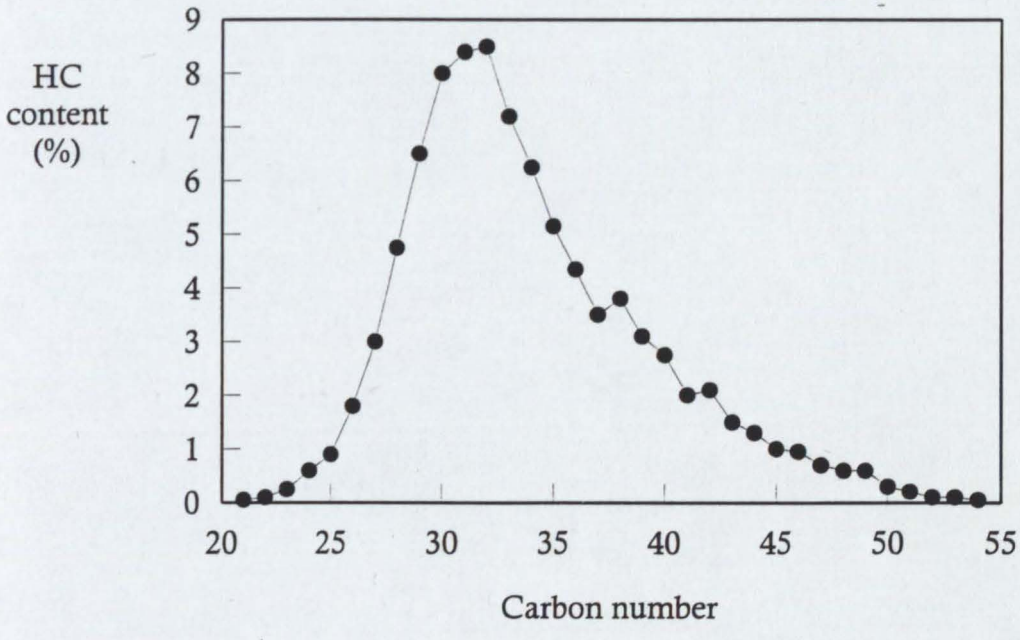

(b)

Fig 30. Typical properties of paraffin wax (Okerin 236H). (a) DSC thermogram showing congealing behaviour C, and (b) typical hydrocarbon content (carbon number distribution). Manufacturer's data, see text.

determined. However, a good indication of the distribution is the carbon number distribution and a typical trace for the wax is shown in Fig 30b. The antioxidant package contained 50% of a primary antioxidant (stearically hindered phenol type) that acts as a free radical scavenger (Ciba Additives, Irganox 1076) and an organophosphite secondary antioxidant (Uniroyal Speciality Chemicals, Polygard HR) which works in conjunction with the primary antioxidant to decompose hydroperoxides. This combination gives synergistic stabilisation at a high level with hot melt adhesives containing rosin based tackifying resin [180].

The adhesives (Table 5) were formulated so that the effects of EVA composition, melt flow index, and crystallinity could be systematically investigated. For identification, a coding has been introduced in Table 5 which reflects these quantities. For example, 28/400XL refers to a sample containing 28% vinyl acetate with a melt flow index of 400, that is crystalline. It is important to note that the notation is used in a dual rôle. In addition to identifying the copolymer, it is also used to identify the adhesive containing the copolymer. In situations where it is not immediately obvious which sample is being discussed, the copolymer sample will be identified by the prefix EVA and the adhesive by ADH.

Small samples of 100 g were prepared as required. The ingredients were weighed to an accuracy of 0.1 g into a 75 mm diameter steel slip-lid can in the order: antioxidant, half the amount of EVA, wax, resin, and finally the remaining half of the polymer. They were mixed using a steel rod and then the can was sealed. After heating for 15 minutes at 180°C in an air-circulating oven (Gallenkamp Oven 300 Plus) the partially molten components were again mixed, by hand, with a steel rod. Heating and mixing was repeated three times, by which time the adhesive was fully molten, smooth and homogeneous. The melt was air cooled in the sealed can and stored until required. Although the effects were not investigated in the present work, other extensive studies have shown, *e.g.* [181] that thermal degradation can occur. However, it was considered that using a small sample and a strict preparation procedure reduced the amount of degradation, and any other variation between the samples, to a

level sufficiently low that they did not influence the present results.

3.2 Differential scanning calorimetry

A Mettler TC11 Thermal Analysis Station with a DSC-30 extended temperature differential scanning calorimeter (DSC) module was used to thermally analyse the EVA polymers and adhesives. The system was fully automated with respect to operation and data collection but required operator input for analysis of the data and presentation of the results. Calibration of the DSC consists of scanning pure substances which have melting/freezing changes in the temperature range of interest. A special program analyses these thermograms and electronically applies corrections to the output to minimise errors. In the present work *n*-octane, analytically pure water, and indium with melting points of -57°C, 0°C and 156.8°C, respectively were used for calibration. The thermal behaviour of the pans used for holding the samples was also measured (prepared and weighed as described later), so that it could be electronically subtracted from the composite thermogram of the sample and pan to give the thermogram of the adhesive. A series of three empty pans were run alongside a reference pan (also empty), and from this an average value of the thermal properties of the pans was calculated and stored in the instrument.

Samples were prepared for testing in the following way. The adhesive (or polymer) was melted in an air-circulating oven for 30 minutes at 180°C and approximately 5 g was smeared onto silicone-coated release paper to form a layer about 2 mm thick. After the sample had cooled naturally in air, a small disc was cut from the sheet using a 5 mm diameter cork borer. An aluminium crucible (and lid) of 40 µl working capacity (supplied by Mettler-Toledo Limited, Leicester) was inserted into the base of a crucible sealing press using stainless steel tweezers, and the assembly (crucible, lid and base) weighed on an analytical balance to ± 0.1 mg. Discs were put in the crucible and the weight of the crucible, lid, base, and sample measured. When the crucible contained 10 - 20 mg of sample, the crucible and lid was crimp sealed and a small hole pierced in the lid to allow gas exchange. Extreme care was taken to avoid any contamination. The empty crucible, cork borer, and sealed crucible were

carefully cleaned with ethyl acetate, and tweezers were used to handle the cleaned crucible. The sealed crucible was then carefully placed on the sample thermopile of the DSC. The reference sample pan was checked to ensure that it was seated correctly and the furnace enclosure was sealed. Nitrogen (white spot, oxygen-free, BOC Limited) was used to continuously purge the furnace at a rate of 5 cm^3 min^{-1}. The thermal cycle consisted of : heating from room temperature to 160°C at a rate of 10°C min^{-1}; equilibrate at 160°C for 3 minutes; cool to -100°C at a rate of -10°C min^{-1}; hold equilibrate at -100°C for 3 minutes; and then heat from -100°C to 160°C at a rate of 10°C min^{-1}. The initial heating to 160°C was to melt the sample, and to ensure that the thermal histories of all the samples were the same.

A series of preliminary experiments had shown that the sample size and rate of heating/cooling significantly affected both the size and temperature of a number of thermal events that were observed during the heating/cooling cycle of an adhesive sample. A simple two level factorial experiment was designed to gain insight into the influence of each variable. A single adhesive sample (28/40NC) was analysed in a series of experiments in which the scanning rate was varied from 1°C min^{-1} to 100°C min^{-1} and the sample weight from 1 mg to 76.3 mg (the maximum capacity of an aluminium crucible). The thermograms of the final heating cycle were analysed in order to determine the melting peak temperature, the enthalpy of melting and any glass transition temperature. The quality of the scans was determined by visual inspection whilst numerical data was analysed by the software package Design Expert (version 3 by Statease Inc, Minneapolis, USA) using ANOVA techniques.

The responses fitted quadratic-type models, with plateaus of little change obtained at sample weights between 15 - 20 mg and scan rates between 10°C min^{-1} and 40°C min^{-1} . Faster scanning rates tended to give distorted traces with considerable loss of detail, which made accurate determination of thermal properties difficult and unreliable. There were also practical difficulties linked to very rapid cooling rates due to the high volumetric flow rate of nitrogen required. This high flow rate occasionally caused the sample pan to become dislodged from the temperature sensing elements within the sample furnace.

This led to sharp discontinuities in the sample trace. Small sample weights, and slow scan rates were plagued by large amounts of instrument noise on the DSC signal. The slower scan rates acted to anneal the samples which made determination of both semi-crystalline (melting) and amorphous (glass transition) features very difficult. It was therefore decided to standardise on sample weights between 10 and 20 mg, with scanning rates of 10°C min^{-1}, as described previously.

A typical adhesive thermogram (cooling) is shown in Fig 31. The ordinate was originally in power (mW) but has been converted to power per unit mass (W g^{-1}). Key features of the curve are labelled A to J. The initial response of the instrument before dynamic heat flow equilibrium is reached is represented by A - B; the baseline corresponding to the melt cooling with no change of phase is B - C; C represents the onset of solidification of the adhesive, typically the wax component. The curve from C - E represents complete crystallisation of the adhesive, D being the congealing peak point of the wax (modified by the presence of copolymer and resin) whilst the tail D - E represents the partial crystallisation of the polymer/resin matrix. The deflection in the baseline E - G is due to the second order glass transition with F representing the midpoint T_g. The curve from G - H corresponds to the continued cooling of the brittle adhesive until H is reached where the program holds the temperature at -100°C for 3 minutes. H - I represents the machine coming to equilibrium whilst I - J is the isothermal portion of the curve. The data was analysed to give the total energy required for the sample to solidify, the peak temperature and the glass transition midpoint (T_g). Similar analyses were performed on the heating thermograms in order to determine energies and temperatures of melting.

There are a number of ways of constructing a baseline to the thermogram. Some of these are shown in Fig 32, together with the values they give when applied to the calibration of the area under a crystallisation peak. It is seen that the difference in the enthalpies is generally small, at worst it is equivalent to 6% of the average value. The spline baselines are very sensitive to the starting and ending points chosen as limits. Figure 33a illustrates the different ΔH values obtained from just small (0.1°C) variations in the limits, whilst Fig 33b illustrates

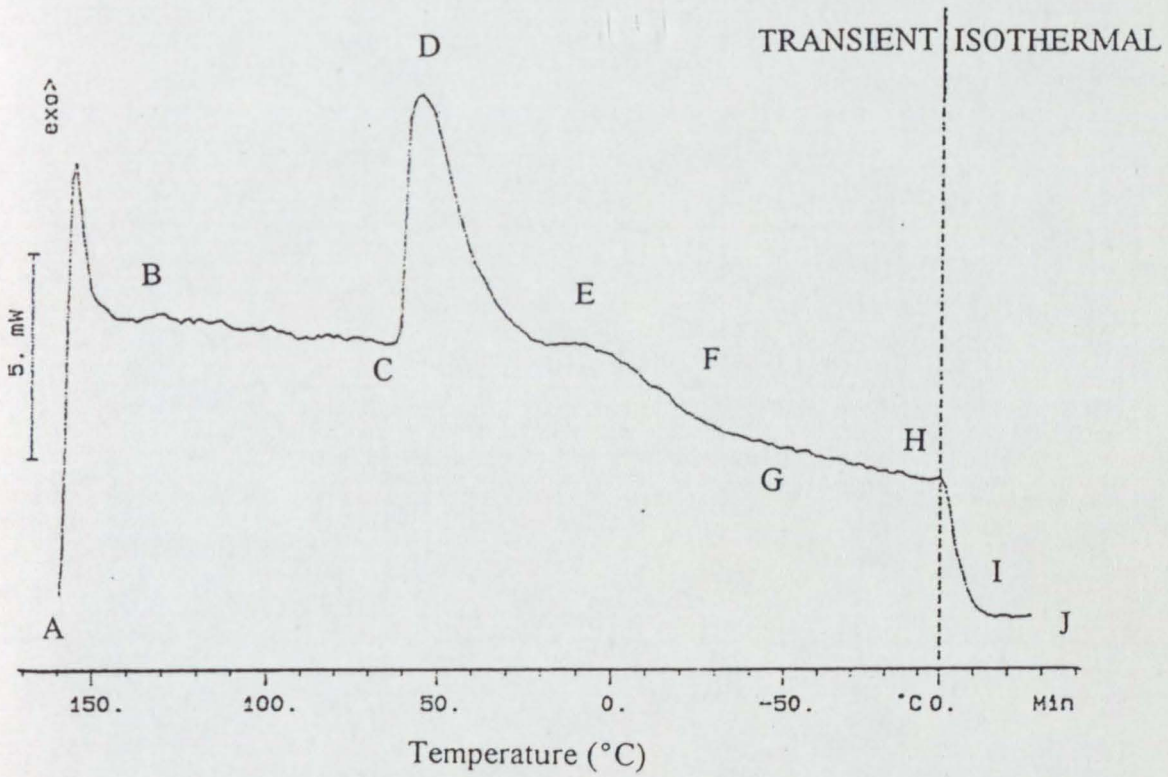

Fig 31. DSC thermogram of ADH 28/40NC showing key features during cooling. Note change of experimental mode from dynamic to isothermal at -100°C. A = initial response, B = equilibrium established, C = adhesive solidification commences, D = congealing peak point of wax, E = crystallisation of polymer/resin, F = Midpoint T_g, G = equilibrium cooling, H = isothermal program commences, I = initial response, and J = isothermal equilibrium established.

ΔH	J g^{-1}
A	31.6
B	29.9
C	30.6

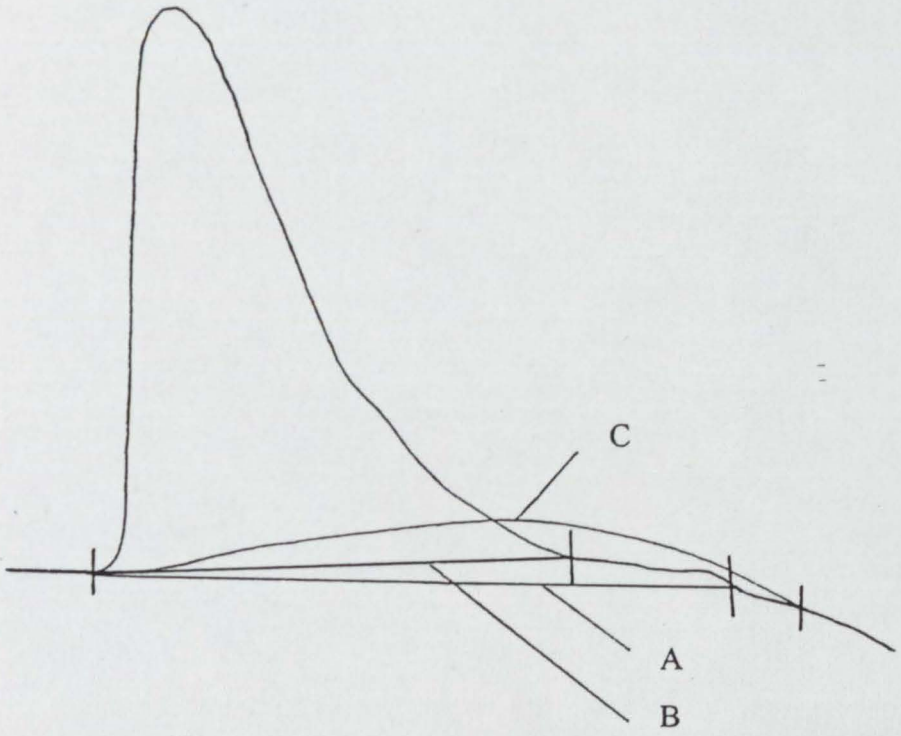

Fig 32. Types of baseline used to calculate the enthalpy changes ΔH from a thermogram. A = tangent of thermal baseline preceding peak, B = point-to-point (horizontal), and C = cubic spline. Note largest difference in ΔH is 1.7 J g^{-1}.

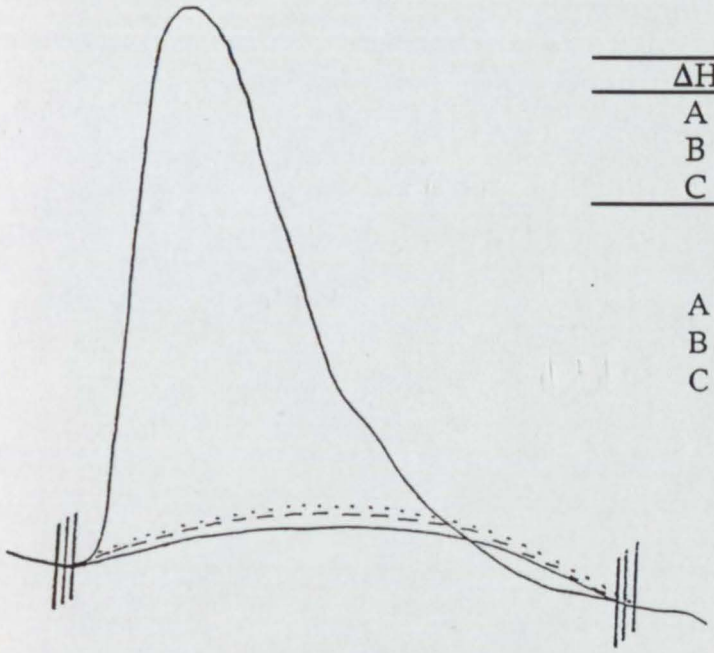

ΔH	J g^{-1}
A	30.6
B	29.1
C	27.4

A ——
B – – –
C . . . . .

(a)

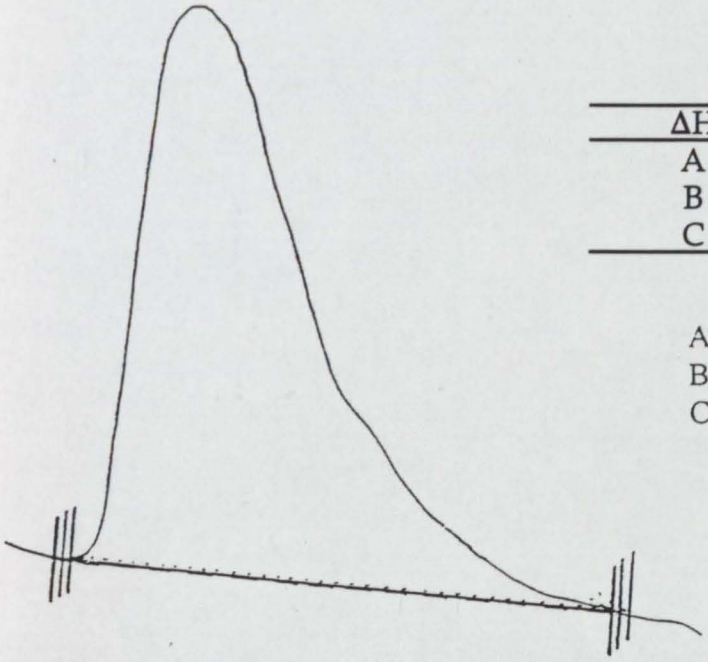

ΔH	J g^{-1}
A	29.8
B	29.5
C	27.4

A ——
B – – –
C . . . . .

(b)

Fig 33. The effect of small variations in the limit determination on the enthalpies calculated from the thermogram (a) with cubic spline baselines, and (b) tangential baselines (see text).

the differences in ΔH obtained by using straight baselines under the same conditions. A horizontal line drawn as an extension of the horizontal baseline preceding the peak (curve A in Fig 32) was used in the present work. Although this is not the most rigorous method [182], it is simple and practical and has been found by the present author to be generally the most useful over many years in analysing the thermograms of complex hot melt adhesives. It also has the advantage of not being as sensitive to absolute start values as some other methods. Two other quantities were routinely obtained from the thermograms. The glass transition temperature was determined by first selecting limits manually on the thermogram, and drawing tangents to the baseline above and below the deflection (E - G in Fig 31). The software then calculated the start, end, middle and inflection points of the transition.

3.3 Softening point and cloud point

The softening point can be defined in several ways. The most common techniques are the "Ring-and-Ball" softening point (ASTM E 2867) and a modification of ASTM D3104 : Standard test method for softening point of pitches (Mettler Softening Point Method), which is the preferred method in this work due to it's high reproducibility and precision. A Mettler FP83 Drop/Softening point apparatus which permitted controlled thermal programming was used to determine the point. Sample preparation consisted of heating the adhesive at 180°C for 30 minutes, and then gently pouring the molten adhesive into a sample cup (6.35 mm orifice) that stood on silicone release paper, ensuring that there was a slight excess and no bubbles present. After cooling, any excess adhesive was removed from the side of the cup and the solidified adhesive cut flush with the top of the cup with a heated knife. The cartridge assembly (containing the cup with adhesive) was then inserted into the sample furnace which had been stabilised at 50°C for at least 1 minute. After a further 30 seconds, the assembly was heated at a rate of 2°C min^{-1} until at some temperature (which was recorded), the adhesive flowed through the orifice and interrupted a light beam which automatically switched off the furnace and the assembly cooled. The sample cartridge was immediately removed to check that

the adhesive had truly flowed and the remaining adhesive was removed from the cup. It was found necessary to clean the sample cups by immersing them in hot mineral oil for a period of 30 minutes to ensure all traces of the adhesive were removed. It was also essential to ensure that every trace of the oil was removed prior to using the sample cup again. The reproducibility of the instrument is quoted as being 0.2°C.

Cloud point temperature was measured according to AMS 360-22. The adhesive was first brought to a sufficiently fluid state by heating in an air-circulating oven at 180°C for a maximum period of 30 minutes. A thermometer bulb (certified to ASTM E1) was dipped into the molten hot melt and withdrawn so that the bulb was completely covered. The thermometer was slowly rotated (so that molten adhesive did not drip from the bulb) and the adhesive was closely observed under bright light conditions. The temperature at which noticeable turbidity first occurs was recorded and the procedure repeated twice. The arithmetic mean of the three readings was taken to be the cloud point temperature. A skilled operator can expect to measure the cloud point reproducibly to within 0.5°C.

3.4 Tensile testing

An Instron 4302 tensile testing machine controlled by Instron Series IX Automated Materials Testing System version 4.09a software, was used to determine the tensile behaviour of adhesive samples and peel tests, at speeds of 0.5, 5, 50 and 500 mm min^{-1} at room temperature. A 100 N load cell with a sensitivity of ± 0.1 N was used with test speeds up to 5 mm min^{-1} and a 10 kN load cell with a sensitivity of ± 10 N was used with the higher speeds. The machine was calibrated by means of a 2 kg reference weight. Although this was strictly unnecessary as the machine had electronically-calibrated load cells, it was considered a useful check to ensure that the equipment was working properly.

Specimens of adhesive were cast in silicone rubber moulds. A poly (methyl methacrylate) die (machined to conform with ASTM D638a : Standard test method for tensile properties of plastics) was used to form the silicone rubber

moulds. The adhesive was first brought into a sufficiently fluid state by heating, for a maximum period of 30 minutes, in an air-circulating oven held at 180°C. The silicone moulds were also heated at 180°C for ten minutes. This was to prevent premature cooling of the adhesive when cast into the mould and to reduce the likelihood of large air bubbles occurring within the sample. After removal of the moulds from the oven, a sufficient quantity of molten adhesive was carefully poured into each mould with the aid of a spatula. A slight excess of adhesive was used so that the profile of the molten material was proud of the surface of the mould. Any bubbles that had formed at this stage were pricked by a heated needle until the sample was void-free within the gauge length. A sheet of silicone release paper was placed on top of the mould and a 500 g brass weight was placed onto the paper to ensure that a flat adhesive sample was obtained. The samples were allowed to air-cool to room temperature in the moulds before the weight was removed. Removal of the sample from the mould was facilitated by flexing the mould slightly. Excess adhesive (in the form of flashing) was removed with a hot scalpel (which both cuts and melts the excess away). Extreme care was required at this stage to ensure that the adhesive sample was not cut into, giving an area of stress concentration, so as to prevent premature failure of the sample under load. The test specimens were loosely wrapped in silicone release paper and stored for seven days in a controlled temperature and humidity laboratory at 21°C and 50% relative humidity. Immediately prior to testing, the sample thicknesses were measured and samples that did not conform to the required dimensional requirements were discarded. Test specimens were clamped in the machine by means of pneumatically-operated jaws. The nature of the adhesive samples necessitated the serrated faces of the jaws being protected by thin silicone release paper (50 μm thick). This also required careful adjustment of the air pressure so that sample deformation was kept to a minimum whilst sample slippage was eliminated. After input of the sample data, the testing, results, and calculation of the required parameters was automatic.

A number of test methods and standards exist for determining peel strengths. The present work used British Standard Method of Test for

Adhesives: Part C12, 180° 't' peel test for a flexible-to-flexible assembly (BS 5350: Part C12), but this was extended to include peel strengths at different testing speeds. Making peel test specimens with constant adhesive thickness is a critical and difficult procedure, and there are various ways the joints may be made. The method used in the present work had the advantages of being simple, requiring only small amounts of adhesive and giving satisfactory and reproducible results.

A fully hard 42 μm thick commercial aluminium foil in the as-rolled condition (grade 1201, Star Aluminium Company Limited, Bridgenorth) was used as the substrate. A soft temper was found unsuitable since it deformed during manufacture of the joint. Individual sections of foil (approximately 100 mm by 200 mm) were cleaned of oxidation products and lightly etched in a 10% (volume by volume) solution of Pyroclean 208 (aqueous solution of phosphoric and hydrofluoric acids with a sequestrant and a surfactant, supplied by Brent Chemical International, Iver) for a period of three minutes, washed immediately in hot water (60°C) for 30 seconds, dried with clean, lint-free tissue paper, and stored temporarily between fresh clean tissues. The cleaned foils were bonded within one hour. Tests showed that the cleaned foils did not loose their wettability until after a few days. Peel specimens were cut from aluminium/ adhesive/aluminium laminates made in the following way. A 6 mm-thick butyl rubber smooth mat was clipped on an electric, thermostatically-controlled hot plate and heated to a surface temperature of 120 - 125°C (measured with a digital thermometer) and then covered with a thin sheet of silicone release paper. A cleaned foil sheet was held in place on the surface by a 500 g weight (Fig 34) and 15 - 20 g of adhesive (at 180°C) was very gently poured on the foil and smeared over it with a heated stainless steel K-bar (previously heated to approximately 180°C). Although this technique is routinely used to give constant thickness coatings of inks and water-based adhesives it has not previously been reported as a method for producing hot melt adhesive coatings. Work by the present author showed that it could be used successfully with hot melt adhesives, providing that the adhesives at application were sufficiently fluid and had melt viscosities of the same order of magnitude. The coated foil was removed from the hot plate, and

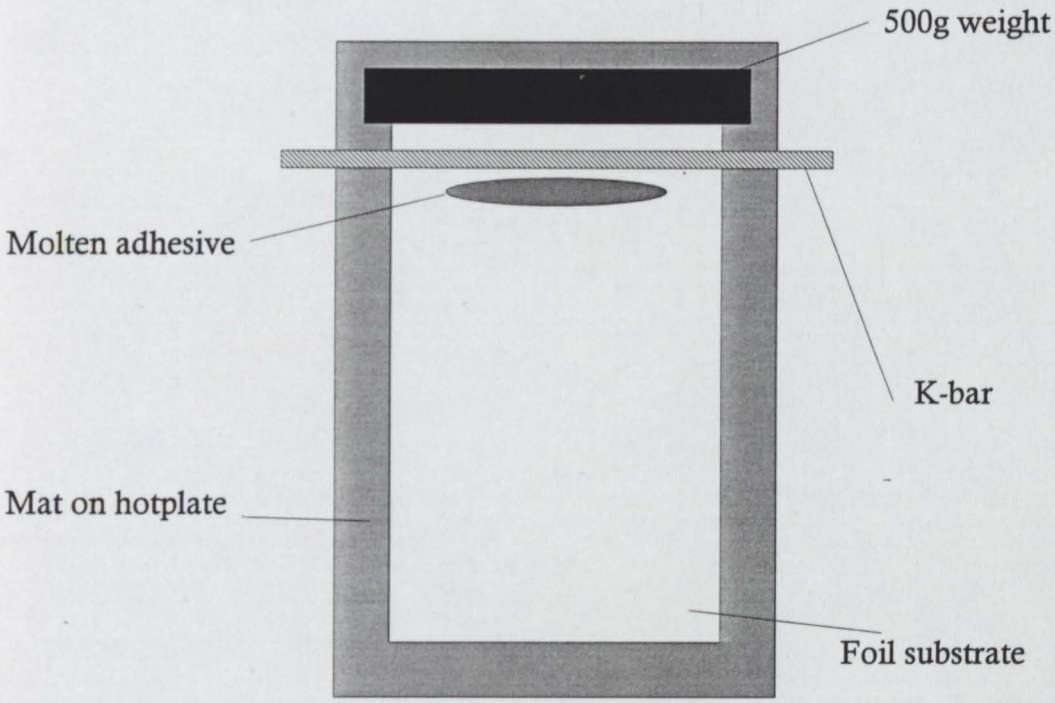

Fig 34. Schematic showing plan view of the arrangement used to prepare peel specimens.

the second (uncoated) foil was heated on the plate for 2 minutes. The coated foil was then carefully placed on the second foil to form a laminate. This was covered with silicone paper and rolled with a 10 kg roller five times in each direction, parallel to the test direction at a speed of approximately 200 mm s^{-1} . The laminate was air-cooled and conditioned (21 ± 2°C, 50 ± 2% RH) for a constant period of 14 days to ensure consistent properties. Strips 25mm wide were carefully cut with a rotary cutter (scalpel cut samples failed prematurely at adventitious nicks), and test pieces were formed by bending the uncoated ends of the laminated strip back at 90°. It was found that by very careful attention to the procedure, satisfactory samples of thickness 40 ± 6 μm could be reliably produced. The average thickness of each specimen was determined from five measurements (digital electronic micrometer). Specimens were clamped using the pneumatic jaws, and the peeling force as a function of grip separation was measured. The type of failure (adhesive, cohesive, mixed-mode or slip-stick) was observed.

3.5 Open time and setting time

The open time and setting time of an adhesive is related intimately to both the properties of the adhesive, and to the method of determination. The present work measured these quantities using a Kanebo bond-tester (manufactured by Kanebo-NSC, Osaka, Japan). The instrument was fully automated and applied the adhesive to corrugated board, formed the board-adhesive-board bond, and tested the bond under precisely controlled conditions. Figure 35 shows the construction and orientation of the bond. Sample preparation consisted of heating 100 g of adhesive in an air-circulating oven (at 180°C) for 30 minutes. The molten adhesive was transferred to the heated glue tank on the bond-tester and the electronic thermostat was adjusted to hold the adhesive at the application temperature (160°C). It was necessary to carefully flush the apparatus through with the molten adhesive to ensure that traces of previous samples were not present. The bond-tester was manually adjusted to give a constant substrate velocity of 30 m s^{-1} and the machine was calibrated (under software control) to give an adhesive bead quantity of 1 g m^{-1}. The

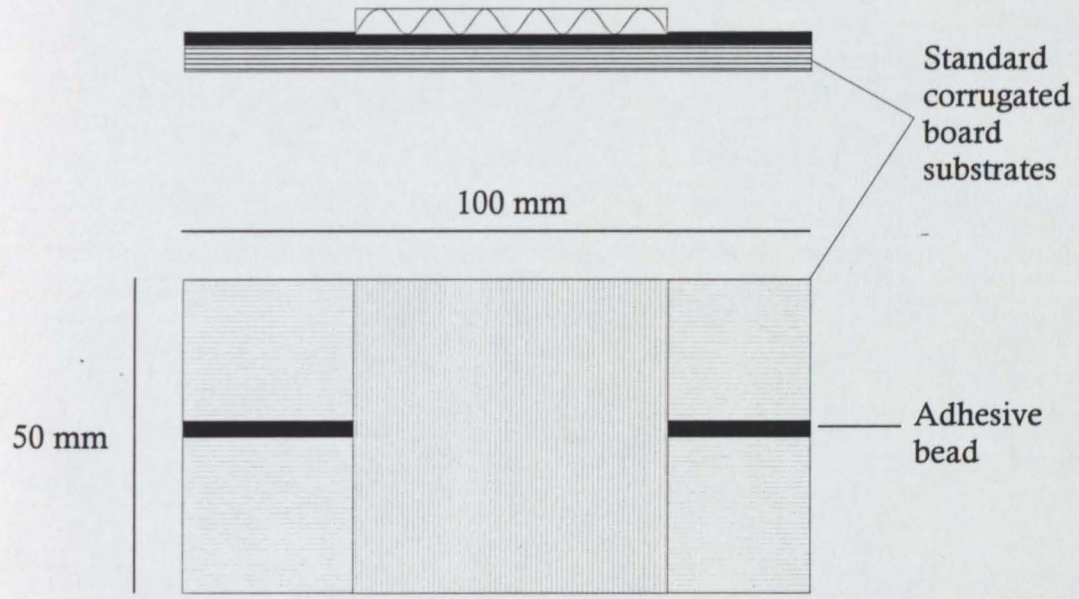

Fig 35. Diagram showing the construction and orientation of bonds used in open time and setting time determination. Note crossed flutes in corrugated board.

compression pressure was adjusted to give a load of 1 kg over the area of the upper substrate (50 mm × 50 mm).

Open time and setting time measurements were both performed using the same machine settings. Standard corrugated board (100% recycled fibre, 4 mm corrugate, supplied by Munksjö Kraftemballage AB, Norrköping, Sweden) was used as substrate material and was conditioned under controlled conditions (21 ± 2°C; 50 ± 2% RH) for a minimum period of three days prior to testing. Only sufficient board that was required for each test was removed from the conditioning room. At the start of each test, the temperature and relative humidity of the atmosphere around the bond-tester was recorded. The substrates were loaded into the machine and the test was controlled from the attached computer. After the bond was made and compressed, the bond-tester pulled the laminate apart in tension. The substrates were then examined for damage. A widely used measure of adhesive performance, fibre tear, was determined, together with the width of the flattened adhesive bead, and these values were entered into the control computer. Fibre tear describes the amount of fibrous substrate that is retained within the flattened adhesive bead when a bond is torn apart. Often quoted as a percentage, 100% fibre tear represents a well made bond whilst amounts less than 100% indicate either the bond was made after the adhesive's open time had elapsed, or the bond was pulled apart before the adhesive had fully set. The measurement of open time or setting time was performed by the systematic variation of one variable whilst a constant value was assigned to the other. For setting time measurements, the time from adhesive application to bond formation (open time) was set at one second. Open time measurements were made using a compression time of five seconds, unless the adhesive had a setting time longer than this, in which case a compression time of two seconds longer than the measured value was used. The setting time of a sample was determined first.

The interpretation of setting time results was straightforward. The adhesive was judged to be fully set once a fully fibre tearing bond was consistently obtained. Figure 36 shows the printout of an adhesive with a setting time of 5½ seconds. In order to determine the open time of an adhesive it was

Set time (sec)	Hot tack (kg)	R e m a r k s
0.5	2.0	Not enough strength
0.5	2.2	Not enough strength
1.0	2.8	Partial fiber tear
1.0	2.7	Not enough strength
2.0	4.3	Partial fiber tear
2.0	4.7	Partial fiber tear
3.0	3.4	Partial fiber tear
3.0	6.1	Partial fiber tear
4.0	4.0	Partial fiber tear
4.0	4.5	Partial fiber tear
5.0	5.5	Full fiber tear
5.0	6.3	Full fiber tear
5.0	6.3	Partial fiber tear
5.5	7.4	Full fiber tear
5.5	4.2	Full fiber tear
6.0	5.2	Full fiber tear
6.0	5.5	Full fiber tear
7.0	6.0	Full fiber tear
7.0	7.9	Full fiber tear

Fig 36. Kanebo bond-tester printout showing the setting time of an adhesive sample to be 5½ seconds *i.e.* at start of full fibre tear. See text for details.

necessary to consider both the amount of fibre tear obtained and the amount by which the adhesive bead had been compressed. When the adhesive is compressed, the beat is flattened and, providing the adhesive is still sufficiently fluid, it attains a width of, typically, 7 - 8 mm. As the adhesive cools it becomes harder and less easy to compress. Assuming a constant compression pressure this reduction in the compressed bead width relates directly to the adhesives ability to wet out a substrate. The open time of adhesive was therefore considered to be the point at which bead compression and fibre tear start to decrease. Figure 37a shows a sample printout of an adhesive with an open time of 2 seconds. A less clear-cut example is also presented (Fig 37b) where full fibre tear is still evident at bead width of 50% of the original value. In this case the open time is judged to be where the bead flatness becomes 70% of it'soriginal value *i.e.* 3½ seconds.

3.6 Heat resistance tests

The heat resistance of an adhesive, in both shear and peel modes, was determined according to a modification of ASTM D 4498 with elements of FINAT standard test method FTM 8 (Resistance to shear from a standard surface). The shear adhesion failure temperature (SAFT) is used to indicate the resistance of an adhesive to shear failure at elevated temperatures whilst the peel adhesion failure temperature (PAFT) represents resistance to peel failure. Sample preparation was identical for both tests, although the bonding configurations are different.

Adhesive/aluminium foil laminates were prepared as described in section 3.4 (Tensile testing). After the foils had been cleaned and etched, and adhesive had been smeared onto the foil by means of the K-bar, the as-coated foils were allowed to air-cool and were cut into 25 mm wide strips by a rotary cutter. The coated foil strips were then heated singly to 120°C on the butyl rubber mat (in order that the adhesive was reactivated) and laminated onto 100 mm × 50 mm sections of standard corrugated board, as described in section 3.5 (Open time and setting time). A standard FINAT 2 kg rubber roller (available from Buro Mayr, Riemerling, Germany) was used to roll the laminates twice in each

Open time (sec)	Tension peak (kg)	Fiber tear	Bead flatness
0.5	6.1	Full	Full
0.5	5.2	Full	Full
1.0	6.5	Full	Full
1.0	7.3	Full	Full
2.0	6.3	Full	Full
2.0	6.9	Full	Full
3.0	5.1	~75%	70%
3.0	5.2	~75%	70%
4.0	4,8	~25%	Half
4.0	4.8	~50%	Half
5.0	3.0	~25%	Half
5.0	4.0	~25%	Half
6.0	3.7	~25%	Half
7.0	3.0	Slight	Slight

(a)

Open time (sec)	Tension peak (kg)	Fiber tear	Bead flatness
0.5	6.1	Full	Full
1.0	6.2	Full	Full
2.0	8.1	Full	Full
3.0	5.8	Full	Full
3.0	4.2	Full	Full
3.0	6.6	Full	Full
3.5	5.9	Full	70%
3.5	6.7	Full	70%
3.5	5.0	Full	70%
4.0	4.0	Full	70%
4.0	6.3	Full	70%
4.0	4.4	Full	70%
4.0	5.2	Full	70%
4.5	6.1	Full	Half
4.5	4.6	Full	70%
4.5	6.2	~75%	Half
4.5	3.6	Full	70%
5.0	5.0	~75%	Half
5.0	6.8	~75%	Half
6.0	4.6	~75%	Slight

(b)

Fig 37. Kanebo bond-tester printouts for adhesive samples with various open times. (a) 2 seconds, *i.e.* time at which fibre tear starts decreasing, and (b) 3½ seconds, *i.e.* time at which bead is 70% of its original width. See text for details.

direction (parallel to the test direction) at a speed of approximately 200 mm s^{-1} in order that intimate contact was established between the adhesive and both substrates. The test pieces for both SAFT and PAFT tests are illustrated in Fig 38. The board adhesive/foil laminates were allowed to air-cool and were stored for a period of seven days in constant conditions (21 ± 2°C, 50 ± 2% RH) to ensure consistent properties.

For the determination of SAFT, the laminates were suspended in an air-circulating oven at an angle precisely 2° from the vertical. A 500 g weight was suspended from the bottom of each specimen. The oven controller was programmed to raise the air temperature from ambient to 70°C in 20 minutes (2.5°C min^{-1}). Subsequently the oven temperature was increased by 5°C over 1 minute and the temperature held constant for five minutes until failure of the specimen occurred. The average failure temperature for five test laminates was recorded as the SAFT. For PAFT determination the laminates were suspended horizontally in an air-circulating oven. A 100 g weight was fixed to the free end of the coated foil. The oven temperature was raised from ambient to 50°C in 10 minutes (3°C min^{-1}). Subsequently the temperature was raised by 5°C over 1 minute and held constant for five minutes until failure of the specimen occurred. The average failure temperature for five test laminates was recorded as the PAFT.

3.7 Rheological testing

Four kinds of rheological tests were made: (a) apparent melt viscosity of the hot melt adhesives, (b) controlled strain dynamic mechanical analysis in the oscillatory mode, (c) controlled stress dynamic mechanical analysis in the oscillatory mode and (d) controlled stress analysis of creep behaviour.

Apparent melt viscosity of the adhesive samples was determined according to the test method given in ASTM D 3236, using a Viscometers UK ERV-8 digital viscometer, together with a TCU3 proportional-heating thermosel system. Various spindle sizes were used dependant upon the viscosity of the adhesive at the test temperature. Table 8 lists the spindle reference numbers, the corresponding "Brookfield" spindle number, and the viscosity range (as a

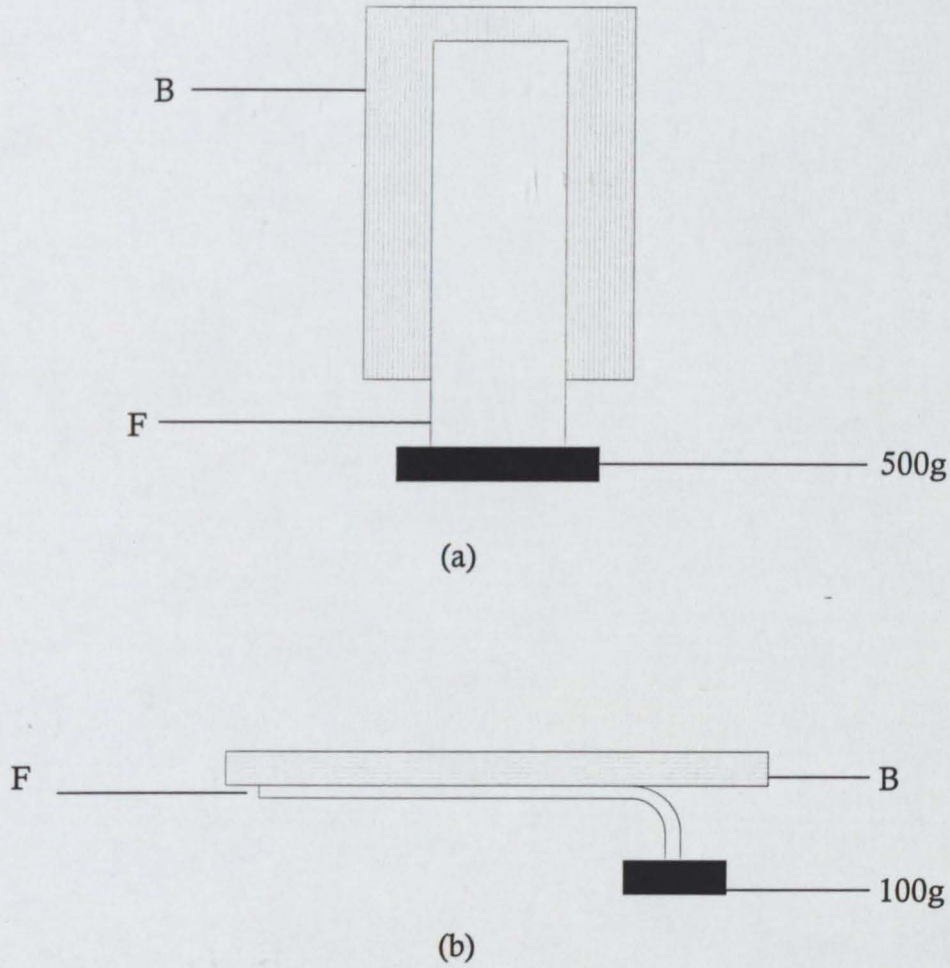

Fig 38. Arrangement of test specimens. (a) shear adhesion failure temperature (SAFT), and (b) peel adhesion failure temperature (PAFT). B = standard corrugated board, F = foil substrate with adhesive coating. See text for details.

Table 8 Viscometer spindles and viscosity ranges

Spindle number[a]		Shear rate[b]	Maximum viscosity (Pa s) at rotational speed (r.p.m.)							
V UK	B	(s^{-1})	0.5	1	2.5	5	10	20	50	100
TR 8	21	0.93N	100	50	20	10	5	2.5	1	0.5
TR 9	27	0.34N	500	250	100	50	25	12.5	5	2.5
TR10	29	0.28N	1 000	500	200	100	50	25	10	5

(a) V UK = Viscometers UK, London; B = Brookfield Instruments, Harlow
(b) N = rotational speed in r.p.m.

function of spindle rotation speeds). The present work used predominantly spindles TR8 and TR9. Sample preparation consisted of melting the adhesive sample for 30 minutes in an air-circulating oven at 180°C followed by filling the sample cell to the correct level. The apparent viscosities were measured at 20°C intervals, increasing from 120°C to 180°C, so that a viscosity profile was obtained for each sample.

It is of critical importance that viscosity measurements are performed in a controlled manner. Hot melt adhesives tend to be slightly shear thinning [183] and this has been observed in the present work. It is, therefore, essential that a suitable period of shearing is allowed before taking a measurement to ensure that a quasi-equilibrium, fully shear-thinned condition has been established. For the majority of samples, a period of 20 minutes shearing was sufficient to reach equilibrium. Five successive scale readings were taken, and if there was still evidence of non-equilibrium behaviour a further 10 minutes of shearing was allowed. The apparent viscosity was an average of at least three successive scale readings.

Although the Viscometers UK ERV-8 is a fully digital instrument, it was still necessary to ensure that the equilibrium scale readings fell between 10% and 90% of the full-scale range. Readings taken outside of these limits are prone to systematic error caused by the non-linearity of the torque spring measurement system used. If the scale reading was not within the desired limits, it was necessary to adjust the spindle and/or speed combination until this was so. The units are considered reproducible to within 1% of full scale deflection *e.g.* within 0.1 Pa s up to 10 Pa s.

Controlled strain rheometry was carried out on a Rheometrics RDS II rheometer using concentric parallel plate geometries. Analysis of data and control of the instrument was performed by Rheometrics RHIOS operating system loaded onto a Compaq i486 computer. The instrument was capable of being cooled to -130°C with liquid nitrogen and heated to temperatures greater than 500°C. The rheometer was programmed to operate in a dynamic mode which permitted fixed frequency oscillations to be carried out during heating from -100°C upwards. The ultimate temperature reached was dependent upon

the experimental geometry employed and the characteristics of the sample.

Samples were prepared for analysis in the following way. The adhesive, or polymer, sample was heated in an air-circulating oven for 30 minutes at 180°C and approximately 10 g was smeared onto silicone release paper to form a layer about 3mm thick. The sample was allowed to air-cool and discs were cut from the layer using cork borers of 5 mm and 12 mm diameters (previously cleaned in ethyl acetate). The discs were then loaded into the rheometer and placed onto the bottom parallel plate. The furnace surrounding the test plates was heated to 160°C to melt the sample and the top plate was lowered onto the molten sample and adjusted to the desired gap size.

The samples were analysed using concentric parallel plates of diameter of either 7.9 mm (for temperature scans from -70°C to about 70°C) or 25 mm (for temperature scans from about 50°C upwards). The gap between the plates was kept as constant as practicable taking such constraints such as normal force development and sample dimensional changes into account. It was considered necessary to check this aspect of the analysis in detail because it has been frequently found that small but significant errors in sample properties can be attributed to differences in stated and actual test geometries. A curve of sample dimensional changes versus temperature is given as Fig 39. The test geometry was selected so as to give a constant stress distribution throughout the sample. Similarly, a small gap size was required so that thermal gradients and induced standing-wave shear patterns were not significant within the sample. Standard texts [184] illustrate the effects of sample thickness and the introduction of thermal gradients.

It was necessary to consider the generation of test protocols for each sample individually due to the differing viscoelastic properties. The first step was the identification of the region of linear viscoelastic response. Strain sweeps at fixed temperatures were performed, in which the rheometer applies an oscillatory sinusoidal waveform to the sample whilst measuring the linear viscoelastic function G' (the elastic, or storage, modulus). The point at which it starts to deviate from linear behaviour is denoted γ_c, the critical strain. This represents the maximum strain that can be applied to the sample during

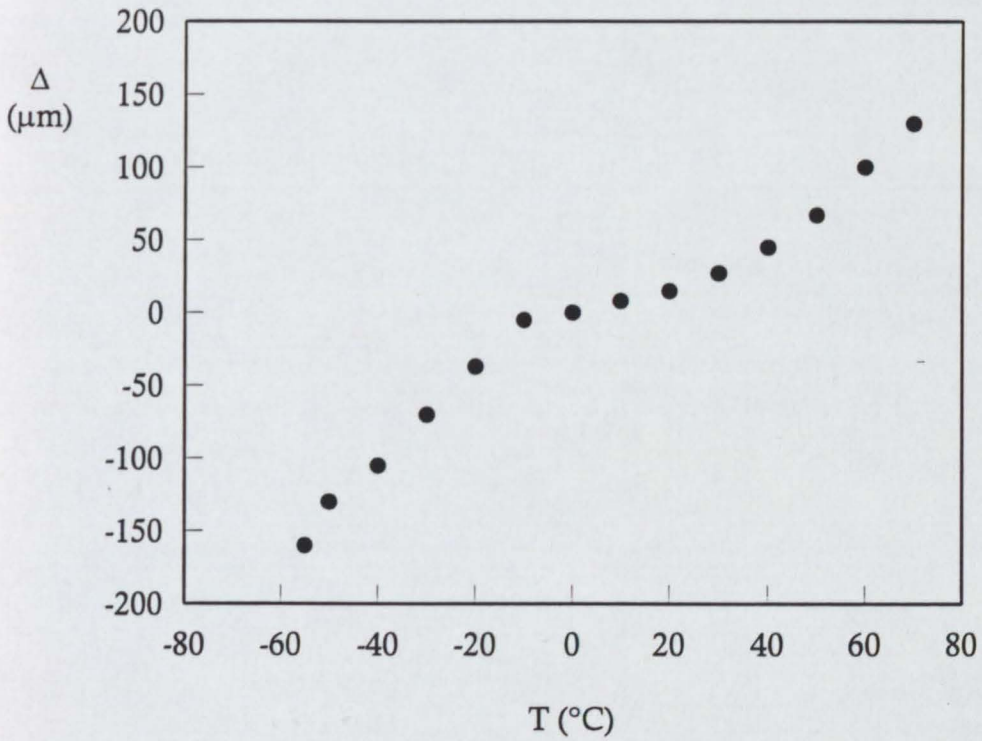

Fig 39. Change in geometry gap Δ as a function of temperature T. Parallel plates of 25 mm diameter. Original gap = 500 μm at 0°C.

subsequent analysis if meaningful linear visco-elastic data is to be obtained. Figure 40 shows the values of γ_c for a particular sample at different temperatures. Having determined γ_c at a number of temperatures it was necessary to construct a temperature sweep protocol that ensured it was not exceeded during the scan and that sufficient strain was applied in order to get reproducible, non-noisy data. Temperature sweeps required careful consideration regarding equilibration times and heating rates. At low temperatures (-100°C to -20°C) it was necessary to allow a considerable period to elapse before measurements at a particular temperature were taken, however this period decreased as the sample temperature increased. The temperature sweep protocols were divided into zones in which suitable values of applied strain and equilibration times could be programmed.

After the correct values for strain and equilibration time had been determined for each sample, temperature sweep scans were performed at a single frequency (ω = 10 rad s^{-1}) from approximately -70°C to 60°C using the smaller diameter parallel plates and from 50°C to approximately 130°C using the 25 mm diameter plates. The resulting rheograms were plotted out on semi-logarithmic scales for the following parameters; storage modulus (G'), loss modulus (G") and *tan* δ (ratio of G"/G'). Figure 41 shows a typical rheogram (sample 28/400NC EVA) with key features labelled A to G for the storage modulus curve, A' to G' for the loss modulus curve and A" to F" for the *tan* δ curve. The G' curve from A to B illustrates the glassy plateau of the specimen with a G' value of approximately 10^8 Pa. The modulus value of this plateau is said to be approximately the same for most carbon-based polymeric materials [8]. From B to D, the specimen passes through it s glass transition temperature and softens appreciably. The glass transition is reflected by the peaks in both the G" curve (at C') and *tan* δ curve C" (signified by T_L). The curve represented by D to E is analogous to the rubbery plateau observed in thermoplastic rubber-based systems however it is significantly shorter and more steeply sloping due to the branched and semi-crystalline nature of EVA. The curve from E to G shows the sharp transition from a viscoelastic solid (G'>G") to a viscoelastic liquid (G">G'). The region from the crossover point F is known as the melt/flow region.

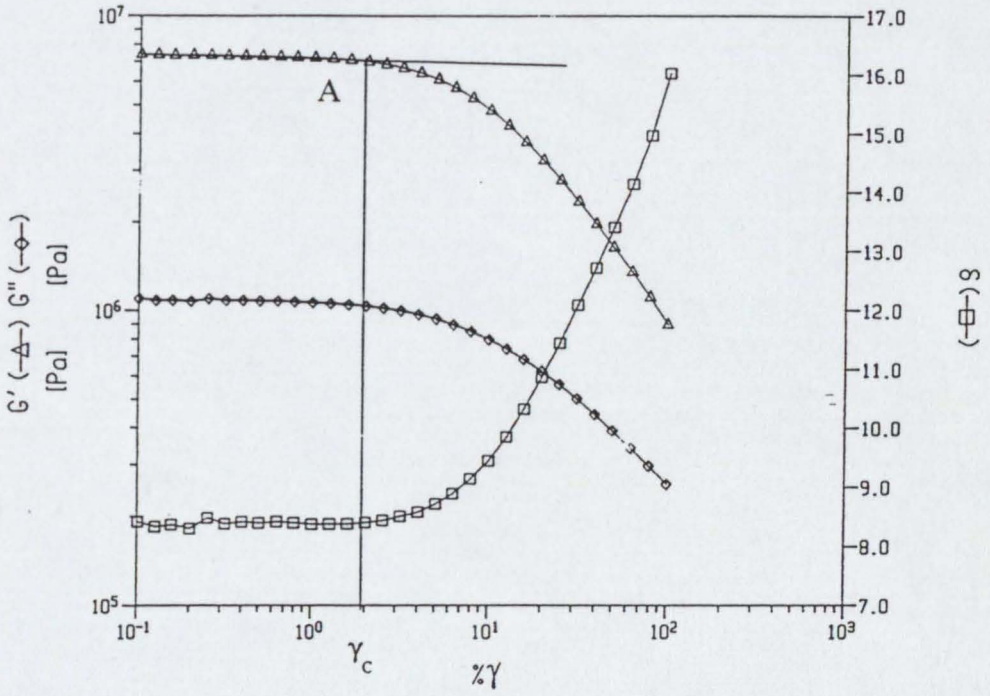

Fig 40. Rheogram illustrating the behaviour of storage modulus G', loss modulus G" and phase angle δ as a function of strain γ. A = the critical strain γ_c at which G', G" and δ deviate from linear viscoelastic behaviour. ADH 28/40NC; 25 mm diameter parallel plates; 40°C.

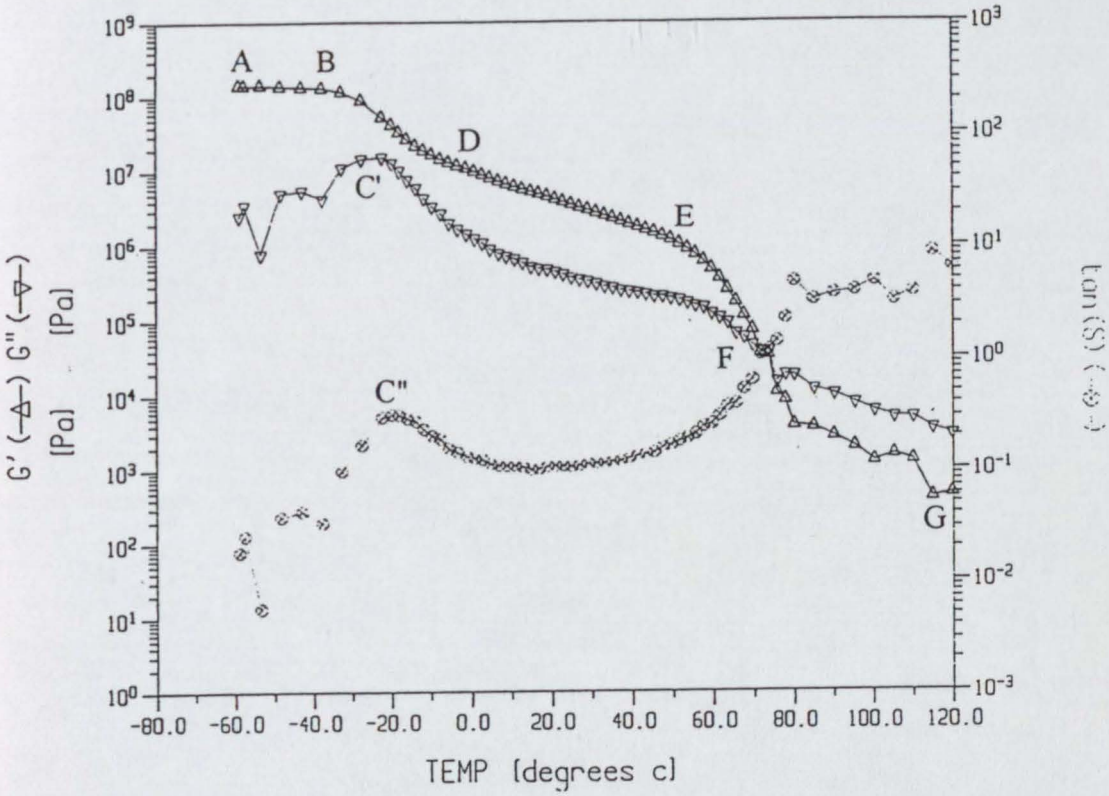

Fig 41. Sample rheogram showing the storage modulus G', loss modulus G" and phase angle δ (*tan* δ) as a function of temperature. EVA 28/400NC; 7.9 mm parallel plates. A - B = glassy plateau, B - D = glass transition region, C" = local maximum in *tan* δ curve at temperature T_L, D - E = rubbery plateau, E - G = transition from viscoelastic solid to viscoelastic liquid, F = crossover point (G' = G" = G_X; *tan* δ = 1) at temperature T_X.

At F, *tan* $\delta = 1$ (F") *i.e.* the phase angle is 45° and G'=G". This is signified T_X.

Controlled stress rheometry was facilitated by the use of a Carrimed CSL² 500 rheometer with control, data logging, and analysis performed by DOS and Windows versions of the Carrimed operating system running on a personal computer. Two geometry systems were found necessary for accurate analytical work over the wide temperature ranges studied in the present work. The geometries were circular parallel plates of 8 mm and 25 mm diameter. The region of linear viscoelastic behaviour was identified in a manner similar to that described above except that the controlled variable was stress and hence the linear viscoelastic region was defined by a critical stress τ_c rather than a critical strain γ_c. The determination of τ_c over a range of temperatures allowed the selection of a suitable oscillatory stress for each sample so that the data collected was within the linear viscoelastic region (LVR) and hence rheologically significant.

Sample preparation was performed by melting the sample at 160°C and placing a sufficient quantity onto the exact centre of the base surface of the CSL²500. The pneumatic ram was then raised to within 1 200 μm of the upper plate. The sample was then cooled to 120°C and held there for a period of three minutes, after which time it was cooled at a rate of -15 °C min^{-1} to -50°C prior to commencement of the test. During the cooling stage, the gap between the parallel plates was reduced, in 50 μm steps, to 1 000 μm which was the final gap used for all testing purposes. The CSL²500 rheometer has a sophisticated servo-mechanism which continuously adjusts the vertical position of the lower parallel plate with respect to the upper plate ensuring that the gap remained constant throughout the whole temperature range. It was necessary to calibrate this mechanism prior to sample testing and this calibration was performed daily throughout the period of study. Once the correct operating parameters had been determined for each sample, the rheometer automatically collated, stored and plotted the data.

Temperature sweeps at a fixed frequency of 10 rad s^{-1} were performed using a heating rate of +5°C min^{-1} and curves similar to that shown in Fig 41 were obtained. It was possible to confirm that readings were within the LVR of

the sample during an experimental run by observing the input and output waveforms generated by the rheometer. Any deviation from a sinusoidal strain signal (in response to a sinusoidal stress input) clearly showed that the critical value of oscillatory stress had been exceeded. These waveforms were stored digitally and allowed checks to be made of each datapoint. Data collected from outside of the LVR was discarded from this study. Low temperature data required the use of the 8 mm diameter plate whilst higher temperature data was obtained using the 25 mm diameter plate. There was substantial overlap in data from both geometries and after an extensive amount of preliminary study, the data given herein is a composite of the two methods. There is considerable justification for such an approach [185] and example data is presented in Fig 42.

In addition to the controlled stress oscillatory measurements, it is also possible to operate the CarriMed CSL^{2}500 rheometer with strain as the controlled variable. Again, a substantial amount of initial work by the present author shows that the agreement between data collected on this instrument when operated in controlled stress or controlled strain modes was well within the limits of experimental accuracy, and consequently, only the controlled stress data is presented herein.

The advantages of a controlled stress rheometer over a controlled strain instrument include the ability to apply small stresses and monitor the resulting small strains, down to 1×10^{-5} rad of angular displacement. This allows the possibility to perform transient creep tests. In order that a creep test be performed in a rheologically significant manner it is important to again operate within the constraints of the LVR which must be determined for each sample at each temperature of test. There are several ways of determining the LVR for the purposes of a creep test. One method is the manual variation of the applied stress until that point at which movement is just discernable to the rheometer's sensing equipment [186, 187]. Another method, employed by workers studying the creep deformation of foams [188], involves the application of a creep stress which is related to the complex modulus of the sample at the test temperature. An initial study was performed to investigate the validity of this approach compared with the former method. It was found that the manual method

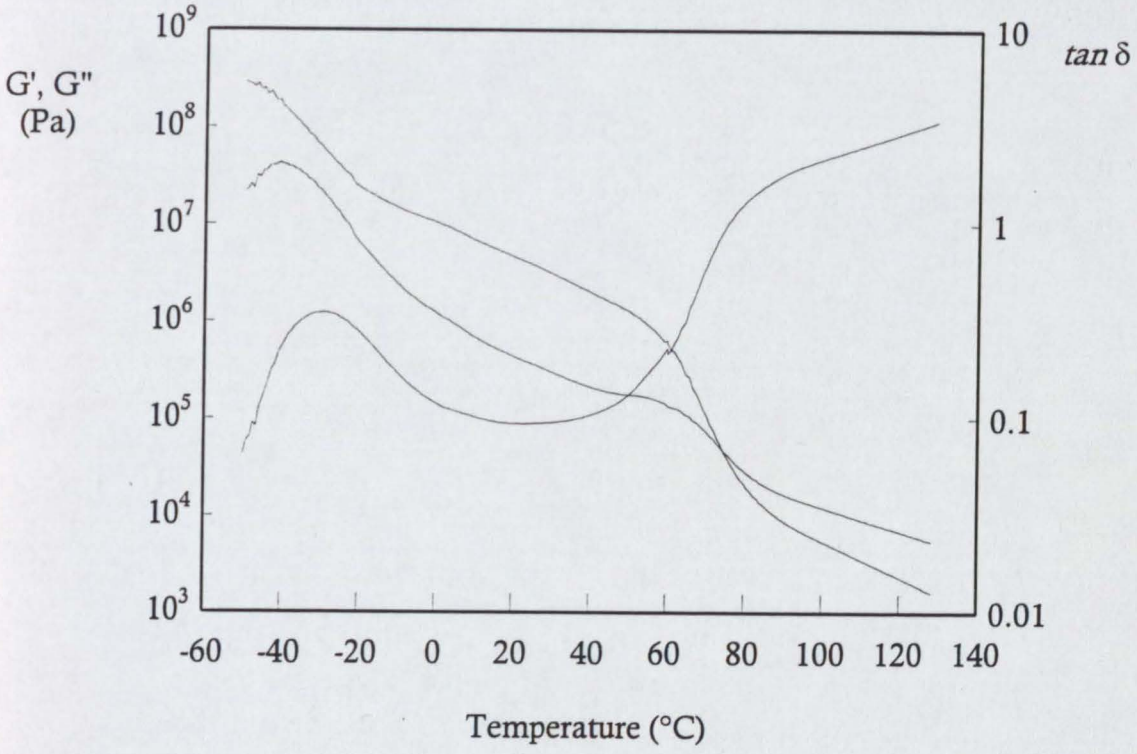

Fig 42. Rheogram showing the storage modulus G', loss modulus G" and phase angle δ (*tan* δ) as a function of temperature T. EVA 28/145NC; 8 mm parallel plate used from -50°C to 60°C; 25 mm diameter parallel plate used from 50°C to 120°C; 1 000 μm gap; 5°C min^{-1} heating rate; controlled stress.

required several attempts at each temperature in order to determine a level of applied stress that gave reproducible, non-noisy data that satisfied the constraints of linear viscoelasticity, *i.e.* the determined property, creep compliance J(t), was independent of applied stress. Due to the crystalline nature of the samples used, it was necessary to reapply a fresh sample after every determination so that annealing of the sample did not occur. This was a very time-consuming process. The alternative method, choosing an applied stress related to the complex modulus G* at the temperature of interest, was investigated by choosing fractional values of the modulus and monitoring the creep compliance at each temperature. Of the samples tested in the initial study (EVA 28/400NC and ADH 28/40NC) it was found that applied stresses of value up to 5% of G* at the test temperature were found to be within the LVR of the samples. To this end, creep tests were performed in the present work with an applied stress equivalent to 1% of the complex modulus at the test temperature to ensure that the LVR was not transgressed.

Data obtained from the creep tests was analysed according to the phenomenological model for creep after Berger (four-parameter model) with the addition of further Voigt/Kelvin units as appropriate. A typical curve (EVA 14/2500NC) obtained during creep testing is illustrated in Fig 43. There is an initial elastic deformation upon application of the stress (A) with a corresponding initial compliance J_0. Note that the creep compliance is simply the ratio strain/applied stress and is a common technique used to normalise curves obtained with different applied stresses. This is immediately followed by the characteristic shaped portion of the curve corresponding to the full extension of Voigt/Kelvin units. In the Berger model (Chapter 2.2, p37) only one Voigt/Kelvin unit was illustrated however additional units may be added in order to fit the data more perfectly. The compliancies and relaxation times of these *i* Voigt/Kelvin units are represented in equation (22) by J_i and τ_i. Point B indicates the point at which all the Voigt/Kelvin units have extended and further deformation is solely by means of viscous flow. This parameter is denoted by the zero shear viscosity η_0. When the applied stress is released at C there is an instantaneous elastic recovery D (denoted by J_r) followed again by

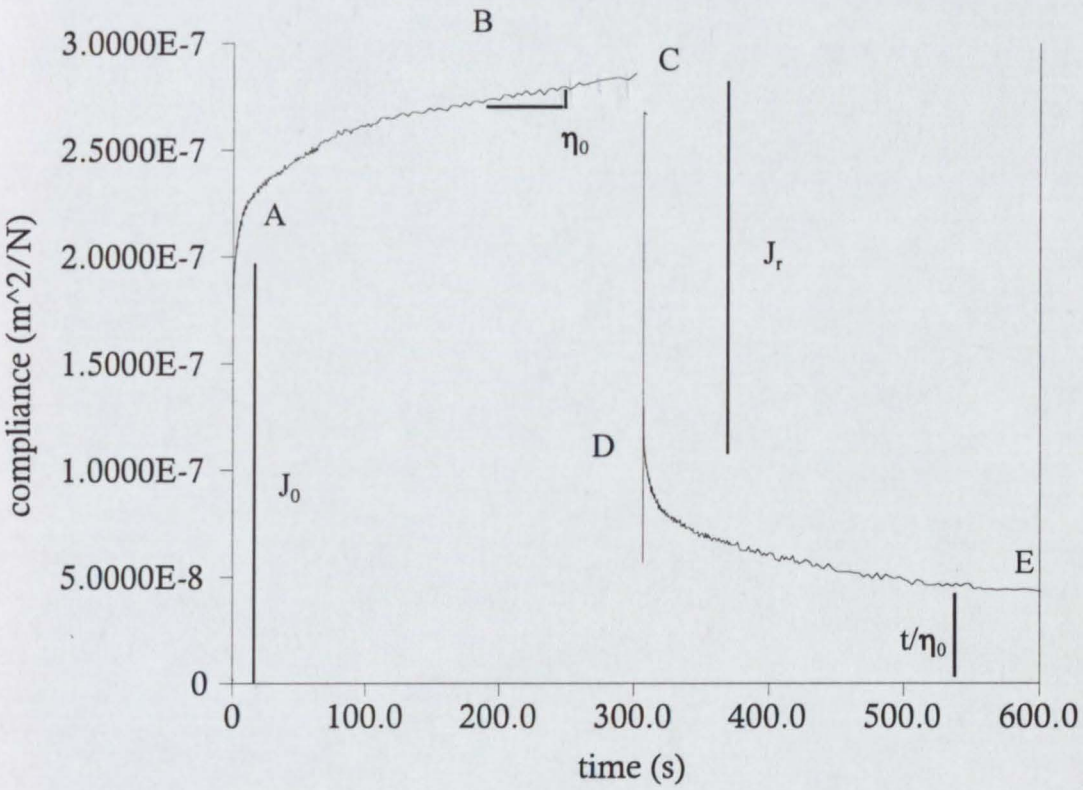

Fig 43. Rheogram illustrating the behaviour of creep compliance J(t) as a function of time t during a creep test. A = initial application of applied stress with the intial compliance indicated by J_0; B = viscous flow indicated by the zero shear viscosity η_0; C = removal of applied stress; D = recoverable compliance J_r; E = permanent deformation given as t/η_0. EVA 14/2500NC; 8 mm parallel plate; 1 000 μm gap; 40°C.

Voigt/Kelvin relaxation until E where the degree of permanent deformation can be calculated from t/η_0. Creep curves for all the polymers and adhesive samples were obtained at 10°C intervals between 20°C and 80°C (120°C for the low MI samples).

Chapter 4 - Results

CHAPTER FOUR

RESULTS

The properties of the adhesive are first given. These are the thermal transitions of the individual components of the adhesive and of the adhesive, softening points, compatibilities, viscosity, and viscoelastic behaviour. Results are then given on the development of the adhesive bond (open times and setting times), the strength of adhesives and adhesive joints (peel tests), and the strength of the adhesive bond at elevated temperatures measured in terms of maximum temperatures that a bond can satisfactorily withstand.

4.1 Thermal transitions in the adhesives and their components

A typical differential scanning calorimeter trace has been given in Fig 31 (p 85), and the information that may be extracted from the curve and its accuracy has been discussed in detail in section 3.2. The main results for the adhesives and for the components of the adhesives are shown in Tables 9 and 10 respectively. Several points should be noted regarding the presentation and nature of these results. In each case the property was determined from a heating and cooling scan, and where neccessary, these will be distinguished by subscripts h and c, *e.g.* ΔH_h and ΔH_c. The enthalpy of the adhesive (Table 6a) is a combination of the enthalpies of the vinyl acetate and of the wax (see Fig 30a, p 80). The glass transition has been taken from the midpoint of the curve (see Fig 31 and associated discussion). Results of the glass transition taken from the inflection on the curve was also determined. They were always within 4°C of the midpoint T_g and are not presented. Each result in Tables 9 and 10 are the average of at least two tests. In the adhesives, the least accurate results were obtained on cooling, and for these the maximum differences observed in any adhesive for the enthalpy, wax peak temperatures, and glass transition were 2.1 $J\ g^{-1}$, 0.6°C, and 3.9°C respectively. For convenience in viewing this large amount of data, the results are also shown as a function of melt index in Fig 44.

Table 9 Transition enthalpies, wax peak temperatures, and glass transitions of various poly(ethylene-*co*-vinyl acetate) adhesives obtained using differential scanning calorimetry[a]

Adhesive	Enthalpy, ΔH ($J\ g^{-1}$)		Wax peak temperature (°C)		Glass transition[b], T_g (°C)	
	Heating	Cooling	Heating	Cooling	Heating	Cooling
14/2500NC	38.5	41.4	71.6	61.7	-10.0	-19.5
19/150NC	40.6	43.3	73.0	57.3	-21.8	-5.4
28/7NC	36.8	36.2	66.9	53.8	-16.5	-13.2
28/25NC	37.4	36.5	66.0	54.6	-19.1	-14.7
28/40NC	35.5	32.7	65.5	56.8	-18.4	-14.4
28/145NC	34.7	31.1	64.7	58.7	-17.9	-11.9
28/400NC	33.7	31.0	64.2	59.3	-19.3	-17.3
28/2500NC	31.1	29.0	63.5	58.4	-19.5	-15.9
28/40NC*	36.9	32.7	66.0	58.9	-22.1	-10.7
28/420NC*	35.4	30.7	62.4	56.4	-27.1	-24.4
33/400NC*	29.4	23.4	60.7	58.2	-21.0	-19.3
28/400XL	35.6	33.1	65.8	59.8	-16.0	-12.8
28/2500XL	29.5	31.8	65.9	59.3	-12.0	-13.3
33/400XL	31.1	28.3	63.3	59.1	-19.0	-17.3

(a) See section 3.2 for typical DSC curves and the definition of and derivation of the properties from the curves. Each value is the average of at least two scans. See text for details.
(b) Midpoint T_g.

Table 10 Transition enthalpies, wax peak temperatures, and glass transitions of the components in various poly(ethylene-*co*-vinyl acetate) adhesives obtained using differential scanning calorimetry[a]

Adhesive components	Enthalpy, ΔH ($J\ g^{-1}$)		Temperature of melting/crystallisation (°C)		Glass transition[b], T_g (°C)	
	Heating	Cooling	Heating	Cooling	Heating	Cooling
14/2500NC	67.9	50.6	79.8	57.8	-26.9	-34.9
19/150NC	65.8	51.7	77.5	58.4	-27.0	-35.0
28/7NC	54.6	39.0	74.1	48.3	-26.4	-38.0
28/25NC	54.4	44.6	73.7	47.3	-26.5	-38.1
28/40NC	54.7	47.1	72.6	46.4	-26.5	-37.7
28/145NC	53.7	49.9	66.7	44.7	-27.8	-35.8
28/400NC	53.1	51.7	62.6	43.3	-26.5	-35.3
28/2500NC	49.1	55.0	60.3	42.1	-26.6	-44.3
28/40NC*	57.9	54.9	74.7	47.4	-26.3	-35.8
28/420NC*	55.6	53.7	65.6	45.6	-26.7	-32.0
33/400NC*	46.8	46.3	56.7	40.2	-26.3	-40.3
28/400XL	54.0	52.6	63.0	44.4	-26.7	-32.6
28/2500XL	50.4	56.8	61.0	43.8	-25.7	-36.0
33/400XL	45.1	58.7	60.3	39.5	-25.6	-37.1
Resin	ND[c]	ND	ND	ND	37.5	30.9
Wax	190.1	172.9	65.7	56.8	ND	ND

(a) See section 3.2 for typical DSC curves and the definition of and derivation of the properties from the curves. Each value is the average of at least two scans. See text for details.
(b) Midpoint T_g.
(c) ND = Not detected.

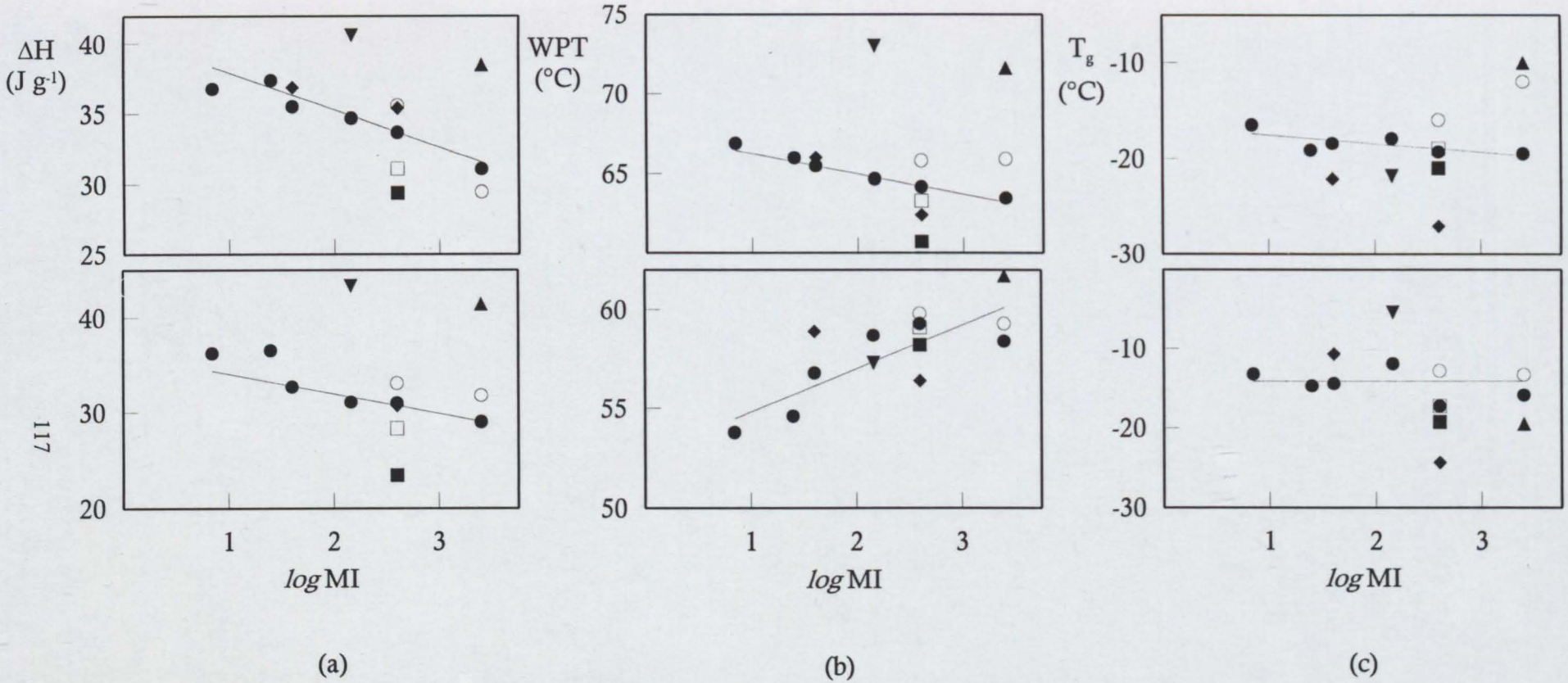

Fig 44. (a) Transition enthalpies ΔH, (b) wax peak temperature WPT, and (c) glass transition T_g on heating (h) and cooling (c) of various adhesives as a function of the logarithm of the melt index MI. See Table 9. The full line is the regression on the 28% VA results. Symbols: ▲ 14% VA; ▼ 19% VA; ● 28% VA;○ 28% VA XL; ■ 33% VA; □ 33% VA XL; ◆ 28% VA* (AtEV).

It is emphasised that the logarithmic function is used simply because of the large range and uneven distribution of melt indices used, and its use does not necessarily imply any physical basis. The largest number of adhesives with different melt indices and the same amount of vinyl acetate are those containing 28%, and the regression on these is shown as a full line in the figures.

There are a large number of relationships to be considered in these results. In addition to the differences between the properties during heating and cooling, there is for the adhesives (Table 9), the effects of crystallinity (comparing the crystalline and non-crystalline grades), manufacturer (considering the consistency of behaviour of the Elf Atochem grades), vinyl acetate concentration, and melt index. Similar relationships exist for the components of the adhesive (Table 10), and then also the relation of the components to the adhesive. These are discussed in detail later along with other properties. Here we may note that many of the properties follow an expected pattern of behaviour, and the main purposes of the differential scanning calorimetry was to characterise the thermal properties of the adhesives as a basis for a wider understanding of the adhesives and the adhesive joints.

4.2 Softening and compatibility behaviour of the adhesives

The softening points and cloud points of the adhesives are given in Table 11. The reproducibility of the test methods are good (to within 0.2 and 0.5°C respectively, see section 3.3) and the small changes in the results are significant. Within the adhesives containing 28% vinyl acetate, there is a general decrease in the softening point as the melt index increases. The results of the 28/7NC, 28/40NC*, 128/420NC* are outside this trend and it is notable that two of these are from a different manufacture and may reflect a different molecular structure of the EVA within the adhesives. The vinyl acetate concentration appears to have a noticeable effect on the softening point.

There is a general trend that the cloud point decreases as the vinyl acetate concentration increases. The cloud point of the adhesive containing 28% vinyl acetate is independent of the melt index.

Table 11 Softening point and cloud point

Adhesive	Softening point (°C)	Cloud point (°C)
14/2500NC	89	69
19/150NC	85	63
28/7NC	97	62
28/25NC	106	62
28/40NC	101	62
28/145NC	91	62
28/400NC	82	60
28/2500NC	82	62
28/40NC*	109	63
28/420NC*	94	58
33/400NC*	83	59
28/400XL	88	64
28/2500XL	85	62
33/400XL	87	61

4.3 Viscosity and viscoelasticity of the adhesives

Viscosities obtained using the rotational viscometer are shown in Table 12. The results are the average of two measurements. It is considered that the viscosities are accurate to within 1% of the full scale deflection (see section 3.7). Some of the results are also shown in Figs 45, 46, and 47. The relationship between the viscosity and melt index is expected, since the melt index is a measure of the viscosity. Indeed from the present results (Fig 45), there is a power relation $\eta = (MI)^k$ where k is a constant and is simply the same slope $k = (log\,\eta)/(log\,MI)$ at any temperature. Viscosity is a thermally activated process (equation 1, section 2.1) and this is clearly seen in Fig 46. The effects of crystallinity appear to be not significant and the more crystalline grades tend to have similar viscosities at any given temperature to their non-crystalline counterparts. This is illustrated for the adhesives with a MI of 400 in Fig 47. The amount of vinyl acetate also appears to have no appreciable effect on the viscosity.

A typical controlled strain rheogram for an adhesive is shown in Fig 48, and data obtained from this rheogram are given in Table 13. The storage modulus G' is given at 40°C intervals, starting at -20°C, together with the value of the loss tangent *tan* δ over the same range of temperatures. Other values include the value of the loss tangent at its lower maxima, together with the temperature at which it occurs, $tan\,\delta_L$ and T_L respectively. Similar data is given for the local maxima in the loss modulus *i.e.* $G''_{L"}$ and $T_{L"}$. The gradient of the curve $d(log\,G')/dT$ was obtained manually from the average gradient of the curve constructed 5°C either side of the temperature where $tan\,\delta = 1$, *i.e.* T_X. Results from other adhesives are also given in the table. Similar data was also obtained for the components of the adhesives, excluding local maxima data, albeit over a reduced temperature range. These are given in Table 14. Tables 15 and 16 contain data obtained using the controlled stress rheometer although the temperature range for the controlled stress data for the adhesive components was wider than that used for the controlled strain experiments. A sample controlled stress adhesive rheogram is given as Fig 49. Some of the results are shown in Fig 50 which illustrates the variation in the storage modulus of the adhesive

Table 12 Viscosity of adhesives at various temperatures obtained using a rotational viscometer[a]

Sample	Viscosity, η (Pa s) at			
	120°C	140°C	160°C	180°C
14/2500NC	2.1	1.2	0.8	0.5
19/150NC	21.3	10.4	8.0	3.4
28/7NC	360.0	147.7	70.1	39.1
28/25NC	84.0	37.0	26.3	14.5
28/40NC	77.5	33.7	18.2	10.2
28/145NC	22.3	10.3	5.4	3.1
28/400NC	12.4	5.4	2.9	1.8
28/2500NC	2.8	1.4	0.8	0.5
28/40NC*	73.0	31.4	16.3	9.2
28/420NC*	9.7	4.7	2.8	1.4
33/400NC*	10.4	4.9	2.7	1.5
28/400XL	12.8	6.0	3.2	1.9
28/2500XL	2.7	1.3	0.8	0.5
33/400XL	10.6	5.2	2.7	1.6

(a) Each value is the average of at least two tests.

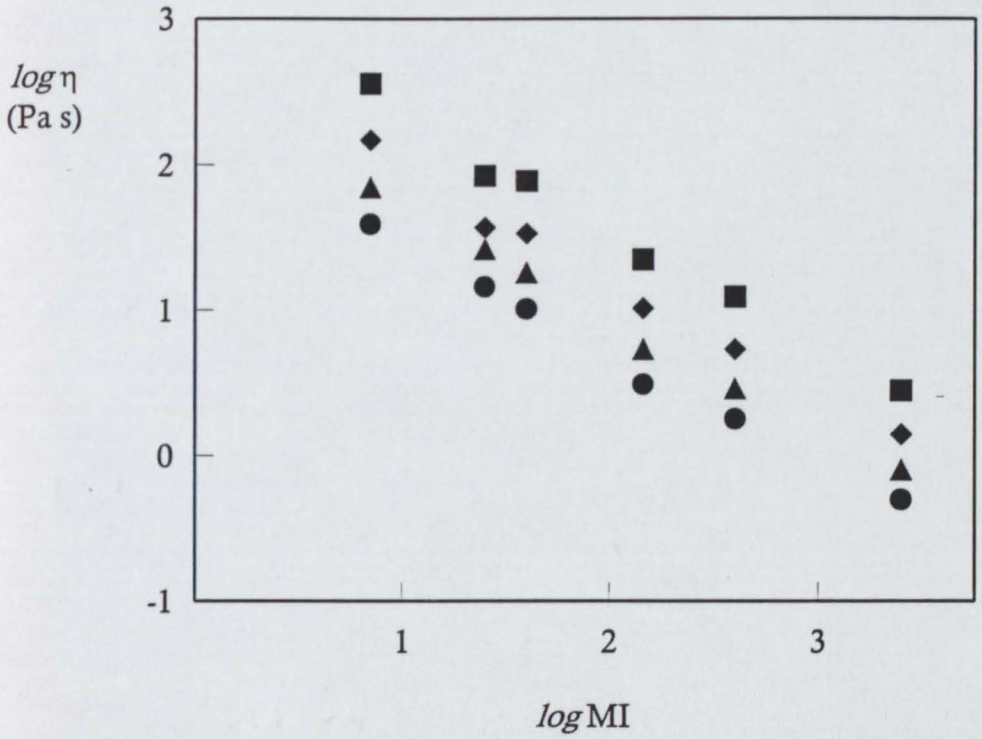

Fig 45. Viscosity η at various temperatures as a function of the logarithm of the melt index MI for 28% VA adhesives. See Table 12. Symbols: ● 180°C; ▲ 160°C; ◆ 140°C; and ■ 120°C.

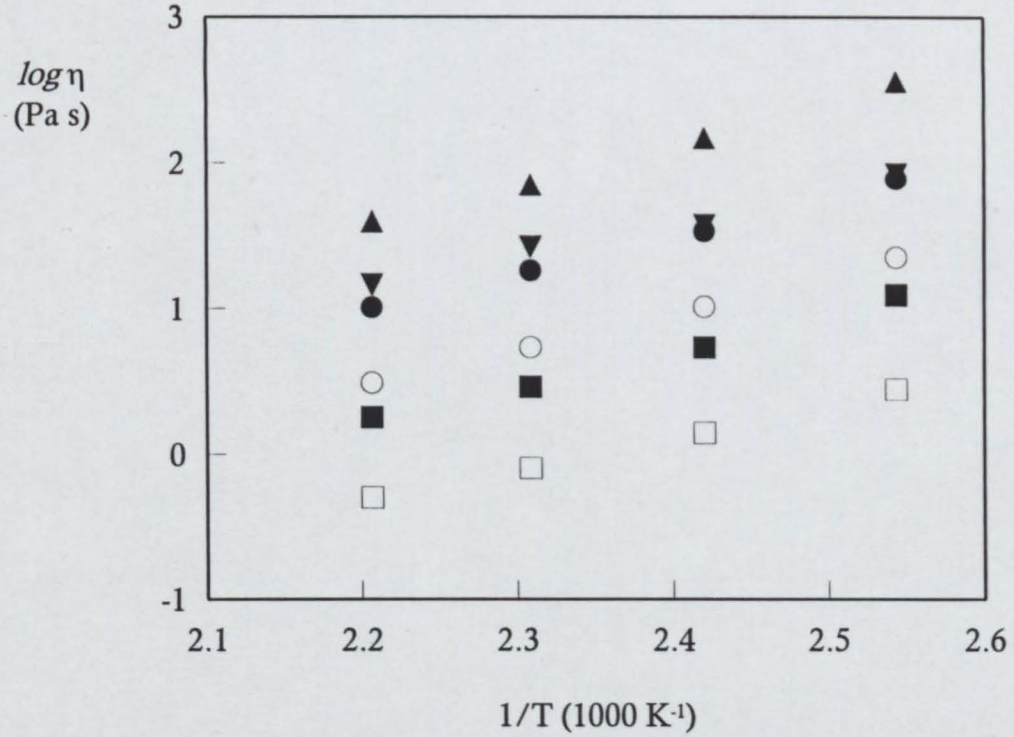

Fig 46. Arrhenius function of the viscosity η as a function of the reciprocal absolute temperature 1/T. Symbols: ▲ 28/7NC; ▼ 28/25NC; ● 28/40NC; ○ 28/145NC; ■ 28/400NC; and □ 28/2500NC.

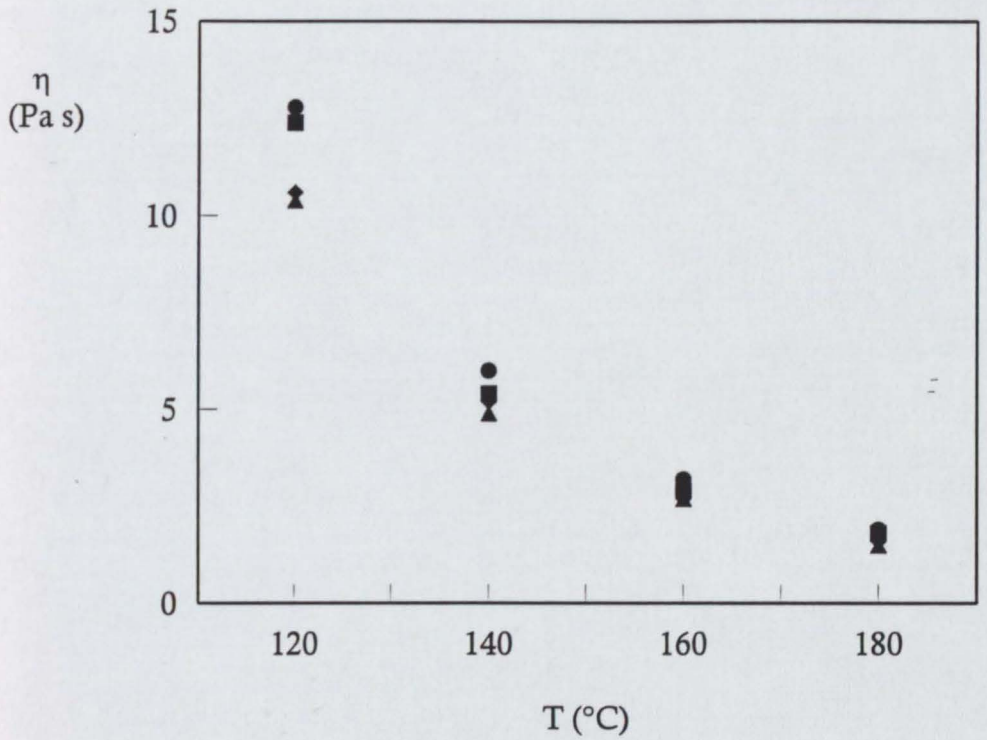

Fig 47. Viscosity η as a function of temperature T showing the effect of crystallinity in adhesives of EVA melt index 400 with concentrations of 28% and 33% vinyl acetate. See Table 8. Symbols: ● 28/400NC; ■ 28/400XL; ◆ 33/400NC*; and ▲ 33/400XL.

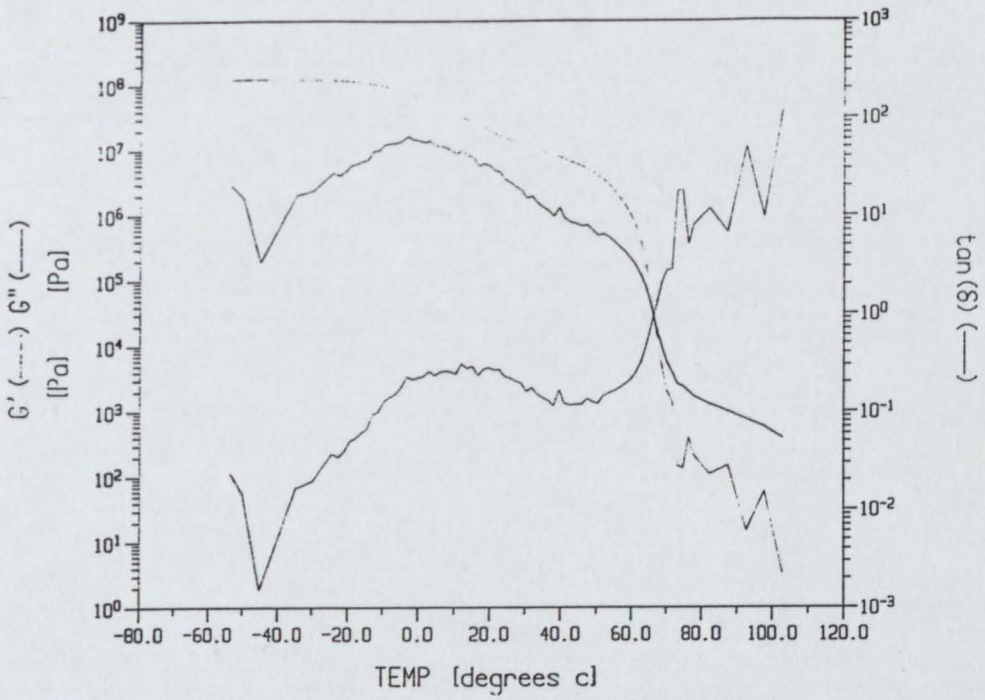

Fig 48. Rheogram showing the storage modulus G', loss modulus G", and tangent of the phase angle *tan* δ as a function of temperature. ADH 28/400NC; 7.9 mm parallel plates; nominal heating rate 5°C min^{-1}; controlled strain.

Table 13 Rheological properties of adhesives at a frequency of 10 rad s^{-1} and constant strain during a temperature scan from -50°C to 100°C[a]

Adhesive	Storage modulus G' at				Loss tangent *tan* δ at				G', G" crossover point			Maximum *tan* δ		Maximum G"	
	-20°C	20°C	60°C	100°C	-20°C	20°C	60°C	100°C	G_X	T_X	(d(*log* G')/dT)[b]	T_L	*tan* δ_L	$T_{L"}$	$G"_{L"}$
	(10^8 Pa)	(10^7 Pa)	(10^5 Pa)	(10^2 Pa)	($\times10^{-2}$)	($\times10^{-1}$)	($\times10^{-1}$)	($\times10^{0}$)	(10^3 Pa)	(°C)	(°C^{-1})	(°C)	($\times10^{-1}$)	(°C)	(10^6 Pa)
14/2500NC	0.79	2.47	0.49	ND	2.3	3.0	1.9	ND	4.2	76	0.400	31	3.5	11	7.2
19/150NC	0.68	2.84	17.70	2.94	4.5	2.6	1.5	3.6	8.8	81	0.201	34	3.3	14	7.1
28/7NC	0.75	2.07	9.10	25.40	2.1	3.3	1.8	2.1	17.5	75	0.115	26	3.7	11	8.6
28/25NC	0.70	1.90	4.90	15.10	2.7	3.7	2.8	3.1	24.3	71	0.138	24	3.9	7	4.2
28/40NC	0.71	1.90	8.60	9.64	2.6	2.9	2.4	3.5	30.2	70	0.173	21	2.9	7	10.0
28/145NC	0.59	1.70	4.00	1.69	3.7	3.2	3.3	6.1	18.9	68	0.228	20	3.0	9	8.9
28/400NC	0.75	1.62	3.40	0.04	4.6	3.1	3.8	56.6	18.4	66	0.346	16	3.2	5	10.0
28/2500NC	0.66	1.31	0.21	ND	4.2	3.4	6.5	ND	9.2	64	0.394	14	3.8	-6	9.0
28/40NC*	0.68	1.75	6.33	10.20	5.2	3.6	2.6	3.5	26.1	73	0.156	24	3.7	6	10.7
28/420NC*	1.20	1.40	7.10	0.04	3.8	3.2	2.2	182.0	35.0	66	0.250	12	3.1	4	10.8
33/400NC*	1.20	1.30	3.90	0.06	5.8	2.1	4.1	165.0	40.0	63	0.298	5	3.2	-8	16.4
28/400XL	1.20	1.70	1.70	0.14	4.3	3.7	3.9	38.5	15.0	64	0.171	19	3.8	3	15.0
28/2500XL	1.20	1.40	0.24	ND	4.7	2.8	6.9	ND	9.0	61	0.249	14	3.1	-6	14.2
33/400XL	1.40	1.60	0.48	ND	3.5	2.8	8.8	ND	23.0	61	0.231	14	3.2	-5	18.7

(a) See Fig 16 and text for explanation of properties.
(b) Actual slope negative. Positive value (the magnitude) given in table.

Table 14 Rheological properties of components of various poly(ethylene-*co*-vinyl acetate) adhesives at a frequency of 10 rad s^{-1} and constant strain during a temperature scan from 40°C to 160°C[a]

Component	Storage modulus, G' at				Loss tangent, *tan* δ at				G', G" crossover point		
	40°C	60°C	80°C	100°C	40°C	60°C	80°C	100°C	G_X	T_X	(d(*log* G')/dT)[b]
	(10^6 Pa)	(10^5 Pa)	(10^4 Pa)	(10^3 Pa)	($\times10^{-2}$)	($\times10^{-1}$)	($\times10^{0}$)	($\times10^{0}$)	(10^3 Pa)	(°C)	($°C^{-1}$)
14/2500NC	0.45	3.71	5.69	0.01	0.30	0.40	0.24	35.21	5.3	86	0.284
19/150NC	4.30	17.90	18.40	3.38	9.98	0.92	0.33	2.48	27.3	85	0.169
28/7NC	1.87	7.58	7.64	46.35	7.36	1.45	0.72	0.89	34.2	117	0.010
28/25NC	1.85	7.31	4.82	23.75	7.32	1.57	0.90	1.20	38.6	83	0.026
28/40NC	1.47	5.72	3.87	18.10	8.97	1.81	1.08	1.43	45.3	78	0.053
28/145NC	1.15	3.34	0.75	3.01	11.00	1.58	1.49	2.09	32.6	75	0.085
28/400NC	0.87	1.92	0.28	0.75	14.00	2.05	3.03	4.84	22.0	69	0.119
28/2500NC	0.51	0.54	0.01	0.004	15.60	3.15	28.50	91.10	11.4	67	0.157

continued

Table 14 continued

Component	Storage modulus, G' at				Loss tangent, *tan* δ at				G', G" crossover point		
	40°C	60°C	80°C	100°C	40°C	60°C	80°C	100°C	G_X	T_X	$(d(log\,G')/dT)^b$
	(10^6 Pa)	(10^5 Pa)	(10^4 Pa)	(10^3 Pa)	($\times10^{-2}$)	($\times10^{-1}$)	($\times10^{0}$)	($\times10^{0}$)	(10^3 Pa)	(°C)	($°C^{-1}$)
28/40NC*	1.69	6.59	4.02	17.40	8.22	1.61	0.98	1.38	38.9	80	0.041
28/420NC*	0.50	0.87	2.15	0.56	1.17	4.10	2.05	5.84	18.4	67	0.109
33/400NC*	0.26	0.19	0.12	0.68	8.10	6.15	2.09	2.18	7.2	63	0.095
28/400XL	1.42	4.90	0.67	1.47	9.65	1.73	2.05	3.86	28.1	75	0.144
28/2500XL	0.40	1.42	0.02	0.005	0.55	2.10	8.10	12.20	10.9	69	0.173
33/400XL	0.68	1.76	0.27	0.69	15.90	3.32	3.24	5.72	24.7	70	0.124
Resin	8.50	84.00	0.15	0.003	1.00	6.75	18.10	ND	ND	ND	ND
	40°C	50°C	60°C	70°C	40°C	50°C	60°C	70°C			
	(10^5Pa)	(10^5Pa)	(10^4Pa)	(10^0Pa)	($\times10^{-2}$)	($\times10^{-2}$)	($\times10^{-1}$)	($\times10^{0}$)			
Wax	5.29	5.30	6.50	15.50	1.05	7.48	20.96	3.24	37.3	61	0.390

(a) See Fig 16 and text for explanation of properties.
(b) Actual slope negative. Positive value (the magnitude) given in table.
(c) See text for explanation. Actual slope negative. Positive value (the magnitude) given in table.

Table 15 Rheological properties of adhesives at a frequency of 10 rad s^{-1} and constant stress during a temperature scan from -50°C to 100°C[a]

Adhesive	Storage modulus, G' at				Loss tangent, *tan* δ at				G', G" crossover point			Maximum *tan* δ		Maximum G"	
	-20°C	20°C	60°C	100°C	-20°C	20°C	60°C	100°C	G_X	T_X	(d(*log*G')/dT)[b]	T_L	*tan* δ_L	$T_{L"}$	$G"_{L"}$
	(10^8Pa)	(10^7Pa)	(10^5Pa)	(10^2Pa)	(×10^{-2})	(×10^{-1})	(×10^{-1})	(×10^0)	(10^3Pa)	(°C)	(°C^{-1})	(°C)	(×10^{-1})	(°C)	(10^6Pa)
14/2500NC	3.04	3.51	14.20	ND	9.5	3.4	3.5	ND	17.6	67	0.229	26	3.5	-7	36.8
19/150NC	2.90	3.37	19.10	ND	7.9	3.4	1.8	ND	22.3	74	0.161	29	3.9	-11	33.3
28/7NC	3.43	5.44	14.40	36.80	3.0	3.0	2.1	2.1	52.4	71	0.126	28	3.1	0	36.4
28/25NC	2.59	1.63	6.09	9.84	12.0	4.0	3.3	3.4	53.3	67	0.157	10	4.4	-14	38.5
28/40NC	2.87	1.96	7.59	6.90	12.1	3.7	3.9	4.5	87.7	65	0.181	12	4.1	-11	47.5
28/145NC	2.77	1.81	2.81	0.41	13.7	3.6	7.4	164.0	86.2	62	0.209	10	4.1	-14	46.3
28/400NC	2.33	1.51	0.98	ND	15.6	3.4	10.5	ND	103.0	60	0.329	10	4.3	-14	42.4
28/2500NC	2.39	1.24	0.06	ND	16.2	3.3	42.4	ND	74.2	55	0.511	5	4.5	-14	44.8
28/40NC*	2.21	1.73	6.39	11.10	16.2	3.7	3.1	1.1	31.4	67	0.123	13	4.2	-14	39.4
28/420NC*	2.44	1.27	2.20	ND	13.1	4.0	7.7	ND	130.0	61	0.294	8	4.6	-14	38.7
33/400NC*	2.49	1.35	0.47	ND	17.7	2.8	13.6	ND	46.9	60	0.303	3	4.2	-16	49.1
28/400XL	2.04	1.90	7.30	ND	10.8	3.9	4.4	ND	208.0	63	0.339	15	4.1	-9	34.6
28/2500XL	0.96	1.57	0.25	ND	17.1	3.4	18.3	ND	315.0	57	0.388	10	4.1	-6	29.4
33/400XL	2.71	2.02	0.89	ND	12.3	3.2	11.9	ND	342.0	59	0.347	8	4.1	-12	49.1

(a) See Fig 16 and text for explanation of properties.
(b) Actual slope negative. Positive value (the magnitude) given in table.

Table 16 Rheological properties of components of various poly(ethylene-*co*-vinyl acetate) adhesives at a frequency of 10 rad s^{-1} and constant stress during a temperature scan from -50°C to 120°C[a]

Component	Storage modulus, G' at				Loss tangent, *tan* δ at				G', G" crossover point			Maximum *tan* δ		Maximum G"	
	-20°C	20°C	60°C	100°C	-20°C	20°C	60°C	100°C	G_X	T_X	(d(*log*G')/dT)[b]	T_L	*tan* δ_L	$T_{L"}$	$G"_{L"}$
	(10^7Pa)	(10^6Pa)	(10^5Pa)	(10^4Pa)	($\times10^{-1}$)	($\times10^{-1}$)	($\times10^{-1}$)	($\times10^{0}$)	(10^4Pa)	(°C)	(°C^{-1})	(°C)	($\times10^{-1}$)	(°C)	(10^7Pa)
14/2500NC	6.15	13.30	25.87	0.10	1.89	0.95	0.94	8.51	3.42	79	0.363	-29	2.08	-40	2.82
19/150NC	6.79	13.10	34.39	0.50	2.09	0.78	0.85	2.26	7.14	85	0.141	-25	2.12	-36	2.89
28/7NC	4.27	8.01	19.48	8.14	2.60	0.66	1.30	0.85	4.59	125	0.010	-26	2.99	-36	4.12
28/25NC	3.47	6.68	14.83	3.56	2.66	0.82	1.50	1.17	5.62	88	0.025	-27	3.13	-37	4.55
28/40NC	2.41	5.41	10.78	2.22	2.53	0.84	1.67	1.34	5.14	84	0.059	-31	3.25	-42	3.07
28/145NC	2.54	4.81	6.32	0.57	2.79	0.94	2.23	2.20	4.88	75	0.086	-30	3.49	-40	4.33
28/400NC	3.61	3.72	5.28	0.17	2.53	1.36	2.64	4.09	5.65	72	0.074	-29	3.00	-38	3.69
28/2500NC	1.55	1.88	0.66	ND	2.78	1.51	5.72	ND	2.72	63	0.168	-32	3.80	-42	3.10

continued

Table 16 continued

Component	Storage modulus, G' at				Loss tangent, *tan* δ at				G', G" crossover point			Maximum *tan* δ		Maximum G"	
	-20°C	20°C	60°C	100°C	-20°C	20°C	60°C	100°C	G_X	T_X	(d(*log*G')/dT)[b]	T_L	*tan* δ_L	$T_{L"}$	$G_{L"}$
	(10^7Pa)	(10^6Pa)	(10^5Pa)	(10^4Pa)	($\times10^{-1}$)	($\times10^{-1}$)	($\times10^{-1}$)	($\times10^{0}$)	(10^4Pa)	(°C)	(°C^{-1})	(°C)	($\times10^{-1}$)	(°C)	(10^7Pa)
28/40NC*	5.16	7.86	15.80	2.99	2.81	0.91	1.42	1.25	5.81	87	0.036	-25	3.07	-34	4.83
28/420NC*	2.83	4.24	35.84	0.16	2.72	1.20	3.21	4.45	5.50	70	0.090	-30	3.49	-41	3.93
33/400NC*	2.38	2.97	1.41	0.17	3.01	1.83	6.87	4.69	6.78	65	0.087	-31	4.12	-38	5.11
28/400XL	4.56	7.15	13.33	0.19	3.03	0.89	1.51	4.36	8.11	75	0.135	-24	3.26	-31	3.88
28/2500XL	3.91	6.00	4.91	ND	3.12	1.49	2.38	ND	4.69	70	0.169	-25	3.38	-35	4.25
33/400XL	2.76	4.26	4.01	0.26	3.65	1.28	3.90	3.92	9.34	67	0.114	-26	4.29	-35	4.56
Resin	24.52	56.75	156.90	5×10^{-4}	0.45	0.72	17.15	ND	4115	57	0.006	ND	ND	55	4.52
Wax	21.24	257.00	0.54	ND	0.57	0.82	15.40	ND	4.29	63	0.457	ND	ND	61	2.69

(a) See Fig 16 and text for explanation of properties.
(b) Actual slope negative. Positive value (the magnitude) given in table.
(c) See text for explanation. Actual slope negative. Positive value (the magnitude) given in table.

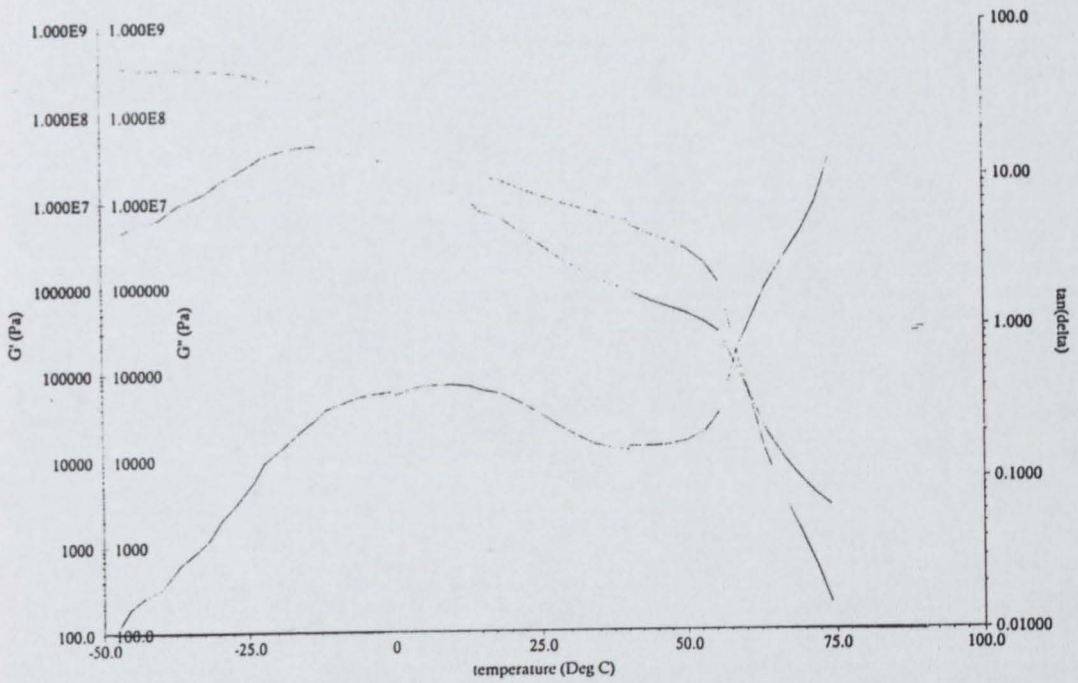

Fig 49. Rheogram showing the storage modulus G', loss modulus G", and tangent of the phase angle *tan* δ as a function of temperature. ADH 28/400NC; 8 mm parallel plates; actual heating rate 5°C min^{-1}; controlled stress.

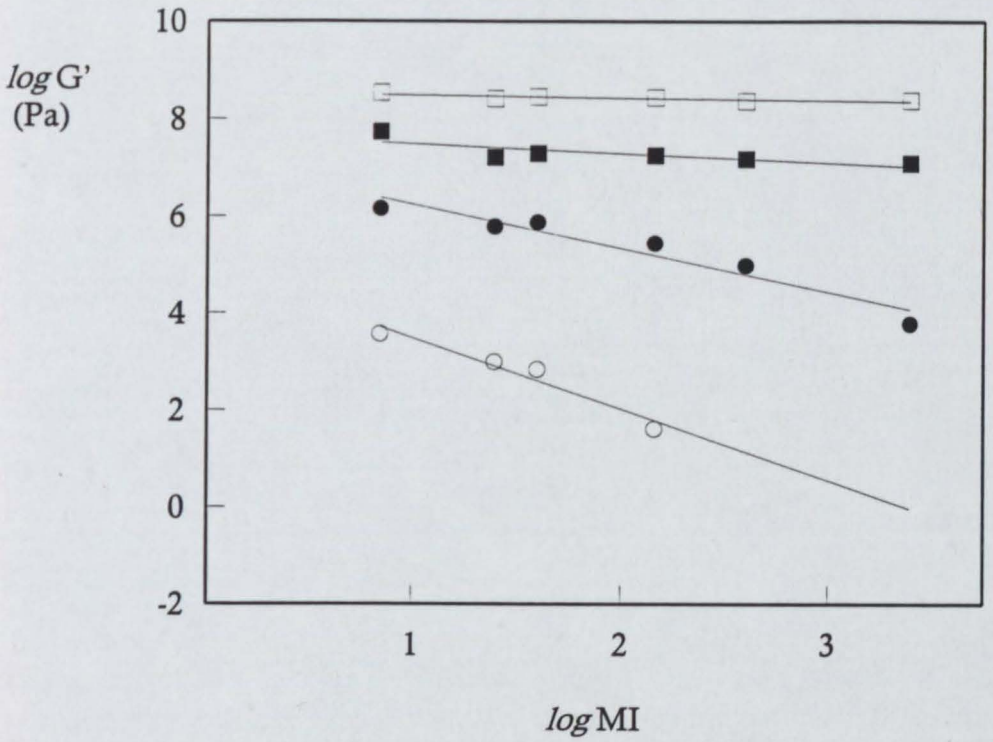

Fig 50. Graph showing the storage modulus G' as a function of the logarithm of the melt index MI for ExUL 28% VA EVAs at four temperatures. Regression lines are shown for clarity. Symbols: □ -20°C; ■ 20°C; ● 60°C; and ○ 100°C. See text for details.

components G' at each of the temperatures in Table 16 as a function of the logarithm of the melt index of the EVA. Regression lines are shown for clarity and are discussed in greater detail in Chapter 5.

Tables 17 and 18 contain data obtained from transient (creep) testing performed on the controlled stress rheometer. Table 17 contains the creep data for the adhesives. Creep tests were performed from 20 - 80°C and the resulting curves were analysed using a four- or six-element model according to Berger (see Chapter 2), *i.e.* they were analysed with one or two Voigt/Kelvin units. The data given in the table corresponds to the parameters obtained from the use of the model. Each result is the average of at least two sample runs on the rheometer and two attempts at modelling the raw data. A typical creep curve is shown in Fig 51. The variation of the initial compliance J_0 of the adhesive as a function of the logarithm of the melt index of the EVA is given in Fig 52. Regression lines are again for the 28%VA series and are given for the sake of clarity. Further discussion appears in Chapter 5. Table 18 gives data for the components of the adhesives. Note in this case only the initial compliance and zero shear viscosity η_0 are given. It was not possible to obtain lower temperature data for the resin due to the sample fracturing. Figure 53 shows a typical creep curve obtained for EVA 28/400NC.

4.4 Adhesive bond development

Five separate tests were conducted to determine the open time and setting time for each adhesive/standard corrugated substrate bonds using the Kanebo bond tester (see Sections 2.3 and 3.5). The maximum differences observed between replicates in both open time and setting time measurements were 1 s and 1½ s, respectively. The average results are given in Table 19. It is considered that the average results are reproducible to within half a second.

A broad pattern of behaviour occurs with the open time. There is a tendency for the open time to decrease as the amount of vinyl acetate increases, and, more clearly, for the bonds made with 28% vinyl acetate adhesive, the open time increase with an increase in melt index from 7 to 40, and thereafter decreases as the melt index increases. The pattern of behaviour in the setting

Table 17 Creep properties of adhesives as determined by controlled stress rheometry[a, b, c]

Adhesive	Temperature (°C)	J_0 (Pa^{-1})	η_0 (Pa s)	J_1 (Pa^{-1})	η_1 (Pa s)	τ_1 (s)	J_2 (Pa^{-1})	η_2 (Pa s)	τ_2 (s)	S.E.	J_r (Pa^{-1})
14/2500NC	20	9.6×10^{-8}	1.8×10^{10}	2.8×10^{-8}	1.1×10^{8}	17.4	-	-	-	16	9.6×10^{-8}
	30	1.2×10^{-7}	1.1×10^{10}	4.3×10^{-8}	3.8×10^{8}	16.5	-	-	-	26	1.2×10^{-7}
	40	1.9×10^{-7}	9.4×10^{9}	6.5×10^{-8}	1.9×10^{8}	12.5	-	-	-	20	1.9×10^{-7}
	50	2.6×10^{-7}	5.7×10^{9}	1.2×10^{-7}	1.5×10^{8}	17.9	2.3×10^{-8}	2.5×10^{7}	0.6	24	2.6×10^{-7}
	60	4.2×10^{-7}	3.1×10^{9}	2.6×10^{-7}	8.4×10^{7}	22.1	5.6×10^{-8}	9.2×10^{6}	0.5	20	4.2×10^{-7}
	70	2.0×10^{-6}	6.3×10^{8}	8.4×10^{-7}	2.7×10^{7}	22.4	-	-	-	8.1	2.0×10^{-6}
	80 §	4.3×10^{-5}	3.2×10^{4}	8.5×10^{-3}	9.4×10^{3}	79.5	2.5×10^{-4}	7.5×10^{3}	1.9	4.3	2.4×10^{-4}
	85	2.4×10^{-4}	6.4×10^{2}	-	-	-	-	-	-	5.5	2.4×10^{-4}
19/150NC	20	8.0×10^{-8}	2.4×10^{10}	2.2×10^{-8}	7.3×10^{8}	16.1	-	-	-	13	8.0×10^{-8}
	30	1.1×10^{-7}	1.1×10^{10}	2.9×10^{-8}	6.2×10^{8}	17.9	-	-	-	18	1.1×10^{-7}
	40	1.6×10^{-7}	1.0×10^{10}	4.3×10^{-8}	3.4×10^{8}	14.6	-	-	-	15	1.6×10^{-7}
	50	2.1×10^{-7}	5.9×10^{9}	6.1×10^{-8}	2.2×10^{8}	13.6	-	-	-	10	2.1×10^{-7}
	60	3.0×10^{-7}	4.1×10^{9}	1.3×10^{-7}	1.3×10^{8}	17.3	-	-	-	15	3.0×10^{-7}
	70	7.7×10^{-7}	1.6×10^{9}	3.4×10^{-7}	5.2×10^{7}	17.4	-	-	-	21	7.7×10^{-7}
	80 §	7.5×10^{-6}	2.3×10^{7}	7.4×10^{-5}	3.2×10^{5}	23.3	1.4×10^{-5}	1.4×10^{5}	2.0	18	7.5×10^{-6}
	85	1.1×10^{-5}	5.2×10^{4}	9.4×10^{-4}	5.6×10^{4}	52.8	3.9×10^{-5}	4.8×10^{4}	1.9	3.2	1.1×10^{-5}
28/7NC	20	1.7×10^{-7}	1.5×10^{10}	4.4×10^{-8}	6.7×10^{8}	29.8	-	-	-	11	1.7×10^{-7}
	30	2.2×10^{-7}	7.6×10^{9}	5.0×10^{-8}	3.0×10^{8}	14.9	-	-	-	10	2.2×10^{-7}
	40	3.2×10^{-7}	7.2×10^{9}	5.5×10^{-8}	3.1×10^{8}	16.7	-	-	-	7.0	3.2×10^{-7}
	50	4.0×10^{-7}	6.3×10^{9}	1.2×10^{-7}	1.2×10^{8}	13.7	-	-	-	15	4.0×10^{-7}
	60	6.2×10^{-7}	1.8×10^{9}	2.5×10^{-7}	6.1×10^{7}	15.1	-	-	-	15	6.2×10^{-7}
	70 §	2.5×10^{-6}	9.2×10^{7}	6.9×10^{-6}	4.8×10^{6}	33.3	2.0×10^{-6}	1.0×10^{6}	2.0	13	2.5×10^{-6}
	80	6.3×10^{-6}	7.2×10^{5}	6.4×10^{-5}	4.1×10^{5}	26.2	9.6×10^{-6}	1.5×10^{5}	1.5	5.4	6.3×10^{-6}

continued

Table 17 continued

Adhesive	Temperature (°C)	J_0 (Pa^{-1})	η_0 (Pa s)	J_1 (Pa^{-1})	η_1 (Pa s)	τ_1 (s)	J_2 (Pa^{-1})	η_2 (Pa s)	τ_2 (s)	S.E.	J_r (Pa^{-1})
28/25NC	20	1.6×10^{-7}	1.4×10^{10}	3.9×10^{-8}	2.8×10^{8}	10.8	-	-	-	14	1.6×10^{-7}
	30	2.4×10^{-7}	4.9×10^{9}	7.7×10^{-8}	2.4×10^{8}	18.6	-	-	-	9.2	2.4×10^{-7}
	40	3.3×10^{-7}	4.0×10^{9}	1.2×10^{-7}	1.4×10^{8}	16.9	-	-	-	14	3.3×10^{-7}
	50	4.7×10^{-7}	2.3×10^{9}	2.1×10^{-7}	9.9×10^{7}	20.7	-	-	-	15	4.7×10^{-7}
	60 §	9.4×10^{-7}	8.3×10^{8}	5.5×10^{-7}	4.3×10^{7}	23.7	2.4×10^{-7}	6.8×10^{6}	1.6	12	9.4×10^{-7}
	70	5.5×10^{-6}	1.3×10^{6}	2.9×10^{-5}	1.3×10^{6}	38.2	5.2×10^{-6}	5.0×10^{5}	2.6	9.4	5.5×10^{-6}
	80	8.8×10^{-6}	2.0×10^{5}	9.2×10^{-5}	1.9×10^{5}	17.8	1.5×10^{-5}	6.5×10^{4}	1.0	3.8	8.8×10^{-6}
28/40NC	20	2.5×10^{-7}	5.7×10^{9}	7.2×10^{-8}	2.2×10^{8}	15.7	-	-	-	11	2.5×10^{-7}
	30	3.0×10^{-7}	5.9×10^{9}	1.1×10^{-7}	2.1×10^{8}	23.0	-	-	-	14	3.0×10^{-7}
	40	5.2×10^{-7}	2.2×10^{9}	1.4×10^{-7}	1.9×10^{8}	27.0	-	-	-	14	5.2×10^{-7}
	50	7.7×10^{-7}	1.6×10^{9}	4.0×10^{-7}	7.4×10^{7}	29.7	-	-		15	7.7×10^{-7}
	60	1.8×10^{-6}	4.2×10^{8}	9.9×10^{-7}	4.0×10^{7}	40.0	6.3×10^{-7}	4.7×10^{6}	3.0	7.0	1.8×10^{-6}
	70	1.0×10^{-5}	4.3×10^{6}	1.1×10^{-4}	5.0×10^{5}	57.0	1.6×10^{-5}	2.2×10^{5}	3.6	7.4	1.1×10^{-5}
	80	6.5×10^{-6}	6.5×10^{4}	2.4×10^{-4}	6.0×10^{4}	14.8	-	-	-	6.6	6.5×10^{-6}
28/145NC	20	2.4×10^{-7}	9.1×10^{9}	8.5×10^{-8}	3.5×10^{8}	29.7	-	-	-	11	2.4×10^{-7}
	30	3.3×10^{-7}	4.1×10^{9}	1.0×10^{-7}	1.7×10^{8}	17.3	-	-	-	15	3.3×10^{-7}
	40	5.2×10^{-7}	1.6×10^{9}	1.9×10^{-7}	6.5×10^{7}	12.8	-	-	-	12	5.2×10^{-7}
	50	7.5×10^{-7}	9.6×10^{8}	4.3×10^{-7}	7.0×10^{7}	30.5	3.0×10^{-7}	4.5×10^{6}	1.4	12	7.5×10^{-7}
	60 §	2.7×10^{-6}	2.1×10^{8}	2.3×10^{-6}	1.1×10^{7}	25.9	1.3×10^{-6}	1.0×10^{6}	1.3	9.4	2.7×10^{-6}
	70	2.0×10^{-5}	4.7×10^{5}	6.7×10^{-4}	9.7×10^{4}	65.2	3.6×10^{-5}	7.1×10^{4}	2.6	7.4	2.2×10^{-5}
28/400NC	20	2.1×10^{-7}	9.4×10^{9}	6.6×10^{-8}	5.2×10^{8}	33.9	3.0×10^{-8}	6.3×10^{7}	1.9	10	2.1×10^{-7}
	30	3.0×10^{-7}	4.1×10^{9}	8.2×10^{-8}	1.7×10^{8}	14.3	6.0×10^{-8}	7.0×10^{6}	0.4	11	3.0×10^{-7}
	40	6.1×10^{-7}	2.1×10^{9}	1.4×10^{-7}	1.4×10^{8}	19.8	-	-	-	16	6.1×10^{-7}
	50	1.1×10^{-6}	9.4×10^{8}	5.6×10^{-7}	5.6×10^{7}	31.7	1.3×10^{-7}	2.0×10^{7}	2.6	8.1	1.1×10^{-6}
	60 §	3.7×10^{-6}	1.9×10^{8}	3.7×10^{-6}	7.2×10^{6}	26.9	1.9×10^{-6}	1.0×10^{6}	1.9	17	3.7×10^{-6}
	70	3.0×10^{-5}	6.6×10^{5}	2.1×10^{-3}	3.4×10^{4}	72.4	6.5×10^{-5}	1.4×10^{4}	2.2	4.1	3.3×10^{-5}
	80	6.1×10^{-5}	3.7×10^{3}	2.7×10^{-4}	2.5×10^{4}	7.0	-	-	-	0.46	6.1×10^{-5}

Table 17 continued

Adhesive	Temperature (°C)	J_0 (Pa^{-1})	η_0 (Pa s)	J_1 (Pa^{-1})	η_1 (Pa s)	τ_1 (s)	J_2 (Pa^{-1})	η_2 (Pa s)	τ_2 (s)	S.E.	J_r (Pa^{-1})
28/2500NC	20	4.3×10^{-7}	2.0×10^{9}	1.6×10^{-7}	7.3×10^{7}	11.6	-	-	-	12	4.3×10^{-7}
	30	8.1×10^{-7}	9.2×10^{8}	4.6×10^{-7}	4.9×10^{7}	22.6	-	-	-	25	8.1×10^{-7}
	40	1.8×10^{-6}	4.2×10^{8}	9.4×10^{-7}	2.3×10^{7}	21.7	-	-	-	30	1.8×10^{-6}
	50	4.5×10^{-6}	1.1×10^{8}	3.1×10^{-6}	6.6×10^{6}	20.5	-	-	-	2.1	4.5×10^{-6}
	60 §	1.1×10^{-5}	8.5×10^{6}	7.1×10^{-5}	2.3×10^{5}	16.3	4.5×10^{-5}	1.9×10^{4}	0.9	18	2.9×10^{-5}
	70	1.1×10^{-5}	9.1×10^{2}	-	-	-	-	-	-	5.1	1.1×10^{-5}
	75	1.5×10^{-5}	3.0×10^{2}	-	-	-	-	-	-	9.2	1.5×10^{-5}
28/40NC*	20	1.4×10^{-7}	9.3×10^{9}	3.0×10^{-8}	3.2×10^{8}	9.4	-	-	-	20	1.4×10^{-7}
	30	2.6×10^{-7}	4.7×10^{9}	6.5×10^{-8}	1.1×10^{8}	73	-	-	-	15	2.6×10^{-7}
	40	3.1×10^{-7}	3.9×10^{9}	1.3×10^{-7}	1.8×10^{8}	24.0	-	-	-	26	3.1×10^{-7}
	50	5.1×10^{-7}	1.6×10^{9}	2.0×10^{-7}	8.3×10^{7}	17.0	-	-	-	18	5.1×10^{-7}
	60 §	9.9×10^{-7}	5.8×10^{8}	6.6×10^{-7}	2.3×10^{7}	14.8	2.0×10^{-7}	4.0×10^{6}	0.8	15	9.9×10^{-7}
	70	4.7×10^{-6}	1.4×10^{7}	3.4×10^{-5}	1.1×10^{6}	35.9	6.2×10^{-6}	3.4×10^{5}	2.1	13	4.7×10^{-6}
	80	9.1×10^{-6}	1.0×10^{5}	1.7×10^{-4}	1.1×10^{5}	18.0	2.2×10^{-5}	4.3×10^{4}	1.0	3.7	9.1×10^{-6}
28/420NC*	20	1.6×10^{-9}	5.9×10^{9}	3.9×10^{-8}	2.4×10^{8}	13.6	-	-	-	8.2	1.1×10^{-7}
	30	4.6×10^{-8}	8.3×10^{8}	3.4×10^{-8}	8.1×10^{7}	31.1	-	-	-	0.8	1.8×10^{-7}
	40	2.5×10^{-7}	1.6×10^{9}	1.7×10^{-8}	7.4×10^{6}	5.2	-	-	-	13.7	3.2×10^{-7}
	50	3.2×10^{-7}	1.6×10^{9}	2.8×10^{-7}	6.8×10^{6}	13.6	-	-	-	1.6	4.5×10^{-7}
	60 §	1.7×10^{-6}	4.8×10^{7}	1.2×10^{-6}	3.6×10^{6}	14.9	1.3×10^{-6}	1.5×10^{5}	1.7	19.4	4.8×10^{-6}
	70	1.6×10^{-5}	1.5×10^{5}	1.5×10^{-5}	4.2×10^{4}	26.8	4.0×10^{-5}	7.6×10^{3}	1.9	3.1	8.4×10^{-4}
	80	6.1×10^{-5}	2.0×10^{3}	7.9×10^{-5}	2.1×10^{4}	1.5	-	-		0.2	6.0×10^{-2}
33/400NC*	20	3.1×10^{-7}	2.2×10^{9}	2.0×10^{-7}	1.4×10^{8}	27.4	2.2×10^{-7}	4.6×10^{6}	1.0	25	3.1×10^{-7}
	30	8.3×10^{-7}	1.8×10^{9}	3.2×10^{-7}	1.2×10^{8}	39.4	9.8×10^{-8}	2.2×10^{7}	2.1	15	8.3×10^{-7}
	40	1.7×10^{-6}	5.3×10^{8}	8.8×10^{-7}	3.5×10^{7}	30.9	6.4×10^{-7}	2.4×10^{6}	1.5	9.5	1.7×10^{-6}
	50	5.3×10^{-6}	1.4×10^{8}	6.4×10^{-6}	4.9×10^{6}	31.8	4.5×10^{-6}	6.4×10^{5}	2.9	15	5.3×10^{-6}
	60 §	2.0×10^{-5}	1.3×10^{6}	1.8×10^{-4}	2.6×10^{5}	47.3	3.1×10^{-5}	1.5×10^{5}	4.8	4.4	2.0×10^{-5}
	70	1.7×10^{-5}	8.5×10^{3}	4.2×10^{-4}	4.3×10^{4}	17.8	3.5×10^{-5}	2.2×10^{4}	0.8	0.77	1.7×10^{-5}

Table 17 continued

Adhesive	Temperature (°C)	J_0 (Pa^{-1})	η_0 (Pa s)	J_1 (Pa^{-1})	η_1 (Pa s)	τ_1 (s)	J_2 (Pa^{-1})	η_2 (Pa s)	τ_2 (s)	S.E.	J_r (Pa^{-1})
28/400XL	20	1.8×10^{-7}	7.1×10^{9}	4.2×10^{-8}	3.1×10^{8}	13.0	1.6×10^{-8}	4.6×10^{7}	0.7	14	1.8×10^{-7}
	30	2.8×10^{-7}	5.0×10^{9}	5.5×10^{-8}	3.2×10^{8}	17.4	-	-	-	6.9	2.8×10^{-7}
	40	4.1×10^{-7}	3.2×10^{9}	7.9×10^{-8}	2.0×10^{8}	16.3	-	-	-	8.5	4.1×10^{-7}
	50	6.3×10^{-7}	1.6×10^{9}	2.3×10^{-7}	1.6×10^{7}	18.0	-	-	-	16.2	6.3×10^{-7}
	60	1.6×10^{-6}	2.8×10^{8}	1.1×10^{-6}	4.3×10^{7}	30.7	-	-	-	21	1.6×10^{-6}
	70	1.6×10^{-5}	2.1×10^{7}	8.2×10^{-5}	1.3×10^{6}	23.9	2.2×10^{-5}	1.2×10^{5}	2.6	12	1.6×10^{-5}
	80	2.4×10^{-5}	5.9×10^{3}	3.1×10^{-4}	1.9×10^{5}	10.1	-	-	-	0.89	2.4×10^{-5}
28/2500XL	20	2.0×10^{-7}	6.9×10^{9}	9.6×10^{-8}	2.4×10^{8}	13.1	-	-	-	22	2.0×10^{-7}
	30	3.0×10^{-7}	3.4×10^{9}	9.9×10^{-8}	3.6×10^{8}	35.9	5.5×10^{-8}	4.7×10^{7}	2.6	7.6	3.0×10^{-7}
	40	6.8×10^{-7}	2.4×10^{9}	2.1×10^{-7}	1.0×10^{8}	20.9	-	-	-	12	6.8×10^{-7}
	50	8.8×10^{-7}	7.5×10^{8}	3.8×10^{-7}	5.1×10^{7}	19.5	8.6×10^{-7}	7.7×10^{5}	0.7	20	8.8×10^{-7}
	60 §	7.0×10^{-6}	2.0×10^{8}	2.2×10^{-6}	1.1×10^{7}	24.7	1.5×10^{-6}	1.1×10^{6}	1.7	10	7.0×10^{-6}
	70	1.1×10^{-4}	5.0×10^{4}	3.4×10^{-3}	1.7×10^{4}	57.5	6.1×10^{-4}	7.1×10^{3}	4.3	4.9	1.3×10^{-4}
	75	4.5×10^{-4}	1.7×10^{3}	5.4×10^{-3}	1.0×10^{4}	55.6	5.6×10^{-4}	1.0×10^{4}	5.8	0.95	1.2×10^{-4}
33/400XL	20	3.0×10^{-7}	3.4×10^{9}	1.0×10^{-7}	1.8×10^{8}	18.9	-	-	-	7.5	3.0×10^{-7}
	30	3.6×10^{-7}	2.8×10^{9}	1.7×10^{-7}	1.5×10^{8}	24.8	7.7×10^{-8}	2.1×10^{7}	1.6	12	3.6×10^{-7}
	40	5.1×10^{-7}	9.5×10^{8}	2.7×10^{-7}	6.6×10^{7}	17.7	1.3×10^{-7}	6.6×10^{6}	0.87	14	5.1×10^{-7}
	50 §	1.3×10^{-6}	4.7×10^{8}	8.6×10^{-7}	3.3×10^{7}	27.9	2.7×10^{-7}	5.4×10^{6}	1.5	10	1.3×10^{-6}
	60	6.4×10^{-6}	5.9×10^{7}	1.0×10^{-5}	3.1×10^{6}	31.5	4.7×10^{-6}	6.3×10^{5}	3.0	9.1	6.4×10^{-6}
	70	8.3×10^{-6}	3.6×10^{4}	2.2×10^{-4}	7.1×10^{4}	15.6	2.3×10^{-5}	2.8×10^{4}	0.7	2.0	8.3×10^{-6}
	75	2.1×10^{-5}	1.3×10^{4}	2.7×10^{-4}	4.9×10^{4}	13.4	-	-	-	1.7	2.1×10^{-5}

(a) J_0, η_0 are initial compliance and zero shear viscosity respectively. J_i, η_i, and τ_i refer to the compliance, viscosity, and relaxation time of the *i* th Voigt/Kelvin (V/K) unit. S.E. is standard error of model fitting. See Fig 43 for further explanation of properties.

(b) Each value is the average of at least two runs and two model fitting attempts.

(c) § denotes sample reanalysed with two V/K units after initial model fit of three V/K units. See Chapter 5 for details.

Table 18 Creep properties of adhesive components as determined by controlled stress rheometry[a, b]

Material	Temperature (°C)													
	20		30		40		50		60		70		80	
	J_0 ($10^{-7}Pa^{-1}$)	η_0 (10^9Pa s)	J_0 ($10^{-7}Pa^{-1}$)	η_0 (10^9Pa s)	J_0 ($10^{-7}Pa^{-1}$)	η_0 (10^9Pa s)	J_0 ($10^{-7}Pa^{-1}$)	η_0 (10^9Pa s)	J_0 ($10^{-6}Pa^{-1}$)	η_0 (10^8Pa s)	J_0 ($10^{-5}Pa^{-1}$)	η_0 (10^6Pa s)	J_0 ($10^{-6}Pa^{-1}$)	η_0 (10^4Pa s)
14/2500NC	0.16	18.30	1.17	11.00	1.85	9.42	2.62	5.74	0.42	30.80	0.20	627.00	43.20	3.24
19/150NC	0.80	24.00	1.13	11.10	1.56	10.20	4.10	5.11	0.30	41.40	0.08	1640.00	7.47	2320.00
28/7NC	1.73	14.80	2.22	7.63	3.23	7.16	4.00	6.26	0.62	18.00	0.25	91.90	6.35	71.80
28/25NC	1.60	14.40	2.36	4.93	3.28	3.99	4.74	2.33	0.95	8.33	0.55	12.80	8.82	20.20
28/40NC	2.46	8.33	2.98	5.33	5.18	2.19	7.70	1.63	1.81	4.19	1.02	4.35	6.52	6.48
28/145NC	2.41	9.11	3.34	4.10	5.20	1.62	8.75	0.86	2.67	2.29	1.99	0.47	7.63	3.73
28/400NC	2.14	9.43	3.03	4.15	6.09	2.11	11.20	0.94	3.74	1.86	3.01	0.07	61.40	0.37
28/2500NC	4.28	1.98	8.11	9.19	0.18	0.42	44.70	0.11	28.70	0.08	1.14	0.001	15.20	0.03
28/40NC*	1.40	5.72	2.04	4.64	3.07	3.92	5.06	1.62	0.99	5.83	0.47	14.30	9.11	10.10
28/420NC*	1.62	6.52	2.97	3.99	4.24	3.14	9.85	0.89	1.74	2.34	2.08	0.11	58.60	0.61
33/400NC*	3.06	2.20	8.26	1.78	0.17	0.53	52.90	0.14	19.70	0.01	1.75	0.01	0.21	0.52
28/400XL	1.77	7.11	2.80	5.03	4.05	3.16	6.32	1.60	1.57	2.80	1.62	21.10	23.80	0.59
28/2500XL	2.03	6.85	2.98	3.36	6.78	2.39	8.77	0.75	0.97	2.03	10.90	0.05	104.00	0.17
33/400XL	3.04	3.43	3.62	2.75	5.07	0.95	12.60	0.47	6.37	0.59	0.83	0.04	21.40	1.28
Resin	ND[c]	ND	0.14	9.55	0.11	9.48	0.02	0.64	0.51	0.01	9.78	0.006	147.70	0.02
Wax	9.57	9.53	9.12	9.60	8.51	9.29	370.00	0.006	283.2	6.5×10^2	46.60	1.1×10^2	447.5	1.5×10^0

(a) J_0, η_0 are initial compliance and zero shear viscosity respectively. See Fig 43 for further explanation of properties.
(b) Each value is the average of at least two runs and two model fitting attempts.
(c) ND = not determined

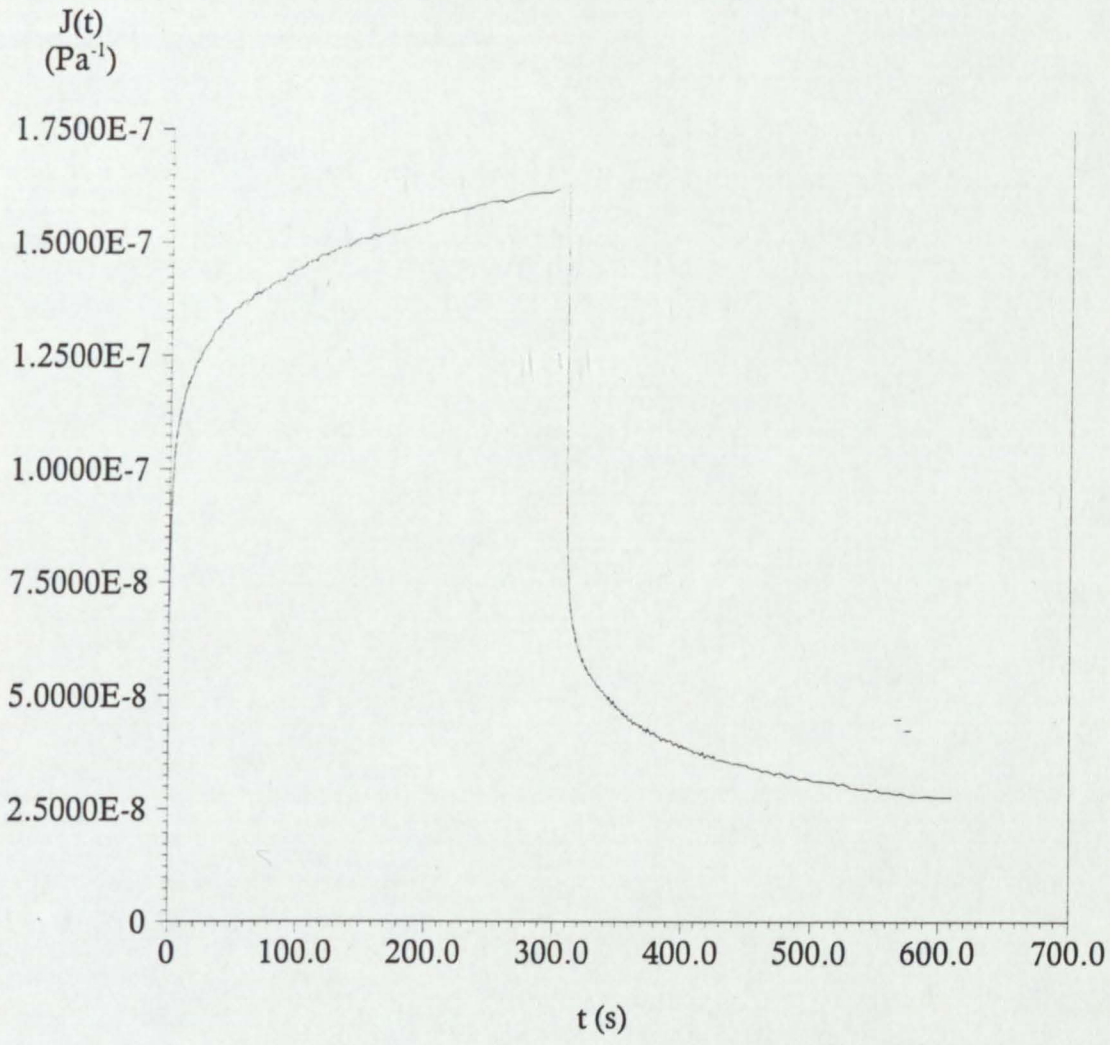

Fig 51. Rheogram showing creep compliance J(t) as a function of time t. ADH 28/145NC. 8 mm parallel plate. Temperature 20°C. Applied stress equal to 1% of G* at test temperature (181 000 Pa).

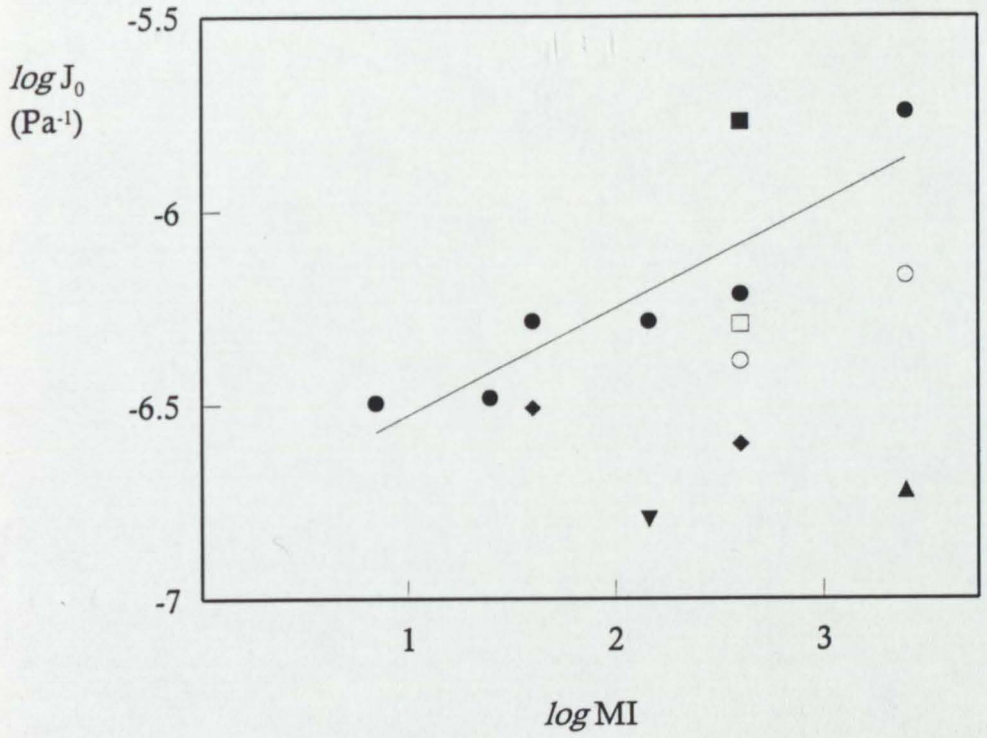

Fig 52. Graph showing the variation of the initial creep compliance J_0 as a function of the logarithm of the polymer melt index MI. Note the use of logarithmic scales on both axes. Regression lines are for adhesives containing Exxon ExUL EVAs of composition 28%VA and are given for the sake of clarity. See text for details. Symbols: ▲ 14/2500NC; ▼ 19/150NC; ● 28% VA; ○ 28% VA XL; ■ 33/400NC*; □ 33/400XL; ◆ 28% VA NC*

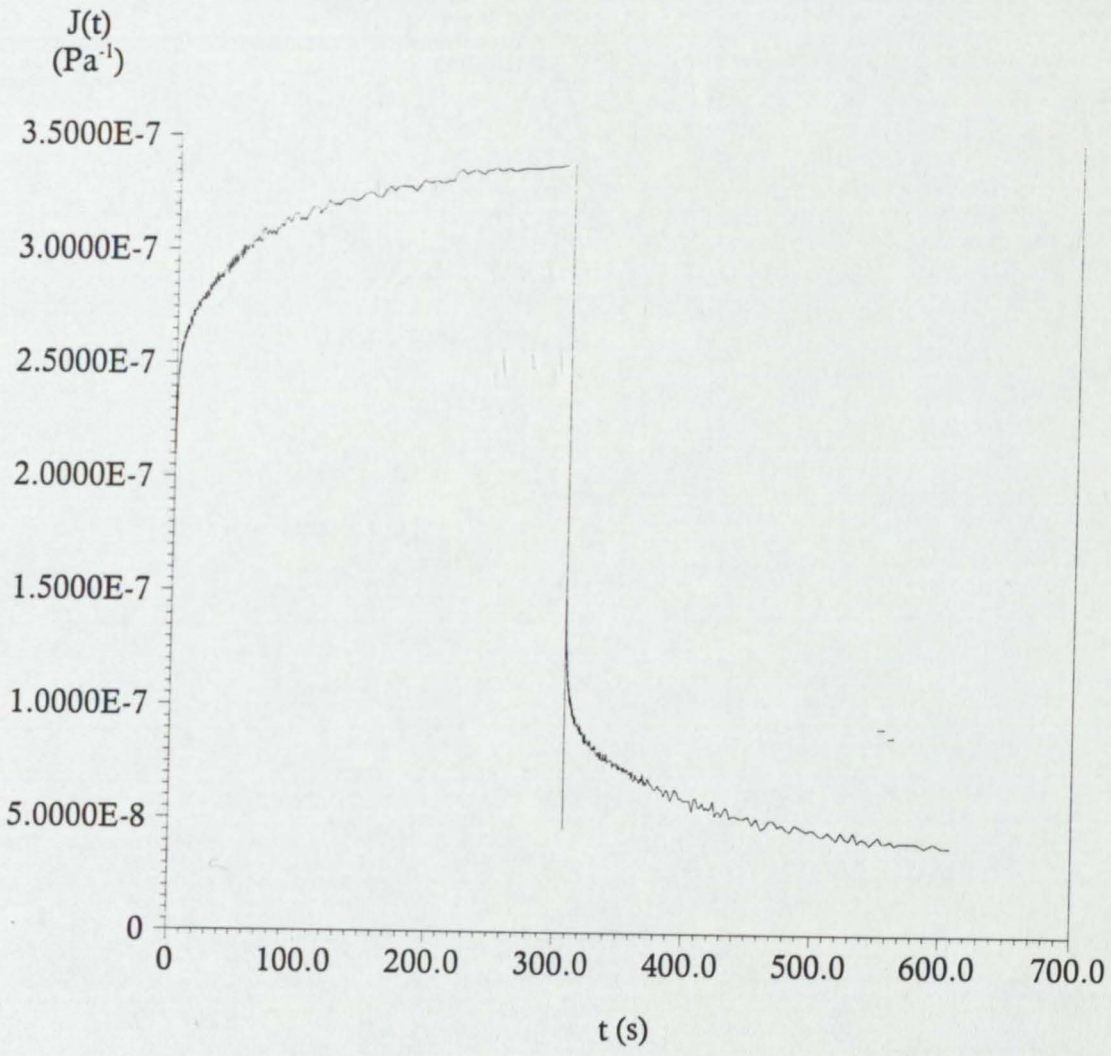

Fig 53. Rheogram showing creep compliance J(t) as a function of time t. EVA 28/400NC. 8 mm parallel plate. Temperature 20°C. Applied stress equal to 1% of G* at test temperature (55 680 Pa).

Table 19 Open time and setting time of adhesives obtained from the Kanebo bond tester[a]

Adhesive	Open time (s)	Setting time (s)
14/2500NC	10.0	4.0
19/150NC	12.0	3.0
28/7NC	6.0	5.0
28/25NC	8.0	6.0
28/40NC	9.0	6.0
28/145NC	8.0	6.0
28/400NC	7.5	5.0
28/2500NC	7.0	4.5
28/40NC*	10.0	4.0
28/420NC*	7.0	5.0
33/400NC*	7.0	6.0
28/400XL	6.0	6.0
28/2500XL	9.0	7.0
33/400XL	4.0	7.0

(a) Each value is the average of five tests.

time is less clear, but it does appear that the influence of the amount of vinyl acetate is opposite to that observed with the open time, and as the concentration increases, the setting time generally increases.

4.5 Strength of the adhesives and adhesive joints

Typical deformation behaviour of the adhesives tested in tension in shown in Fig 54, and the results for all the adhesives are given in Table 20. The results presented are to some extent a matter of choice and the ones given were selected to give a full impression and information on the essentially weak and ductile behaviour of the adhesives. At least three specimens were tested under each condition and the average value is given in the table. The scatter varied with the test speed and the property and is not considered further. Although some of the results followed a pattern that might be expected from an increase in the strain rate of a viscoelastic material, *i.e.* there would be less time for the viscous component to operate many do not show such simple behaviour. There was a distinct, defined initial linear region (Fig 54) and a slope and Young's modulus were calculated. The modulus generally increases with testing speed, for example, with adhesive 14/2500NC the values were 25, 29, 34, and 52 MPa for test speeds of 0.5, 5, 50 and 500 mm min^{-1} respectively. Figures 55 - 58 illustrate the relationships between Young's Modulus, maximum stress, 1% yield stress, and maximum strain for the adhesive samples for each of the testing speeds (0.5, 5, 50, and 500 mm min^{-1}). Linear regression was attempted on the 28% VA series data (illustrated).

A result for an 180°C peel test is shown in Fig 59 and all the results are given in Table 21. Typical scatter in the fracture load is illustrated by the trace for 28/2500NC, and the value in the table is the average of 3 to 5 tests. The effect of melt index and test speed is also shown for some adhesives in Fig 60.

The peel strength generally increases with an increase in the melt index (Figs 60b - d). This effect may be counter to what is first expected (molecular weight decreases with increasing melt index) however it could be explained by the improved wetting of the aluminium adherend by the molten adhesive (higher melt index EVAs give adhesives with lower melt viscosities). The effect of test

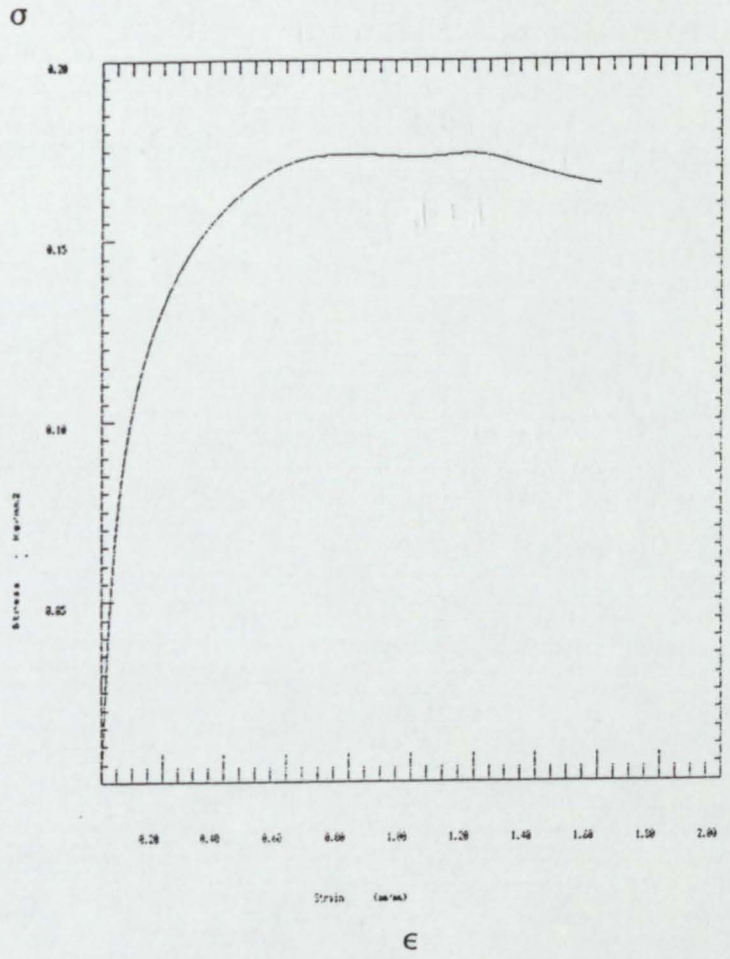

Fig 54. Typical tensile testing trace showing tensile stress σ as a function of strain ϵ. The initial linear region and weak, ductile nature of the adhesive are visible. 28/400NC; 5mm min^{-1} test speed. See text for details.

Table 20 Tensile properties of poly(ethylene-*co*-vinyl acetate) adhesives tested at various test speeds[a]

Adhesive	1% yield stress, σ_y (MPa)				Young's modulus, E_Y (MPa)				Maximum stress, σ_m (MPa)				Strain at fracture, ϵ_f (%)			
	at test speeds, v (mm min^{-1})				at test speeds, v (mm min^{-1})				at test speeds, v (mm min^{-1})				at test speeds, v (mm min^{-1})			
	0.5	5	50	500	0.5	5	50	500	0.5	5	50	500	0.5	5	50	500
14/2500NC	0.69	0.99	1.31	0.76	29	30	34	52	1.9	2.6	2.3	3.5	104	115	70	62
19/150NC	0.74	0.87	1.47	0.53	31	31	33	60	2.3	2.1	2.3	4.5	1500	416	267	155
28/7NC	0.58	1.04	1.38	0.44	24	26	29	60	2.2	2.3	2.3	3.7	1500	598	354	561
28/25NC	0.67	0.73	0.89	0.28	18	19	27	42	2.0	2.2	2.9	3.0	1500	465	939	567
28/40NC	0.57	0.60	0.83	0.30	26	25	27	29	2.1	2.0	2.8	3.4	1500	235	780	1127
28/145NC	0.65	0.85	1.05	0.89	23	23	26	35	1.8	1.9	2.2	2.3	1360	558	880	394
28/400NC	0.60	0.72	0.79	0.27	20	21	21	29	1.7	1.6	1.6	2.0	1500	526	538	315
28/2500NC	0.46	0.53	0.60	0.75	12	14	15	19	1.1	1.1	1.0	1.3	143	156	94	150
28/40NC*	0.49	0.74	0.95	0.85	16	17	18	26	1.8	1.7	2.9	2.6	1500	672	979	771
28/420NC*	0.62	0.74	0.80	1.31	17	17	20	28	1.8	1.6	1.7	1.9	1500	437	445	269
33/400NC*	0.36	0.44	0.54	0.75	18	19	15	18	0.9	1.2	1.1	1.1	1500	517	869	320
28/400XL	0.60	0.88	1.00	0.62	18	17	19	38	1.8	2.0	2.3	2.5	1500	484	538	348
28/2500XL	0.45	0.57	0.79	0.30	12	14	16	28	1.2	1.1	1.3	1.9	133	160	141	141
33/400XL	0.62	0.64	0.68	0.58	18	17	13	23	1.4	1.3	1.6	1.5	1500	836	771	210

(a) Results presented are average of at least three tests. See text for comments on scatter.

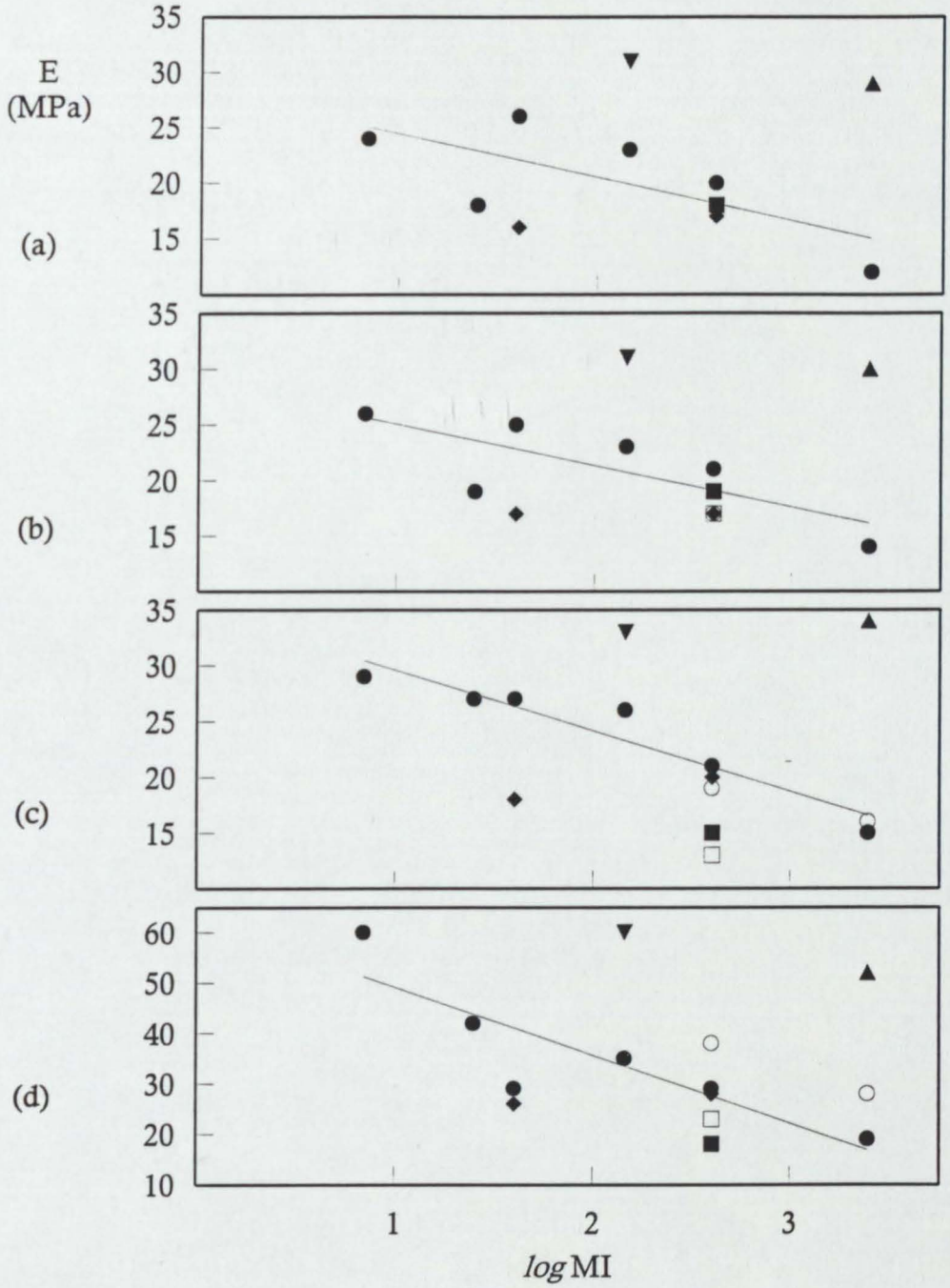

Fig 55. Graph showing the variation in Young's modulus E of the adhesives as a function of the logarithm of the polymer melt index MI at each test speed. (a) 0.5 mm min^{-1}; (b) 5.0 mm min^{-1}; (c) 50 mm min^{-1}; and (d) 500 mm min^{-1}. Regression lines are for adhesives containing Exxon ExUL EVAs of composition 28%VA and are given for the sake of clarity. See text for details. Symbols: ▲ 14/2500NC; ▼ 19/150NC; ● 28% VA; ○ 28% VA XL; ■ 33/400NC*; □ 33/400XL; ◆ 28% VA NC*.

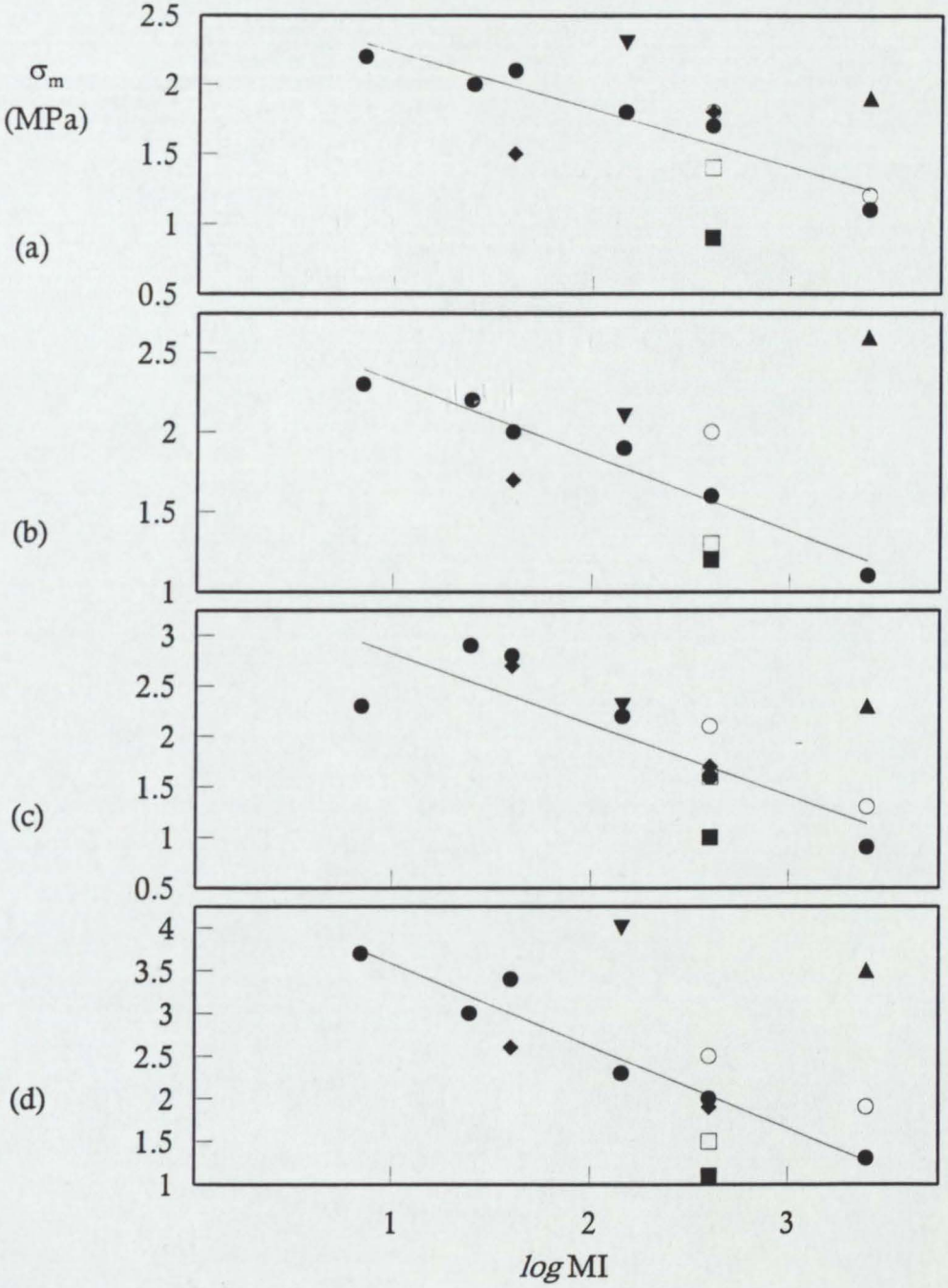

Fig 56. Graph showing the variation in maximum stress σ_m of the adhesives as a function of the logarithm of the polymer melt index MI at each test speed. (a) 0.5 mm min^{-1}; (b) 5.0 mm min^{-1}; (c) 50 mm min^{-1}; and (d) 500 mm min^{-1}. Regression lines are for adhesives containing Exxon ExUL EVAs of composition 28%VA and are given for the sake of clarity. See text for details. Symbols: ▲ 14/2500NC; ▼ 19/150NC; ● 28% VA; ○ 28% VA XL; ■ 33/400NC*; □ 33/400XL; ◆ 28% VA NC*.

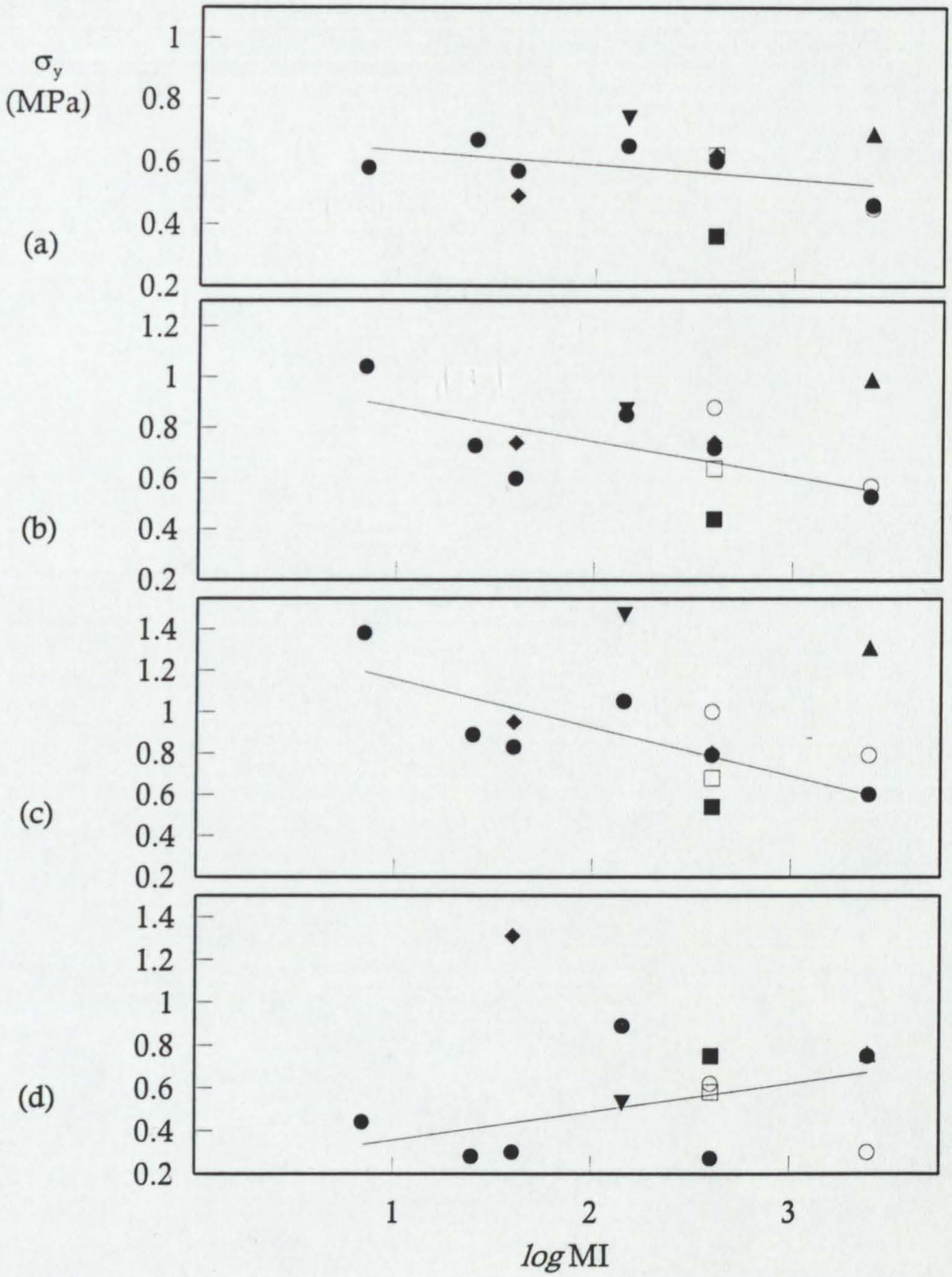

Fig 57. Graph showing the variation in 1% yield stress σ_y of the adhesives as a function of the logarithm of the polymer melt index MI at each test speed. (a) 0.5 mm min^{-1}; (b) 5.0 mm min^{-1}; (c) 50 mm min^{-1}; and (d) 500 mm min^{-1}. Regression lines are for adhesives containing Exxon ExUL EVAs of composition 28%VA and are given for the sake of clarity. See text for details. Symbols: ▲ 14/2500NC; ▼ 19/150NC; ● 28% VA; ○ 28% VA XL; ■ 33/400NC*; □ 33/400XL; ◆ 28% VA NC*.

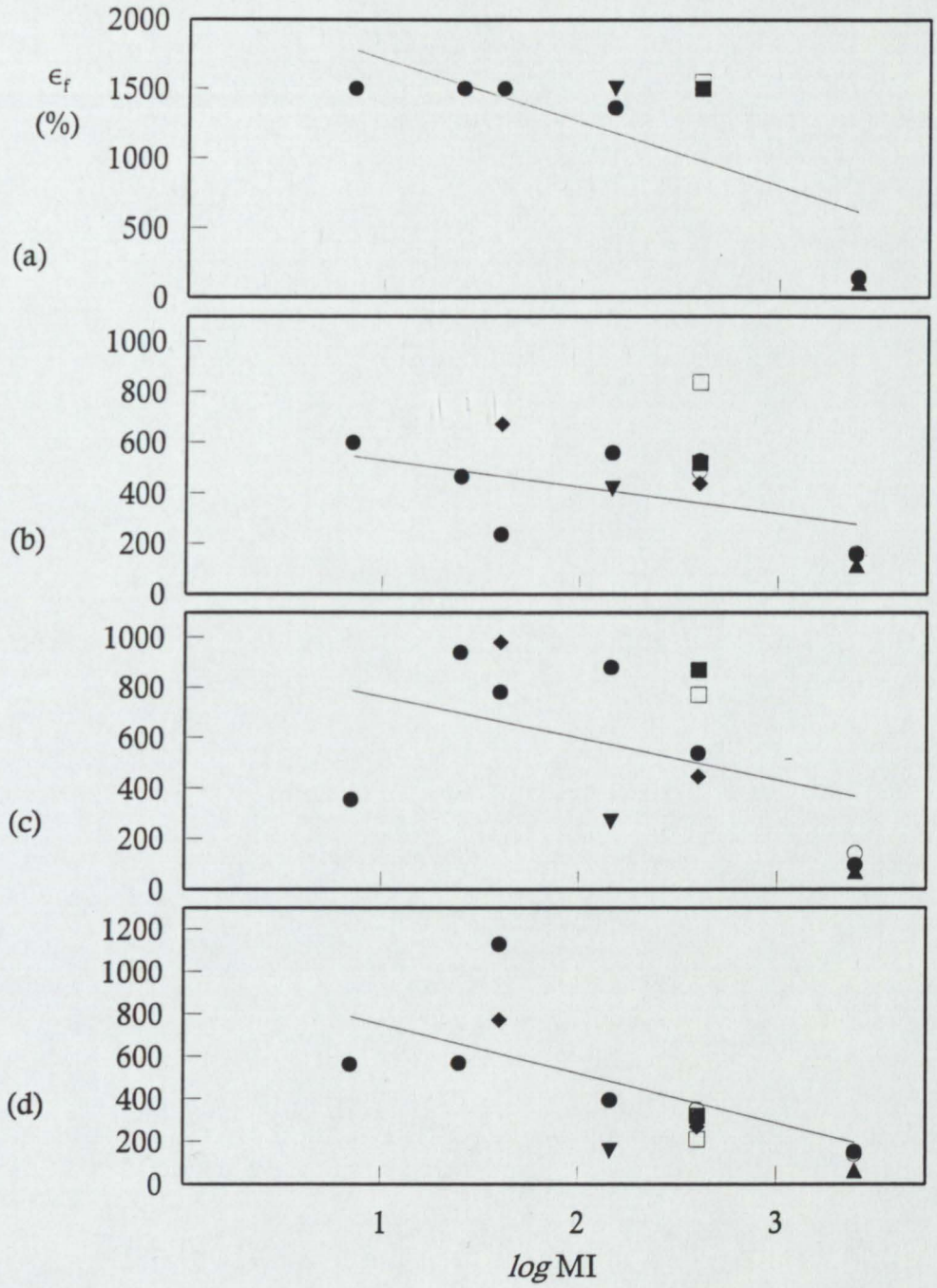

Fig 58. Graph showing the variation in maximum strain ϵ_f of the adhesives as a function of the logarithm of the polymer melt index MI at each test speed. (a) 0.5 mm min^{-1}; (b) 5.0 mm min^{-1}; (c) 50 mm min^{-1}; and (d) 500 mm min^{-1}. Regression lines are for adhesives containing Exxon ExUL EVAs of composition 28%VA and are given for the sake of clarity. See text for details. Symbols: ▲ 14/2500NC; ▼ 19/150NC; ● 28% VA; ○ 28% VA XL; ■ 33/400NC*; □ 33/400XL; ◆ 28% VA NC*.

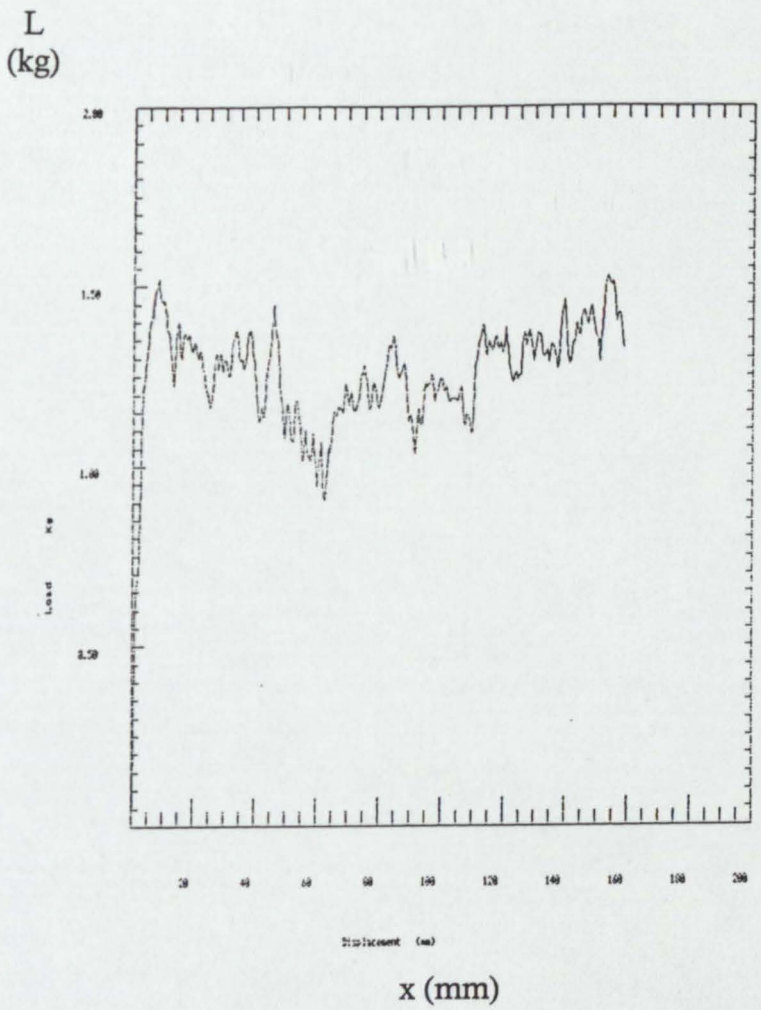

Fig 59. Typical result from a peel test showing peel load at fracture P as a function of crosshead displacement x. ADH 28/2500NC; 500 mm min^{-1} test speed. See Table 12.

Table 21 Load at fracture P and failure mode FM of adhesive peel joints tested at various test speeds[a]

Adhesive	Test speed, v (mm min^{-1})											
	0.5			5			50			500		
	P (g)	sd (g)	FM[b]	P (g)	sd (g)	FM	P (g)	sd (g)	FM	P (g)	sd (g)	FM
14/2500NC	22.0	5.4	coh	22.8	2.7	coh	27.7	3.0	coh	29.2	2.7	coh
19/150NC	37.7	4.3	adh	39.4	3.1	adh	44.6	3.5	mix	49.8	4.2	mix
28/7NC	66.4	3.3	adh	48.2	4.2	adh	54.2	3.9	adh	52.7	4.3	adh
28/25NC	36.6	5.7	adh	38.3	5.0	adh	58.6	3.6	adh	53.2	4.7	adh
28/40NC	49.6	4.2	adh	56.7	3.9	adh	55.0	4.2	adh	54.1	4.9	adh
28/145NC	57.6	3.6	adh	60.1	4.5	adh	63.7	4.1	adh	57.7	5.3	mix
28/400NC	58.0	3.6	adh	65.0	4.3	adh	68.6	4.7	adh	60.8	4.8	adh
28/2500NC	45.1	3.9	coh	63.1	3.7	coh	67.4	3.6	mix	64.7	4.4	adh
28/40NC*	23.1	2.4	adh	44.9	2.2	adh	38.2	3.2	adh	46.8	2.8	adh
28/420NC*	56.0	4.2	adh	65.5	4.0	adh	56.3	4.5	adh	54.5	5.1	adh
33/400NC*	60.1	5.2	mix	57.9	4.6	mix	52.5	5.0	adh	54.0	4.1	adh
28/400XL	25.2	3.3	adh	29.7	3.3	adh	47.7	3.4	adh	37.8	2.9	mix
28/2500XL	36.3	3.1	coh	39.4	3.2	coh	38.0	2.8	coh	41.0	3.1	coh
33/400XL	44.7	4.7	adh	45.3	4.4	adh	51.5	3.3	adh	46.1	3.7	adh

(a) The load is for a specimen 25mm wide. Five joints were tested at each condition and average load P is given along with standard deviation sd.

(b) The failure mode FM is given as cohesive coh, adhesive adh, and mixed cohesive and adhesive mix. See text for details.

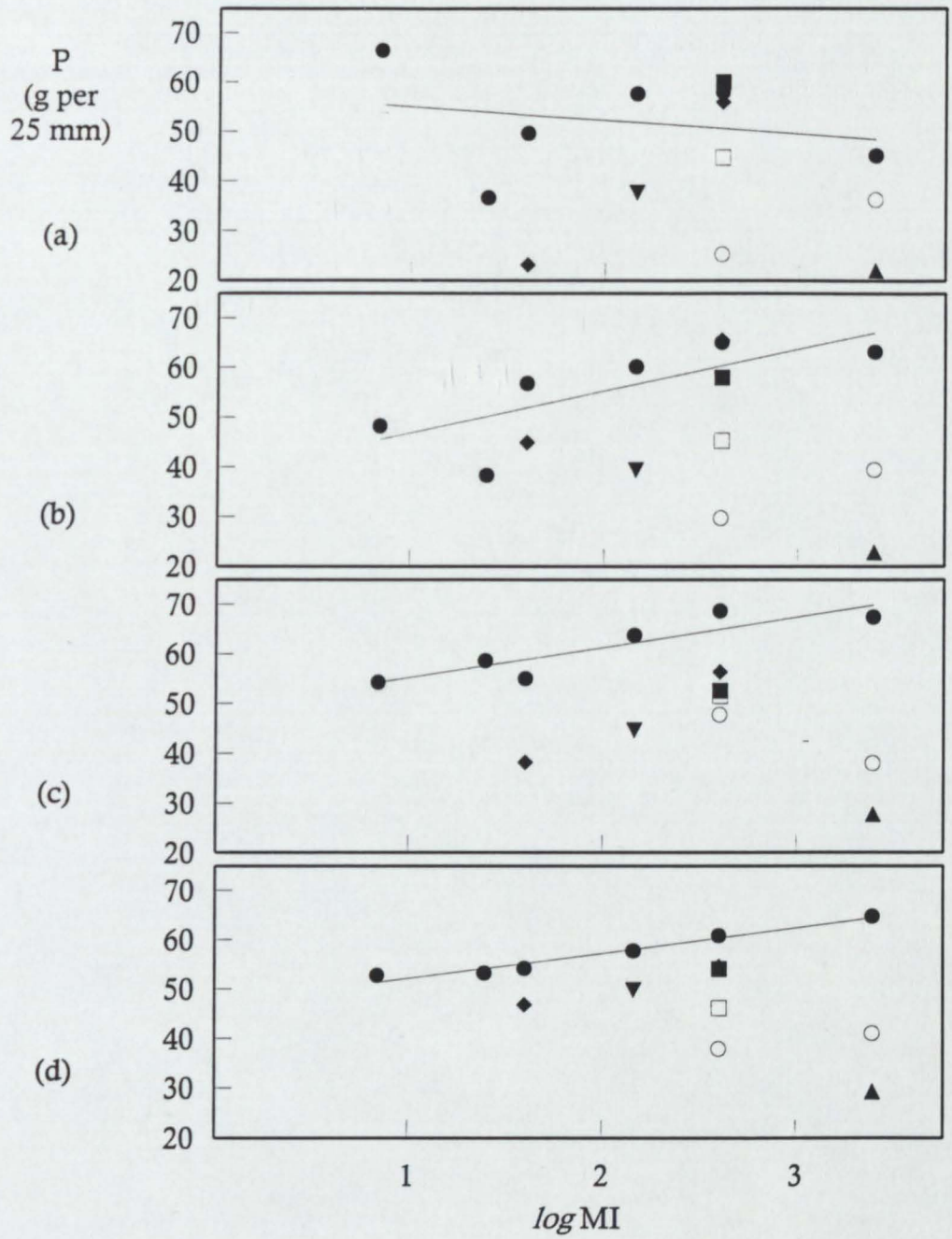

Fig 60. Graphs showing variation of peel strength P as a function of the logarithm of the polymer melt index MI at four different test speeds: (a) 0.5 mm min^{-1}; (b) 5.0 mm min^{-1}; (c) 50 mm min^{-1}; and (d) 500 mm min^{-1}. Note units of peel strength are g per 25 mm width of bond. Symbols: ▲ 14% VA; ▼ 19% VA; ● 28% VA NC; ○ 28% VA XL; ■ 33% VA; □ 33% VA XL; ◆ 28% VA NC*.

speed on the peel strength of the 28%VA adhesive is also shown. In general the peel increased from 0.5 to 50 min min^{-1} and then decreased as the test speed increases to 500 mm^{-1}. However there are a few exceptions, most noticeably 28/7NC (which shows decreasing peel strengths with increased speed of testing) and 28/40NC which displays a maximum at 5 mm min^{-1}. The 28/40NC* sample also has this tendancy to exhibit a maximum at 5 mm min^{-1}. If the grades with different levels of vinyl acetate content are examined, two different effects may be observed. The low %VA grades (14/2500NC and 19/150NC) do not show maxima at 50 mm min^{-1} but show increases in peel strength continuously with testing speed. In contrast, 33/400NC* shows a decrease in peel strength from 0.5 mm min^{-1} upwards.

The effect of crystallinity appears to be varied. At all testing speeds, the peel strengths are decreased, particularly with the 28%VA grades. In the case of the 400MI adhesives, 28/400XL shows a similar pattern to 28/400NC albeit exaggerated and at lower overall levels of peel strength. However if the 28/2500NC data is compared with that of the 28/2500XL, it can be seen that the crystalline peel strength is practically independant of testing speed although it is significantly lower than that of 28/2500NC. In the 33%VA series, the effect of crystallinity appears to shift the behaviour towards that of a 28%VA series adhesive sample, for example with a maximum at 50 mm min^{-1}.

4.6 Strength of adhesive joints at elevated temperatures

Five specimens were tested for each adhesive joint for the shear adhesive failure temprature (SAFT) and the peel adhesion failure temperature (PAFT). The average values are given in Table 22. The time to fail at each temperature is also given. The results are considered to be accurate to well within 4°C, and with the present limited range of temperatures only the broadest of patterns may be distinguished. In general, both the SAFT and PAFT temperatures show a decrease in resistance to heat as the melt index increases. The time for melt indices up to and including 40 is relatively high compared with the lower time observed for adhesive with melt indices above 40.

Table 22 Shear adhesion failure temperatures and peel adhesion failure temperatures of adhesive joints[a]

Adhesive	Shear adhesion failure		Peel adhesion failure	
	Temperature, SAFT	time[b]	Temperature, PAFT	time
	(°C)	(min:sec)	(°C)	(min:sec)
14/2500NC	70.0	19:30	55.0	11:00
19/150NC	79.0	31:00	55.0	16:00
28/7NC	73.0	25:15	57.5	16:30
28/25NC	71.5	23:45	60.0	17:00
28/40NC	69.5	19:15	60.0	18:00
28/145NC	68.5	18:15	55.0	11:00
28/400NC	68.0	18:15	49.0	9:30
28/2500NC	67.0	17:00	55.0	11:15
28/40NC*	70.0	19:30	60.0	18:00
28/420NC*	69.0	18:00	55.0	11:00
33/400NC*	67.0	16:15	55.0	11:30
28/400XL	69.0	18:30	55.0	13:30
28/2500XL	67.5	17:00	55.0	11:00
33/400XL	67.0	17:00	47.5	8:00

(a) Results presented are the average of five test specimens.
(b) Time to failure since the commencement of the test.

Chapter 5 - Discussion and Conclusions

CHAPTER FIVE

DISCUSSION AND CONCLUSIONS

It has been emphasised in the literature survey that the scientific development of hot melt adhesives has been severely limited by the gulf between the firmly established complex industrial practices and the meagre scientific foundations. This has necessitated in the present work, a detailed characterisation of the ingredients and a systematic formulation of the adhesives. On this basis we first discuss the thermal properties and the characterisation of the materials. Next we discuss fully the rheological properties of the adhesives. This then leads to a detailed discussion of the strength of adhesive joints and models describing the properties of the adhesives and joints. Finally we present the conclusions and suggestions for future work.

5.1 Thermal properties and characterisation of materials

A major feature of the present work is that the properties of the adhesives have been measured as a systematic function of the poly(ethylene-*co*-vinyl acetate) copolymer (EVA) properties, namely the melt index, vinyl acetate concentration, and degree of crystallinity. Since commercially available substances were to be used, this placed limitations on the selection of suitable copolymers. In the event, it was possible to obtain, from one manufacturer, samples containing 28% vinyl acetate with six melt indices ranging from 7 to 2 500. These provided the core of the studies. It was also possible to obtain, for comparison, samples with the same melt indices and different amounts of vinyl acetate, and samples with the same melt indices and vinyl acetate concentration with the normal low crystallinity and also in a higher crystallinity version. Unfortunately, to complete the comparisons it was necessary to use three materials from a second manufacturer. While these samples had the required nominal composition, melt index, and crystallinity, there was now present the possible influence of other factors like the nature of the side chain branching on

the properties [11, 189], and this aspect had to be kept fully in mind.

There have been relatively few systematic studies on the properties of hard-setting hot melt adhesives, and most of these have either been qualitative statements *e.g.* [152], or appeared to have deficiencies in the experimental techniques employed. Nowhere was this more evident than in the use of differential scanning calorimetry (DSC). Some of the techniques used by previous workers [12, 88, 190] did not appear to pay sufficient attention to the scan conditions, which enable the more subtle changes and differences in the polymers and adhesives to be measured. The effect of sample size, thermal history, heating and/or cooling rate, baseline selection, and choice of atmosphere have been determined and critically assessed in Section 3.2 and will not be discussed further. It is clear from results and discussions on the experimental techniques, that despite a critical attention to controlling the experimental variables there must necessarily remain an element of uncertainty from such factors as the unambiguous display of a feature on the thermogram, or the interpretation of the feature, *e.g.* in the latter case, selection of the baseline in determining the glass transition. Although ideally to obtain the most sensitive detection and analysis of a thermochemical change it is necessary to finely tune the test conditions for each material, in the present work it was considered important that the same conditions were used so that an effect observed in each different material could be related to systematic changes in the material. Within these constraints and with the purposes of the present work in mind, the enthalpies of melting and crystallisation, the temperature of the largest melting/crystallisation peak, and the locations of the midpoint glass transition temperature, were considered to be of primary importance and use, and are here discussed in detail. Several other features of the thermograms have also been considered in detail, but their significance in the present work is such that only a summary comment on them is given.

The semi-crystallinity of the EVA samples is clearly identified by the presence of a major well-defined crystallisation/melting peak and the wide freezing/melting range associated with the behaviour of the non-crystalline material (Fig 61). In general the melting and crystallisation peaks are broad,

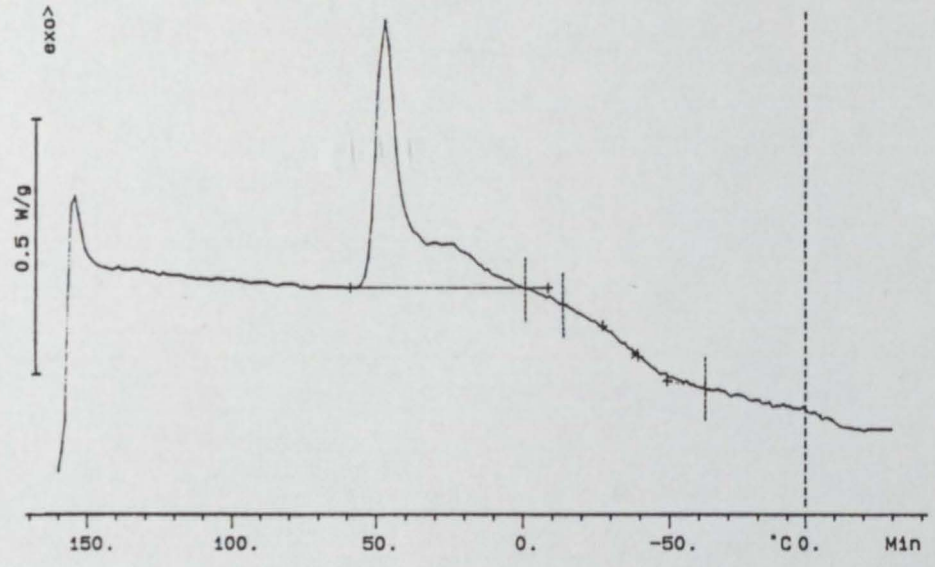

(a)

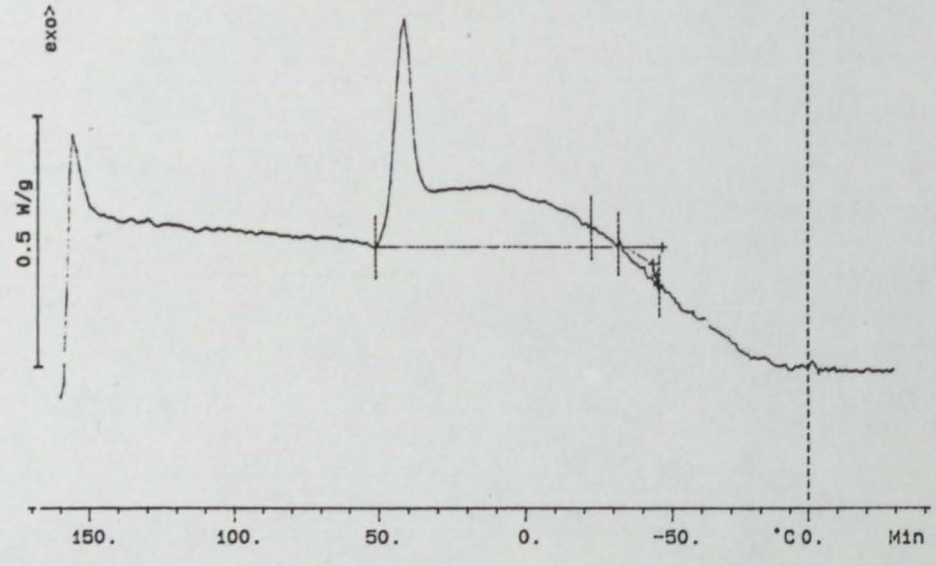

(b)

Fig 61. Thermograms showing heat flow as a function of sample temperature during cooling of two EVAs of 28%VA composition. Melt indices of the polymers are (a) 7 and (b) 2 500. Both polymers are from the Exxon ExUL series.

melting starting around -20°C and continuing up to 60 - 80°C (depending upon grade). Crystallisation starts around 60 to 50°C and finishes at approximately 0°C. The temperature, height, and breadth, of the main peak changes with the MI, but the effects are small and sometimes the interpretation is contentious. For example, there appears to be no relationship between peak height and amount of crystallinity in the present work despite vague suggestions that have been made elsewhere that this may be the case for some polymer systems [190]. It has been suggested that the position of the peak may be related to the open time of the adhesive and this point is considered later in section 5.3. The characterisation and significance of the small extra peak at a lower temperature is indicative of the semi-crystalline nature of the copolymer. This manifestation of a multiple melting phenomenon has been recorded for other polymers, including poly(ethylene) [191, 192] and is open to a wide interpretation as to its explanation, including partial re-melting and re-crystallisation [193] or crystallite structure [194 - 196]. Bugada and Rudin studied this phenomenon in EVA [11] and hypothesised that the lower peak represents the melting behaviour of stable crystallites and support their argument by quench cooling their samples and observing the disappearance of the minor peak. The essentially semi-crystalline nature of the EVA copolymers is shown clearly in the literature, especially with relation to its spherulitic morphology [197 - 199].

Considerable attention to the experimental techniques is necessary in order to obtain reproducible and meaningful results using differential scanning calorimetry. Nowhere is this more important than in the need to establish a reproducible thermal condition and microstructure of the test specimen. For example, in comparable work on an EVA sample similar to the present 28/420 NC*, Komornicki *et al* [88] used data from the initial heating to demonstrate that so-called equilibrium conditions had been established. However, there was only a vague comment ("a fresh sample") on the condition of the sample prior to the initial scan, and the cooling rate was very rapid. These are in sharp contrast to the careful pre-treatment of the sample and the very low scan rate used in the present work. Both these points are critically important: EVA co-polymers are produced such that they have complex mechanical and thermal treatments;

whilst rapid cooling reduces the amount of crystallinity. The main effect is that in Komornicki's work, the untransformed material crystallised (so-called "re-crystallised") on re-heating, and this masked other transitions and limited the information. In contrast, the re-crystallised peak was absent in the present work due to the fact that the cooling rate used in the present work was much slower. This allowed crystallinity to develop fully during the cooling process, thereby eliminating the potentially misleading, uncontrolled variable from the experimental procedure and subsequent analysis. However, agreement was still generally quite good. For example, melting started at -20°C, reached a maximum at 66°C, and finished at 85°C for sample EVA 28/420NC* and these compare with values of -28°C, 57°C, and 83°C respectively which were reported by Komornicki. These differences again are directly related to the extra amount of untransformed amorphous material in the rapidly cooled specimens.

It has been proposed [200] that crystallisation of copolymers follows a non-equilibrium path whereby the longest segments of the crystallisable component do so first at higher temperatures, whilst shorter segments crystallise at lower temperatures. This is supported by observations that low molecular weight homopolymers melt at lower temperatures than higher molecular weight homopolymers [82, 201, 202]. It is also noted that amorphous phases of a semi-crystalline polymer melt before the crystalline material that is present. We can therefore infer that the difference in maximum melting peak temperature is attributable to the difference in thermal treatment. The exact mechanism cannot be determined. However it is either due to minute spherulites of lower molecular weight material crystallising before higher molecular weight material has a chance to organise into a crystalline structure, or it is due to the lack of any crystallisation occurring at all due to the rapid quenching of the sample used by Komornicki. In either case, it emphasises the strict control needed on the thermal history of the EVA samples during any characterisation.

The enthalpies of melting and crystallisation of the EVA copolymers as a function of MI are shown in Fig 62. It can be seen from the first graph that there is a systematic variation of both ΔH_h and ΔH_c as a function of melt index, *i.e.*

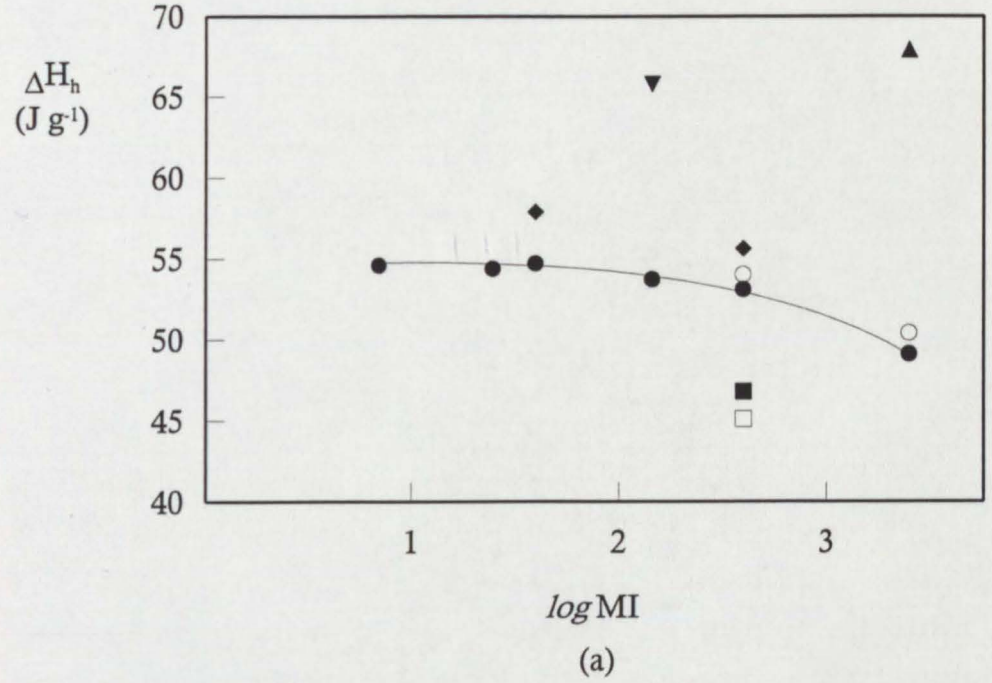

(a)

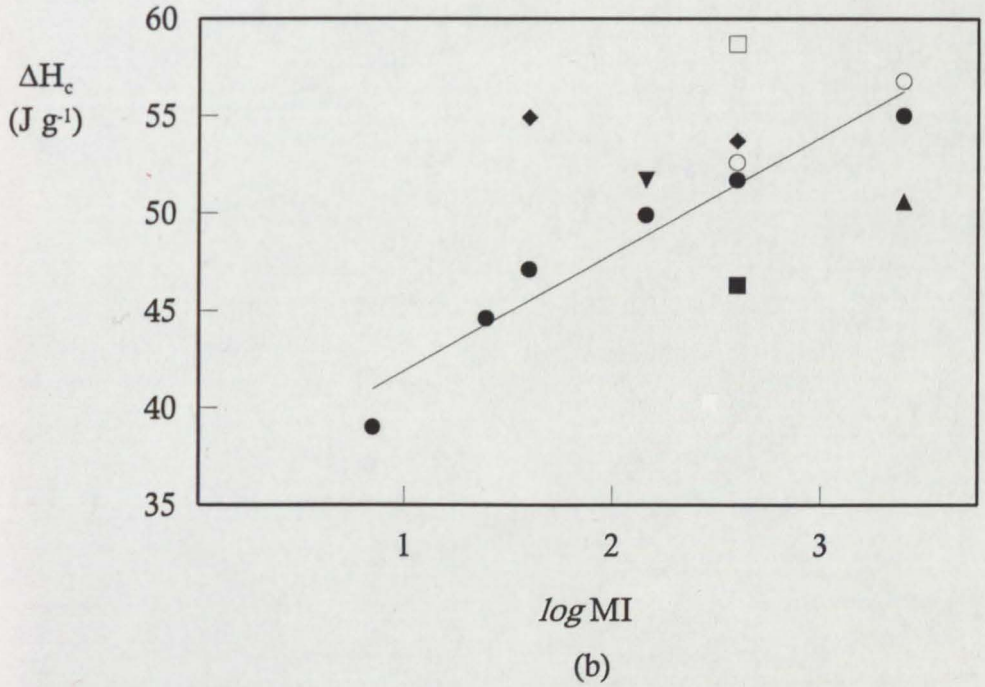

(b)

Fig 62. Graph showing transition enthalpies ΔH_h, ΔH_c on (a) heating and (b) cooling respectively of the polymer as a function of the logarithm of the melt index MI. Symbols: ▲ 14% VA; ▼ 19% VA; ● 28% VA NC; ○ 28% VA XL ■ 33% VA; □ 33% VA XL; ◆ 28% VA NC*.

molecular weight. For melting, the change in ΔH_h for the higher molecular weight polymers (MI less than 150) is not significant, whilst EVAs with MI greater than 150 show a more pronounced effect, with the lowest molecular weight polymers having ΔH_h values approximately 10% lower than the highest. Considering the accuracy of ΔH data this decrease can be considered real but rather small. On cooling the polymers from the melt, the changes in ΔH_c are greater than those described above. There is also a clear trend showing an increase in ΔH_c with reduction in molecular weight. There is an excess of ΔH_h over ΔH_c for all polymers except 28/2500 MI. It is here proposed that these differences reflect the differences in chain morphology and chain mobility during the heating and cooling cycles performed on the DSC. During melting, the long sequences of poly(ethylene) in a high molecular weight polymer fold and rearrange to form a crystalline structure which requires significant amounts of energy to melt. The nature of melting in a highly viscous polymer melt is a slow process in which chain mobility plays a significant part. In a relatively short timescale process, such as the heating scan of a DSC evaluation, the inability of the chains to move apart completely may delay the dissolution of the crystals that are formed in a solid polymer. This rate-dependence is reflected by the apparent independence of ΔH_h and molecular weight, above a certain value of MI. The decrease in ΔH_h with a reduction in molecular weight can be attributable to the greater proportion of free chain ends associated with shorter chains. These chain ends may act to disrupt the regular chain folding and packing sequences and hence reduce the overall amount of crystallinity.

The same factors are equally likely to be responsible for the variation in ΔH_c during cooling scan evaluations. The cooling rate imposed during the DSC experiment gives a specific time for crystallisation to occur. The ability of the chains to reorganise into crystalline structures is governed by the need to disentangle from neighbouring molecules to a greater or lesser degree. This disentanglement takes a longer time in higher molecular weight samples and may not be completed to an equilibrium state during the imposed cooling of the experiment. Conversely, lower molecular weight species may be able to fully rearrange but, as discussed earlier, will not attain such a high degree of packing

due to the greater number of chain ends.

There appears to be an equilibrium melt index at which point there is an equivalence between ΔH_h and ΔH_c. This point (approximately 400 MI) corresponds to a molecular weight M_w of approximately 22 000 g mol^{-1}.

It has been observed in other polymer systems [203], including poly(ethylene), that changes in molecular weight, and molecular weight distribution, affect the crystalline form of the polymeric material in several ways. These can include the formation of different crystal shapes, particularly in single crystals, together with the nature, and amount, of amorphous, *i.e.* non-crystallised, material within the spherulitic structure that forms during cooling from the melt. As discussed earlier, the effect of an increased number of polymer chain ends may reduce the total amount of crystallinity in a solid polymer and evidence supporting this supposition is seen by quantitatively examining the melting peaks taken from the DSC curves. Figure 61 shows the peaks for EVA 28/7NC and EVA 28/2500NC. The lower molecular weight polymer is both shallower and broader which is indicative of a less crystalline material [204].

Figure 63 illustrates the variation in ΔH_h and ΔH_c as a function of EVA copolymer composition. It is immediately apparent that the variation in enthalpy due to composition is much larger and more significant than that attributable to molecular weight. There is a substantial decrease in ΔH_h as the amount of VA increases and, whilst the magnitude is smaller for ΔH_c, the same effect holds upon crystallisation. The spread of ΔH_h results for 28% VA EVAs is less than 5 J g^{-1}, whilst the variation from 14% VA to 33% VA (ignoring differences in manufacturer, crystallinity, or molecular weight) is over four times greater (22.8 J g^{-1}). The lines on Fig 63a are used to illustrate the trends discussed above and join copolymers of similar molecular weight. The trends are in the same direction for all molecular weights, manufacturers, and crystallinities and can be combined into a single broad trend as shown in Fig 63b. The vinyl acetate group in an EVA copolymer is bulky compared to the compact ethylene backbone and acts to stearically hinder the alignment of the molecules required for the formation of crystalline structures.

One significant observation is that the change in ΔH_h attributable to an

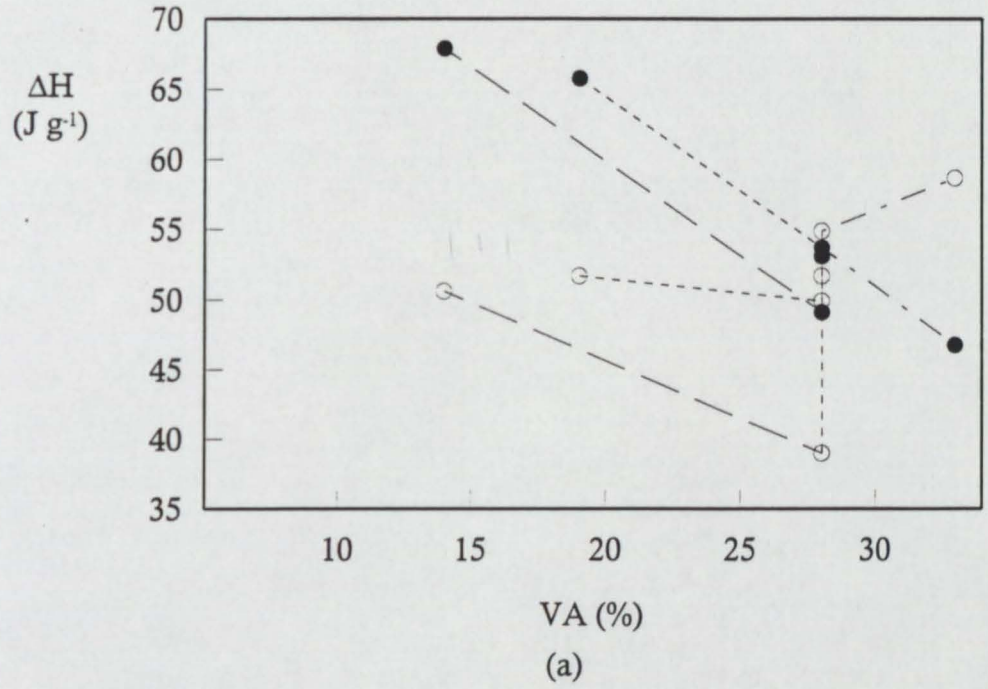

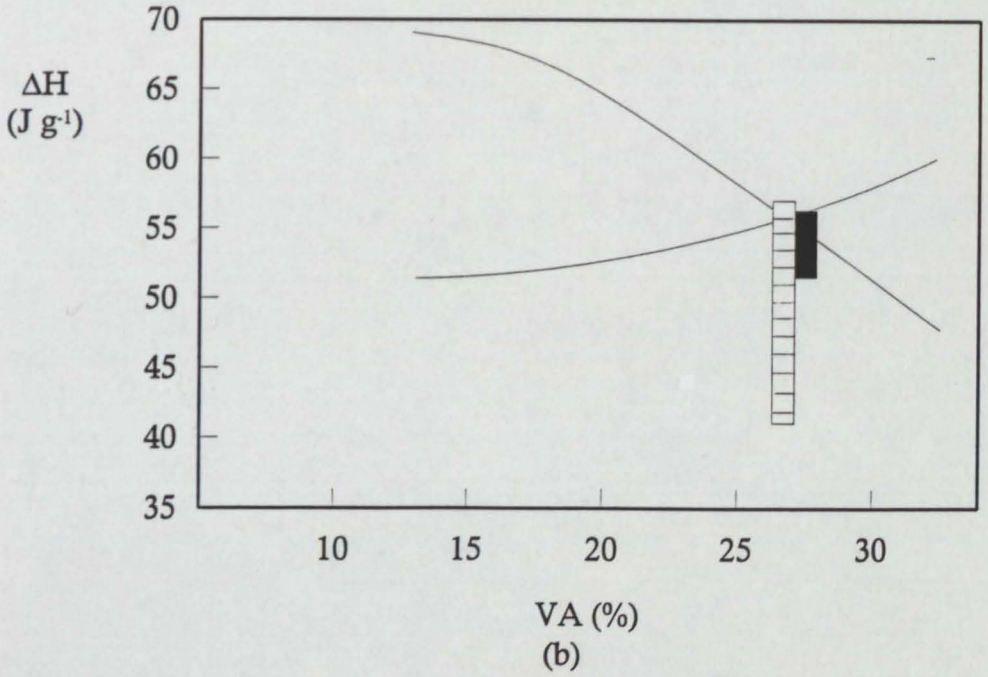

Fig 63. Graph illustrating the variation in enthalpy of melting ΔH_h and crystallisation ΔH_c of the polymers as a function of vinyl acetate content VA. Symbols: in (a) ● heating data; ○ cooling data; ▬▬ effect of molecular weight on ΔH_h; and □□□□□ effect of molecular weight on ΔH_c for 28% VA ExUL polymers; and in (b) general trend lines are shown.

increase in vinyl acetate is constant for all concentrations of vinyl acetate. For example, considering polymers of the same melt index, the difference in ΔH between ΔH_h 14/2500NC and ΔH_h 28/2500NC, Δ , is 18.8 J g^{-1}, or 1.32 J g^{-1} per %VA. Similarly, for 19/150NC and 28/145NC the difference is 1.34 J g^{-1}. This relationship is illustrated in Fig 64 and is consistent with accepted theories of polymer crystallinity [202]. The implications of this observation are that it may be possible to design into the adhesive the desired thermal properties by considering the total amount of VA in the system. This point will be discussed later. It should be noted that the more crystalline XL copolymers do not lie upon the extrapolated curve, which passes through zero at zero vinyl acetate, illustrating that the more crystalline copolymers are more greatly affected by variations in VA concentration than their lower crystallinity counterparts. This is intuitively correct as a small increment in stearic hindrance will have a greater effect on a more closely packing molecule than on a less densely packed system. In addition, the shift in ΔH in the ExAD polymers is also off the ExUL line, indeed it falls exactly upon the point of the AtEV polymers. One interesting point is that it seems that the AtEV polymers with 28% VA appear significantly more crystalline than the ExUL alternatives, and appear to be more crystalline than the ExAD polymers. This is taken as strong evidence that the production method used in copolymer preparation significantly affects the molecular structure and hence morphology of the final product.

Polymers from the higher crystallinity ExAD range (28/400XL, 28/2500XL and 33/400XL), together with those produced by Elf Atochem (28/40NC*, 28/420NC*, and 33/400NC*) show some differences in enthalpy upon heating and cooling when compared with the ExUL grades. During heating there appear to be only minor differences in ΔH_h between the NC and XL polymers : the 28% VA polymers have higher ΔH_h than their NC counterparts (as do the NC* polymers) whilst 33/400XL is lower than 28/400XL. This is a composition effect that has been discussed earlier. As there is no direct comparison possible between grades manufactured by Exxon at 33%VA, high and low crystallinity, we can only note that the difference in ΔH_h between 28/420NC* and 33/420NC* is the same as that between 28/400XL

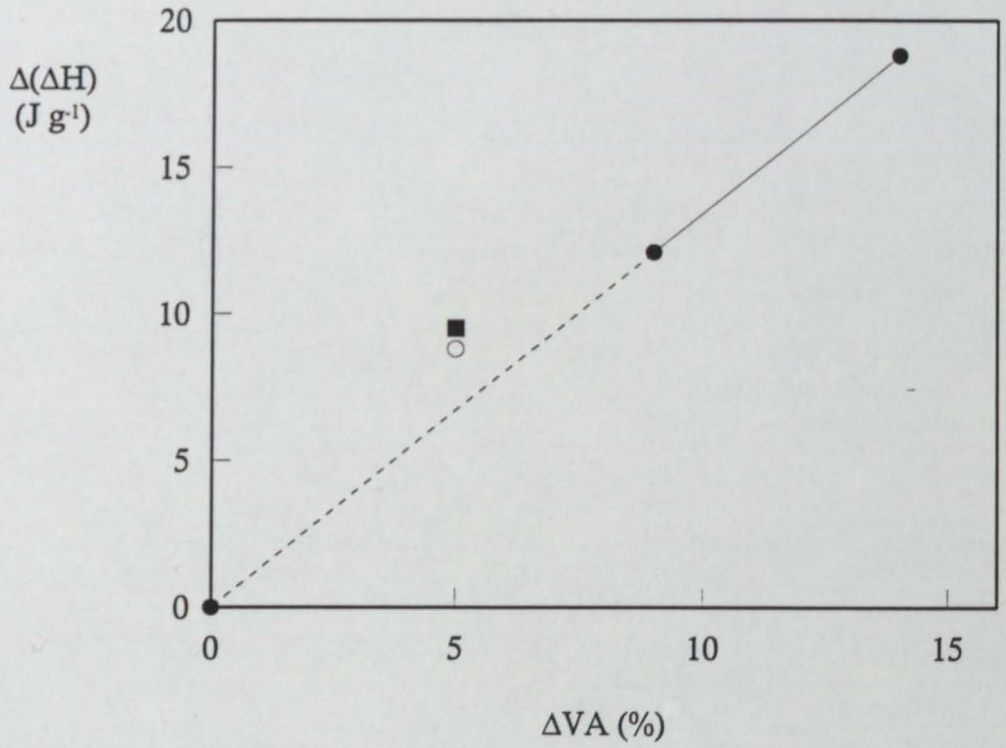

Fig 64. Graph illustrating the differences in enthalpy of melting ΔH_h between copolymers having similar melt indices but different concentrations of vinyl acetate Δ(ΔH) as a function of the difference in VA concentration ΔVA. Symbols: ● ExUL polymers; ○ AtEV polymers; and ■ ExAD polymers. Data pairs are 14/2500NC and 28/2500NC; 19/150NC and 28/145NC; 28/420NC* and 33/400NC*; and 28/400XL and 33/400XL. See text for further details and sample calculation.

and 33/400XL (8.8 J g^{-1}) and that one would expect the same trends to follow through, albeit at a lower value of the difference so as the fall on the line in Fig 64. As stated above, the differences between AtEV and ExUL grades are much larger than those between AtEV and ExAD grades, suggesting that the AtEV grades are more crystalline than their ExUL counterparts. This conclusion is supported by the ΔH_h and ΔH_c data which in all cases are larger than the ExUL grades with similar molecular weights.

Trends in the melting and crystallisation temperatures as functions of the logarithm of the melt index and vinyl acetate content of the copolymer are shown in Figs 65 and 66 respectively. It is seen that the rate of variation in T_h is greatest at the intermediate melt index of approximately 150 g 10 min^{-1}. Both above and below this point (corresponding to a molecular weight M_w of about 49 000) the melting point appears to be independent of molecular weight, albeit at two different levels (28/7NC has a T_h of 74.1°C, 28/2500NC has a T_h of 60.3°C). This effect is also apparent during crystallisation, although the total variation in T_c is much smaller (being only 6°C). It is suspected that the same factors influencing ΔH_h and ΔH_h are also affecting the transition temperature, *i.e.* total crystallinity, polymer/crystalline morphology, and relative ease of chain motion [44]. It is also important to stress that the copolymers tested herein are not at equilibrium and necessarily show a strong dependence of T_h or T_c on the heating/cooling rate of the experiment. However, it is again stressed that the systematic determination of the thermal properties under a set of standard conditions can still yield information useful to the formulator of hot melt adhesives. It can be seen from Fig 66 that the effect of VA concentration is again much larger than that due to molecular weight. The depression of the melting point with increasing VA content is approximately linear, again in accordance with theories on the mixing of crystallising and non-crystallising polymers [82].

Figure 67 shows the variation of glass transition temperature T_g with VA content. For the T_gs determined during the heating cycle T_{gh} there is very little change in the determined values, either with VA content or MI. There is a greater variation if the data from the cooling curve is considered and this is in the

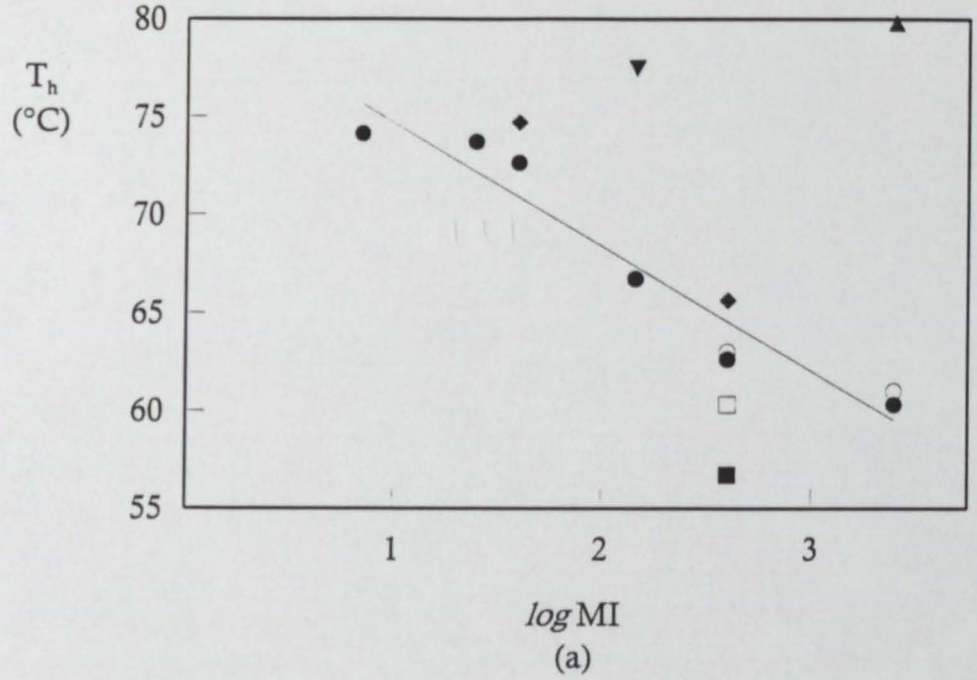

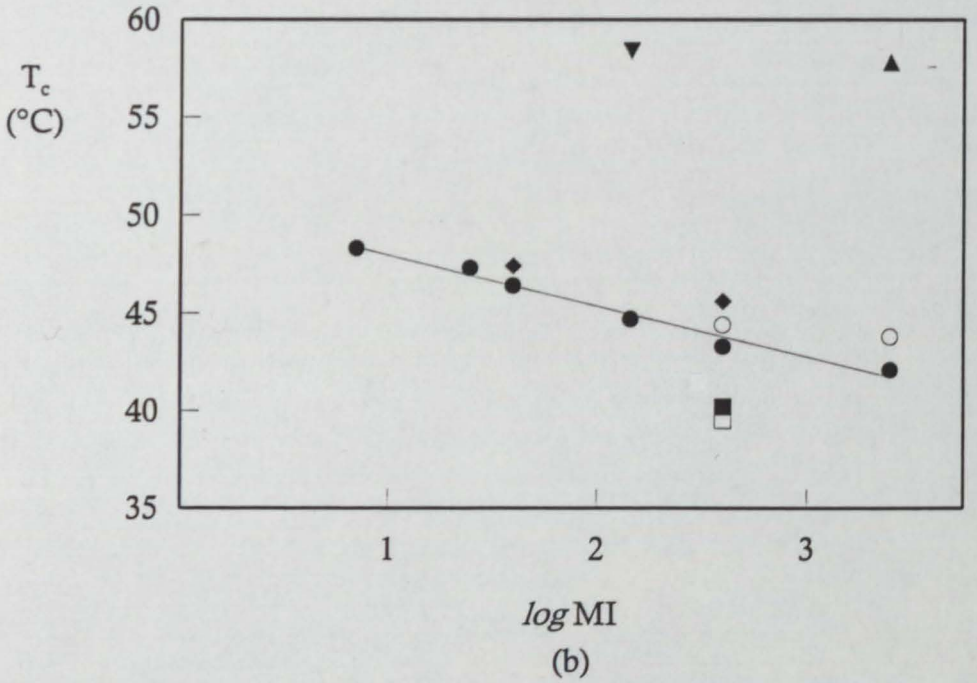

Fig 65. Graph showing temperatures of melting or crystallising T_h, T_c on (a) heating and (b) cooling repectively of the polymer as a function of the logarithm of the melt index MI. Symbols: ▲ 14% VA; ▼ 19% VA; ● 28% VA NC; ○ 28% VA XL; ■ 33% VA; □ 33% VA XL; ◆ 28% VA NC*.

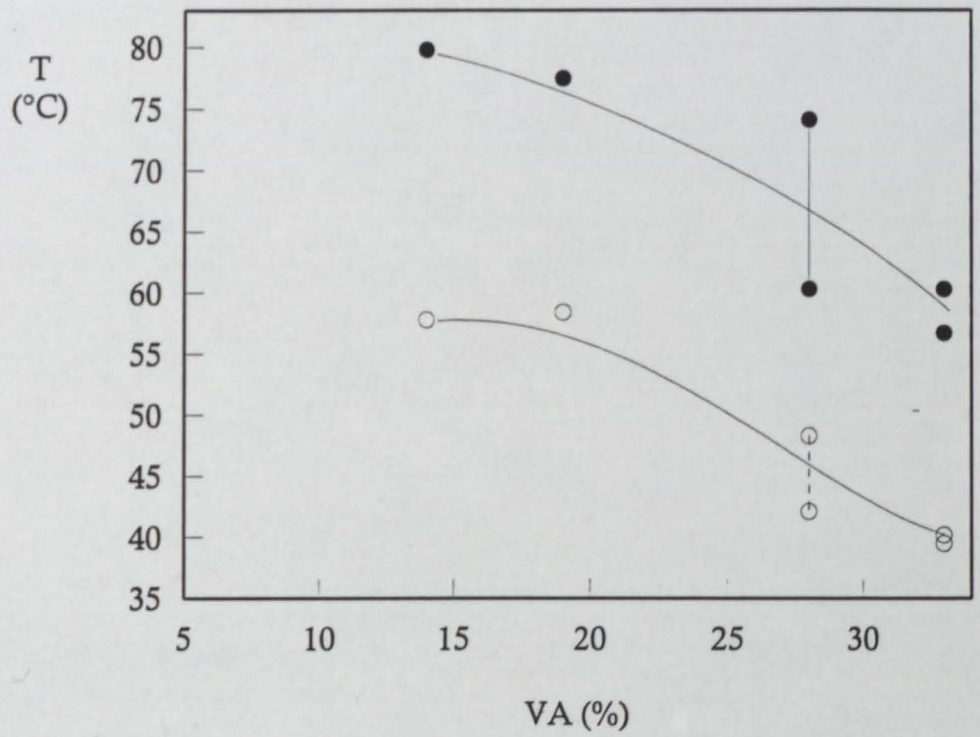

Fig 66. Graph illustrating the variation in temperature of melting T_h and crystallisation T_c of the polymers as a function of vinyl acetate content VA. Symbols: ● heating data; ○ cooling data; ——— effect of molecular weight on T_h; and -------- effect of molecular weight on T_c for 28% VA ExUL polymers.

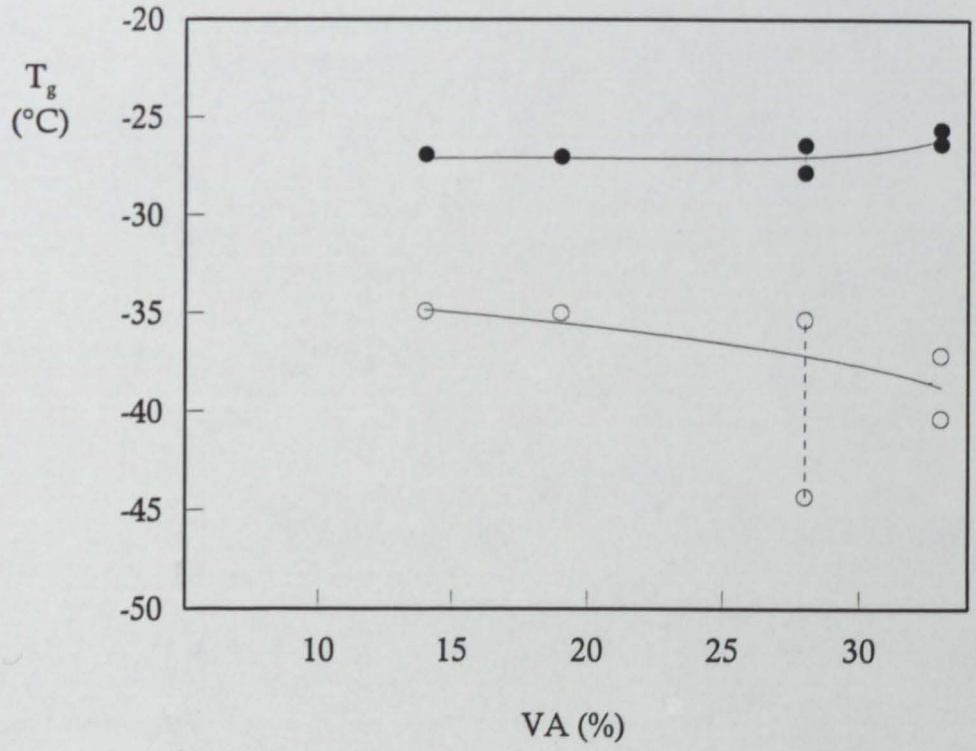

Fig 67. Graph illustrating the variation in glass transition temperature T_{gh}, T_{gc} during heating and cooling respectively of the polymers as a function of vinyl acetate content VA. Symbols: ● heating data; ○ cooling data; ——— effect of molecular weight on T_{gh}; and -------- effect of molecular weight on T_{gc} for 28% VA ExUL polymers.

direction expected *i.e.* the T_g decreases as the amount of poly(ethylene) is reduced and replaced by the more flexible vinyl acetate group. A similar effect has been observed by other workers [59]. Crystalline polymers from the ExAD range have higher T_gs than their lower crystallinity counterparts, and this trend is also detected with the AtEV polymers which, as hypothesised earlier, are suspected to be more crystalline than their ExUL counterparts. If the glass transition temperatures are calculated by reference to the Fox equation (eqn. 32, see p 65), with T_g poly(ethylene) = -120°C and T_g poly(vinyl acetate) = 30°C, then T_gs around -100°C are obtained. These are clearly much lower than those obtained in this work and in previously reported works [88, 190]. At this point it is again essential to remember that the T_g measured here is one of several solid-state transitions that have been observed in ethylene homo and co-polymers. The highest temperature transition, α, is just below the melting region and is assigned to the onset of molecular motion in the crystalline phase [205]. It tends to be very small and is only seen in polymeric materials exhibiting high degrees of crystallinity. The lowest temperature γ-transition is the T_g as calculated by eqn. 32 and is assigned to the cessation/onset of segmental motion in the polymeric backbone. The beta transition is reported [206] to be in the range -12°to -30°C and is associated with a ductile-brittle transition in the long chain branch points close to the surface of crystalline lamellae. It is practically constant for most semi-crystalline ethylene-based copolymers such as EVA at all practical comonomer concentrations. The present data seem to support this view for the heating cycle. However the correlation between T_{gc} and composition can be of use to the adhesives formulator. It has, for example, been noted that the β-transition can be related to fracture propagation mechanisms [*e.g.* 207].

There are few data with which the present results may be compared. The results of Eastman [190] are given in Table 23 and included in Fig 68. In viewing this data it should be kept in mind that Eastman's results are relatively old and obtained using an instrument of uncertain precision; the scan conditions were not detailed (except that the heating and cooling rate was given as 10°C min^{-1}); the method of evaluation was not given; and there is no indication of the

Table 23 Comparison of DSC data from the present work with that of Eastman [190]

	Enthalpy ($J\ g^{-1}$)		Main peak temperature (°C)		Glass transition (°C)	
Polymer	ΔH_h	ΔH_c	Heat	Cool	Onset[a]	Mid-point
LDPE[b]	106.0	96.8	106.4	98.7	ND[c]	ND
18% VA EVA[b]	54.9	48.1	85.3	65.8	-48	-20[d]
28% VA EVA[b]	31.8	35.5	71.3	49.9	-42	-18[d]
33% VA EVA[b]	24.1	26.5	56.4	37.5	-40	-24[d]
19/150NC	65.8	51.7	77.5	58.4	-	-27.0
28/145NC	53.7	49.9	66.7	44.7	-	-27.8
28/400NC	53.1	51.7	62.6	43.3	-	-26.5
28/420NC*	55.6	53.7	65.6	45.6	-	-26.7
33/400NC*	46.8	46.3	56.7	40.2	-	-26.3
28/400XL	54.0	52.6	63.0	44.4	-	-26.7
33/400XL	45.1	58.7	60.3	39.5	-	-25.6

a) Onset T_g determined from heating curve (given data)
b) Data from reference
c) ND; not detected
d) Data is estimated from graphs in reference

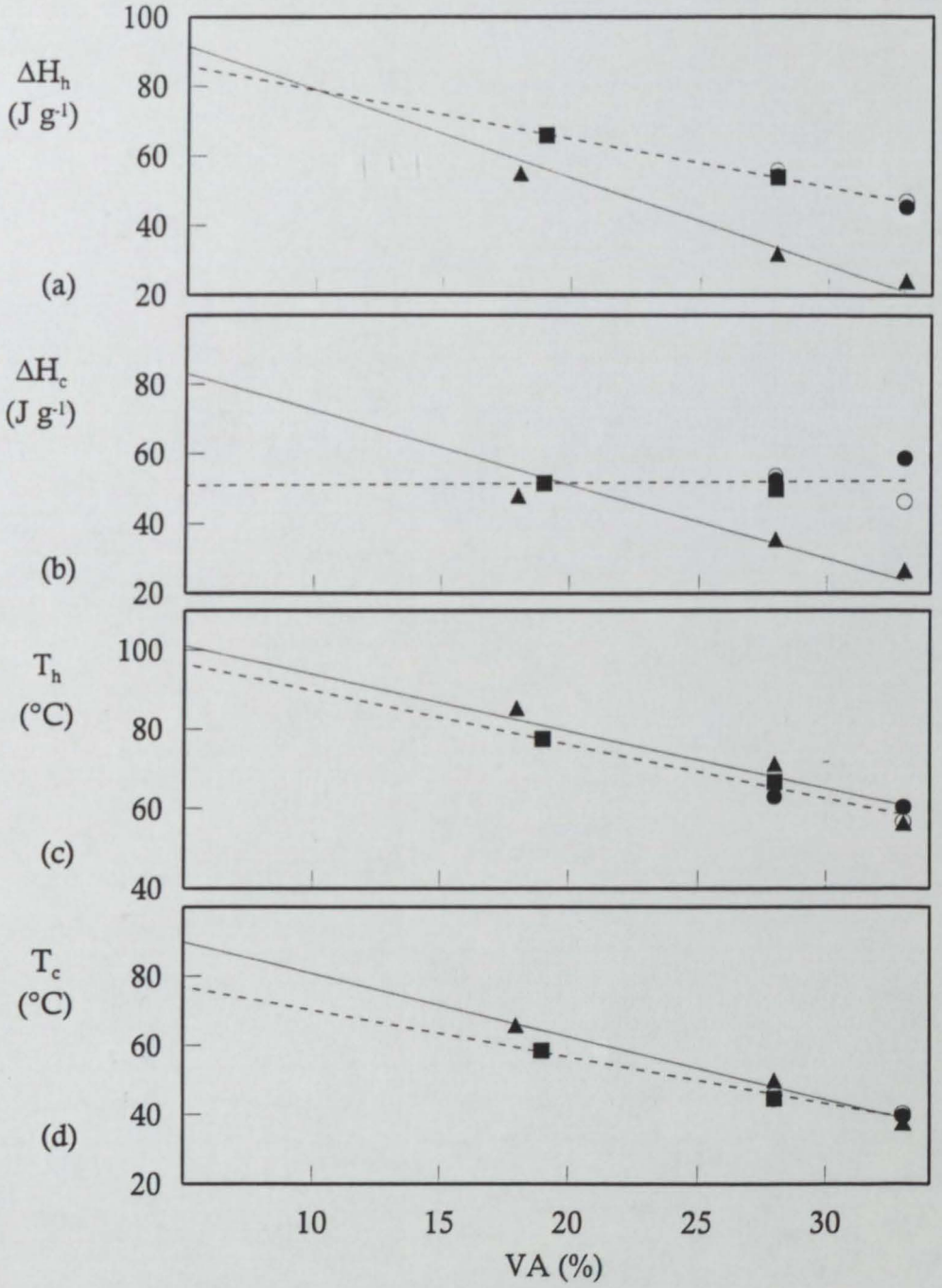

Fig 68. Graphs comparing data illustrating the thermal characteristics of PE and EVA polymers as a function of vinyl acetate concentration of the polymer VA. (a) transition enthalpy during heating ΔH_h; (b) transition enthalpy during cooling ΔH_c; (c) temperature of melting T_h; and (d) temperature of crystallisation T_c. Symbols: ● EVA ExAD (400 MI); ■ EVA ExUL (150 MI); ○ EVA AtEV (400/420 MI); and ▲ data of Eastman [190].

molecular weight or melt indices of the EVA samples. These resulted in significant differences in the detailed shape of the thermograms (not illustrated) and, together with the use of the onset value for the glass transition (in contrast to the mid-point value in the present work), give a substantial element of uncertainty in the results. Nevertheless, the trends are similar to those obtained in the present work. In addition to the data of Eastman, several earlier papers on EVA copolymers have shown the relationships between heats of fusion, melting temperatures and composition. Salyer & Kenyon [59] quote values of heats of fusion for several EVA compositions, and although molecular weights are significantly higher for the polymers used in their work, there is good agreement with the present work (Fig 69).

Paraffin wax is essentially a coarse grained crystalline structure comprised of straight chain and branched hydrocarbons. The DSC curve (Fig 30a) shows the essentially crystalline nature by the single sharp crystallisation peak. Although paraffin wax has two crystalline forms, orthorhombic and hexagonal, depending upon the composition and temperature there is no evidence of these on the thermogram. There is also no evidence of a glass transition in the range studied. The amorphous nature of the resin is apparent from the DSC (Fig 70). The T_g is clearly visible, and noticeably higher than that of the EVAs (see Table 10). There is no evidence of changes due to crystallisation or melting. This contrast sharply with the strong peaks observed with the EVA.

The thermal analyses of the formulated adhesives show some similarity to the analysis of the neat polymers but there are obvious differences owing to the presence of the wax and resin. In exploring the effect of modifiers on the properties of a material, it is necessary to consider the compatibility between them and the possible phases that may exist during the heating or cooling cycle. It has been proposed that EVA/rosin ester/wax systems exist as a homogeneous phase above the wax melting point, but separate into an EVA/resin phase and an incompatible wax phase below the softening point [156]. If this simple model were true then a number of features could be predicted; namely that the wax would crystallise or melt at a constant temperature independent of the EVA

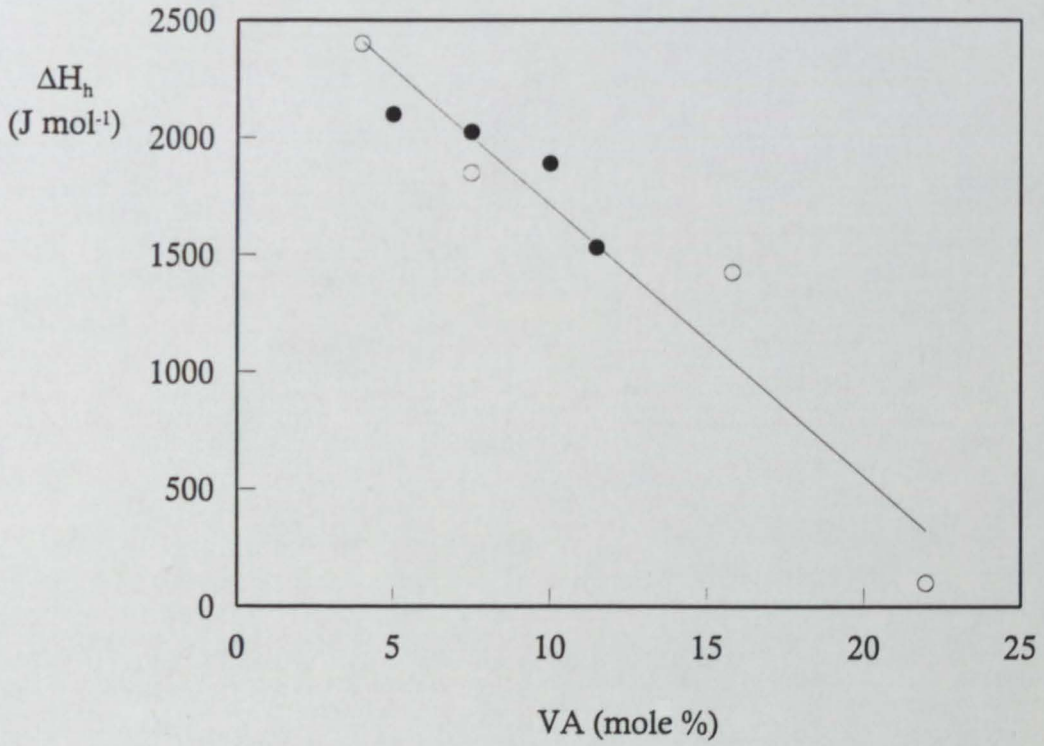

Fig 69. Graph illustrating the transition enthalpy during heating ΔH_h as a function of the vinyl acetate content of the polymer VA (mole %) for a series of EVA copolymers. Symbols: ● data from present work; ○ data of Salyer and Kenyon [59]. Regression line from reference. See text for details.

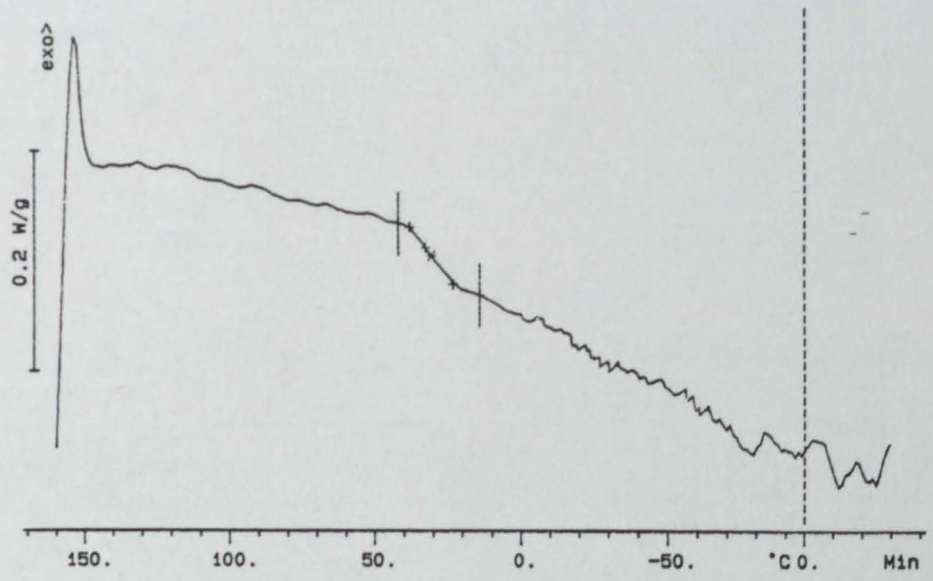

Fig 70. DSC thermogram of Permalyn 5095 illustrating, by way of a lack of any crystallisation peaks, the completely amorphous nature of the resin. Note the extremely well-defined glass transition at approximately 30°C. Cooling scan performed at 10°C min^{-1}.

composition and molecular weight (melt index), and that there would be evidence of two distinct peaks on the DSC thermograms during the analysis. Examination of the present experimental data does not support either of these predictions. There is evidence of a small, but systematic, shift in the wax peak temperature (WPT) as a result of varying the EVA melt index and amount of vinyl acetate comonomers. In the first case, considering the heating data, there is a definite shift in the WPT as a function of M_w (Fig 44a). At higher molecular weights, *i.e.* low MIs, the WPT is shifted upwards towards the higher polymer main peak temperature, whilst in the lower M_w EVAs there is a depression in the WPT. If the wax was truly incompatible with the EVA there should be no shift in the WPT. In fact, there is a limited compatibility between the crystalline material in the wax and the more crystalline regions of the EVA copolymers. Higher molecular weight EVAs are more crystalline than than those of lower M_w hence the reinforcement effect of the wax when high molecular weight material is used in the formulation. The apparent anomaly in compatibility with the EVA 28/7NC is probably attributable to the mobility of the EVA chains. During the time scale of the DSC heating/cooling ramp, the long molecules do not have the chance to attain crystalline positions and hence do not appear to fit the otherwise regular transition of thermal properties. In support of this picture of limited compatibility, the qualitative shape of the wax peak should also be considered. At the relatively slow heating and cooling rates used here it would not be unreasonable to be able to differentiate between thermal events occurring over 14°C from each other (fusion peak of EVA 14/2500NC is 79.8°C, of paraffin wax is 65.7°C) which would be visible if the two components were immiscible however examination of the heating curve of ADH 14/2500NC only shows a single peak at 71.6°C (Fig 71). The composition of the EVA used also has an effect on the thermal properties of the adhesive. In general, the lower vinyl acetate content EVAs give higher crystallisation and fusion temperatures whilst the ADH 33/400NC* sample has significantly lower WPTs than its 28% VA analogue. The more crystalline versions of the 28%VA EVAs had little effect on the fusion or crystallisation suggesting perhaps that the limit of compatibility between the crystalline portions of the wax and polymer is limited

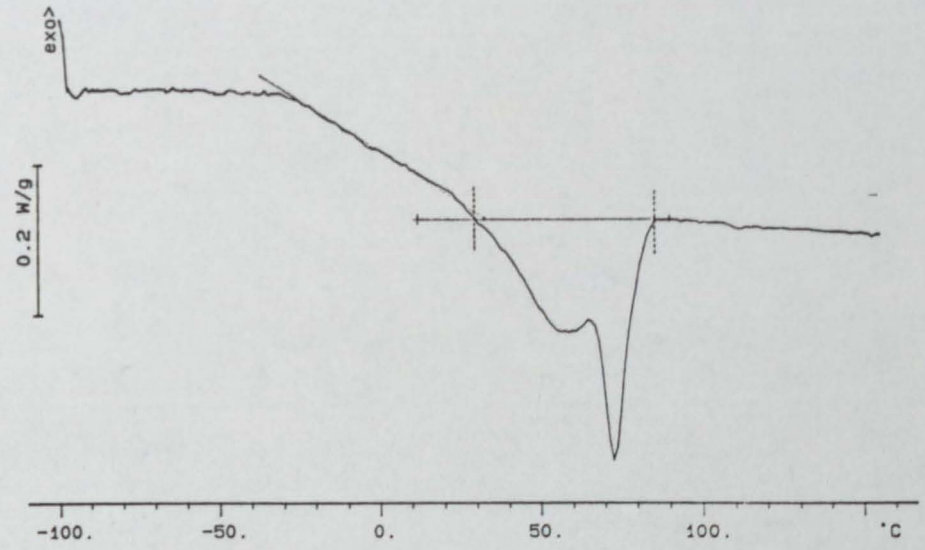

Fig 71. DSC thermogram of ADH 14/2500NC. Heating scan performed at 10°C min^{-1}.

by the wax composition, not that of the EVA.

Further evidence on the supposition of wax compatibility comes from the correlation of the glass transition temperatures (T_g) of the adhesive blends. Marin *et al* [172] performed a series of experiments with EVA/resin blends and showed that the T_g of such a binary blend can be related to the free volumes of the constituents, their T_gs, and certain bulk mobility factors. If the same assumptions are made about the materials in this present work, and if the wax is assumed to be completely incompatible and performs no part in the determination of the T_g of the adhesive, then it is possible to calculate values for the T_g of the adhesive blends using the equation

$$T_g = [\phi\alpha_{1f}T_{g1} + (1 - \phi)\alpha_{2f}T_{g2} - k\phi(1 - \phi)]/[\phi\alpha_{1f} + (1 - \phi)\alpha_{2f}] \quad \ldots (38)$$

where T_g, T_{g1}, T_{g2} are the T_gs of the adhesive, polymer, and resin respectively, ϕ is the volume fraction of the polymer, $\alpha_{1f} = \alpha_{2f} = \alpha_f$ is the free volume expansion factor ($\alpha_f = 6.46 \times 10^{-4}$), and k is a constant ($k = 3 \times 10^{-2}$) (from [172]). These values are given in Table 24 as 'Marin' model, together with the measured values and the difference between the two. As can be seen, the differences are extremely large. The exercise can be repeated with the simpler Fox equation

$$1/T_g = w_1/T_{g1} + w_2/T_{g2} \quad \ldots (32)$$

with w_1, w_2 being the weight fractions of the polymer and resin respectively. The results are shown as 'Fox' model in Table 24 but the differences are still very large. However, if the broad assumption is made that the wax behaves as a low molecular weight poly(ethylene) and hence is at least partially compatible with the resin/EVA blend, then a simple expansion of the Fox equation (with T_g of poly(ethylene) = -120°C) gives

$$1/T_g = w_1/T_{g1} + w_2/T_{g2} + w_3/T_{g3} \quad \ldots (39)$$

with T_g and w having the same significance as before and the subscripts 1, 2, and 3 referring to the polymer, resin, and wax respectively. The values also appear in Table 24. It can be seen that, even with this very crude model, the predicted values are significantly closer to those observed than is the case if the wax component is completely omitted. Previous workers did not find this to be the case [88] and concluded that the wax content had no effect on T_g. This point is important and is worth discussing in greater detail. Komornicki *et al* used a

Table 24 Adhesive glass transition temperature predictions using various models[a]

Adhesive	Measured T_g[b] (°C)		Marin model				Fox model				Present model			
			Predicted T_g (°C)		Difference (°C)		Predicted T_g (°C)		Difference (°C)		Predicted T_g (°C)		Difference (°C)	
	heat	cool	heat	cool	heat	cool	heat	cool	heat	cool	heat	cool	heat	cool
14/2500NC	-10	-20	5	-2	15	18	2	-3	12	16	-19	-23	-9	-3
19/150NC	-22	-5	5	-2	27	3	2	-4	23	2	-19	-23	3	-18
28/7NC	-17	-13	6	-4	23	9	2	-5	18	8	-18	-24	-1	-11
28/25NC	-19	-15	5	-4	24	11	2	-6	21	9	-18	-24	1	-9
28/40NC	-18	-14	5	-3	23	11	2	-5	20	9	-18	-24	0	-10
28/145NC	-18	-12	5	-2	23	10	1	-4	19	8	-19	-23	-1	-11
28/400NC	-19	-17	5	-2	24	15	2	-4	21	14	-18	-23	1	-6
28/2500NC	-20	-16	5	-7	25	9	2	-10	21	6	-18	-27	2	-11
28/40NCA	-22	-11	6	-2	28	9	2	-4	24	7	-18	-23	4	-12
28/420NCA	-27	-24	5	-1	32	23	2	-2	29	22	-19	-21	8	3
33/400NCA	-21	-19	6	-5	27	14	2	-7	23	12	-18	-25	3	-6
28/400XL	-16	-13	5	-1	21	12	2	-2	18	11	-19	-21	-3	-8
28/2500XL	-12	-13	6	-3	18	10	2	-4	14	9	-18	-23	-6	-10
33/400XL	-19	-17	6	-3	25	14	2	-5	21	12	-18	-24	1	-7

(a) Models are described in the text.
(b) Measured T_g refers to midpoint DSC measurements.

system containing EVA 28/420NC*, a highly crystalline Fischer-Tropsch wax, and a phenolic-modified terpene resin. Considering each of these components in turn the present author also finds that the glass transition of the 28/420NC* EVA is not shifted in the adhesive formulation. It has already been hypothesised above that by consideration of the ΔH values of the neat polymer that the process used by this manufacture yields a more crystalline polymer and that this may give different behaviour with respect to compatibility and phase formation in the formulated adhesive. The wax used by Komornicki *et al* is synthesised by the Fischer-Tropsch process and is characterised by a relatively narrow carbon number distribution with practically no branched chain carbons [25]. The lack of low molecular weight tails, coupled with the lack of branched material suggest that the material is less likely to show partial affinity for the EVA and that the original phase model [172] is more appropriate. The extent of differences between paraffinic waxes and synthetic waxes has been extensively discussed [23] and the available evidence seems to support Komornicki's hypothesis that the wax acts as an inert filler with respect to T_g modification. The final point to consider is the choice of resin. The phenolic-modified terpene resin used has a different compatibility profile to the rosin ester used in the present work [208]. This may mean that it too is completely incompatible with the wax and although there is no direct evidence to support this statement, the fact that modified terpene resins give quantitatively and qualitatively different properties to hot melt adhesive formulations is well recorded by resin manufacturers [209], in the literature [210], and by standard texts on adhesives [171].

The enthalpy values for the adhesives are all significantly less than those obtained for the neat polymer (on average 64% of neat polymer value) and there is a general decrease in enthalpy on both heating and cooling with decreasing molecular weight however the change is less pronounced on cooling (Table 9). Komornicki *et al* [88] observed that the energy to melt a simple EVA/resin blend was 3.4 J g^{-1}, and this was increased to 42.2 J g^{-1}, when the blend contained 15 wt. % wax. Assuming the enthalpies are additive, 15% of the sample has an enthalpy of 42.2 - 3.4 = 38.8 J g^{-1}, and therefore 100% wax would have an enthalpy of 250 J g^{-1}. Considering that different waxes have been used, this

value is not too far away from the presently determined value of 190.1 Jg^{-1}. Literature value given for paraffinic waxes of the type used in the present work range from 184.7 J g^{-1} [24] to 196.0 J g^{-1}[25]. The author has independantly determined the enthalpy of the wax type used by Komornicki to be 236.4 J g^{-1}. The enthalpy also decreases as the VA content increases, as with the neat polymer, as the overall crystallinity of the system is decreased. The difference is much less however due to the effect of the wax content which acts as a nucleating agent upon cooling thereby aiding the development of the maximum amount of crystallinity, even in the higher VA, lower crystallinity samples. The effect of increased crystallinity in the 28/400XL and 28/2500XL, containing grades is marginal, however a larger difference in ΔH is seen with the 33/400XL sample where the effects of the co-crystallisation with the wax are more clearly seen.

5.2 Rheological properties and characterisation of materials

The rheological properties are fundamental to the service performance of adhesives, and although oscillatory rheology has been widely used to determine and predict the performance of some types of hot melt pressure sensitive adhesives, there is relatively little information on the rheological properties of hard setting hot melt adhesives. These points have been examined and emphasised in the literature survey, and are the basis for the present broad and systematic determination of the rheological properties of the components of the adhesives and the hard setting hot melt adhesives. In this section we critically assess generally the significance of all of the results and, after a brief discussion of the flow results, we concentrate in particular on the information provided by controlled strain and the more recently introduced controlled stress techniques, the factors influencing the results, and a comparison of the determination of glass transitions by rheological and scanning differential calorimetric techniques. In the following sections the rheological properties are considered especially in terms of their detailed application to the formation, behaviour, and service performance of adhesive joints.

The results for the flow properties of the adhesives were obtained by using

a Brookfield-type rotational viscometer. The instrument operates by measurement of the deflection of a calibrated torque spring caused by the rotation of a bob in a precise volume of fluid. The accuracy of the instrument is limited by two principal factors. Firstly, there are the mechanical constraints that must be considered as a result of the instument's design. The value given for the viscosity measurement is only valid for deflections of the torque spring within 10 - 80% of its full scale deflection due to the effects of spring non-linearity [211]. This limit of the torque also places an upper boundary on the shear rate that can be accomplished, *e.g.* high viscosity samples, which require large amounts of torque in order to shear them, can only be tested at low shear rates. Depending upon the rate of shear, the deflection of the spring can be converted, either manually or electronically, into a viscosity measurement. The highest resolution of the machine is $\pm$ 1% of full scale deflection. The second factor is related to temperature control of the sample during viscosity measurement. The specification of the instrument regarding temperature control is $\pm$ 0.1°C of the set point however differences in temperature as small as 1°C can affect the viscosity in a detectable fashion. Previous work by the present author has demonstrated that small temperature changes can affect the viscosity of EVA-based HMAs by upto 8% [212]. Given the limitations of this instrument it still remains commonly used throughout the adhesives industry and a very large number of quality control, and customer, specifications are made using this instrument.

The effects of melt index, VA concentration, and crystallinity have already been commented upon earlier (Chapter 4). The thermally activated nature of viscosity is evident from the Arrhenius plot of $log\,\eta$ *vs* 1/T shown in Fig 46. The activation energies calculated for the adhesives are dependant upon the MI of the polymer (Fig 72a) and also upon the vinyl acetate concentration. Note that the activation energy required for flow of the low VA concentration samples (14% and 19%) is considerably less than for 28%VA copolymers of the same melt index. It may be hypothesised that this is attributable to the fact that low VA copolymers tend to be more crystalline and have sharper, more clearly defined melting peaks. This could enable a more rapid dissolution of the

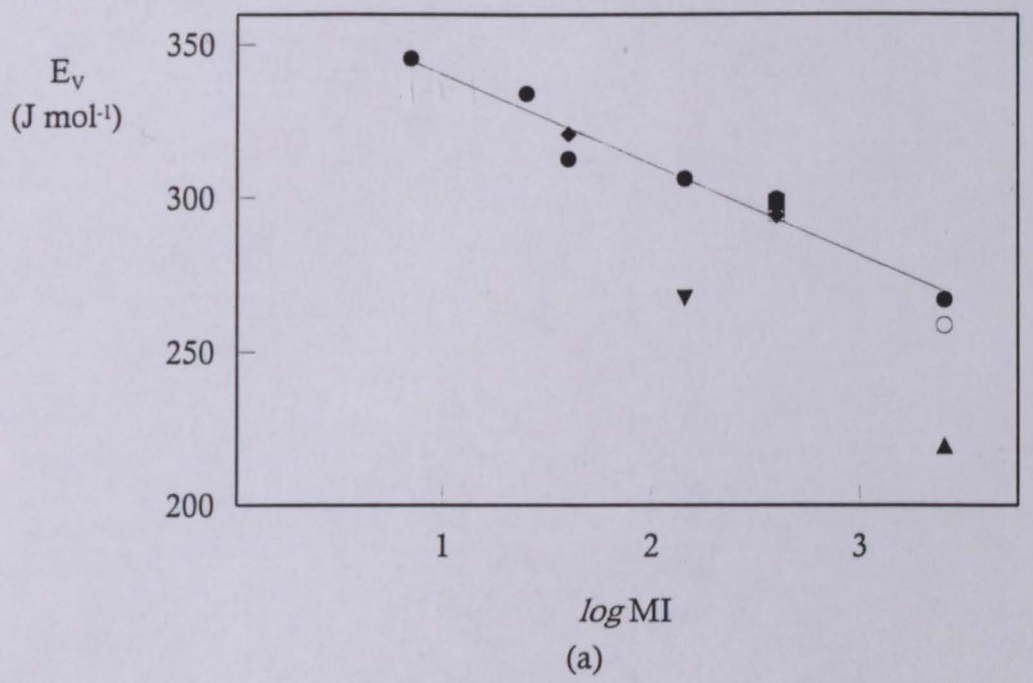

(a)

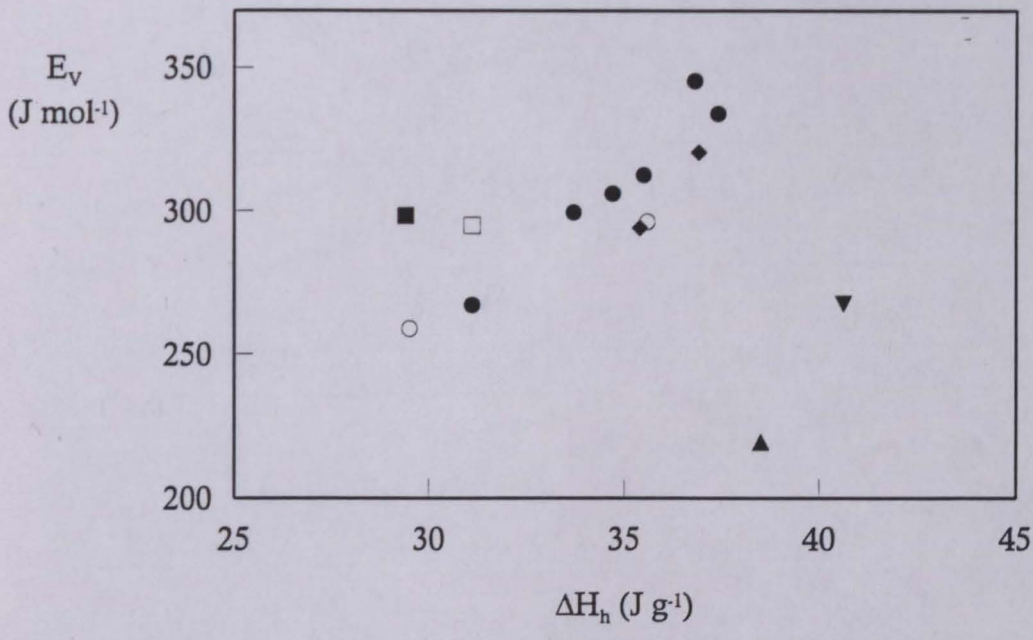

(b)

Fig 72. Graphs comparing data illustrating the activation energy for viscous flow E_v as a function of (a) the logarithm of the polymer melt index MI and (b) the transition enthalpy during heating ΔH_h. Symbols: ▲ 14% VA; ▼ 19% VA; ● 28% VA NC; ○ 28% VA XL; ■ 33% VA; □ 33% VA XL; ◆ 28% VA NC*.

crystallite structure. There appears to be no significant correlation between the activation energy for viscous flow and ΔH_h however (Fig 72b), beyond that of the correlation between ΔHh and MI already discussed.

The double logarithmic relationship between viscosity and melt index is noted and was commented upon in Chapter 4. This dependance upon adhesive viscosity and molecular weight of the polymer must therefore remain a critical factor in determining an adhesive design for a particular application, although recent studies by a large manufacturer of EVA copolymers states the significance of other extrinsic factors which, although outside the scope of the present work, must be taken into account of when a formulating chemist initiates pilot-scale production of an adhesive formulation [213].

Although the use of oscillatory rheometry in determining and predicting the performance of adhesives is critically established for certain kinds of hot melt pressure sensitive types [*e.g.* 169, 214], there is little comparable data for hard setting hot melt adhesives. This work is one of the first to critically examine the results of comparing the controlled strain and newer controlled stress techniques when applied to hot melt adhesives and goes on to examine the rheograms of the materials investigated in this study. Following a brief illustration of the limitations of each technique with respect to the present work, there is a comparison between the two techniques, firstly for the data generated on the adhesive samples and then on the adhesive components. We will then discuss the key rheological features of the EVAs and adhesives, followed by a detailed examination of the differences attributable to molecular weight, composition, crystallinity. A comparison of the glass transition temperatures determined by DSC and rheology will then be discussed, along with other noteworthy observations on the oscillatory rheometry.

The advantages and limitations of either the controlled strain and controlled stress techniques are related to the capabilities of the equipment and it is important to examine these in detail so as to obtain consistent and accurate rheological information. There have been numerous studies involving the use of controlled strain rheometers, *e.g.* Rheometrics RDAII, in the study of adhesive samples whilst there are relatively few giving comparable data obtained under

conditions of controlled stress. This is mainly historical, as reliable and affordable controlled stress instruments are fairly new commercially.

In examining the instruments used in the present work, it is apparent that some of the differences are attributable to machine design. Several of those features have been mentioned earlier (Chapter 3) and these are summarised for this discussion (Table 25). The most significant are the machine compliance effects, the sample preparation, and the efficiency and accuracy of the heating/cooling systems. The first and second factors can be relatively easily quantified, and either accounted for or eliminated to an extent within the experimental variation caused by other factors. The third factor is more difficult.

Figure 73 illustrates the rheograms obtained for the adhesive sample 28/7NC. Qualitatively, the curves are similar and key rheological features such as the position and height of the *tan* δ peak, together with the sudden drop in modulus associated with the melting of the wax in the adhesive, are fundamentally unchanged. However, the absolute values of, for example, the elastic modulus G' appear quite different, especially at lower temperatures and again prior to melting. The difference in the value of the moduli at low temperature are primarily a function of machine compliance. It has been recorded [*e.g.* 215] that polymeric materials attain a modulus of approximately 10^9 Pa after the cessation of polymeric chain motion. Neither the controlled stress nor controlled strain rheometer in the geometries used in the present work can resolve such moduli due to the inherent elastic response of the machine components themselves. This subject has been extensively covered by other workers [*e.g.* 184], suffice to say that the internally stiffer controlled stress instrument gives a greater "headroom" to the measurements and more nearly allows the accurate measurement of the glassy plateau. The modulus determined within the glassy region is therefore primarily a function of machine compliance and not material properties. It has been reported that the use of beam, or rectangular, specimens in conventional dynamic mechanical analyzers gives useful data on moduli and relaxation spectra beyond the glass transition [*e.g.* 216] however, in the present work, more emphasis will be placed on the transition temperature and the relative modulus values and these will be

Table 25 Key features in the design and utilisation of the rheometers in the present work

Feature	Rheometrics RDAII Controlled strain	Carrimed CSL^{2}500 Controlled stress	Additional comments
Machine compliance	Major limitation due to torque transducer. Typical values of machine compliance (10^7 - 10^8 Pa is typical modulus).	Limitations less severe due to lack of transducer in drive system. Compliance determined by spindle (10^8 - 10^9 Pa).	With the lack of a torque measuring sensor, controlled stress gives greater headroom for stiffer materials.
Resolution of strain	At high modulus values, the actual displacement of the sample is extremely small. RDAII can resolve strains as small as 5×10^{-5} rad.	Optical encoder in CSL^{2}500 gives strain resolution of 1×10^{-6} rad.	Neither instruments improve further on resolution which aids accuracy on harder/more viscous specimen.
Torque application/ measurement	Strain is controlled variable however care must be taken to protect torque sensor as sample contracts/expands on heating and cooling.	The maximum torque that can be applied is a limiting factor however reducing the diameter of the measuring system increases applied stress.	Torque overload in the controlled strain system limits the resolution at lower temperatures, in addition to compliance effects.
Heating/ cooling system	Large volume environmental chamber with slow thermal response. Need to condition sample at test temperature prior to measuring.	Induction heating directly to test geometry ensures rapid thermal response allowing true 'dynamic' temperature sweeps.	The 'heat & soak' method is particularly inappropriate for crystallising polymers as the properties change with time - temperature history.
Gap setting	Manual compensation of thermal expansion of geometry required. Actual gap not recorded during run.	Servo controlled micrometer adjusts gap during heating and cooling cycle. Expansion coefficients determined manually.	If the gap changes significantly during the thermal sweep this can have a significant affect on calculated visco-elastic parameters (see Chapter 3).

continued

Table 18 continued

Feature	Rheometrics RDAII Controlled strain	Carrimed CSL^{2}500 Controlled stress	Additional comments
Sensitivity	Torque transducer has lower sensitivity to smaller movements, partially attributable as increased size and complexity in measurement chain.	Air bearing has minimal drag and can be compensated however effect is not significant for highly viscous/solid samples.	Not a major issue in polymer melt rheology.
Sample preparation	Sample preparation is easier. Access to machine and geometry allows formation of cylindrical samples which eliminate 'edge' effects and aid reproducibility.	Samples are formed between small upper plate and larger diameter base plate in form of a fillet. Possible introduction of error due to 'edge' effects or differences in fillet size.	Reproducibility is good for both techniques however the possibility of poorer reproducibility between techniques is high.
Machine inertia	Machine has relatively high inertia due to incorporation of stress transducer into measuring chain.	Extremely low levels of inertia due to 'simple' design.	Especially significant for measuring melt region parameters where high strains are applied/measured.
Accuracy of temperature	Air temperature governed by thermocouple. Additional thermocouple situated in base of bottom parallel plate.	Accuracy quoted to ± 0.1°C determined by platinum resistance thermometer situated below surface of bottom plate.	Previous workers have stressed importance of secondary temperature measurement in RDAII. Soak time elimination in CSL500 is crucial for crystallising polymers.

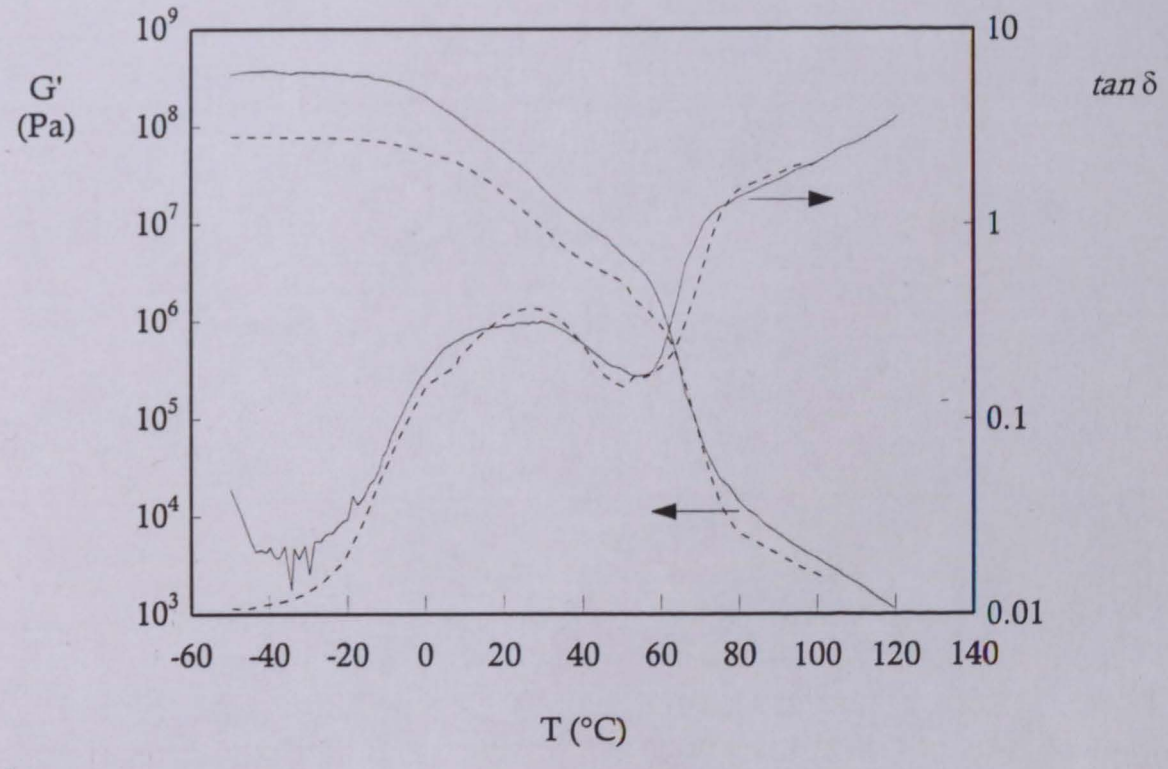

Fig 73. Rheograms of ADH 28/7NC showing the variation of the storage modulus G' and the loss tangent *tan* δ as a function of temperature T obtained using controlled stress (———) and controlled strain (-------) oscillatory rheometry. Conditions (controlled stress): 8 mm diameter parallel plates; 1 000 μm gap; heating rate 5°C min^{-1}; 10 rad s^{-1}. Conditions (controlled strain): 7.9 mm parallel plates; 1 000 μm gap; Soak and step heating parameters: 30s soak time, 1.5°C step; 10 rad s^{-1}. See text for details.

discussed in greater detail later. If sample preparation is considered (Chapter 3), repeat runs on both instruments show minimal differences. Consider Fig 74a which shows repeat runs on fresh samples of adhesive 28/420NC* performed under controlled stress conditions and Fig 74b showing repeat controlled strain runs on adhesive 33/400NC*. It is clear that this is not a major contributory cause to the differences seen between the techniques. The subject of edge effects is also a much discussed subject in standard texts of rheometry [*e.g.* 217] however other workers in fields unrelated to adhesives have not observed major differences between controlled stress and controlled strain oscillatory rheometry [218]. This tends to suggest that the key differences in the results obtained by the two techniques are perhaps due to the thermal history imposed on the samples by the preparation and measurement steps. As has been discussed earlier (*e.g.* p 159 relating to DSC) it is imperative that identical, controlled thermal profiles are imposed on the semi-crystalline polymers and their adhesives, if reproducible and meaningful data are to be obtained. The Carrimed CSL^{2}500 controlled stress rheometer has a low thermal mass, compact environmental chamber, barely larger than the geometry which it contains. It is heated and cooled with a considerable degree of precision which is not matched by the larger, less sophisticated Rheometrics RDA II controlled strain instrument which uses a heated/cooled stream of nitrogen. Whilst it must be stressed that, with care, the repeatability between samples on each machine is excellent (on average, measured differences in properties for both techniques are less than 3½%), the change in measured properties attributable to the different cooling profiles must play a significant part in the discrepancies between the instruments. Evidence to support this hypothesis may be seen by examining the data presented in Tables 13 - 16 and by examining sample rheograms. If the 28% VA adhesive samples are first examined, and G' is considered, it can be seen that there is reasonable agreement between the two techniques at 20°C and that the same overall trends are apparent at -20°C and 60°C (Fig 75). At 20°C there is good agreement between the techniques (less than 8% difference) which, considering the orders of magnitude by which the modulus changes with temperature, is reasonable. The exception in this case is ADH 28/7NC which has a difference of over 20%

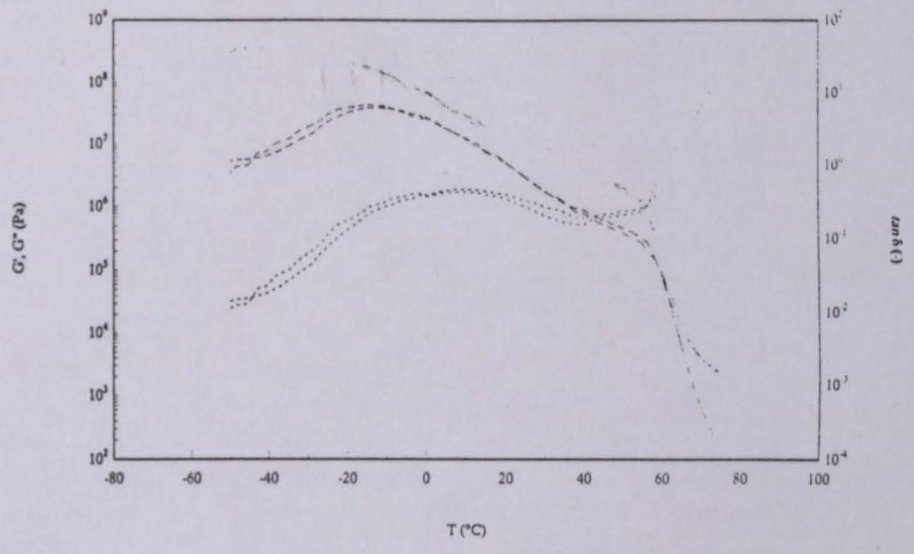

(a)

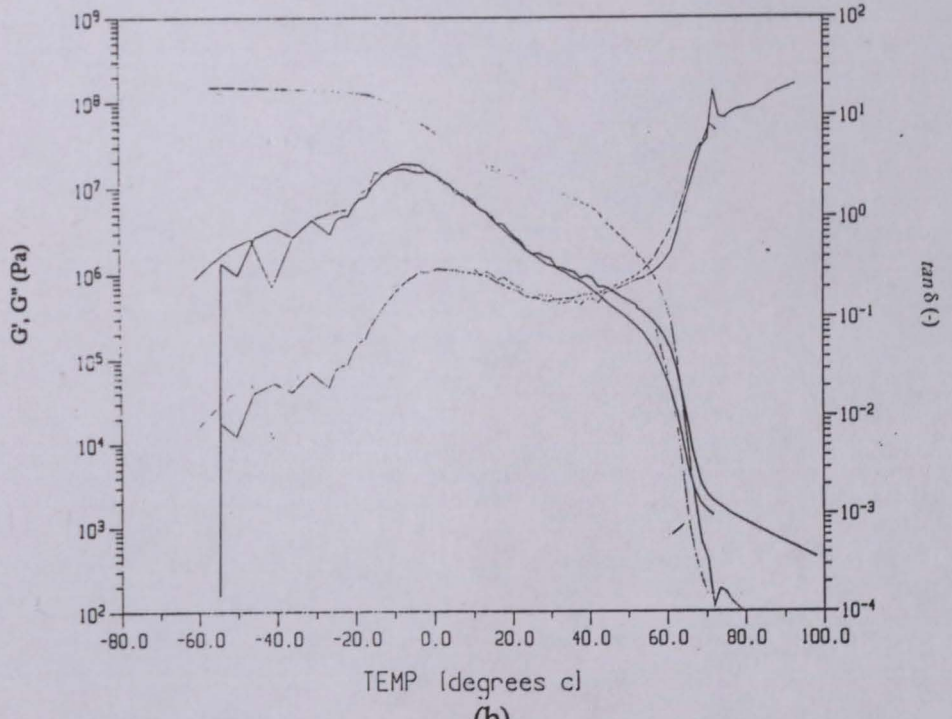

(b)

Fig 74. Rheograms showing variation of storage and loss moduli G', G" and loss tangent *tan* δ as a function of temperature T for two adhesive samples measured under conditions of (a) controlled stress and (b) controlled strain. Conditions (controlled stress): ADH 28/420NC*; 8 mm diameter parallel plates; 1 000 μm gap; heating rate 5°C min^{-1}; 10 rad s^{-1}. Average difference between samples is approximately 3%. Conditions (controlled strain): ADH 33/400NC*; 7.9 mm parallel plates; 1 000 μm gap; Soak and step heating parameters: 30 s soak time, 15°C step; 10 rad s^{-1}. Average difference between samples is approximately 5%.

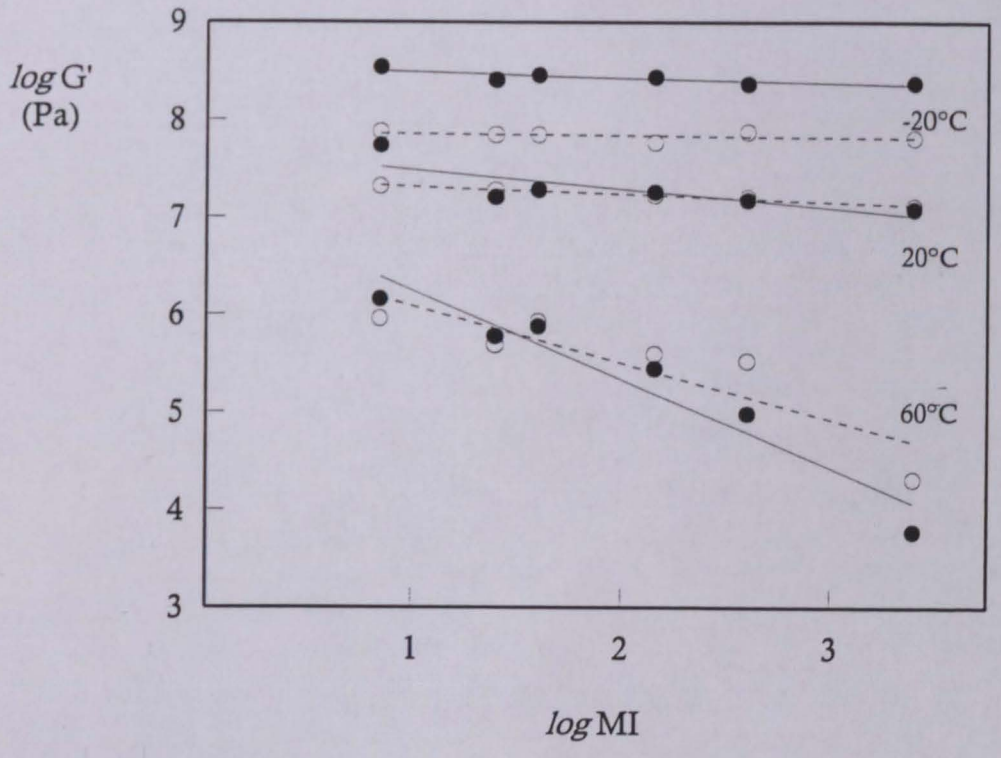

Fig 75. Graph showing variation of storage modulus G' as a function of the logarithm of the polymer melt index MI at three temperatures (-20, 20, and 60°C) as determined by controlled stress rheometry ● and controlled strain rheometry ○. Data presented for adhesives containing ExUL EVA of 28%VA composition. Conditions (controlled stress): 8 mm diameter parallel plates; 1 000 μm gap; heating rate 5°C min^{-1}; 10 rad s^{-1}. Conditions (controlled strain): 7.9 mm parallel plates; 1 000 μm gap; Soak and step heating parameters: 30s soak time, 15°C step; 10 rad s^{-1}. See text for details.

between techniques. From the DSC work discussed earlier, it is known that EVA 28/7NC is a fairly crystalline polymer due to its high molecular weight and hence ability to form regions of undisrupted crystalline material. Whilst the controlled stress instrument can reproducibly cool the sample at any given rate, the controlled strain instrument can only cool relatively quickly and with considerable variation in the rate at which it cools. The hypothesis is that the conditioning received during sample preparation on the controlled stress machine allows additional crystallinity to develop in the sample which subsequently gives higher modulus values when tested. It is important to note that the less crystalline ADH 28/2500NC does not show such differences at 20°C. It would be expected then that other, more crystalline, copolymers would also show similar large discrepancies, and whilst this is broadly true, *e.g.* ADH 14/2500NC and 33/400XL, it is more noticeable with the copolymer having the highest molecular weight. Figure 76 illustrates the measured differences in adhesive crossover temperature T_X for each of the techniques as a function of the melt index of the polymer.

There is evidence in the literature that the rate of cooling grossly affects the dynamic mechanical properties of amorphous polymers [219]. It has been shown that quench-cooled polymers have greater damping, *i.e.* higher values of *tan* δ, than slow cooled polymers [220] and that quenching raises both the T_g and the position of the maximum in the loss tangent curve T_L. It has also been shown [221] that quenching broadens the lower temperature side of the *tan* δ maxima. Work by Kovacs *et al* [222] showed the above phenomenon and related the various degrees of quenching and annealing performed on poly(vinyl acetate) back to changes in the free volume of the sample (as determined by measurements of density). Annealing decreases free volume and causes a decrease in molecular mobility which manifests itself in higher modulus and reduced damping values. If an examination is made of the data in the present work, the slowly cooled controlled stress samples do exhibit higher modulus values although evidence of an increase in damping is not as clear. Examination of sample rheograms also confirms that the rapidly cooled controlled strain specimens tend to have slightly broader *tan* δ_h maxima, although for the

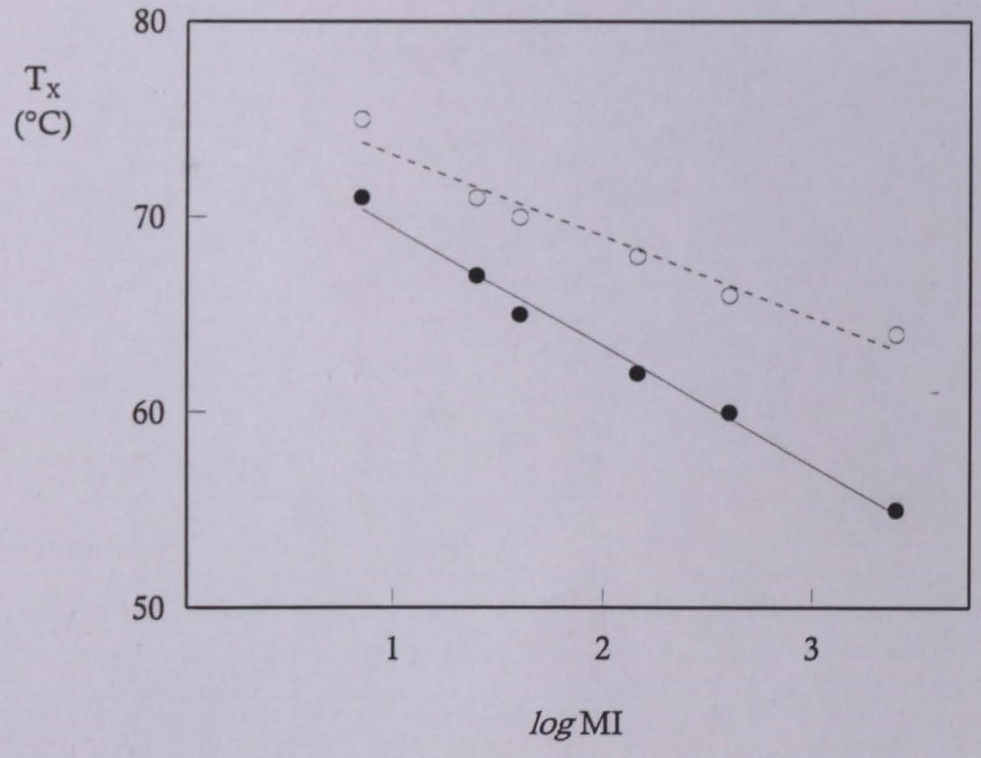

Fig 76. Graph showing variation of modulus crossover temperature T_x as a function of the logarithm of the polymer melt index MI as determined by controlled stress rheometry ● and controlled strain rheometry ○. Data presented for adhesives containing ExUL EVA of 28%VA composition. Conditions (controlled stress): 8 mm diameter parallel plates; 1 000 μm gap; heating rate 5°C min^{-1}; 10 rad s^{-1}. Conditions (controlled strain): 7.9 mm parallel plates; 1 000 μm gap; Soak and step heating parameters: 30s soak time, 15°C step; 10 rad s^{-1}.

adhesive samples this effect is by no means conclusive.

There are other examples of discrepancies between the two techniques, some of which also may be attributable to the cooling process, others to the 'heat and soak' technique versus the 'dynamic' heating method utilised by the controlled stress instrument however the important conclusion remains that the two techniques, for crystalline polymers and compounds of them thereof, although qualitatively giving the same data, are not quantitatively comparable. For the purposes of the modelling of industrial applications, it is probably not critical which technique is selected but care must be taken to treat all samples with an identical thermal history. For this reason the rest of this discussion will concentrate on the controlled stress results, bringing in controlled strain results only when serious discrepancies arise and, if necessary, to confirm key points.

Qualitatively, the rheograms of the EVA copolymers share several of the key features illustrated by Ferry [223] for an amorphous copolymer. These features include the glassy plateau at low temperatures, a 'transition point' (signified by a local maximum in either the loss tangent or loss modulus curve), a region wherein the storage modulus decreases gradually with an increase in temperature, followed by a sharp drop in modulus and increase in loss tangent to greater than unity, and finally a flow region where G' and G" decrease monotonically with temperature. The example used by Ferry was an amorphous poly(styrene) and it is important to note both the striking similarities and the large differences when compared with copolymers containing proportions of a crystallising comonomer. Figure 77a illustrates the variation in storage modulus curves for the ExUL EVA series containing 28% VA. It can be clearly seen that the major effects of increasing MI (reducing molecular weight) are: a shift in the melting point (characterised by the sharp drop in G') towards lower temperatures; lower moduli in the terminal zone, middle region between T_g and melting point; and, to a lesser extent, a reduction in modulus at lower temperatures (keeping in mind earlier comments about measurements in these regions).

The primary feature of the rheograms is the variation in G' and G" as the temperature increases. There is no evidence in any of the rheograms of G" being

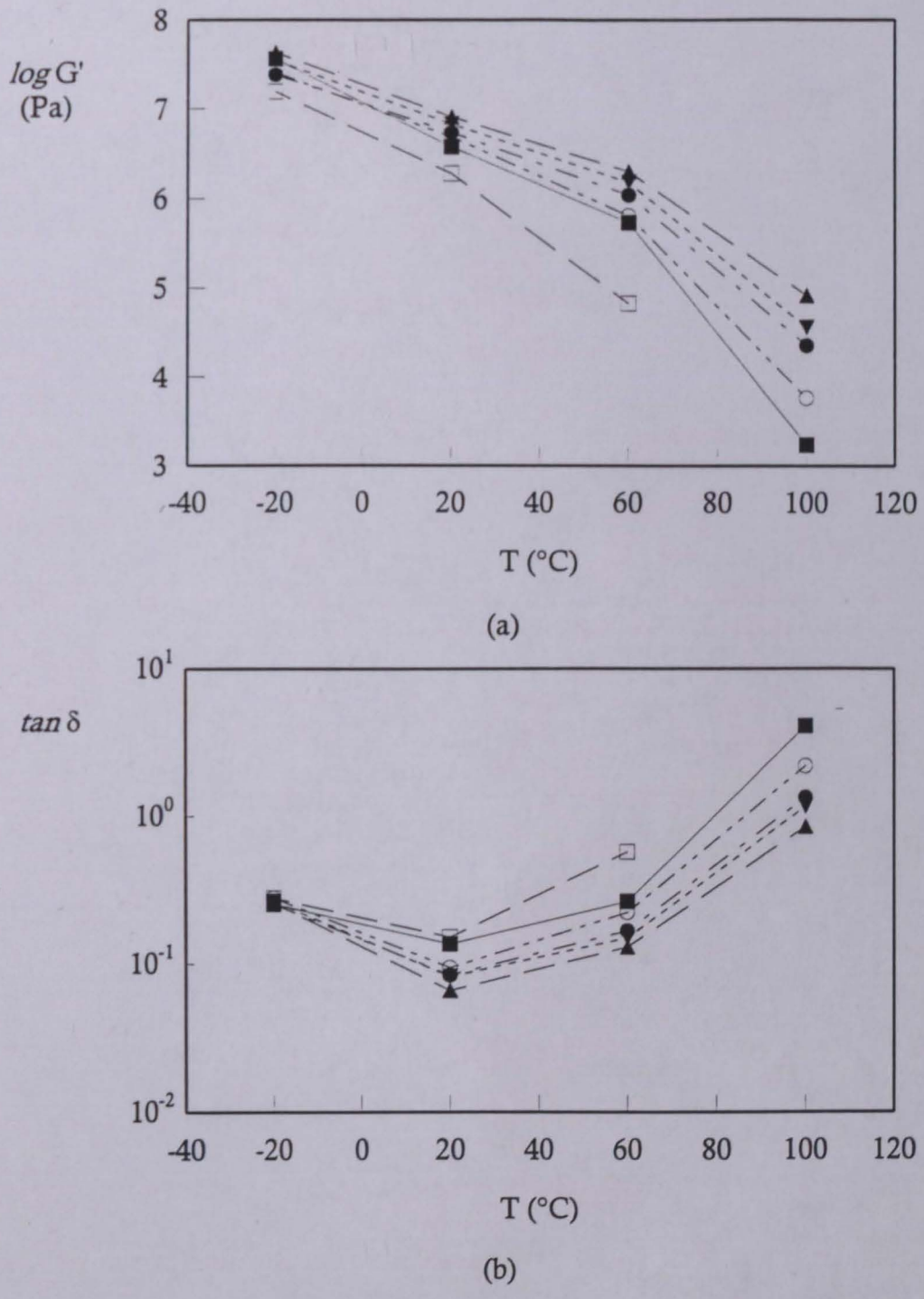

Fig 77. Graphs showing variation of (a) storage modulus G' and (b) loss tangent *tan* δ as a function of temperature T. Data presented for ExUL EVAs of 28%VA composition. Symbols: ▲ 28/7NC; ▼ 28/25NC; ● 28/40NC; ○ 28/145NC; ■ 28/400NC; and □ 28/2500NC. Conditions: controlled stress; 8 mm diameter parallel plates; 1 000 μm gap; heating rate 5°C; 10 rad s^{-1}.

close to G' or greater than it, below the crossover temperature. This implies that the EVAs are behaving as tough, elastic solids. At room temperature, elastic moduli vary from about 8 MPa to 2 MPa as the molecular weight decreases. This decrease occurs at all temperatures but is clearly more visible in the melt region where elastic moduli are very small and for the lowest molecular weight samples (14/2500NC, 28/2500NC and 28/2500XL) are undetectable at 100°C within the limits of the instrument. Figure 50 (p133) shows a plot of the logarithm of G' at each of the temperatures in Table 13 versus the logarithm of the melt index. It can clearly be seen that the variation in G' attributable to molecular weight becomes greater as the temperature increases. Significant points on the graph are the results for 28/400NC at 20°C, 28/7NC at 100°C, and 28/2500NC at 60°C. At a temperature of 100°C, all of the samples have undergone the transition from G' being greater than G" to *vice versa*. The gradient of the line shown on Fig 50 through all the molten samples is -1.11 and is an exceedingly good fit (linear regression coefficient, $r^2 = 0.999$ and standard error, S.E., of 0.6%) however the still solid 28/7NC sample does not fall on that line and the drop in modulus is not as great as with the other molten samples. Similarly, at 60°C the regression line through the still solid samples has a gradient of -0.35 ($r^2 = 0.970$, S.E. = 0.71%). The point for 28/2500NC lies a little off the regression line as, at this temperature, the polymer is very close to the crossover point. Note that there is an estimated uncertainty of ± 1% in the interpolated T_X. The significance of these regression curves is that it allows prediction of the modulus of an EVA copolymer at each of the chosen temperatures which may be a useful first step towards modelling a complete adhesive's behaviour. Figure 77b illustrates the variation in *tan* δ for the same samples. It is important to state again at this juncture that the position of the *tan* δ peak does not truly represent the glass transition temperature however it can be of technological importance. It is also easily measured and has in previous works [88, 156, 172] been used as an indicator of the T_g. This convention is continued in the present work although, as will be seen later, the correlation between DSC-derived T_gs and *tan* δ peak temperatures is not without significant scatter. The maximum in the *tan* δ curve is reasonably well defined however it

does not exhibit a sharp peak as is obtained with polymers with a small polydispersity index [224], nor does it shift to a large degree with molecular weight. This lack of significant shift correlates with the DSC results discussed earlier (p167) which also showed minor variation with molecular weight although it can be said that the measurement of the peak temperature this was easier to determine than the corresponding midpoint T_g from the DSC curves. Figure 78 is similar to that already presented for the neat polymers however this time the results are for the adhesive samples. Immediately apparent is the effect of the wax on the rheogram of the adhesive. The crystalline paraffin wax has a narrow melting range between 60 and 70°C and this is reflected in the extremely steep drop in G' between these two temperatures. Above the softening point of the wax it behaves as an extremely low molecular weight plasticiser which acts to dilute the adhesive, separating the molecules of the EVA and hence reducing the viscosity. Above the softening point, the paraffin wax is insoluble in the EVA/resin system and is precipitated at its freezing temperature which corresponds to the cloud point of the adhesive [156]. It has been proposed that crystalline waxes act as fillers in the solid phase [88] and the usual phenomena associated with filled polymers (increased modulus, broadening of *tan* δ peak) [225] are clearly observed in the data on the present work. In addition, there is a slight increase in the amount of damping (height of *tan* δ peak). Completely inert fillers tend to decrease damping in polymeric materials however the nature of mineral waxes is such that the earlier hypothesis of some compatibility between the EVA and wax, even below the cloudpoint, should be considered. This is especially true of paraffin waxes with their largely random composition of crystalline and amorphous material [20]. The shift in the position of the *tan* δ peak in the adhesive samples is believed to be indicative of compatibility between the copolymer and the amorphous resin. It has been shown extensively for pressure-sensitive adhesives [*e.g.* 165], and in simple EVA/resin blends, that the addition of a compatible resin causes the phenomenon of two separate *tan* δ peaks (corresponding to the resin and copolymer respectively) merging into one (Fig 79). The use of the Fox equation to predict the position of midpoints T_gs (as determined by DSC) has already been discussed and it has also been used to

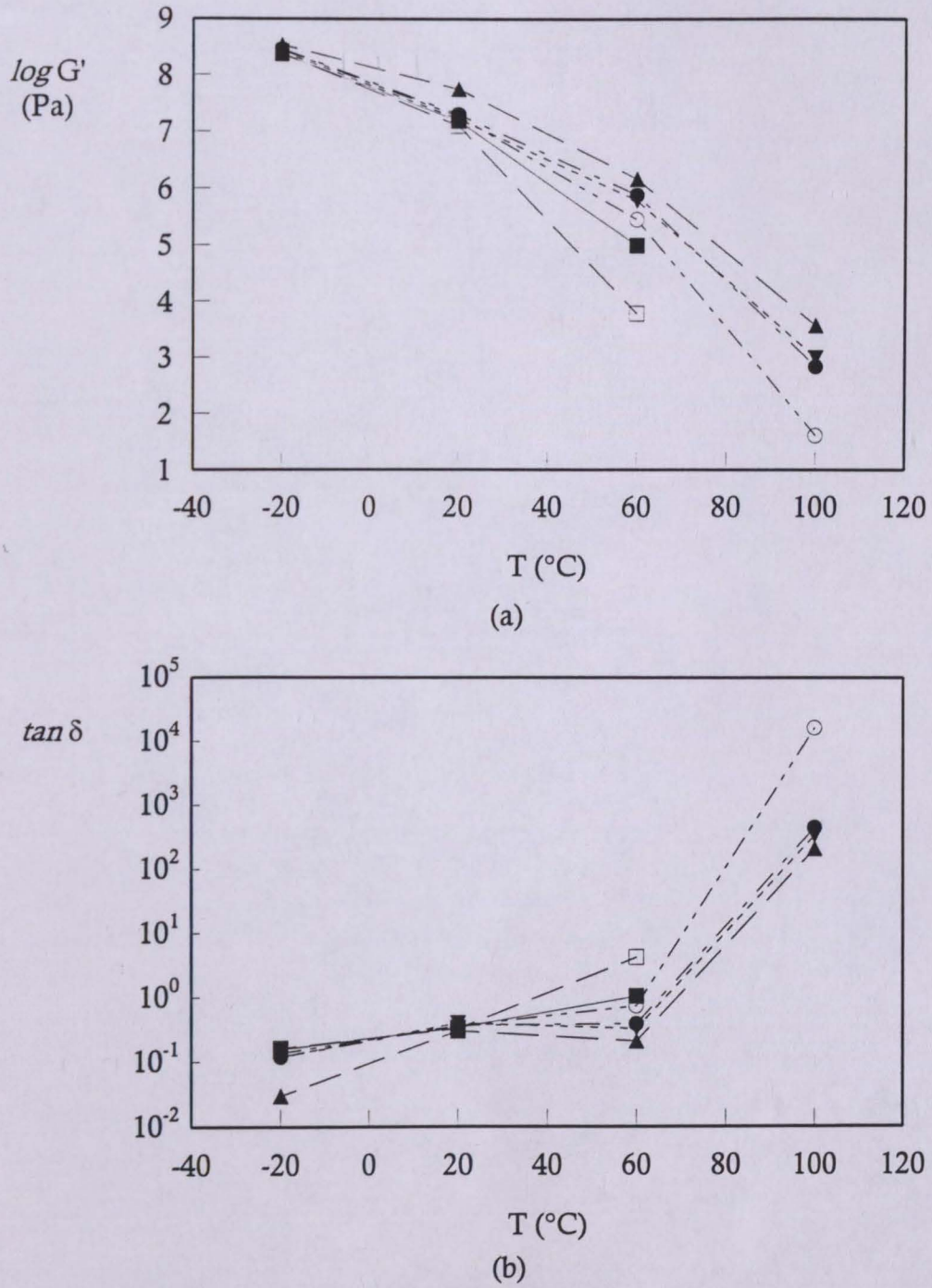

Fig 78. Graphs showing variation of (a) storage modulus G' and (b) loss tangent *tan* δ as a function of temperature T. Data presented for adhesives containing ExUL EVAs of 28%VA composition. Symbols: ▲ 28/7NC; ▼ 28/25NC; ● 28/40NC; ○ 28/145NC; ■ 28/400NC; and □ 28/2500NC. Conditions: controlled stress; 8 mm diameter parallel plates; 1 000 μm gap; heating rate 5°C; 10 rad s^{-1}.

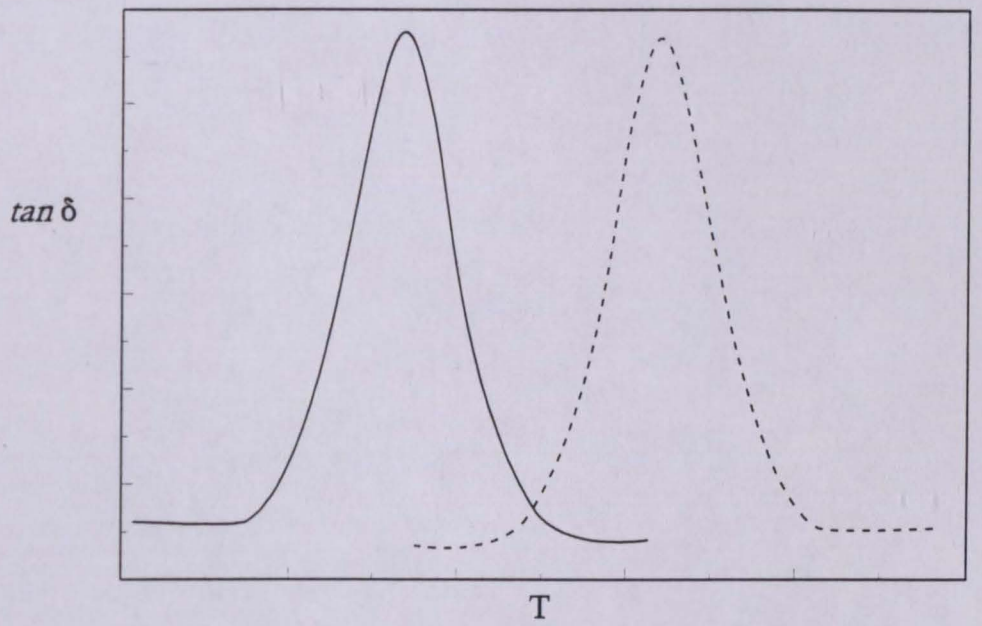

(a)

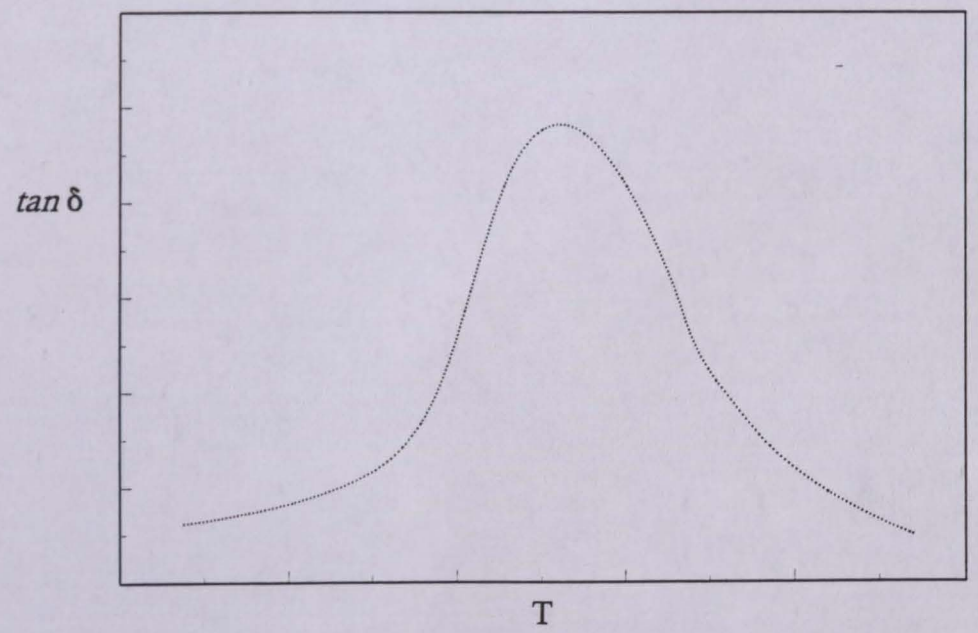

(b)

Fig 79. Schematic diagrams of the loss tangent *tan* δ as a function of temperature T for an idealised polymer (———) and a fully compatible resin (-------), both of which only possess a single peak in the temperature range of interest. (a) individual *tan* δ peaks prior to mixing. (b) single, broader *tan* δ peak obtained after blending (·····). Note that the effect is exaggerated for clarity. See text for details.

indicate the position of *tan* δ peaks however the arguments explored for the DSC work regarding crystalline polymers and co-compatibility remain equally valid in this case. Marin *et al* [172] notes that the resin acts as an anti-plasticising agent in the case where its T_g is greater than that of the polymer, and as a plasticiser when it is below. In the materials used in this study, it is clear that the addition of the rosin ester tackifying resin will have an anti-plasticising effect due to the differences in T_g (T_{gh} = 38°C for the resin *versus* T_{gh} = *c.* -27°C for the EVA copolymers).

The key features of the EVA polymers will now be examined in detail with respect to molecular weight, composition, and crystallinity. Figure 77 shows the variation of storage modulus G' and loss tangent *tan* δ with temperature for the ExUL EVA copolymers containing 28% VA. The general features of the curves have already been discussed, what follows is an attempt to identify particular features of the curves with particular molecular motions. The variation of these motions and the impact on copolymer properties will then be discussed in relation to molecular weight, composition, degree of crystallinity, and manufacturer, with particular reference to the likely implications on adhesive performance. Several authors *e.g.* [223] have, in the past, found it conventional to divide the behaviour of copolymers into zones depending upon modulus or general characteristics. The zones which are of particular significance for semi-crystalline, non-crosslinked polymers are, in order of increasing temperature; the glassy zone (G' $>10^8$ Pa), the rubber-to-glass transition, the rubbery (or leathery) plateau, the order-disorder transition associated with crystalline melting, and the flow (or terminal) region.

Within the temperature region studied in the present work, all of the EVA copolymers show a single maxima in both the loss tangent and loss modulus curves. Both of these maxima are commonly taken to be representative of the glass transition T_g and, as stated before, whilst this is not strictly true [175], the values determined may be of technological importance in the prediction of adhesive properties, as will be discussed later. The phenomenon of the damping peak is associated with a non-specific 'loosening' of the hereto rigid polymer structure as a general consequence of the increase in free volume associated with

increasing amounts of thermal energy. The T_g data generated by DSC measurements have already been discussed with the overall conclusion that there is little variation in the T_g with molecular weight, with more significant variation attributable to copolymer composition. The same conclusions can be drawn if T_L (loss tangent maxima) or $T_{L''}$ (G" modulus maxima) are considered. However it was considerably easier to observe and determine the rheological T_g points than it was to determine the DSC T_gs. It should be remembered that the position of the damping peaks are not just related to free volume changes, but also such parameters as polymer morphology which is of critical importance when considering crystallisable polymers. At low frequencies, it is the maximum in the G" curve that is more closely representative of the T_g [175]. If the *tan* δ maxima is used, care must be taken that the β-transition (which may be used as an indicator of the T_g) is not so close to the α-transition (the transition associated with the order-disorder change of crystalline melting) that interference may result. Interference and superposition of several relaxation mechanisms is especially problematical for semi-crystalline polymers due to the complex nature of their morphologies. Willbourn [205] describes the variables associated with transitions in crystalline regions, variable amounts of crystallinity, and different crystal structures dependant upon the thermal history of the copolymer system. The β-transition was assigned by him to be the T_g of the amorphous regions with γ and δ sub-T_g transitions dependant upon the nature and length of side chain branching. His assignment of the α-transition to crystalline melting was based upon the observation that the intensity of the transition decreased as the crystallinity of the system was reduced. The notion that the β-transition is associated with inter-lamellar non-crystalline regions is popular [226] although more recent work hypothesises that the β-transition is in fact attributable to the more specific relaxation of CH_3-bearing side chains [200]. It is likely however, on the basis of recent work [227], that both the β- and γ-transitions are true T_gs as they have been shown to possess high activation energies and time-temperature superpositionability (so-called WLF dependance). Table 26 and Fig 80 compare T_g data as derived from DSC heating scans with T_L and $T_{L''}$ data. There is a great deal of scatter and correlation is not readily

Table 26 Comparison of glass transition events as determined by differential scanning calorimetry (DSC) and controlled stress rheometry on the components of adhesives.

Adhesive components	Mid point T_{gh} [a] (DSC)	Mid point T_{gc} [b] (DSC)	T_L (*tan δ* maximum) [c] (Rheometry)	$T_{L''}$ (G" maximum) (Rheometry)
	(°C)	(°C)	(°C)	(°C)
14/2500NC	-27	-35	-29	-40
19/150NC	-27	-35	-25	-36
28/7NC	-26	38	-26	-36
28/25NC	-27	-38	-27	-37
28/40NC	-27	-38	-30	-40
28/145NC	-28	-36	-31	-40
28/400NC	-27	-36	-32	-41
28/2500NC	-27	-44	-32	-42
28/40NC*	-26	-36	-25	-34
28/420NC*	-27	-32	-30	-41
33/400NC*	-26	-40	-31	-41
28/400XL	-27	-33	-24	-31
28/2500XL	-26	-36	-25	-35
33/400XL	-26	-37	-26	-35
Resin	38	31	ND[d]	55
Wax	ND	ND	ND	ND

(a) Second heating scan; +10°C min^{-1}.
(b) Cooling scan; -10°C min^{-1}.
(c) Temperature sweep; controlled stress; -50 to 150°C; +5°C min^{-1}; 10 rad s^{-1}; 8 mm parallel plate.
(d) ND; not detected.

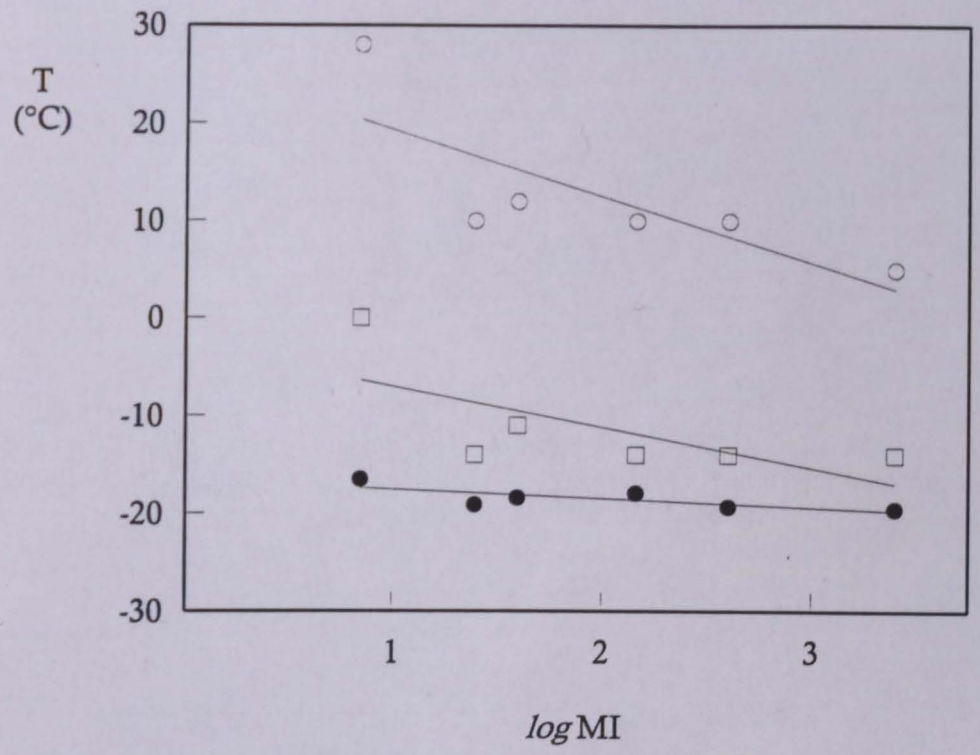

Fig 80. Graph of DSC glass transition temperature T_{gh}, loss tangent maximum temperature T_L, and loss modulus maximum temperature $T_{L''}$ of adhesives containing ExUL EVAs with 28%VA composition as a function of the logarithm of the polymer melt index MI. Symbols: ● data from second DSC heating curve, T_{gh}; ○ data from controlled stress rheometry, T_L; □ data from controlled stress rheometry, $T_{L''}$. See text for details.

apparent. Komornicki *et al* determined the T_g of the EVA 28/420NC* to be -40°C by DSC and approximately -28°C by TMA however they readily admit that the measurement of T_g by DSC is fraught with uncertainty due to the ambiguities of the baseline in a crystallising polymer. In addition they do not make clear the rheological phenomenon which they are taking as their T_g measurement in the rheological work, thereby making meaningful comparisons with the present work difficult.

Greater differences in the glass transition, as determined by either T_L or $T_{L''}$, can be observed if the VA concentration is varied at constant molecular weight. Examining the data in Table 19 we can see that increasing VA from 14 to 28% in a 2 500 MI copolymer gives a T_L shift of -3°C and a $T_{L''}$ shift of -2°C (correspondingly there is no significant shift in the DSC T_g), whilst increasing from 19% VA to 28% VA in a 150 MI copolymer gives T_L and $T_{L''}$ shifts of -6°C and -4°C respectively (-1°C shift in DSC T_g). It was commented upon, in a previous section, that the T_g data collected from the cooling scan was better in terms of repeatability. However, it does not make sense to compare rheological data gained during heating to thermal data from cooling, as the mechanisms responsible for the T_g process are too dependant upon the kinetics of crystallisation or relaxation [228]. The more crystalline ExAD polymers tend to have slightly higher T_L and $T_{L''}$ values than their non-crystalline counterparts. This effect is often seen with crystalline polymers, the crystallites serve to increase the strain on the amorphous regions of polymer, hence requiring additional thermal energy for molecular motion [229], or by a similar argument, due to the reduction in amorphous polymer chain length between crystallites [230]. Earlier comments on the susceptibility of the maxima to be affected by polymer morphology should also be borne in mind. It is likely that the microstructure of the solid polymers compared with that of the non-crystalline material is sufficiently different to cause other relaxation phenomena to influence the positions of the maxima. Similar comments apply to the AtEV polymers which have already hypothesised as being more crystalline than their ExUL counterparts. In summary, it can be said that the relative sensitivity of the T_g of EVA copolymers to molecular weight, composition, crystallinity, and

manufacturer seen in the DSC work is equally confirmed by the results of controlled stress rheometry, although the transitions which can be likened to the T_g, *i.e.* local maxima in *tan* δ and G" curves, are easier and more accurately determined by this technique.

The second zone often examined is the rubbery, or leathery, plateau. The distinction in nomenclature is based upon the value of the modulus in this region. The crystalline regions of the EVA copolymers act to dramatically increase the modulus within this zone to values much higher than that would be expected from an ideal rubber of similar molecular weight. The effect of crystallinity in a polymer modifies the modulus curve of an idealised amorphous polymer above its T_g by several mechanisms [231]. Firstly, the crystallites act as crosslinks by tying segments of several molecules together. Secondly, the crystallites themselves are reported as having very high moduli [232] compared with the rubber-like amorphous phase; in effect they behave as rigid fillers in an amorphous matrix. The effect is most noticeable in this second zone due to the large relative differences in moduli: below the T_g, the glass has a sufficiently high modulus to be affected only minimally by additional hard particles [233]. Figure 81 presents the complex shear modulus G* data as a function of temperature for the 28% VA ExUL EVAs. Note the qualitatively similar curve shape to the dominant G' curves at lower temperatures, whilst there is a manifestation of the G" data to the right of the crossover point. The data in the present work matches remarkably well to the established literature [*e.g.* 234] which describes the effects of crystallinity in an amorphous polymer both with respect to the values of the modulus in the plateau regions (changing as a function of molecular weight) as well as the shape of the curve in the plateau region. In reality, the plateau is not truly flat but has a negative temperature coefficient as a result of small, imperfect crystallites melting, which reduces the filler and crosslinking effects, and as a natural consequence of the polymer structure loosening. The effect of EVA composition can now be explained in terms of how it affects the size and distribution of crystallite formation. For example, the low vinyl acetate content, highly crystalline EVA 14/2500NC has a significantly higher modulus across the temperature range up to the melting point (which is

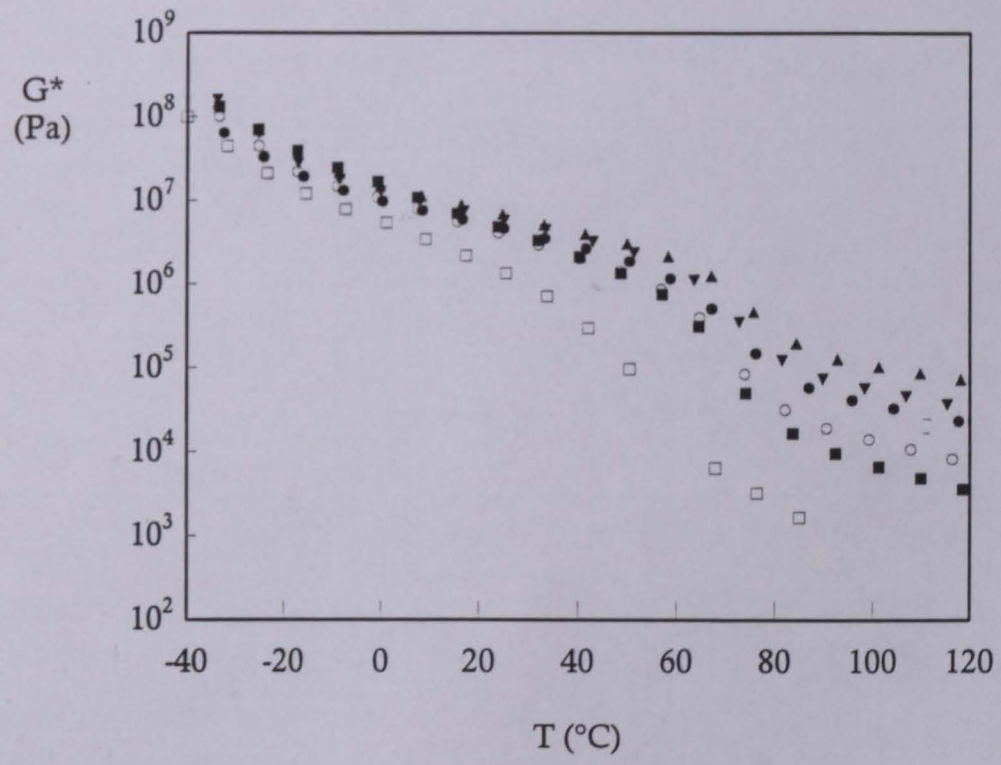

Fig 81. Graph of complex shear modulus G* as a function of temperature T. Data presented for ExUL EVA samples of 28%VA composition. Symbols: ▲ 28/7NC; ▼ 28/25NC; ● 28/40NC; ○ 28/145NC; ■ 28/400NC; and □ 28/2500NC. Conditions: controlled stress; 8 mm diameter parallel plates; 1 000 μm gap; heating rate 5°C; 10 rad s^{-1}.

itself increased) whilst the 33/400NC* polymer (which is considerably more amorphous than its 28/420NC* counterpart) has a lower modulus value. The steep slope evident in the plateau region of the 2 500 MI modulus curve prompts the discussion of the entanglement molecular weight (M_e). This is the minimum value of molecular weight required for the formation of the crosslinks that leads to the formation of the plateau. It is possible to estimate the entanglement molecular weight from the pseudo-equilibrium plateau modulus G_N^0 using the following [234]

$$G_N^0 = \rho RT/M_e \qquad \ldots (40)$$

where ρ is the density of the polymer at temperature T and R is the gas constant. G_N^0 itself may be determined indirectly with a reasonable degree of accuracy by considering literature values for the plateau moduli of poly(vinyl acetate), G_{N1}^0 and poly(ethylene), G_{N2}^0 hence [235]:

$$log\, G_N^0 = v_1\, log\, G_{N1}^0 + v_2\, log\, G_{N2}^0 \qquad \ldots (41)$$

where v_1, v_2 are the volume fractions of VA and ethylene in the EVA copolymer repectively. Substituting $G_{N1}^0 = 2.586 \times 10^5$ Pa and $G_{N2}^0 = 1.524 \times 10^6$ Pa (taken from ref [234]) with $v_1 = 0.22$ for a 28% VA EVA, $G_N^0 = 1.032 \times 10^6$ Pa and hence, using a temperature of 23°C as reference and $\rho = 0.95$ g cm^{-3} at 23°C, M_e = 2 265 g mol^{-1}. Inspection of the molecular weight data in Table 5 (Chapter 3) indicates that, even for the 2 500 MI samples, the M_n values are greater than M_e. Clearly from the above calculation, it can be seen that varying the composition of the copolymer will affect the plateau modulus (and by inference the critical molecular weight). As the volume fraction of the VA is decreased, the contribution to G_N^0 by the plateau modulus of the poly(ethylene) is increased and G_N^0 is larger in magnitude. In fact the same argument can be applied to the value of G at any point, and this effect is clearly seen in Fig 82 whereby the increase in modulus due to reduction in VA generation, and *vice versa*, are shown for ExUL 2 500 MI and AtEV 400 MI EVAs. Note that, for the 14/2500NC EVA, the plateau is considerably more well defined and extends over a broader temperature range - this is a direct consequence of the higher G_N^0 value obtained *via* eqn. (41). The higher value of G_N^0 implies a lower M_e and indeed M_e of EVA 28/2500NC ≈ 2 265 g mol^{-1} whilst M_e of EVA 14/2500NC ≈ 2 150 g mol^{-1}.

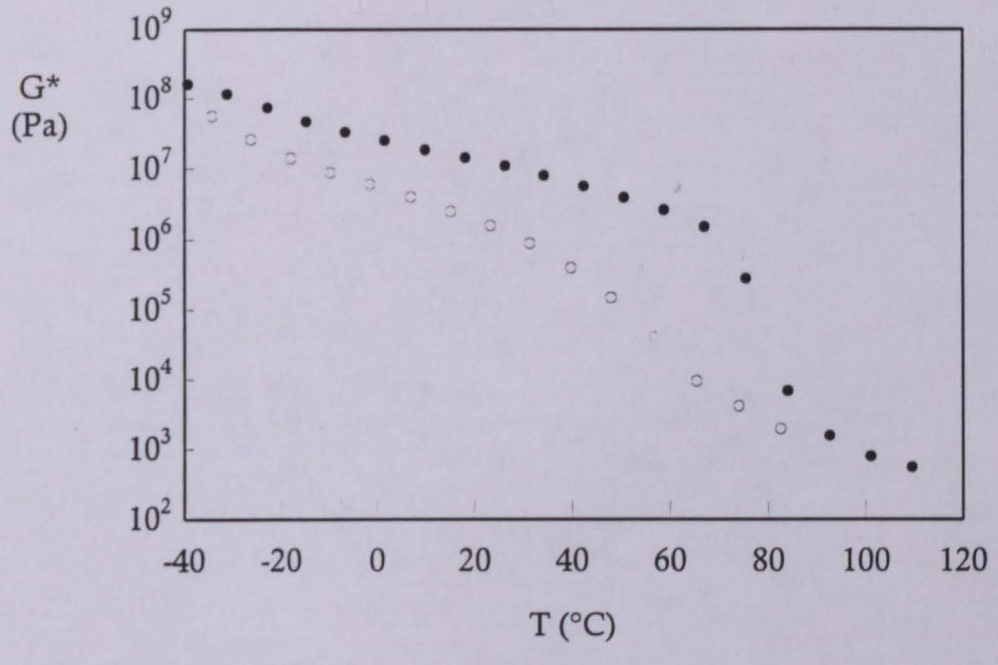

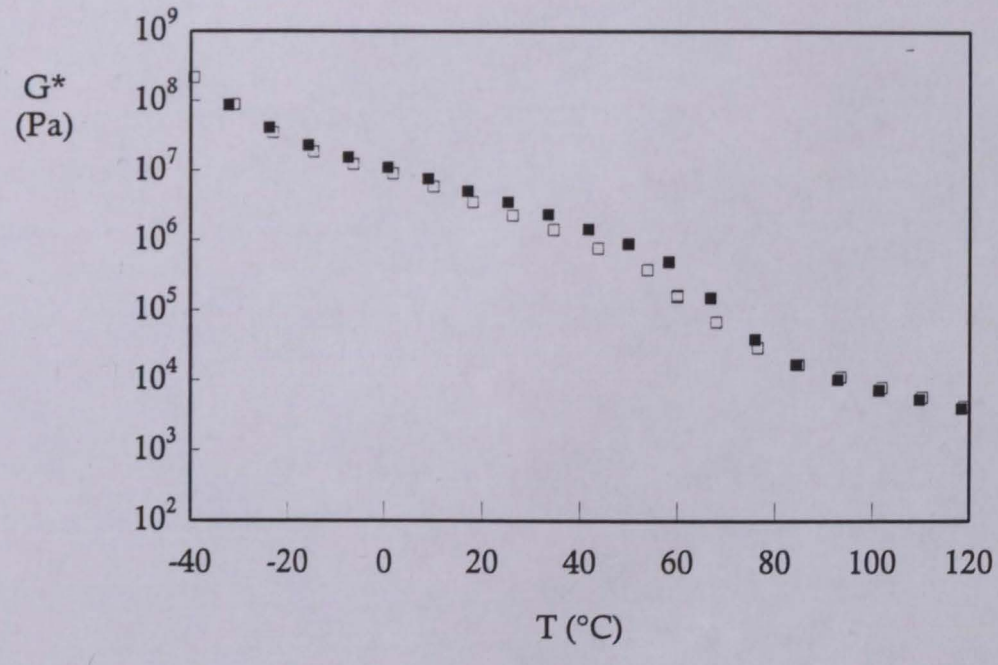

Fig 82. Graphs showing variation of complex shear modulus G* as a function of temperature T. (a) ExUL EVAs ● 14/2500NC and ○ 28/2500NC; and (b) AtEV EVAs ■ 28/420NC* and □ 33/400NC*. Conditions: controlled stress; 8 mm diameter parallel plates; 1 000 μm gap; heating rate 5°C; 10 rad s^{-1}.

In addition, the presence of fewer VA groups to disrupt the formation of regions of high crystallinity gives a sharply defined melting point. The effect of increasing the amount of vinyl acetate in the copolymer is illustrated in Fig 82b for the AtEV polymers. Due to the much higher molecular weight of the 400 MI EVA, the differences caused by an additional 5% VA are more subtle than in the previous example. However a reduction in plateau modulus and a lowering of softening point are clearly visible and commensurate with a less crystalline polymer. If the high crystallinity versions of two EVA copolymer pairs are examined (Fig 83) the effect of crystallinity hypothesised, and discussed, above is observed and the two key parameters, plateau modulus and melting point are clearly increased with increasing crystalline content.

The final zone of interest is that immediately beyond the sudden drop in modulus which we have denoted the crossover point. It is interesting to note that the point at which G" becomes larger than G' (denoted T_X in this work) occurs within the region of the sudden drop for all polymer samples save those with the highest molecular weights, in practice ExUL 28/7NC and ExUL 28/25NC, which occur some way beyond that point. The sudden drop in modulus is generally associated, in crystalline polymers, with the melting of the crystals to give an amorphous, rubber like material which either flows (if G" > G') or persists in the rubber plateau for an additional temperature range. This point may be of significant technological importance as it would allow materials to soften and deform under applied stresses but not start flowing until some higher temperature was reached. This could be useful in applications such as bookbinding adhesives where adhesive properties under a wide variety of environmental conditions is required.

In considering the crossover point further (called the 'cohesion point' by Komornicki) there are, perhaps, three key parameters which may be influenced by molecular weight, composition, and crystallinity. Those are the temperature of crossover T_X, the modulus value at this point G_X, and the slope of the tangent drawn to the modulus curve at this point. On the semi-logarithmic plots normally employed, this is denoted $(d(log\, G')/dT)_{Tx}$ (see Chapter 2). Upon initial examination of the data it is immediately apparent that T_X is related to,

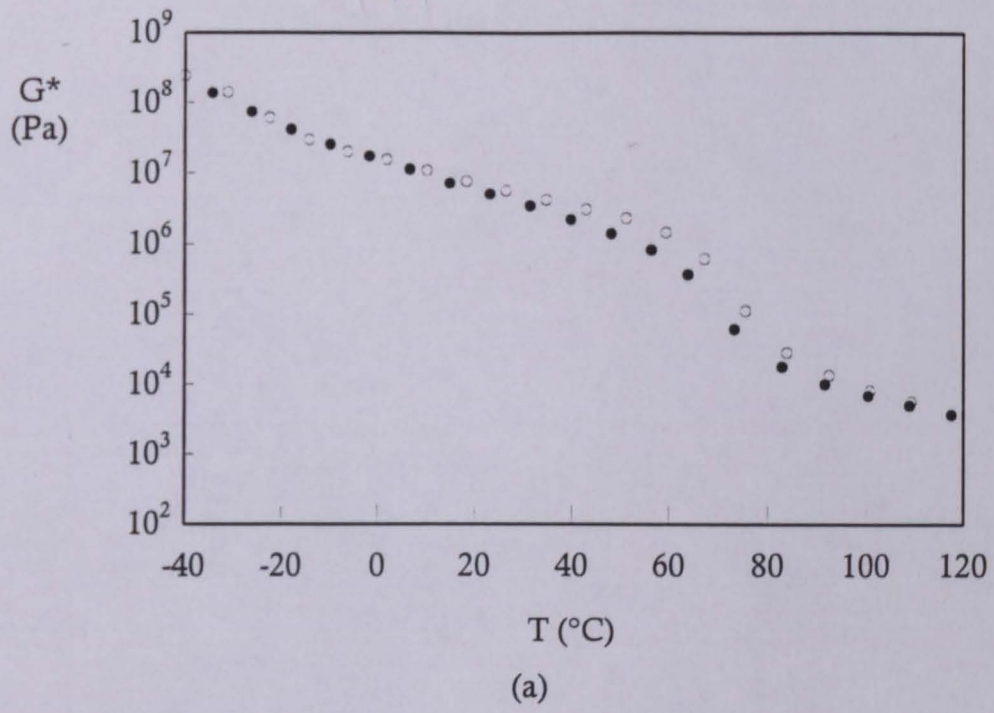

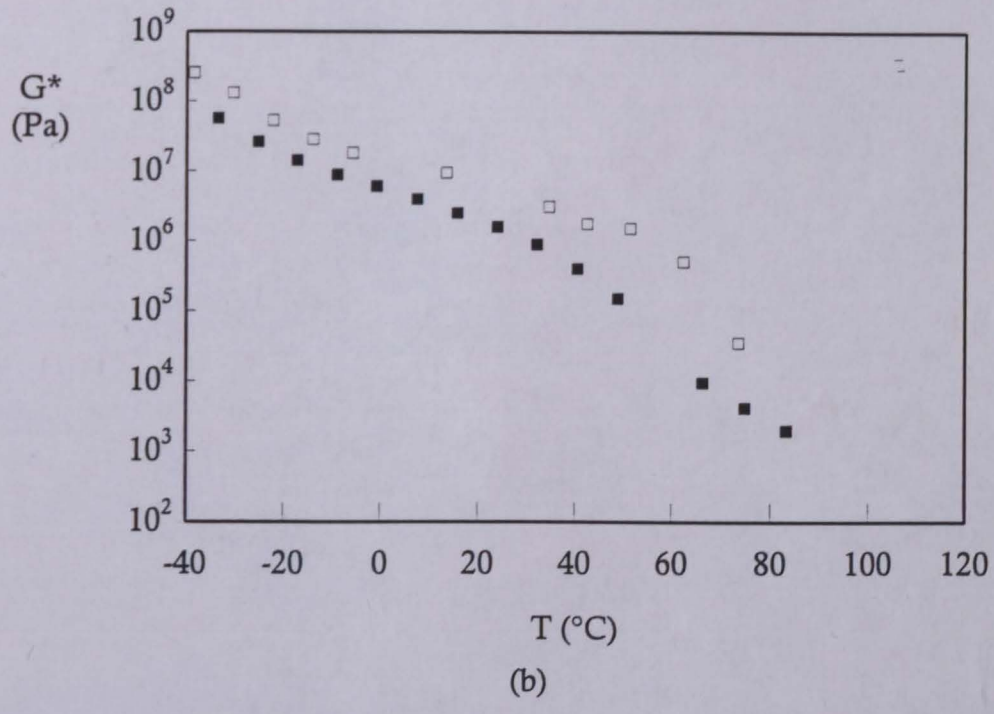

Fig 83. Graphs showing variation of complex shear modulus G* as a function of temperature T. (a) ● EVA 28/400NC and ○ EVA 28/400XL; and (b) ■ EVA 28/2500NC and □ EVA 28/2500XL. Conditions: controlled stress; 8 mm diameter parallel plates; 1 000 μm gap; heating rate 5°C; 10 rad s^{-1}.

and affected to the same extent by, the parameters already discussed in relation to the behaviour of the polymers in the plateau zone (Fig 84) however the trends visible with the crossover modulus G_X are not as clear (Fig 85). Figure 85a shows the relationship between G_X and MI. There is a considerable amount of scatter and no clear correlation can be drawn between MI or % VA (Fig 85b). There may be some suggestion that higher crystalline contents give higher G_X values but this is self-evident if the arguments considered previously are taken as being true. The cohesion rate is also plotted *vs* MI in Fig 86 and the correlation is quite good as the line of best fit drawn through the 28% VA NC ExUL data points illustrates ($r^2 = 0.899$). Examining the graph indicates that the vinyl acetate concentration is also significant. It is possible, though the evidence is scant, that the variation in cohesion rate attributable to VA concentration is a function of the relative monomeric friction coefficients of VA and ethylene. The monomeric friction coefficient is defined as a measure of the frictional resistance to translational movement of a monomer unit on a sufficiently long molecule, *i.e.* the effects of free chain ends is considered negligible [34]. Although data for poly(ethylene) is not given in this reference, it may be reasonable to assume that it is approximately 6 500 Pa s m^{-1} at 373K based on the data given for a number of polyolefin polymers. In contrast, the value quoted for poly(vinyl acetate) is 4 870 Pa s m^{-1} at 373K. Following this line of reasoning, one may expect that polymers containing more vinyl acetate may, irrespective of the actual temperature of melting, undergo flow more easily than those polymers with little VA. If this were true, the low VA polymers would require greater thermal energy to undergo movement and, under conditions of fixed heating rates, would appear to suddenly melt as opposed to a gradual softening, *i.e.*they would have a greater cohesion rate. It is stressed that this hypothesis is highly speculative but it may give an insight into the true nature of the molecular relations and movements happening around this point. It should be noted that the correlation between activation energy for viscous flow and the cohesion rate is not significant and so meaningful conclusions on the cohesion rate cannot be drawn from a consideration of viscosity data alone. This is not surprising considering the differences in rheological behaviour of the adhesive under

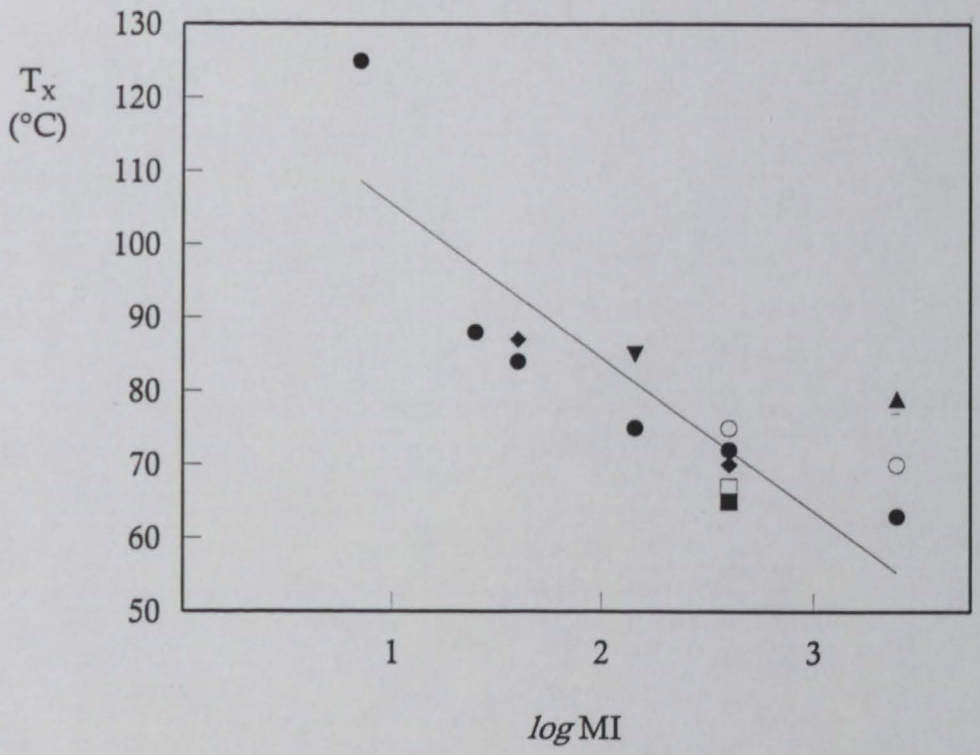

Fig 84. Graph of modulus crossover temperature T_X for the EVA copolymers as a function of the logarithm of the melt index MI. Symbols: ▲ 14% VA; ▼ 19% VA; ● 28% VA NC; ○ 28% VA XL; ■ 33% VA; □ 33% VA XL; ◆ 28% VA NC*. Conditions: controlled stress; 8 mm diameter parallel plates; 1 000 μm gap; heating rate 5°C; 10 rad s^{-1}.

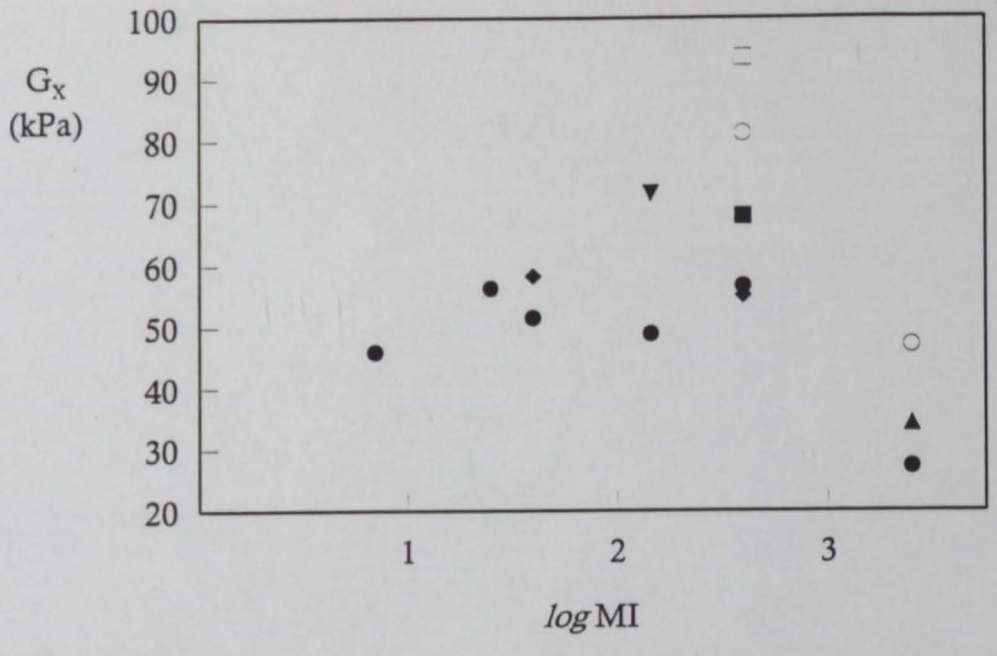

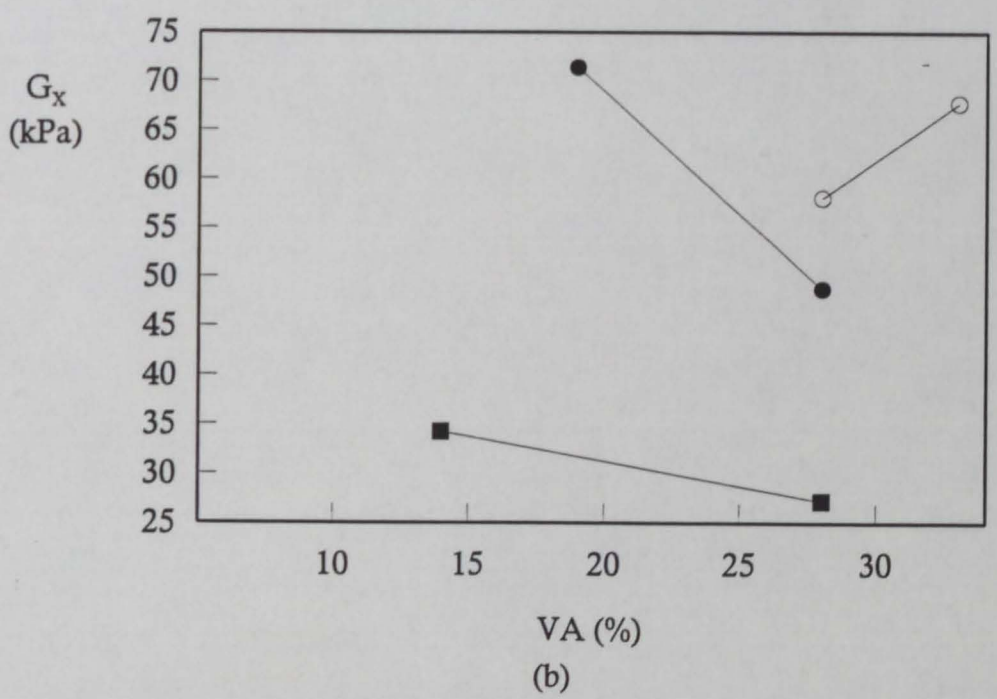

Fig 85. Graphs showing variation of EVA crossover modulus G_x as a function of (a) the logarithm of the melt index MI and (b) vinyl acetate concentration %VA. Symbols: in (a) ▲ 14% VA; ▼ 19% VA; ● 28% VA NC; ○ 28% VA XL; ■ 33% VA; □ 33% VA XL; ◆ 28% VA NC*, and in (b) ● ExUL 150MI NC; ○ ExUL 2500MI NC; ■ AtEV 400MI NC*. Conditions: controlled stress; 8 mm diameter parallel plates; 1 000 μm gap; heating rate 5°C; 10 rad s^{-1}.

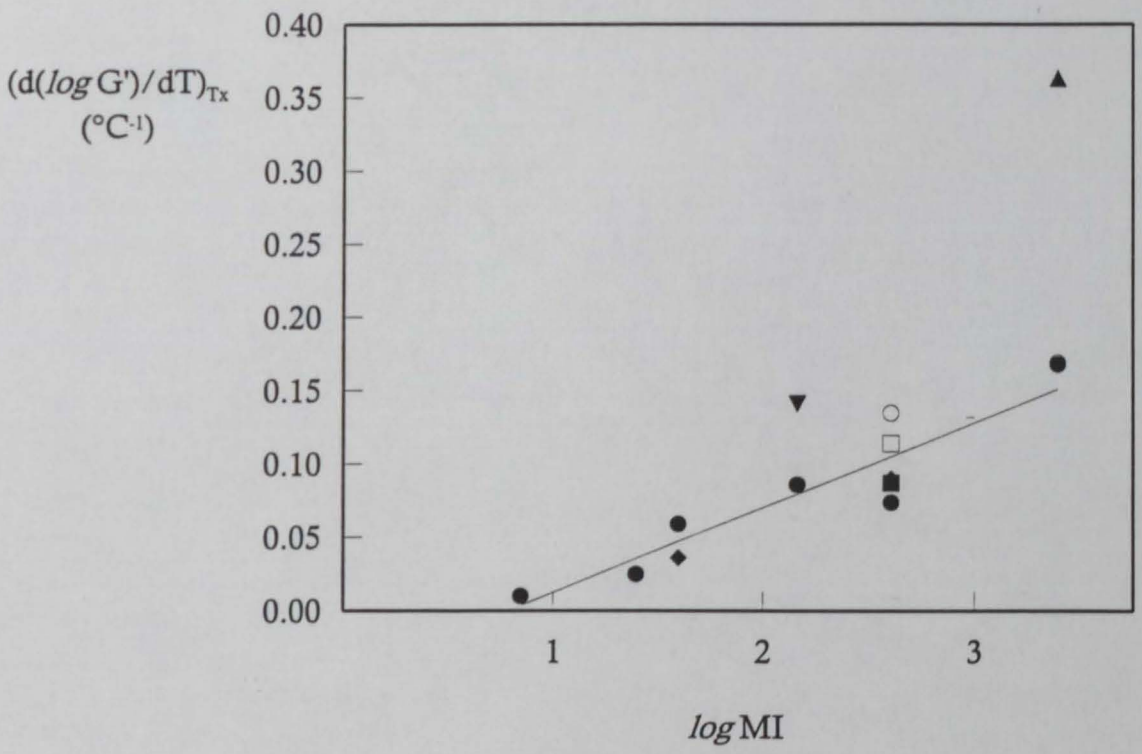

Fig 86. Graph of cohesion rate $(d(log\,G')/dT)_{Tx}$ for the EVA copolymers as a function of the logarithm of the melt index MI. Symbols: ▲ 14% VA; ▼ 19% VA; ● 28% VA NC; ○ 28% VA XL; ■ 33% VA; □ 33% VA XL; ◆ 28% VA NC*. Conditions: controlled stress; 8 mm diameter parallel plates; 1 000 μm gap; heating rate 5°C; 10 rad s^{-1}. Regression line is least squares fit of the 28%VA NC ExUL datapoints.

conditions of flow and oscillatory rheological testing. The composition theory also relates back to considerations of copolymer crystallinity (as in other examples). Examination of the highly crystalline sample datapoints *e.g.* low VA, AtEV, or ExAD grades is not conclusive, however in most cases the more crystalline grades have a slightly higher cohesion rate.

Once past the crossover point, G' diminishes rapidly to almost vanishingly small values, and indeed was not detectable in the experimental configuration herein for 2 500 MI EVAs whilst G" dimishes more slowly with temperature. This has the effect of letting the melt behave as a predominantly viscous liquid although the examination of high temperature data, particularly for the higher molecular weight EVAs shows that there is still considerable elastic nature at temperatures well within the typical range of hot melt adhesive application conditions, typically between 120 - 180°C. Figure 87 illustrates G' and G* respectively for EVA 28/145NC.

The adhesive rheograms show the similar pattern of zones as the EVA polymers they contain, with the general observations that the plateau between the glass/rubber and the plateau/flow transitions is both higher in modulus and slightly shorter. The increase in modulus has been discussed earlier whilst the foreshortening effect of the plateau region is attributable to the effective broadening of the molecular weight distribution caused by the addition of low molecular weight tackifying resin and wax. This effectively reduces the entanglement molecular weight M_e of the adhesive as a whole which in turn governs the length of the plateau. It can be noted that the plateau length in a double logarithmic plot of modulus *vs* frequency can be empirically calculated [34, 236] as:

$$\text{length of plateau} \propto 3.4 \; log\,(M_w/M_e) \qquad \ldots (42)$$

where M_w is the weight average molecular weight. Given the general equivalence of viscoelastic functions in the time and temperature domain, it is perhaps not unreasonable to expect that a similar relationship exists for modulus/temperature graphs, and this effect is visible to some limited extent in the rheograms in the present work (Fig 88).

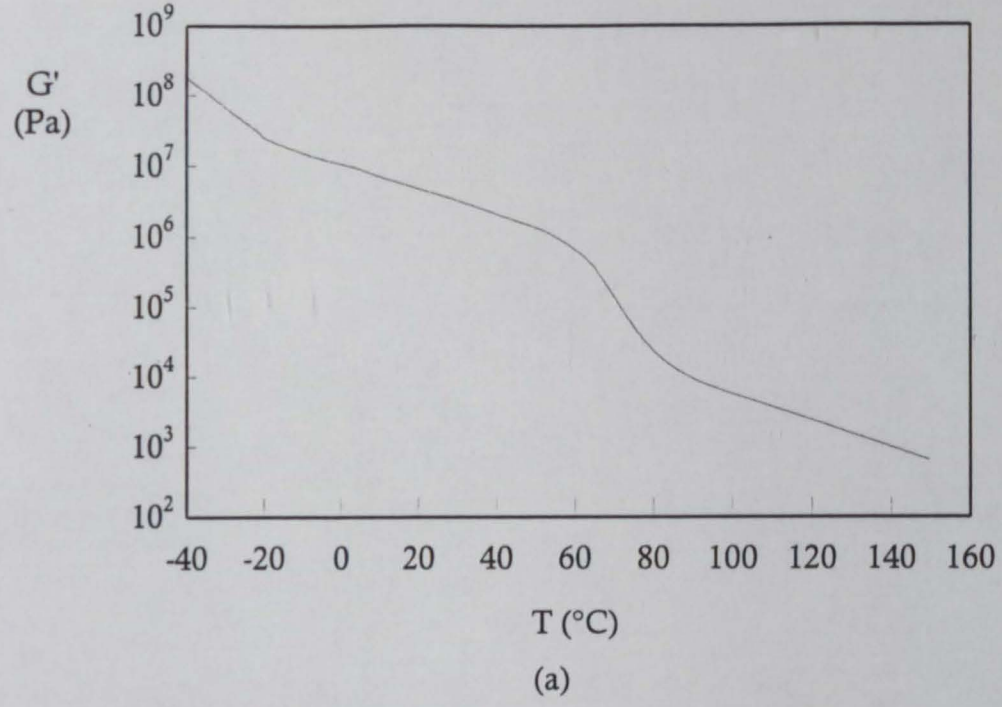

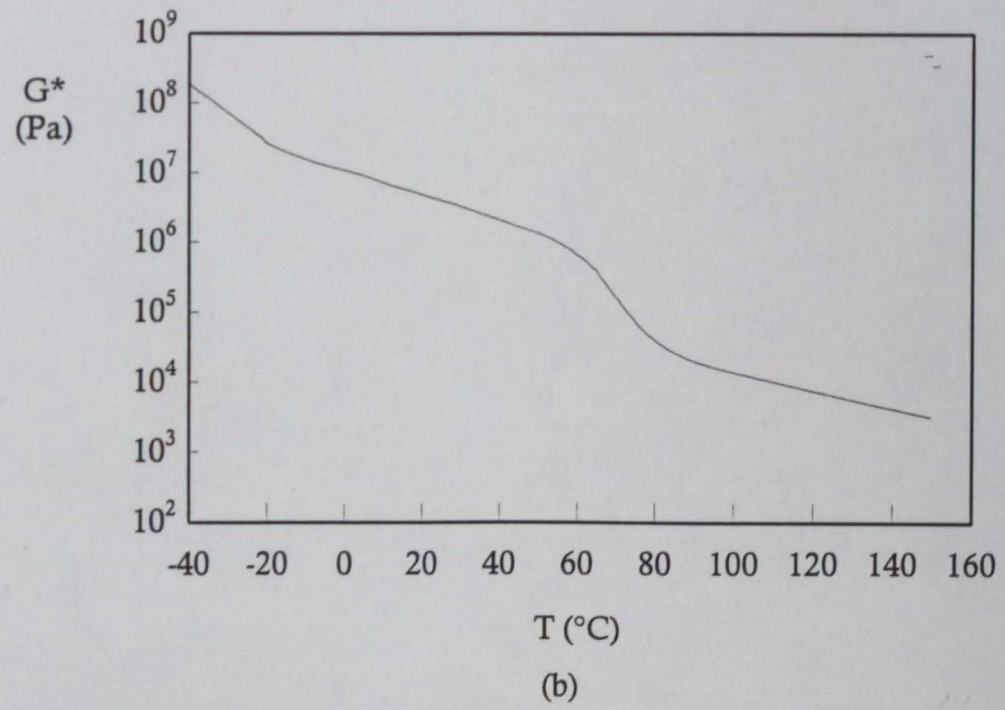

Fig 87. Rheograms showing the variation of (a) elastic modulus G' and (b) complex shear modulus G* for EVA 28/145NC as a function of temperature T. Conditions: controlled stress; 8 mm diameter parallel plates; 1 000 μm gap; heating rate 5°C; 10 rad s^{-1}.

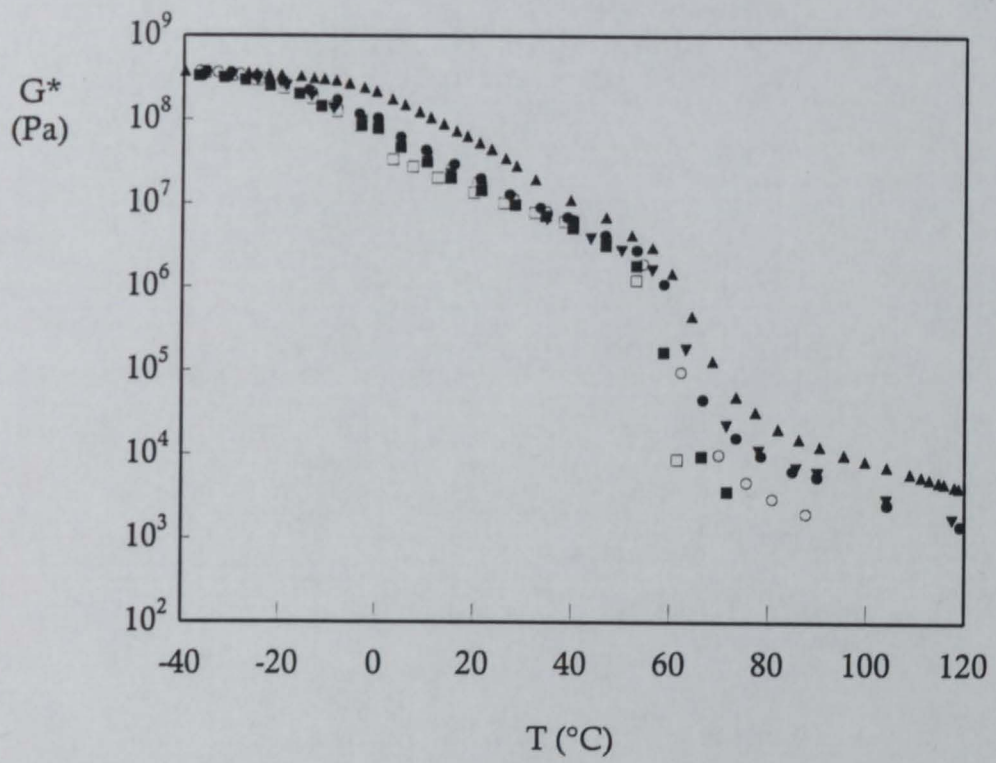

Fig 88. Graph of complex shear modulus G* as a function of temperature T. Data presented for adhesives containing ExUL EVA samples of 28%VA composition. Symbols: ▲ ADH 28/7NC; ▼ ADH 28/25NC; ● ADH 28/40NC; ○ ADH 28/145NC; ■ ADH 28/400NC; and □ ADH 28/2500NC. Conditions: controlled stress; 8 mm diameter parallel plates; 1 000 μm gap; heating rate 5°C; 10 rad s^{-1}.

The variation in rheological properties attributable to molecular weight has been briefly illustrated (Fig 78) and discussed earlier. The variation attributable to composition is just as significant as can be seen in Fig 89 which illustrates the variation in temperature response of the complex shear moduli of two pairs of adhesives with differing %VA EVAs. As is expected, the grades containing more VA are generally softer over the whole temperature range and have lower crossover temperatures.

In an adhesive formulation, the rheological behaviours of polymers are substantially modified by the addition of crystalline waxes and amorphous, low molecular weight tackifying resins. Figures 42 and 49 have already been presented which illustrate the qualitative differences between neat polymers and formulated adhesives, however it is prudent to examine this data more critically. It has been shown [172] that for simple polymer/tackifying resin binary blends that the linear viscoelastic properties are altered by the anti-plasticising action of the resin (it having a higher T_g than the polymer). To recap, the elastic properties such as plateau modulus and limiting compliance, depend only upon the polymer concentration, independent of resin type (providing that there is some compatibility) whilst the resin changes the viscosity and relaxation times of the adhesive by two mechanisms: a topological effect which can be modelled using a relatively simple structure factor, linked to concentration; and secondly a change of glass transition temperature which can raise or lower the viscosity depending upon the T_g of the resin. This model was later expanded to try and predict the effect of wax concentration on the adhesives properties [88] and finally the whole package was used to try and predict adhesive performance, albeit with only limited success [176]. The addition of wax to a polymer/resin blend causes the properties of the blend to vary according to the level of compatibility that the wax has with the polymeric phase. In the simplest case, for a tackifying resin similar to the one in the present work, it has been suggested by Bamborough and Dunkley [156] that a complicated phase structure can exist over the temperature range the adhesive is exposed to. At high temperatures (such as those used for application) an essentially single phase system exists with mutual solubility between the adhesive components. This phase exists until the

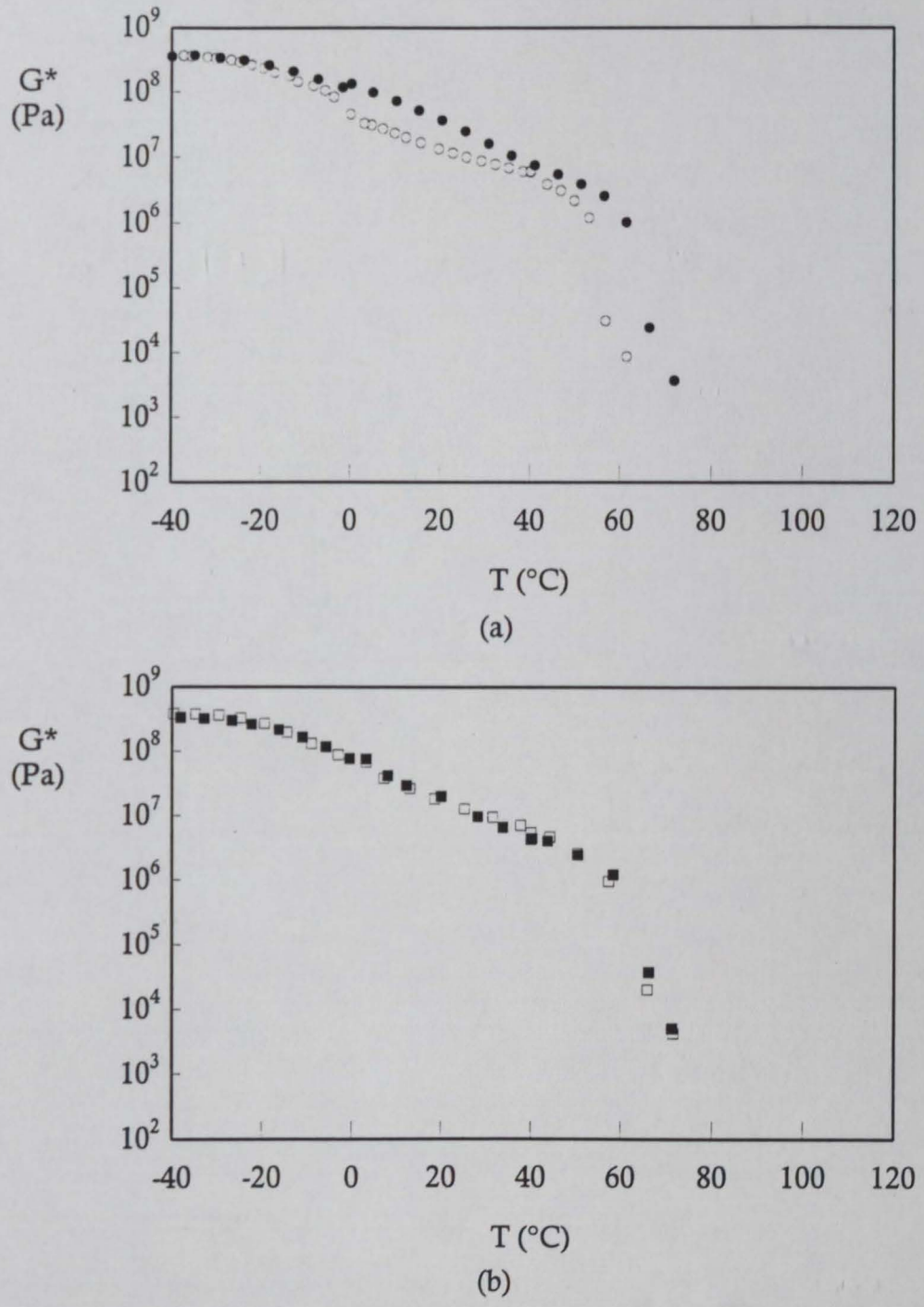

Fig 89. Graphs showing variation of complex shear modulus G* of adhesives as a function of temperature T. (a) ● ADH 14/2500NC and ○ ADH 28/2500NC; and (b) ■ ADH 28/420NC* and □ ADH 33/400NC*. Conditions: controlled stress; 8 mm diameter parallel plates; 1 000 μm gap; heating rate 5°C; 10 rad s^{-1}.

congealing point of the wax when it starts to precipitate from the single solution phase. The start of this precipitation is measured as the cloudpoint temperature, which for the majority of the adhesives in the present work is approximately 62°C and, this value is invariant for all of the adhesives containing 28% VA, irrespective of the polymer molecular weight. Below the cloudpoint, two phases have been reported, a continuous EVA/resin phase and a precipitated wax phase. It is generally assumed that there is little co-compatibility between the EVA and wax however, as has been demonstrated with the calculations of T_g in an earlier section, it is our belief that such co-compatability and, indeed, co-crystallisation does occur. Furthermore, the presence of the wax modifies the crossover temperature (as expected) but not by a uniform amount which could perhaps be expected if wax phase were truly immiscible. Figure 90a shows the relationship between the crossover temperature of the EVA and adhesive, $T_{X\,EVA}$ and $T_{X\,ADH}$ respectively, whilst Fig 90b shows the difference Δ plotted against the logarithm of the melt index. The solid lines are drawn through the 28% VA NC ExUL data to illustrate the variation attributable to molecular weight. The lowest molecular weight polymer is modified least by the wax perhaps suggesting that substantial compatibility is present between wax and EVA/resin phase whilst the highest molecular weight shows the greatest Δ indicating perhaps that the more rubbery nature of this polymer is less compatible with the crystalline wax. The significance of the shapes of the moduli curves and those associated with *tan* δ have been explored by Bamborough and Dunkley [156]. The area between the G' and G" curves was taken to be an indication of cohesive strength and, of course, this area can be directly correlated to the *tan* δ value *i.e.* those adhesives with lower *tan* δ values at, say, 20°C would be more cohesive, but less flexible than other adhesives with higher *tan* δ values. The *tan* δ curves for adhesives containing 28% VA show that there is little variation in *tan* δ with molecular weight and, indeed that there is comparatively little variation attributable to composition. Qualitatively however, differences in the *tan* δ curves are immediately apparent as the amount of VA is increased (Fig 91) although the effect is most apparent with the lower molecular weight polymers (Fig 91a). Increasing the amount of VA reduces the temperatures at which the

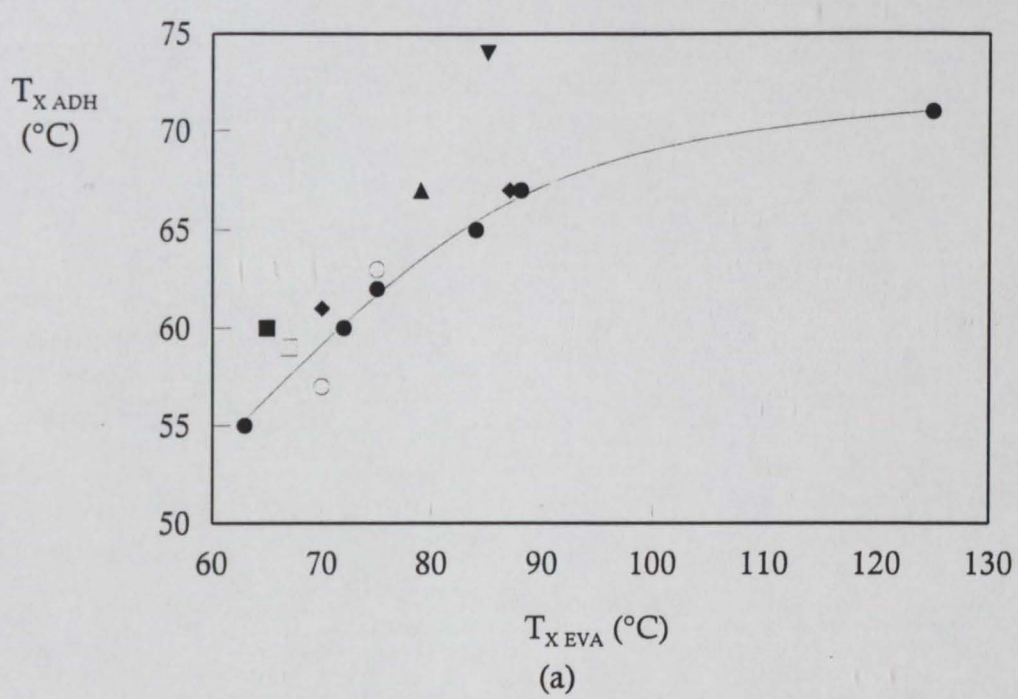

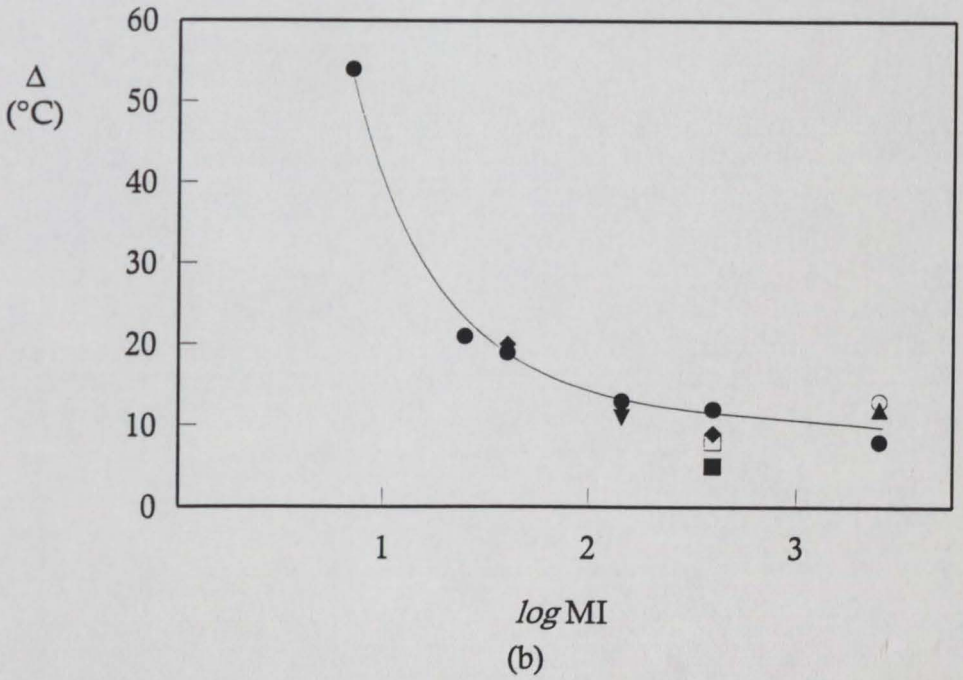

Fig 90. Graphs showing relationship between (a) crossover temperature of EVA $T_{X\,EVA}$ and crossover temperature of the adhesive $T_{X\,ADH}$ and (b) difference between $T_{X\,EVA}$ and $T_{X\,ADH}$, Δ, as a function of the logarithm of the polymer melt index MI. Symbols: ▲ 14% VA; ▼ 19% VA; ● 28% VA NC; ○ 28% VA XL; ■ 33% VA; □ 33% VA XL; ◆ 28% VA NC*. Conditions: controlled stress; 8 mm diameter parallel plates; 1 000 μm gap; heating rate 5°C; 10 rad s^{-1}.

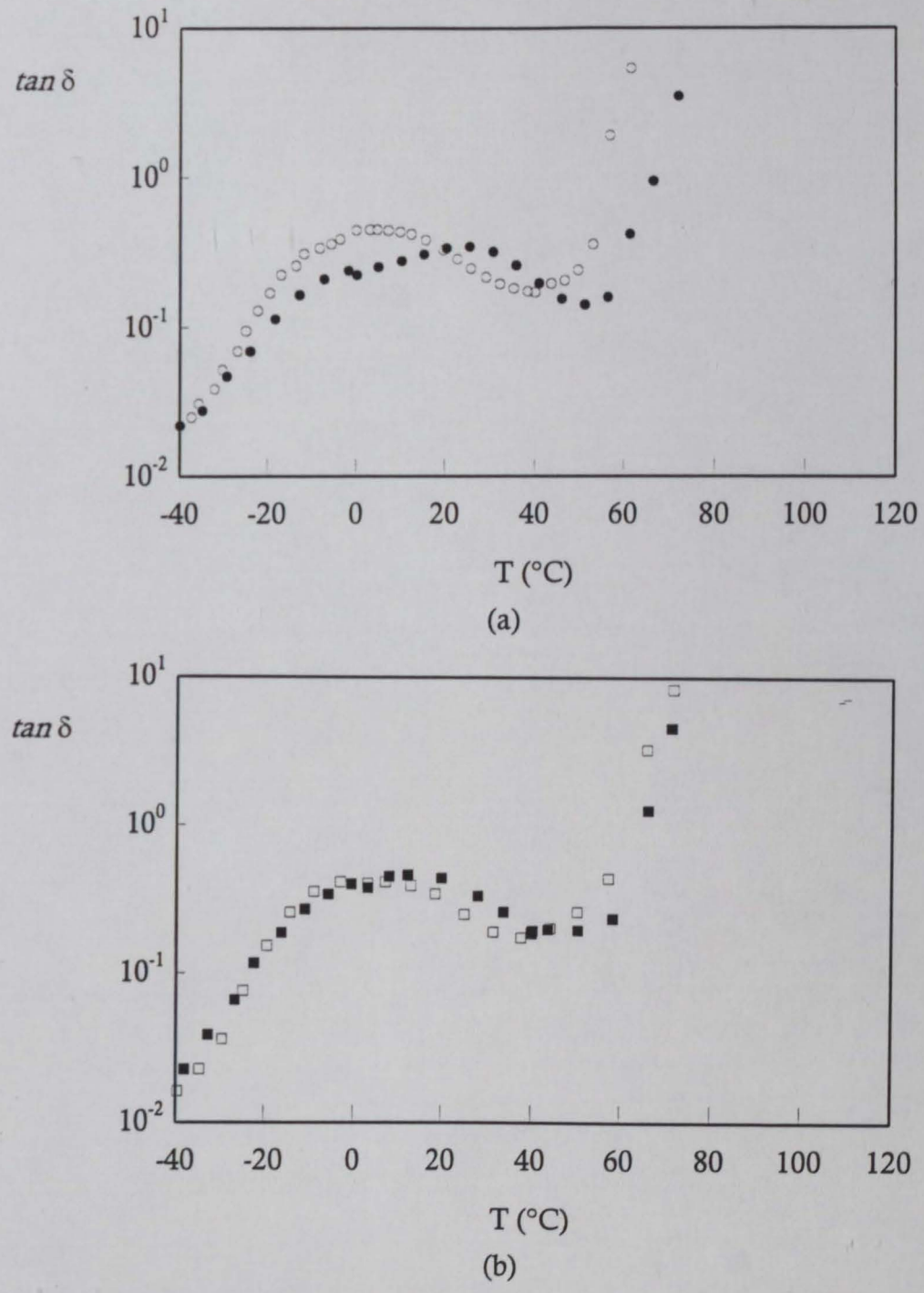

Fig 91. Graphs showing variation of loss tangent *tan* δ of adhesives as a function of temperature T. (a) ● ADH 14/2500NC and ○ ADH 28/2500NC; and (b) ■ ADH 28/420NC* and □ ADH 33/400NC*. Conditions: controlled stress; 8 mm diameter parallel plates; 1 000 μm gap; heating rate 5°C; 10 rad s^{-1}.

tan δ peak occurs. Correlations between tensile data and *tan* δ values were attempted by Bamborough and Dunkley. These will be commented on later.

The addition of wax to an adhesive formulation has been reported by Komornicki [88] to increase the cohesion rate (defined as d(*log* G')/dT) at the crossover temperature T_X due to the sharp melting point of the crystalline wax. The greater the amount of wax, the greater the cohesion rate. This effect is clearly visible in the present work. Cohesion rates are dramatically increased with the addition of the wax into the adhesive formulation, so much so that the cohesion rate differences seen for the neat polymers are, to some extent, masked. Komornicki gives this cohesion rate (which strictly speaking is a melting rate, although the assumption is made that a similar change in modulus is seen under approximately equivalent conditions upon cooling) for a system containing 28½% EVA, 27½% resin, and 14% wax as being 0.42 MPa K^{-1} (absolute value). Despite using a different wax and different resin, the 28/420NC*, which is the nearest equivalent in the present work, has a cohesion rate of 0.33 MPa K^{-1} (absolute value) which is a reasonable comparison. Just as increasing the amount of wax increases the cohesion rate, increasing the VA concentration also increases the cohesion rate. This is initially surprising as it would be expected that the more crystalline, lower VA polymers would assist the crystallisation and hence the cohesion rate as discussed earlier. Given the more amorphous nature of these polymers however, there is perhaps a greater opportunity for the crystalline wax to nucleate crystalline growth. There may also be some effects due to increased incompatibility between the polar VA species and the apolar paraffin wax. This is speculative though as there is no real difference in cloud point data. The wax peak temperature determined by the DSC also does not seem to support this.

Overall, the adhesives share many of the rheological features of the polymers that comprise them. Differences attributable to the wax and resin content are mainly limited to shifting the position of the curve along the temperature, or moduli, axes. Some differences, such as length of the leathery plateau and moduli values in the terminal region are due to a dilution effect that is significant and needs to be taken account of. To summarise then, at low

temperatures, upto a sharply defined melting temperature, the wax acts as a crystalline filler, albeit of low molecular weight, which shows signs of being at least partially compatible with one of the other phases present at lower temperatures. Around the transition to flow, the wax starts to melt rapidly and there are signs of increased compatibility with the EVA/resin phase causing a shift in the crossover temperature, the magnitude of which is dependent upon the molecular weight, crystallinity, and composition of the EVA.

The results of the transient, or creep, tests performed on the adhesives and polymers are presented in Tables 17 and 18, and illustrative creep curves for EVA 28/400NC and ADH 28/145NC are given, as a function of temperature, in Fig 92. The extremely large variation of J(t) with temperature necessitates the use of a logarithmic scale which tends to mask the qualitative change in curve shapes - however these become apparent when logarithmic scales are used. The change in curve shape reflects the change in the properties of the material from solid-like to liquid-like behaviour and this point will be discussed in greater detail.

The vast amount of data generated during transient rheological testing requires observations to be made both qualitatively (for example when describing curve shapes, as above) and quantitatively. This is aided by the fitting of mathematical models to the data in such a way that a few meaningful parameters be obtained which uniquely describe and relate the behaviour to fundamental molecular properties. The use of spring-and-dashpot models in creep and stress relaxation experiments has already been described (Chapter 2, p32) and the Berger and Voigt/Kelvin models introduced and illustrated. In order to quantitatively describe the data within the present work, the creep data was analysed (using Version 2.1 of TA Instruments Data Software) to yield values of the initial compliance J_0 and zero shear viscosity η_0, together with the parameters associated with an appropriate number of Voigt/Kelvin (V/K) units. In general, it was found that all of the samples could be modelled with a sufficient degree of accuracy by Berger models with one or two V/K units. On the rare occasions when the software attempted to use additional V/K units, the data was reanalysed with two and the standard error was examined. The

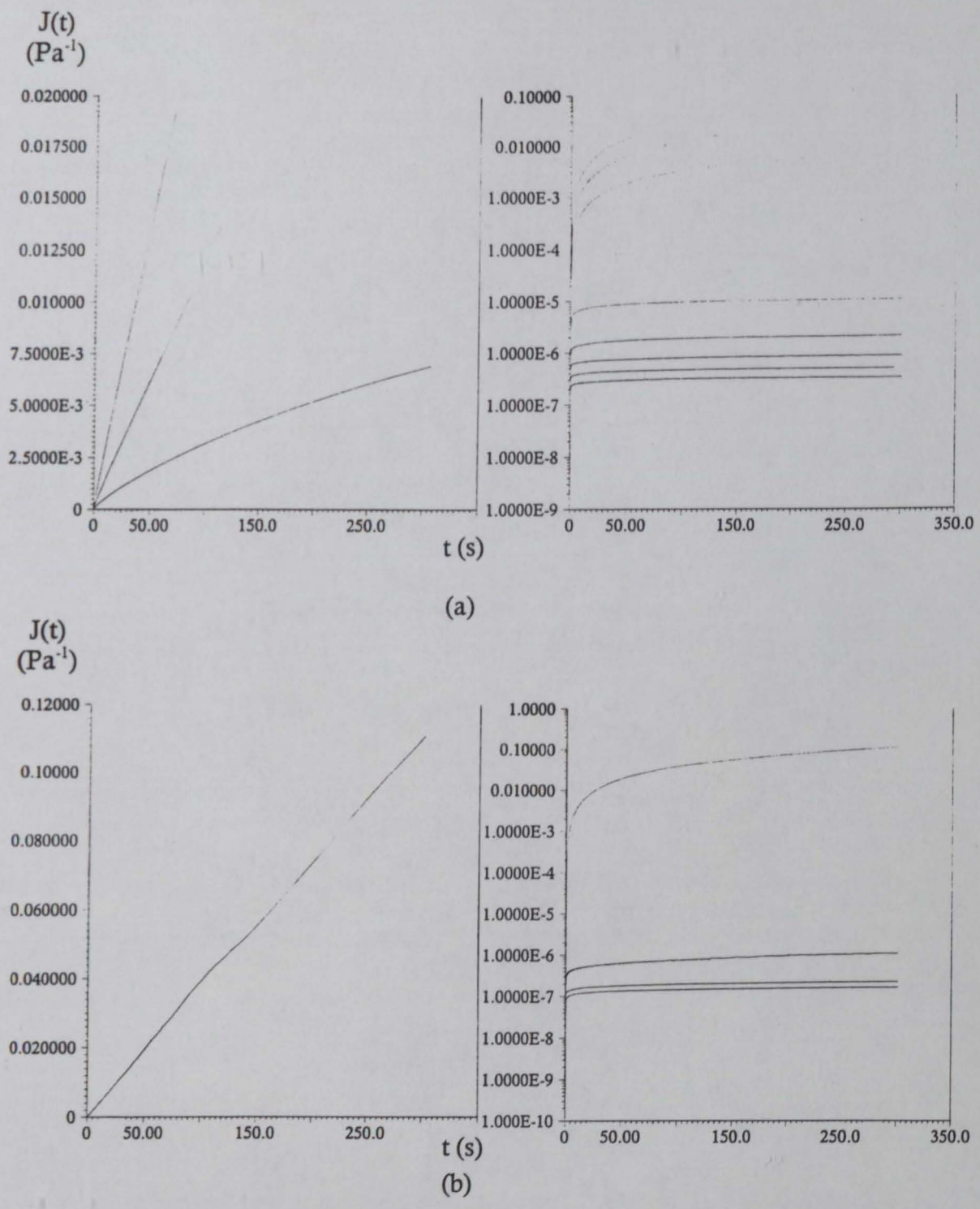

Fig 92. Graphs illustrating the variation of time dependant creep compliance J(t) as a function of time t for (a) EVA 28/400NC and (b) ADH 28/145NC for a series of temperatures. The data is presented in both linear (left) and semi-logarithmic (right) form as an illustration of the very large changes in J(t) experienced as the temperature of test is varied.

subsequent discarding of the extra V/K did not significantly affect the goodness of fit and was thought to add little to the process of understanding the phenomenological and morphological processes occurring within the sample during the process of creep. Data points affected thus are indicated by the symbol § in the tables. The justification for discarding extra V/K units comes from the consideration of the theories of molecular entanglement and the influence of polymer morphology on viscoelastic behaviour *e.g.* [92]. It has been proposed, for polymeric materials in general, that the elements of Berger's model can be linked to polymeric rotational/configurational changes which do not involve the requirement for co-operative segmental rearrangement of polymer units (the response of the initial spring); the disentanglement and co-operative motion of low molecular weight chains, or sidebranches (first V/K unit); the cooperative segmental movement of main chains (second V/K unit); and finally the transitional movement of polymeric chains following the breaking/ disentanglement of localised crosslinks (the final dashpot). Putting these back into the data obtained in the present study we obtain J_0; J_1, τ_1; J_2, τ_2; and η_0. Derived data from the analysis also includes the recoverable compliance J_r which can be calculated from the final compliance values obtained during the application and removal of the stress.

In contrast to the earlier section on oscillatory rheometry, there is an additional variable to consider when looking at the rheological characteristics of the polymers and adhesives. This variable is temperature. Figure 93 illustrates the response of the 28% VA polymers to an applied stress over a range of temperatures. The value of the stress was selected according to the procedure described in Chapter 3, and the results are presented as graphs of creep compliance J(t) as a function of time t. The graphs are again presented in linear and semi-logarithmic form so that the shapes of the curves and the changes can be clearly seen. It should be noted that the curves are illustrated upto a value of 150 s. In reality the creep test was performed for a much longer time (10 minutes), but in all cases, the system had reached equilibrium after approximately 120 s and the zero shear rate viscosity was able to be determined from the curves with a considerable degree of confidence (regression analysis

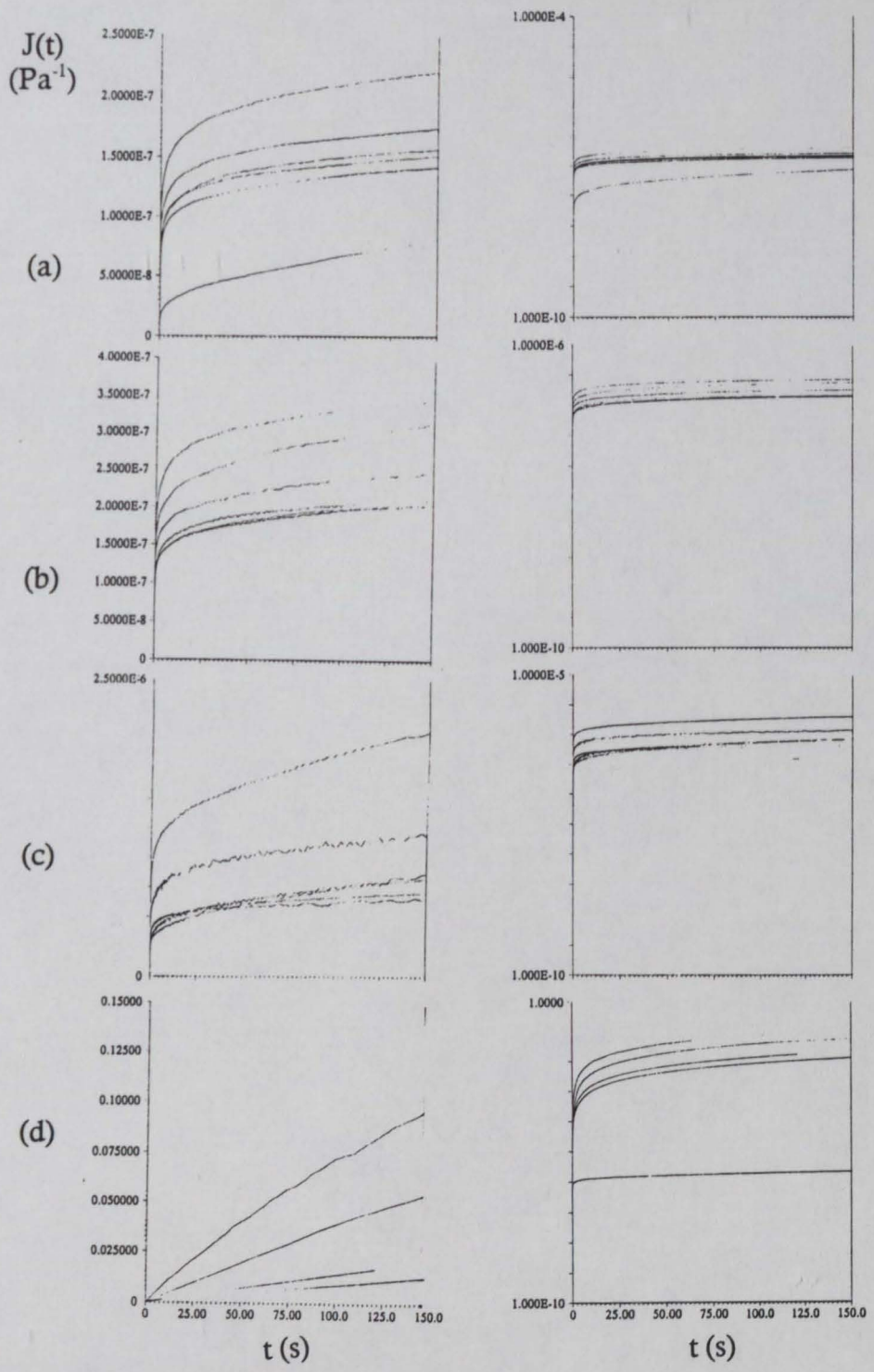

Fig 93. Rheograms illustrating the variation in time dependant creep compliance J(t) of adhesives containing 28%VA ExUL EVAs as a function of time t at a series of temperatures: (a) 20°C; (b) 40°C; (c) 60°C; and (d) 80°C. The data is presented in both linear (left) and semi-logarithmic (right) form as an illustration of the very large changes in J(t) experienced as the temperature of test is varied. See text for identification.

gave r^2 values of >0.950). With the exception of the 20°C data illustrated, clear patterns were observed at all other temperatures, with low MI polymers (such as 28/7 NC and 28/25 NC) consistently showing lower values of J(t) and higher calculated values of η_0. The curves clearly fall in the same order, from top to bottom, of highest MI to lowest. Qualitatively, the curve shapes vary little with MI, at least at the lower temperatures. At higher test temperatures the low molecular weight samples flow more easily and rapidly attain large compliances. The rapid breakdown of strength and increased tendency to show flow behaviour has also been observed with oscillatory testing where the samples containing 400 and 2 500 MI polymers showed a rapid decrease in modulus at elevated temperatures. The 20°C curves shown in Fig 93a do not fall into the regular pattern seen at other temperatures. This is thought likely to be attributable to experimental uncertainty given the hard nature of the polymeric samples and the typically small strain resolutions experienced during the test (of the order of 1×10^{-5} rad). It should be borne in mind that the curves illustrate the arithmetic mean of datapoints collected from three runs and that the level of experimental scatter at lower temperatures (± 9% at 20°C) is significantly higher than that at higher temperatures (± 2½% at 80°C). There is an internal consistency to the results in the fact that the number of V/K units required to model the polymers at lower temperatures are equal between samples. As the temperature increases, the curve shapes tend to alter more rapidly and different models (number of V/K units) are required to give good fits to the data.

As the temperature increases there is a subtle shift from viscoelastic solid to viscoelastic liquid-like behaviour. The exact transition point is not clear and attempts to correlate the temperature at which a certain zero shear viscosity (10^6 Pa s; called here the flow point) is obtained with DSC data shows that the relationship is not linear (Fig 94). Although the overall trends are the same, *i.e.* lower molecular weight gives lower DSC melting peak and lower flow point temperature, differences arise presumably due to the different mechanisms being characterised by DSC, a zero shear thermal technique determining crystalline dissolution, and creep, an applied low shear technique measuring the onset of chain disentanglement and molecular rearrangement. It may be reasoned then

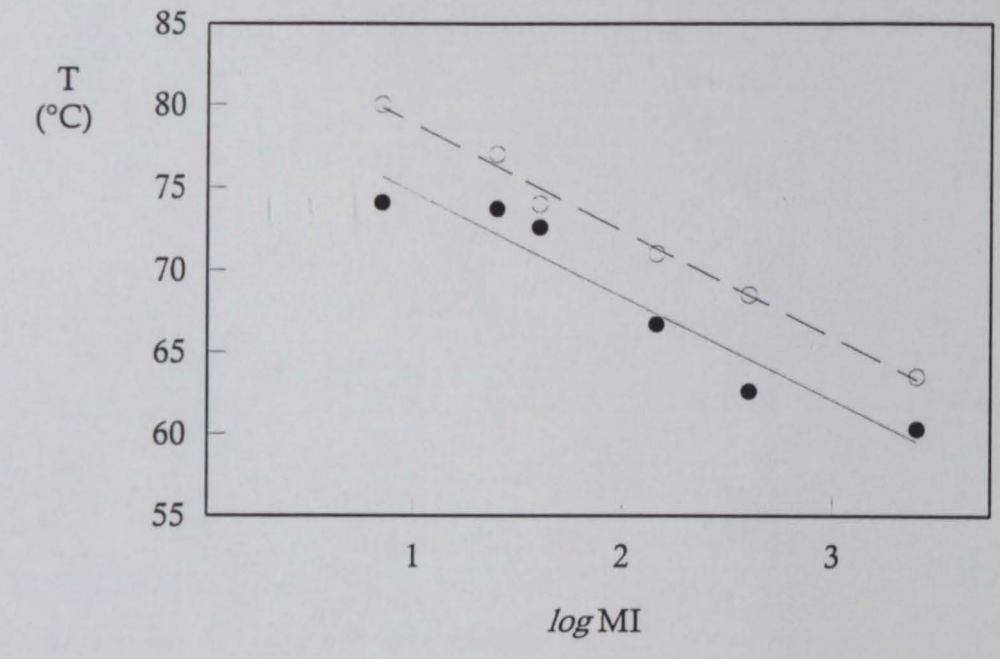

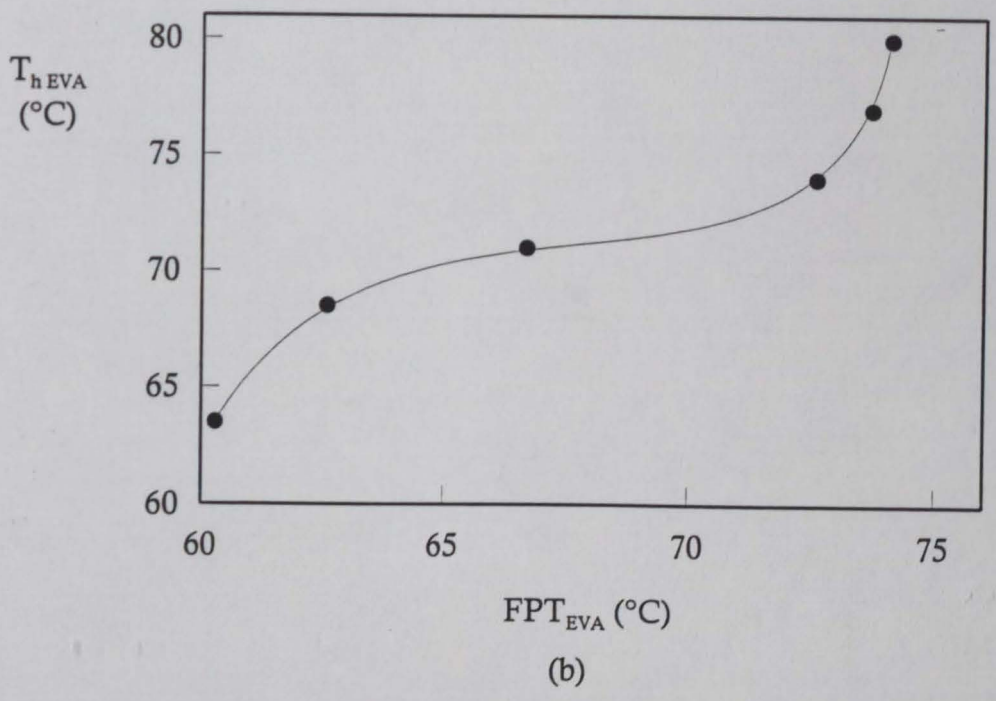

Fig 94. Graph showing relationship between (a) melting point $T_{h\,EVA}$ (DSC data) and flow point temperature FPT_{EVA} as a function of the logarithm of the melt index MI and (b) the non-linear relationship between $T_{h\,EVA}$ and FPT_{EVA} for ExUL 28%VA polymers. Symbols: in (a) ● $T_{h\,EVA}$; ○ FPT_{EVA}. See text for details.

that the softening point of the adhesive sample be related to the flow point temperature of the polymer however Fig 95 illustrates that this, whilst true for some adhesives (namely those based upon 28%VA ExUL EVA), falls short of predictive modelling by some degree. It is possible that differences are attributable to mixing and phase morphology effects, in addition to the compatibility effects expected due to the composition of the polymer.

Graphs of instantaneous (initial) compliance J_0 and zero shear viscosity η_0 as functions of temperature are given in Fig 96. It is interesting to note (but not suprising) that the trends relating to melt index, composition, and crystallinity already discussed in relation to oscillatory rheometry are equally valid here in so much as high molecular weight gives rise to high η_0, lower J_0, and lower flow point. If the mathematical models for creep behaviour are considered, it can be seen that the need for a second V/K unit is dependant upon both temperature and molecular weight. For example, the use of the second V/K unit for the EVAs occurs at 70°C for 28/7NC, 60°C for 28/25NC, 60°C for 28/40NC, 50°C for 28/145NC and indeed 20°C for 28/400NC. EVA 28/2500NC appears to exhibit very different behaviour and it was not possible to fit a second V/K unit until 60°C. This is thought to relate back to the idea of reduced chain entanglement associated with smaller polymeric molecules, even though the M_w of the polymer is above the critical value. The onset of viscous flow occurs very rapidly after the relaxation of the short molecules and the differentiation between side chain and main chain co-operative rearrangement is not thought possible.

It can be noted if the temperature of testing is not too close to the T_g of the polymer then J_0 is of the same order of magnitude as the plateau compliance J_N^0 (reciprocal of the plateau modulus G_N^0) and therefore, at around frequencies of 1 Hz (10 rad s^{-1} ≈ 1.6 Hz), $J_0 \approx 1/G'$. This relationship is illustrated in Table 27 and is valid for the 20°C data but is clearly not valid for temperatures near the flow region of the polymers either. This was also noted by Komornicki *et al* [88].

The data of Komornicki generally relates solely to polymer/resin/wax blends and cannot be directly compared with the polymeric results, however, the

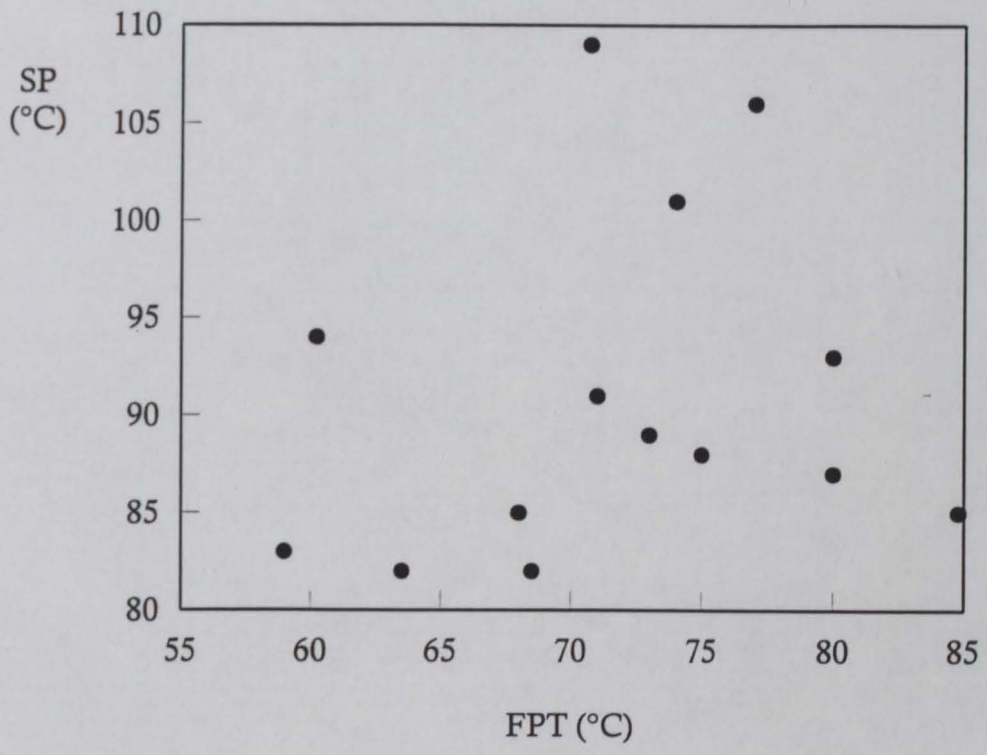

Fig 95. Graph showing relationship between flow point temperature FPT of the copolymer and softening point SP of the adhesive.

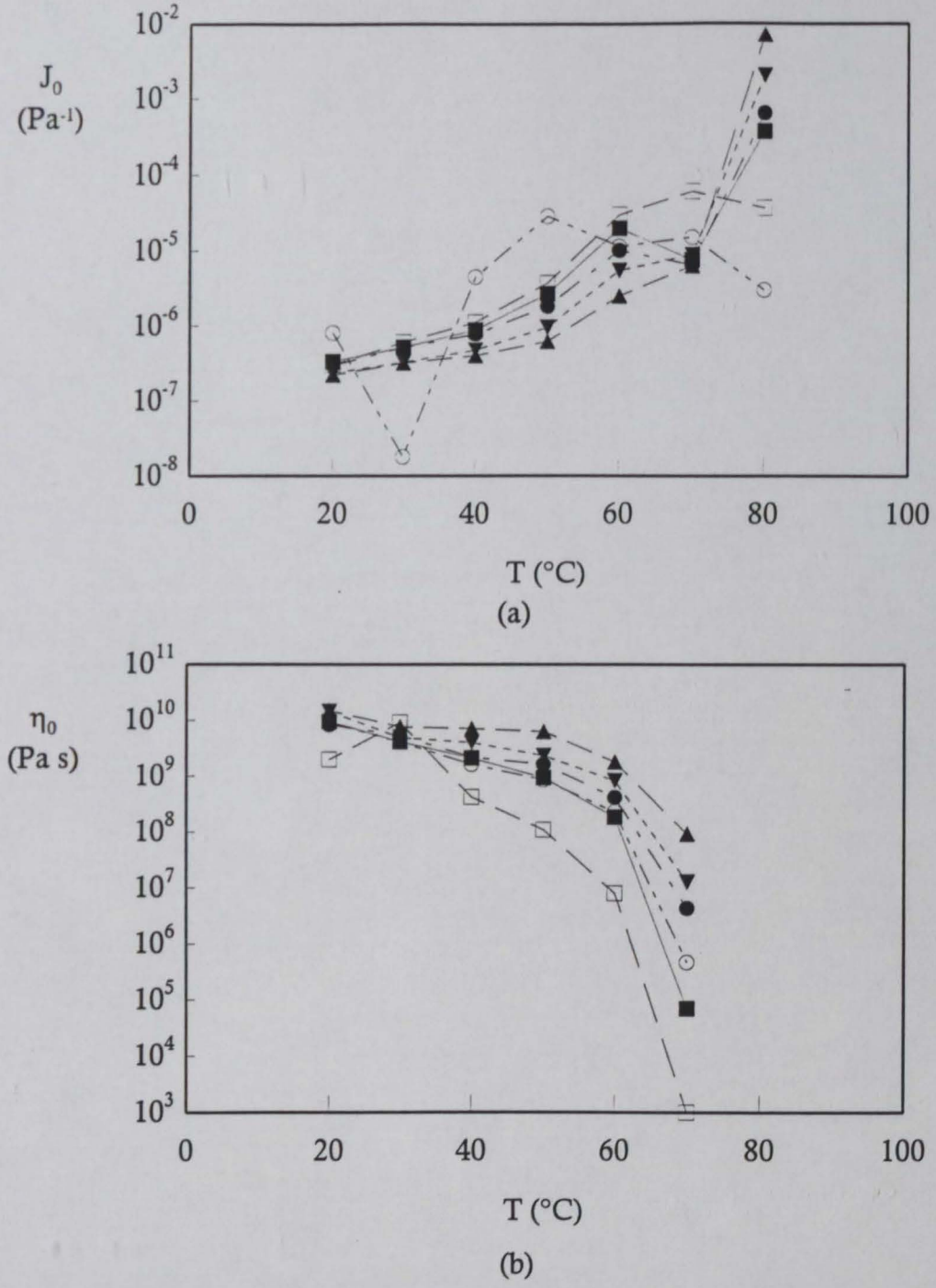

Fig 96. Graphs illustrating the variation in (a) instantaneous creep compliance J_0 and (b) zero shear viscosity η_0 for the ExUL 28%VA EVAs as a function of temperature T. Symbols: ▲ EVA 28/7NC; ▼ EVA 28/25NC; ● EVA 28/40NC; ○ EVA 28/145NC; ■ EVA 28/400NC; and □ EVA 28/2500NC.

Table 27 Comparison of oscillatory (G') and transient (J_0) rheological data for the components of poly(ethylene-*co*-vinyl acetate) adhesives.

Component	20°C			60°C		
	G' (10^6 Pa)	1/G' (10^{-8} Pa^{-1})	J_0 (10^{-8} Pa^{-1})	G' (10^5 Pa)	1/G' (10^{-7} Pa^{-1})	J_0 (10^{-7} Pa^{-1})
14/2500NC	13.3	7.5	1.6	25.9	3.9	4.2
19/150NC	13.1	7.6	8.0	34.4	2.9	3.0
28/7NC	8.0	12.5	17.3	19.5	5.1	6.2
28/25NC	6.7	14.9	16.0	14.8	6.7	9.4
28/40NC	5.4	18.5	24.6	10.8	9.3	1.8
28/145NC	4.8	20.8	24.1	6.3	15.8	2.7
28/400NC	3.7	27.0	21.4	5.3	18.9	3.7
28/2500NC	1.9	52.6	42.8	0.7	15.2	28.7
28/40NC*	7.9	12.7	14.0	15.8	6.3	9.9
28/420NC*	4.2	23.8	16.2	35.8	2.8	17.4
33/400NC*	3.0	33.3	31.6	1.4	70.9	19.7
28/400XL	7.2	13.9	17.7	13.3	7.5	15.7
28/2500XL	6.0	16.7	20.3	4.9	20.4	97.0
33/400XL	4.3	23.3	30.4	4.0	24.9	63.7
Resin	56.8	1.8	ND[a]	156.9	0.7	5.1
Wax	257.0	0.4	95.7	0.5	200.0	2832.0

(a) ND = Not detected.

comments regarding the qualitative changes in curve shape do apply. In general, the EVA samples have very high zero-shear viscosities and, certainly at room temperature exhibit the characteristics of viscoelastic solids. Komornicki comments upon an "exponential" decrease in elasticity observed in samples with different wax contents. A similar decrease, although not exponential (although neither is Komornicki's) is observed as a function of compositions and molecular weight. The crystalline XL samples appear more elastic than their NC counterparts whilst the AtEV samples also show more crystalline behaviour than their ExUL analogues. This compares extremely well to the trends already seen from the work on the DSC and oscillatory rheometry data.

When considering the results of creep tests on the adhesives themselves it is helpful to follow the same pattern as earlier chapters, *i.e.* a review of the data and an examination of its accuracy followed by an interpretation of the results.

The data presented in Table 17 follows the same format adopted for the raw materials, in so much as a maximum of two V/K units were used to fit the data and this was verified as a valid approach by the consideration of the standard error associated with the model. Again, standard errors were generally kept below 30 at lower temperatures. These fell to less than 5 at temperatures above 50°C where the material was considerably softer and the nature of the samples changed significantly from viscoelastic solid-like behaviour to a more liquid-type response. There is little published literature available which records the typical standard errors associated with modelling using Berger (V/K) type models, however verbal communication with expert users [237 - 241] seems to confirm that the modelling accuracy improves with the softening associated with elevated temperatures. For very hard solids (such as the adhesive samples at lower temperatures) the larger magnitude of the zero shear viscosity (typically $>10^{10}$ Pa s) coupled with very small compliancies, typically $<10^{-7}$ Pa^{-1}, can lead to relatively large standard errors often encountered as a result of the subtraction of one large number from another. Indeed, the standard errors achieved here are better than can be expected. This can be attributed to the care taken in the preparation and loading of the samples, together with the precisely controlled thermal history. The other point to consider when examining the response of

hard materials is that the rheometer has a finite compliance. Although this is typically three orders of magnitude smaller than that of the material under test it may possibly contribute to the increase in the error of measurement seen at lower temperatures. It is concluded then that, as before, it is probably better to concentrate on the trend, and magnitudes of compliancies and viscosities so determined by the creep process rather than the absolute numerical values. As before, the actual qualitative shapes of the creep curves are also of use and will be discussed.

When examining the creep results of the adhesives themselves, it is necessary to consider the nature of the adhesive with respect to its components. Komornicki *et al* [88] observed that the addition of wax to binary polymer/resin blends shifted the nature of the blends to more viscoelastic solid-like behaviour, *i.e.* at lower temperatures it increased the amount of elastic creep recovery and the wax acted as if it were a filler. In addition, at higher temperatures, and higher concentrations of wax, the resultant zero-shear viscosity profiles were shifted to a higher level, although melt viscosities were undoubtedly reduced, as has been seen in the present work. With this in mind, it can be seen that the adhesive samples in the present work show a similarly increased elasticity, *i.e.* smaller J_0, and increased η_0 at temperatures significantly lower than the softening point of the wax (Fig 97). It is important to once again note that the waxes used in this work and the ones in the reference are significantly different as has already been discussed. Komornicki uses a synthetic Fischer-Tropsch wax of melting range 63 - 120°C (peak at 105°C) whilst the present author's fully refined paraffin wax shows melting in the range 60 - 70°C. Despite these obvious differences, the results obtained for both J_0 and η_0 data are of comparable magnitude, taking into account that the different EVA compositions, melt indices, and manufacturers will obviously affect the properties as discussed before.

The initial compliancies of the adhesives formulated around 28% VA EVAs show remarkable similarity at temperatures below 40°C. Above this temperature, however, it can be seen that the compliance is more dramatically affected by molecular weight. For example, at 20°C ADH 28/25NC has a J_0 of

approximately 2×10^{-7} Pa^{-1} whilst ADH 28/2500NC has a $J_0 \approx 4 \times 10^{-7}$ Pa^{-1}. At 70°C (above the melting point of the wax) ADH 28/25NC has $J_0 \approx 6 \times 10^{-6}$ Pa^{-1} compared with $J_0 \approx 1 \times 10^{-5}$ Pa^{-1} for ADH 28/2500NC. These differences are illustrated in Fig 97. Similar trends are experienced with zero shear viscosities η_0. At lower temperatures the viscosities are so high ($\approx 10^{10}$ Pa s) as to render differences between them somewhat academic, if indeed they are real differences, however at higher temperatures differences attributable to the molecular weights of the polymers become discernable. It should be noted that the η_0 values do not significantly alter, for the majority of the samples, until temperatures greater than the melting point of the wax are exceeded. Above this temperature, the trends in η_0 follow closely the patterns observed for the melt viscosities discussed earlier in this chapter. Similar trends with high and low vinyl acetate contents are seen, as are comparisons between high and low crystallinity versions of polymers. The only exception to the above trend appears to be ADH 28/7NC, which shows abnormally high J_0, and low η_0 values. These are in stark contrast to the creep data obtained on the neat polymer which clearly shows the trends in MI/molecular weight over the whole range of polymers studied. It may be recalled that similarly anomalous results were observed in some of the thermal data (Section 5.1). The argument was put forward there was that the mixture was not at equilibrium because of inadequate mixing (physical) and/or kinetically supressed chemical equilibration as a result of inhomogeneity or unstable phases. Phase seperation could occur, if the material was held at elevated temperatures for extended periods of time, by either nucleation and growth or spinodal decomposition [242]. This could leave the adhesive consisting of polymer-rich and wax/resin-rich "phases" or regions of inhomogeneity.

It is helpful at this point to stress again one of the assumptions made by Komornicki *et al* in their model of the adhesive, that the wax acts as an inert filler. This compares with the hypothesis put forward by the present author in Section 5.1 on the basis that the T_g of the blended adhesive is lowered, that the paraffin wax has a limited, but significant, mutual compatibility with the other components, particularly the EVA copolymer. Unfortunately, the creep data are

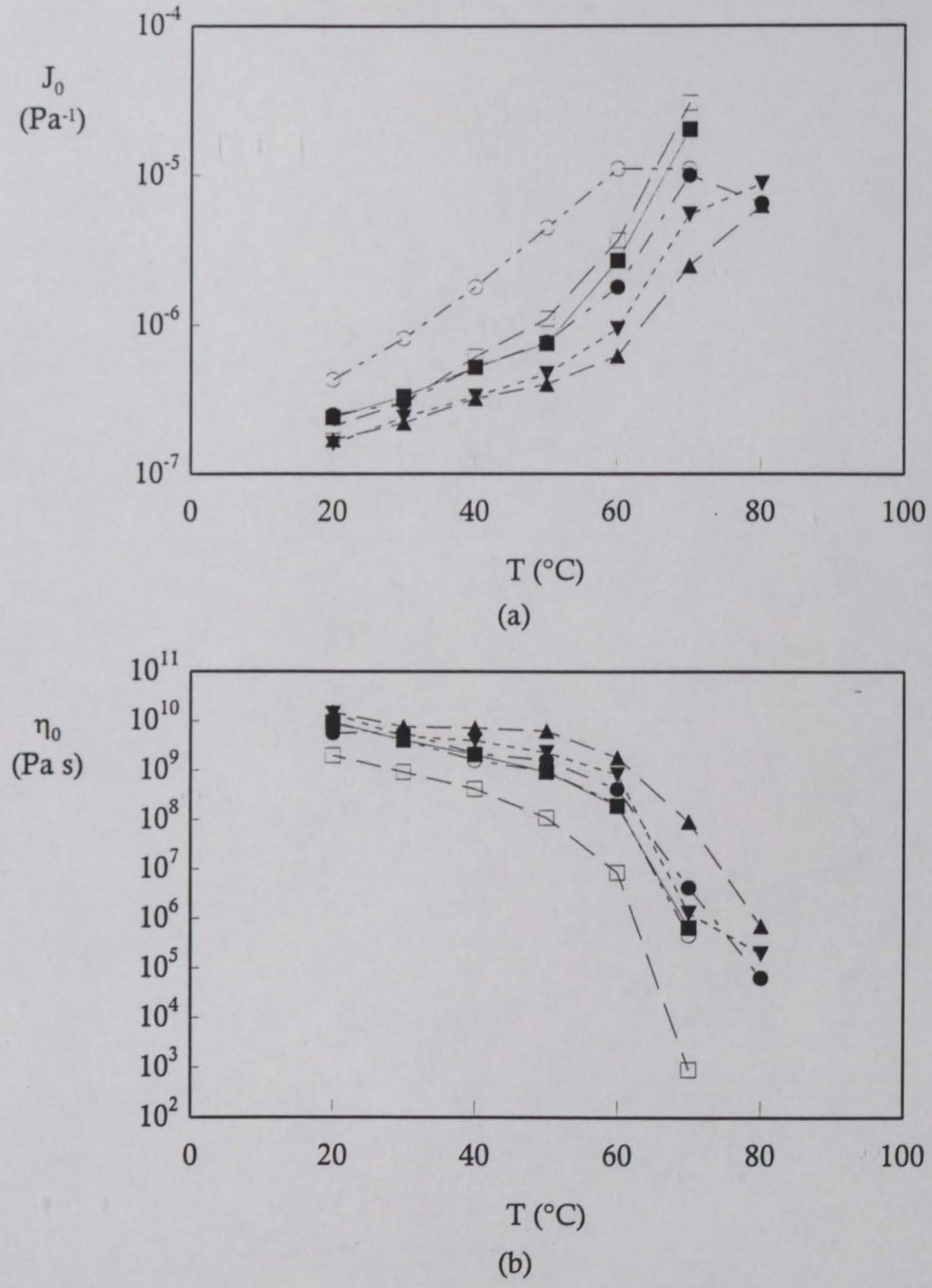

Fig 97. Graphs illustrating the variation in (a) instantaneous creep compliance J_0 and (b) zero shear viscosity η_0 for adhesives containing ExUL 28%VA EVAs as a function of temperature T. Symbols: ▲ ADH 28/7NC; ▼ ADH 28/25NC; ● ADH 28/40NC; ○ ADH 28/145NC; ■ ADH 28/400NC; and □ ADH 28/2500NC.

not sufficiently sensitive on this point.

5.3 Formation and testing of adhesive bonds

After considering the thermal and rheological properties of the adhesives and their components, it is necessary to critically examine and discuss the data generated in the industrial tests, and also to see what relevance the scientific theories and rheological results have in understanding, interpreting, and developing the tests. These tests are often qualitative or semi-quantitative in nature and often performed on a comparative basis due to the lack of a critically evolved, scientifically-based grounding. The data which will be discussed here can be conveniently split, for the purposes of this discussion, into two sections: adhesive properties which affect the formation of joints; and adhesive properties which govern the strength of joints. Examples of the former include open and setting time, softening point, and cloud point whilst the tensile strength and heat resistance tests fall into the latter category. Because of the lack of scientifically established data on these commercial materials a very large amount of work characterising the materials was necessary. This invariably leads to an enormous amount of data and therefore it is essential that careful consideration is given to the critical selection of these data for further analysis. However, this must be balanced by the potential usefulness of predicting adhesive performance in a systematic and efficient manner by the utilisation of screening techniques.

In order to form a bond, a hot melt adhesive must first be melted. It is common practice amongst a number of adhesive suppliers [*e.g.* 243 - 245] to quote softening points on adhesive data sheets as an indication of the adhesive's performance. The softening point test method as given in ASTM D 3104 is a classic example of an industrial test that cannot be trivially reduced to a simple scientific basis. The principle of the test requires an undefined mass of adhesive, being heated at a constant, ideally slow, rate until such time as the adhesive flows sufficiently to break a beam of light. This test encompasses the variables of adhesive density, heat capacity, melting points of the adhesive constituents, and rheological characteristics such as viscosity, non-Newtonian behaviour and/or viscoelasticity. On the basis of such a simple, single-point measurement a

number of claims are made. These will be critically examined in turn.

It is sometimes taken as a given fact that the softening point measurement can give definitive data on such characteristics as heat resistance, open time, and setting speed. Figures 98 and 99 illustrate the variations of these parameters as a function of the measured softening point of the adhesive. In Fig 98a, the actual SAFT and PAFT temperatures show little dependance upon the adhesives softening point - indeed, even if a linear regression were attempted, one can observe that the difference in SAFT for a 20°C increase in softening point is just 2°C. Taking into account the accuracy of both measurements (± 0.2°C for softening point, ± 2°C for SAFT and PAFT) it would appear that, in the first instance, that any predictions of heat resistance based upon softening point are spurious. Figure 98b in which failure times are considered for each heat resistance test reveals a slightly greater observed change, however the experimental scatter seems greater. Incidently, the use of heat resistance temperature or time is equally valid, the parameters show a linear relationship with $r^2 = 0.966$, S.E. = 0.614 for SAFT and $r^2 = 0.745$, S.E. = 1.914 for PAFT. Note that the PAFT data is slightly more scattered (Fig 98). This is thought to be attributable to the nature of the bond geometry which is not as simply expressed in terms of forces over bond area as the straightforward shear joint. It will be recalled that (p 47), in a peel joint

$$P = ab[(K\sigma_0)/((2E)^{½}) + (\tau_o \cos\omega)/((2G/3)^{½})]^2 (1 - \cos\omega)^{-1} \quad \ldots (29)$$

where a, b refer to the width and thickness of the adhesive bond, E, G are tensile and shear moduli respectively, and K is a complex function relating to the stress intensity factor of cleavage failure. K is a function of peel angle ω and it can be shown that, when $\omega = 90°$, equation (29) reduces to

$$P = (abK^2\sigma_0^2)/2E \quad \ldots (43)$$

compare this with the equivalent equation for shear

$$S = (EL^2b)/a \quad \ldots (44)$$

where L is the length of the overlap (for limiting conditions). The dependance upon the angle of peel for equation (29) to reduce to equation (43) is very strong such that even small (<½°) variations will result in contributions to the overall peel strength from other resolved components of the stress distribution. The

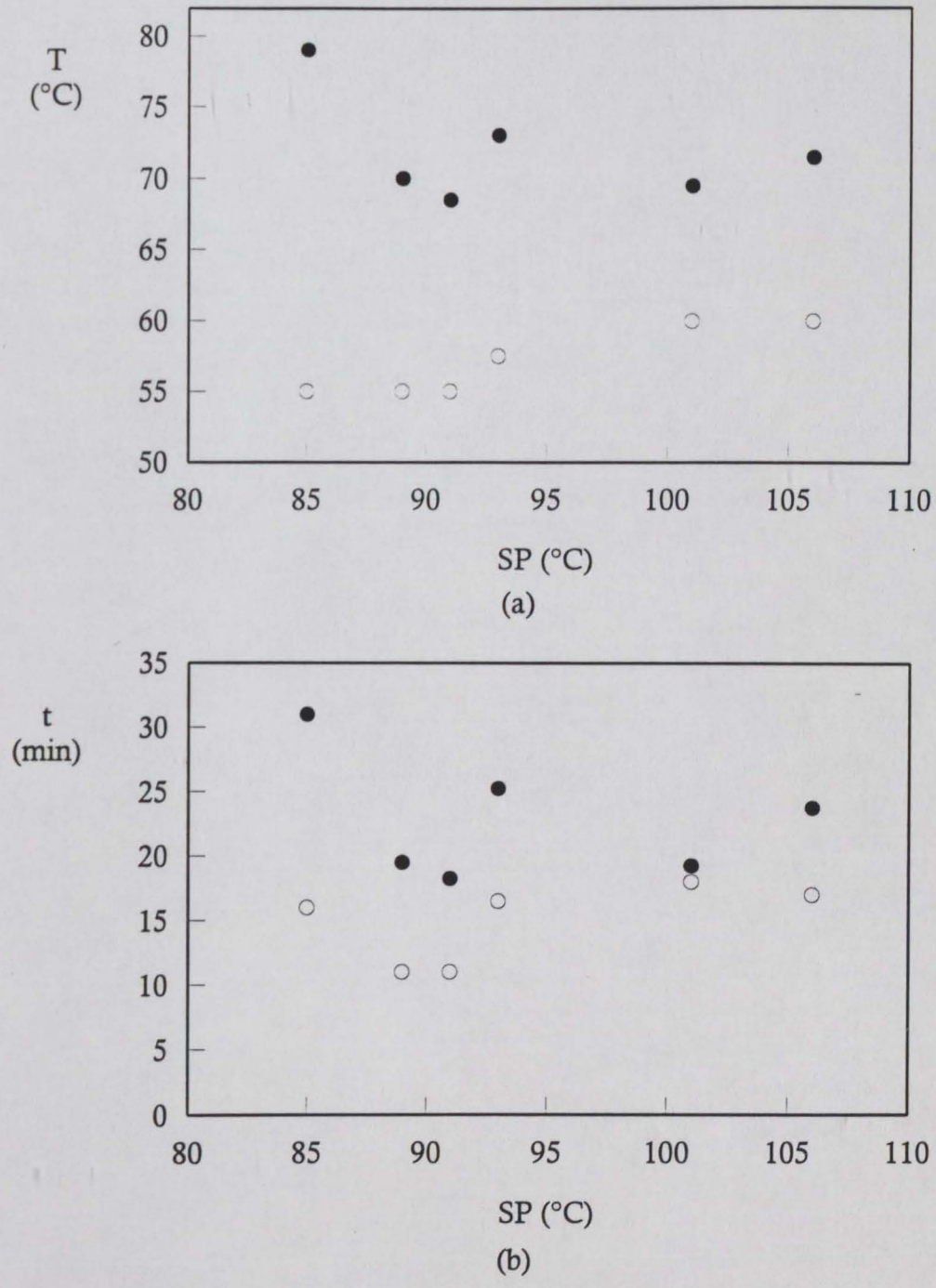

Fig 98. Graphs illustrating the variation of (a) the heat resistance failure temperature T and (b) the heat resistance failure time t of the adhesive as a function of its softening point SP. Symbols: ● SAFT, ○ PAFT.

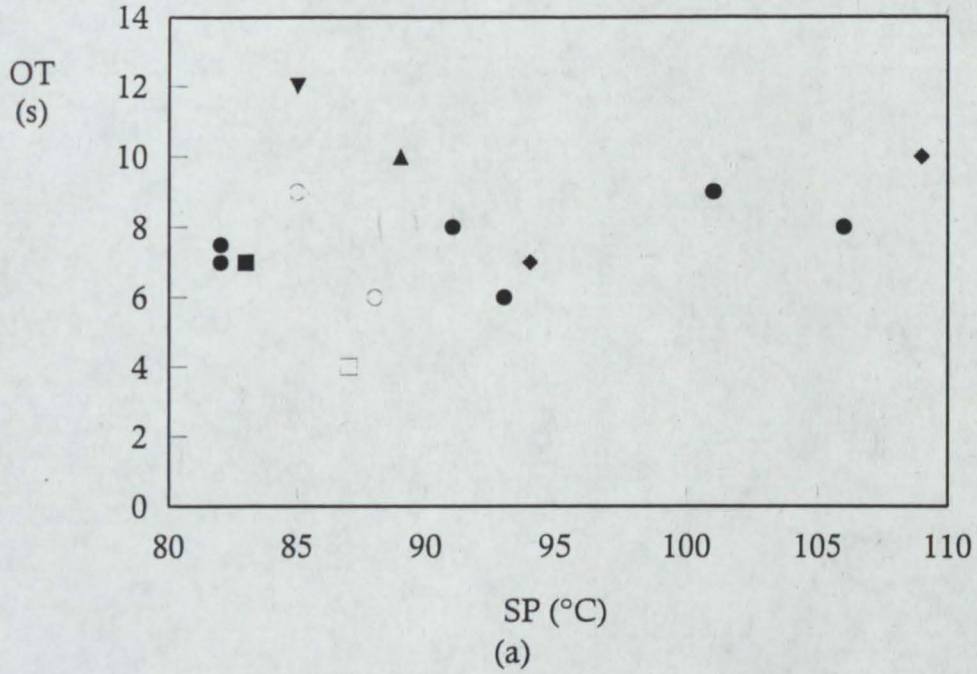

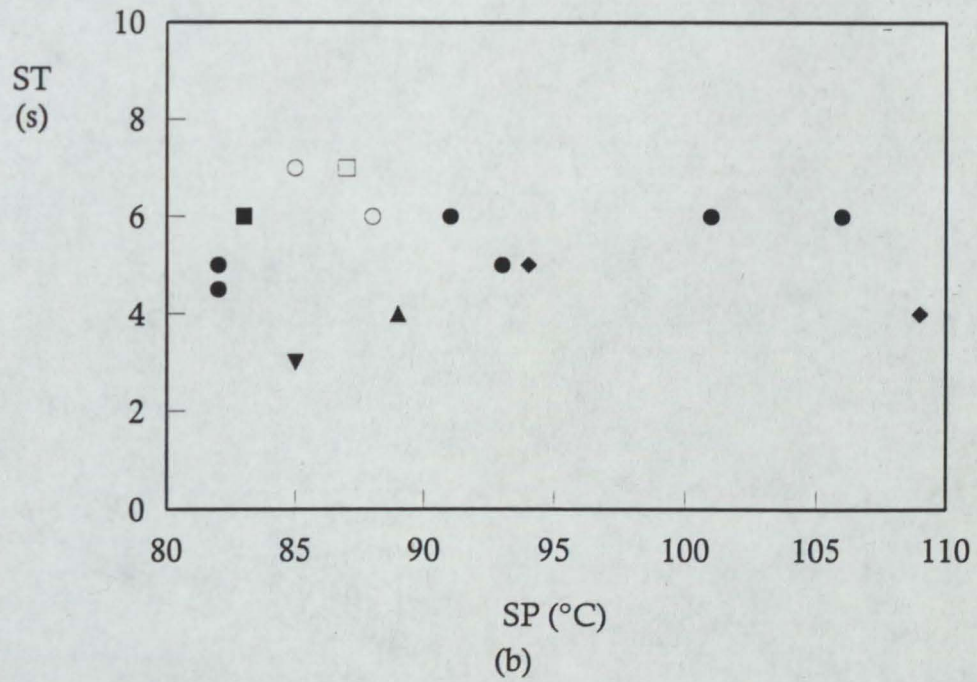

Fig 99. Graphs illustrating the variation of (a) the open time OT and (b) the setting time ST of the adhesive as a function of its softening point SP. Symbols: ▲ 14% VA; ▼ 19% VA; ● 28% VA NC; ○ 28% VA XL; ■ 33% VA; □ 33% VA XL; ◆ 28% VA NC*.

source of the resultant variation in apparent peel strength thus becomes more identifiable and explicable. Note that in both of the above analyses, the adhesive is assumed to behave as an elastic solid which, has already been made clear from the rheological data presented and discussed earlier, is not necessarily the case under the conditions used in the present work.

Returning to the relevance of the softening point to open time and setting time (Fig 99) it can be seen that there is again a considerable spread of data points with no apparent relationships for either phenomenon; indeed the scatter amongst the data points (greatest for the open time measurements) precludes the use of softening point as a clear indication of performance. It is possible to see the same picture of scatter when relating the DSC wax peak temperature on heating (WPT_h) to the softening point (Fig 100). These observations serve to reinforce the point made above that the adhesives' softening points cannot be trivially related to fundamental properties of the adhesive.

One can also compare the softening point with the rheological properties of the adhesive. Figure 101 illustrates the relationship between the crossover temperature T_X and the softening point. It is clear that there is no significant correlation if all of the samples are considered together (Fig 101a) however if the 28% ExUL EVAs are considered then the situation becomes a little clearer. A first attempt at linear regression fails on the ExUL EVAs due to the outlier results of ADH 28/7NC and ADH 28/2500NC. Removing these two points gives a regression coefficient of 0.988 with an S.E. of approximately 7%. The justification for removing these data is based upon discussions that have already been put forward in earlier sections. The ADH 28/7NC has shown anomalous behaviour in both the DSC and rheological tests performed upon it in relation to the rest of the ExUL series and this has been explained by consideration of the possibility that the high molecular weight material dephases or does not mix completely with the other adhesive components. This may give rise to an artificially low softening point as the wax and resin may flow from the measurement cup before the EVA has had a chance to flow. At the other end of the molecular weight range, the lack of difference observed between ADH 28/400NC and ADH 28/2500NC is perhaps attributable to the fact that the

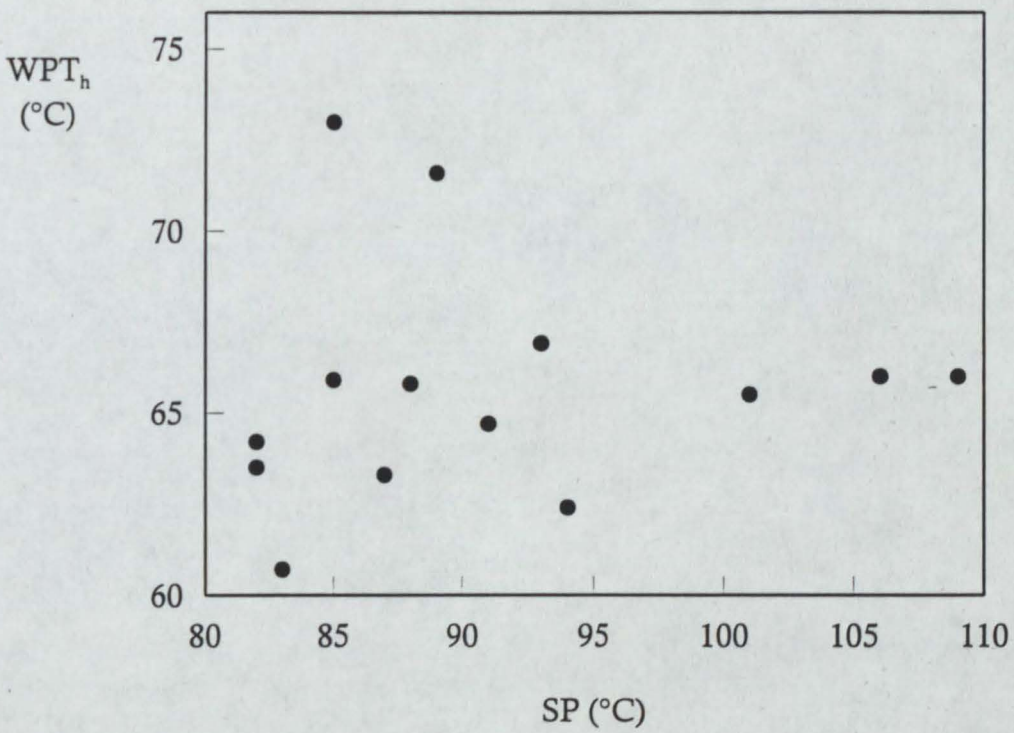

Fig 100. Graph illustrating the relationship between DSC wax peak temperature on heating WPT_h and the softening point SP of the adhesives.

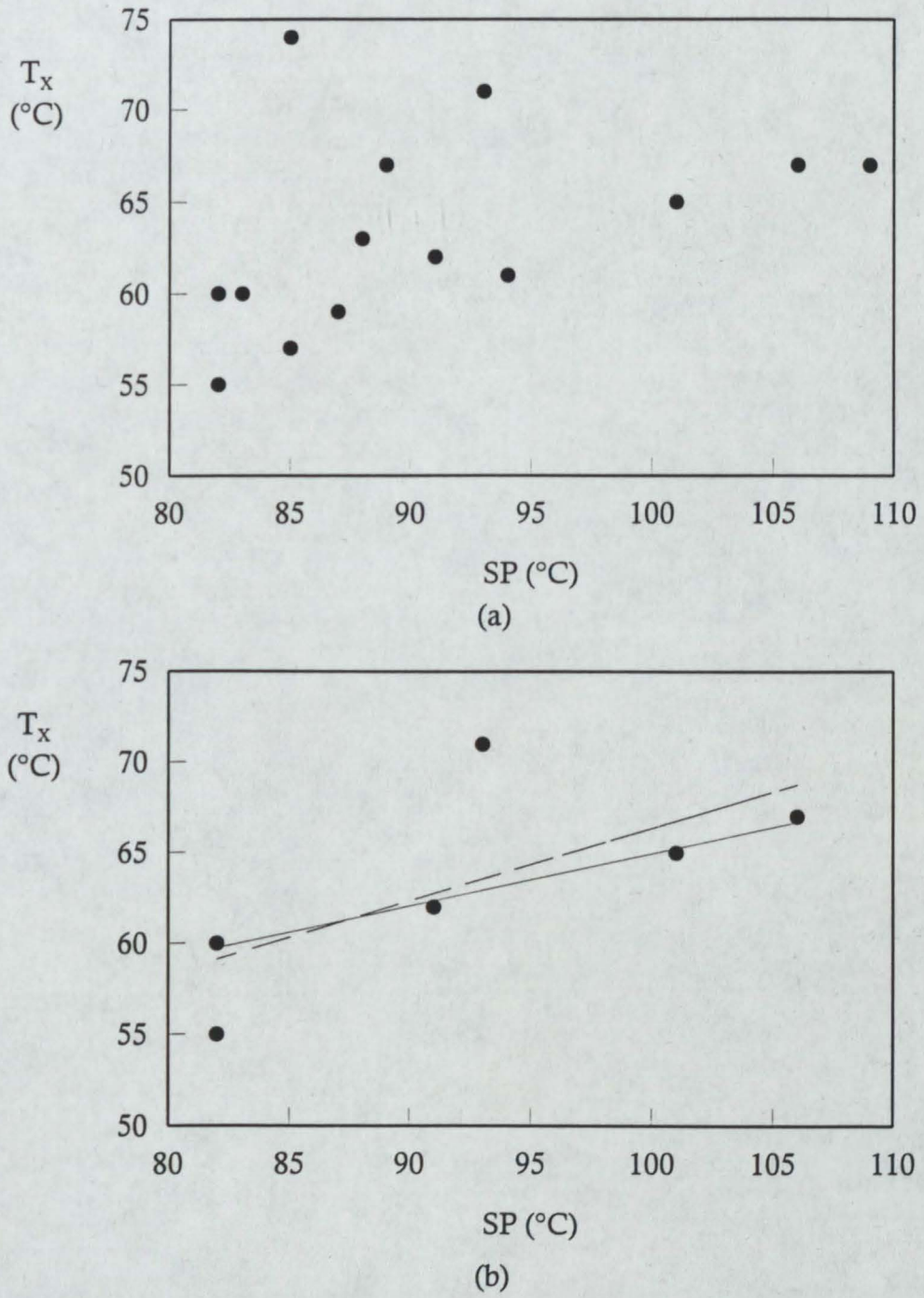

Fig 101. Graphs illustrating the relationship between crossover temperature T_x and the softening point SP of the adhesive samples. (a) data for all samples; (b) data for the adhesives containing 28%VA ExUL EVA. (— — —) linear regression performed on all ExUL 28%VA samples; (———) regression performed after discarding of ADH 28/7NC and ADH 28/2500NC results. See text for details.

dominant component with respect to flow in the softening point test is not related at all to the polymer but is governed by the other components in the system. The detection of T_X by rheometry in this case then gives a much more reliable picture of adhesive behaviour at this important phenomenological region of the adhesive and is a better indication of onset of flow of the adhesive.

The cloud points of the adhesive samples are usually taken as an indication of the compatibility of a system with regards to the suitability of a particular resin for a certain polymer [15, 156]. Although often applied to complete systems, as in the present work, an indication of resin/polymer compatibility is only really possible with a binary system, or with a pressure-sensitive adhesive that does not contain a wax. The cloud point represents the temperature at which a noticeable turbidity appears within the adhesive sample upon cooling and for wax containing systems this is strongly influenced by the wax's crystallisation temperature. Considering initially the binary polymer/resin system. It has been widely shown in the literature that gum rosin esters are extremely compatible with EVA copolymers for all concentrations of VA, *e.g.* [171]. Indeed, this compatibility was a primary justification for the selection of the resin used in the present study. The addition of a third component to the binary blend complicates matters and this is especially true if, as in this case, the third component precipitates on cooling. The theory relating to the mutual solubility/ immiscibility of ternary systems has been extensively expounded [82] however in most cases the studies have involved the determination of critical solution temperatures as a function of blend composition, rather than investigating the effects of varying the characteristics, such as molecular weight or composition, of the polymer itself.

It can be seen from Table 11 that there are three broad categories of adhesive cloud point behaviour: (a) the 28% VA series ExUL adhesives appear to all have invariant cloud points suggesting that molecular weight is not the most significant factor; (b) polymers which are less compatible than their 28%VA counterparts; and (c) polymers which are more compatible with the adhesive system, *i.e.* lower cloud points. Considering these points in turn. The invariance of cloud point as a function of molecular weight is not entirely

surprising given that one of the primary considerations for compatibility is polarity [208]. Mixtures of polymeric materials, and in fact most organic materials, require similar degrees of polarity if they are to be mutually soluble, *i.e.* like dissolves like. In a copolymer such as EVA comprising non-polar and polar comonomers, it is obvious that greater concentrations of the polar monomer will give a more polar copolymer. Of course, there will generally be residual polarity in any polymeric system due to the nature of the species at the ends of the chains however in typical polymers, such as those considered here with $M_w > 15\,000$ the change in polarity attributable to the greater concentration of chain ends in a lower molecular weight polymer cannot be detected within the scope of the industrial test performed here.

Of greater significance is the observation that the cloud point for the 28% VA series adhesives almost exactly corresponds to the point of initial crystallisation as seen as the DSC trace of the neat wax (Fig 30a, Chapter 3). It must be borne in mind that the cooling rates of the two techniques are almost certainly different and this exact correspondence is probably co-incidental, however it is still valid to conclude that the initial change here is due to precipitation of the wax phase, modified only to a very small extent by the presence of the 28% VA polymer. If one considers the precipitation of the crystalline wax phase then it follows that another important factor when describing the compatibility of a system must be that of crystallinity of the polymer. If the crystallinity of the polymer is such that co-crystallisation with the wax is possible, it would be expected that a modification of both the wax and polymer crystallisation temperatures would be observed. The low VA 14/2500NC-containing adhesive shows this type of behaviour. From a polarity viewpoint, the less polar 14/2500NC might be expected to be more compatible with the non polar wax, leading to a decrease in cloud point, however the opposite is observed. This is believed due to the more crystalline nature of the 14/2500NC. The increased crystallinity initiates crystallisation of the wax at a higher than normal temperature. Similar effects were noted and discussed earlier in relation to the DSC data (p181). A similar effect, albeit to a much lesser extent, was observed with 19/150NC.

The third effect observed was a decrease in the cloud point compared with the baseline 28%VA series. This depression (indicative of increased compatibility) primarily consisted of polymers manufactured by Elf Atochem. The 28/420NC* and 33/400NC* adhesives both showed increased compatibility. The differences in thermal and rheological behaviour have already been extensively commented upon and it has been hypothesised that the different manufacturing conditions gives rise to these changes. There is ample support in the literature for such conclusions and these differences could be expected to manifest themselves in compatibility terms also.

Overall there do not appear to be extremely large differences between the samples, considering the relatively precise determinations (estimated error in cloud point determination is ± ½°C). In the wide industrial experience of the author, and by example in trade literature [246], and published articles *e.g.* [25, 179], much greater differences in cloud points are obtained by substituting different resins or waxes into a polymer/wax/resin system. In some cases, cloud point differences of greater than 30°C have been reported. In this context then, we may view the present results as giving some indication of polymer/resin/wax compatibility, however the overriding observation is that wax precipitation is the predominant effect and this occurs at more or less the same temperature.

The phenomenon of cloud point as an indicator of wax precipitation leads to the question of whether useful adhesive parameters can be elicited from it's measurement. The obvious first correlation to investigate would be that of DSC wax peak temperature (WPT_c) on cooling *vs* cloud point. This is illustrated in Figs 102a and 102b for both WPT_c of the adhesive and of the neat polymers. It can be seen that there is considerable scatter on both graphs and, as we have already seen for softening point, any simple attempt to correlate cloud point temperature and WPT must be discarded. If the cloud point is taken as a solubility limit then it should theoretically be possible to perform the same comparison on DSC heating WPTs (Fig 102c) however scatter is again significant. The suggestion therefore that the cloud point indicates a major thermal effect needs further examination. Firstly, in the definition of the cloud point test method, it is stressed that the cloud point represents the first point of

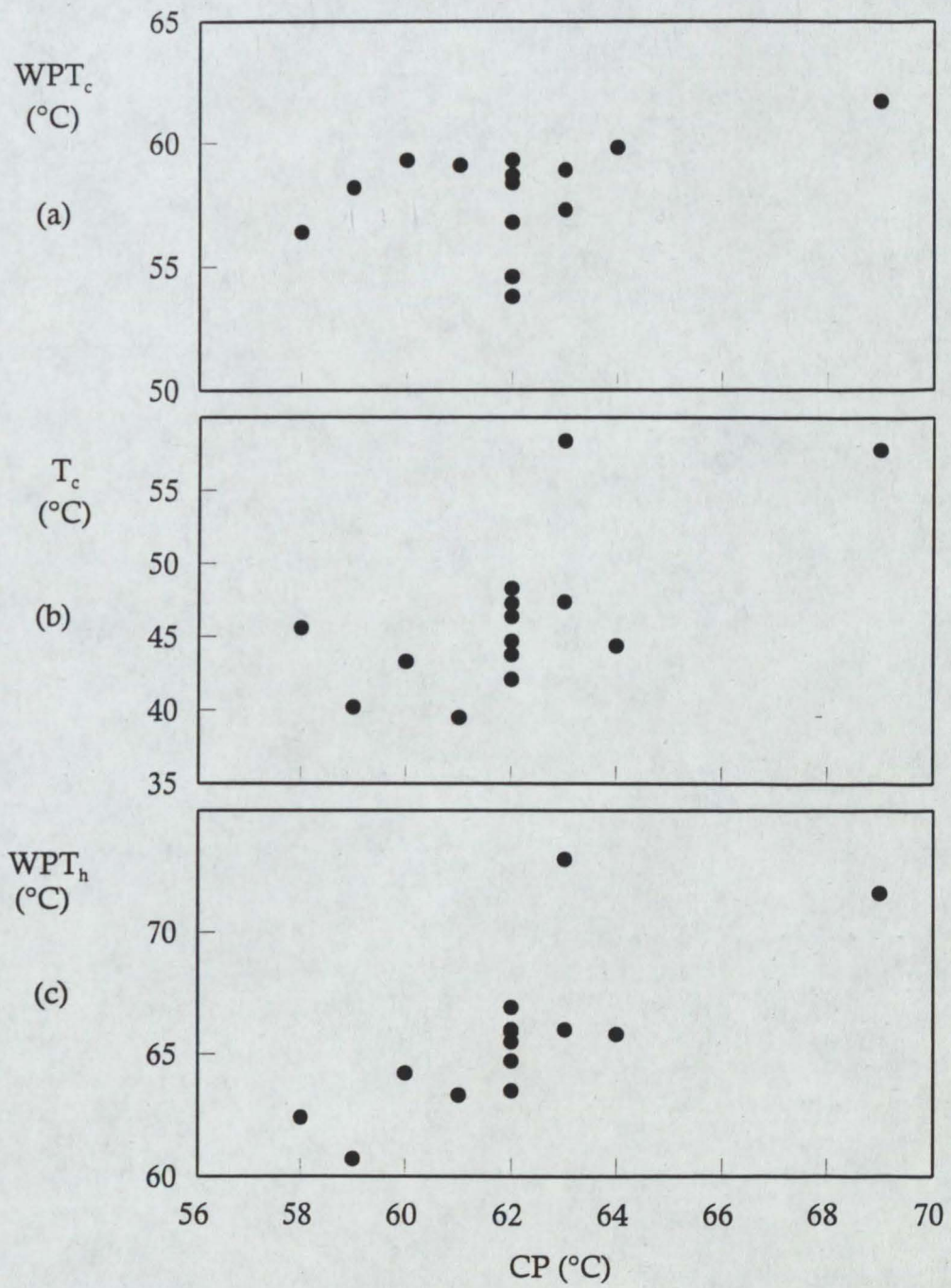

Fig 102. Graphs showing the relationship between (a) DSC wax peak temperature on cooling WPT_c of the adhesives, (b) DSC crystallisation temperature of the EVA copolymers T_c, and (c) DSC wax peak temperature on heating WPT_h of the adhesives as a function of the cloud point CP of the adhesive.

initial turbidity. As an experiment, reproducibility is quite good (for a trained operator) however repeatability between operators is dependant very much on interpretation of turbidity. Secondly, the appearance of turbidity gives an indication of the start of the wax precipitation or crystallisation phenomenon, whereas the WPT determined by DSC indicates the point of maximum crystallisation rate. Figure 103 illustrates DSC cooling curves for two 2 500 MI EVA-based adhesives. Cloud point measurements of ADH 14/2500NC and ADH 28/2500NC show values of 69 and 62°C respectively whilst cooling WPT are < 62 and 58°C. In this case we could reasonably expect to relate the difference in cloud point to the different crystallisation peak profile, *i.e.* start point or WPT, arising from different composition. If, however, we examine two 28% VA - based adhesives, made of EVAs from different manufacturers, then the obvious differences in Fig 103 are not visible and the small but significant shift in the cloud point temperature is not really reflected in any feature of the DSC curve except by a small difference in the slope of the initial crystallisation peak. This minor difference however may not be suitable as a robust enough tool for the industrialist to use when trying to predict hot melt adhesive performance.

The third industrial test mentioned in connection with bond formation was that of open time and setting time determination. These properties are of critical importance in a hard setting HMA, second only to the HMAs ability to adhere to the substrates. The definitions of open time and setting time have been given earlier (Chapter 1, p4) and it will be recalled that the definitions given relate not just to the adhesive properties, but also to external factors such as the nature of the adhesives, the amount of adhesive, and environmental considerations. These factors greatly influence the transfer of heat from the molten adhesive and hence affect its cooling rate and how rapidly the adhesive becomes unable to wet the substrate to which it is applied. Practically, these considerations can lead to significant differences in the precise and reproducible determination of open time and setting times of adhesives unless considerable attention to detail is paid to the environment, and means, of the determination.

There are many standard test methods for the determination of hot melt

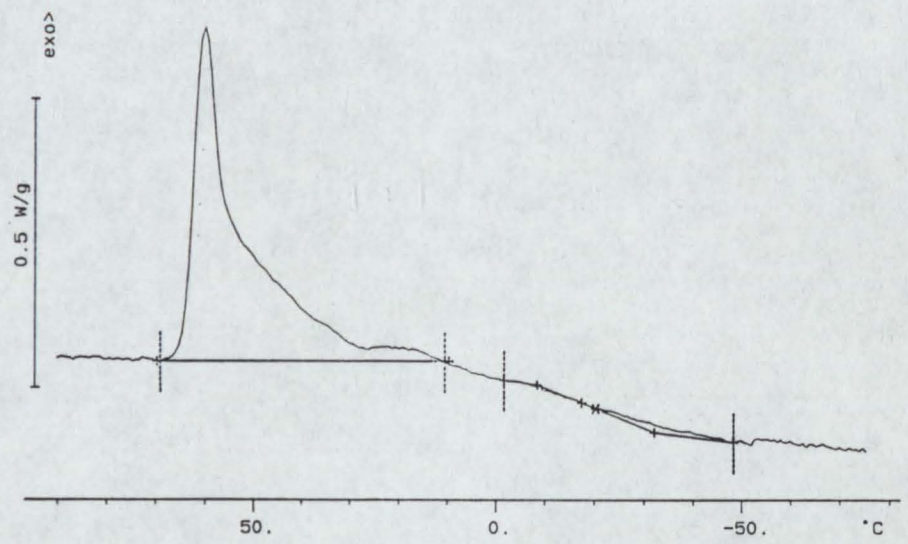

(a)

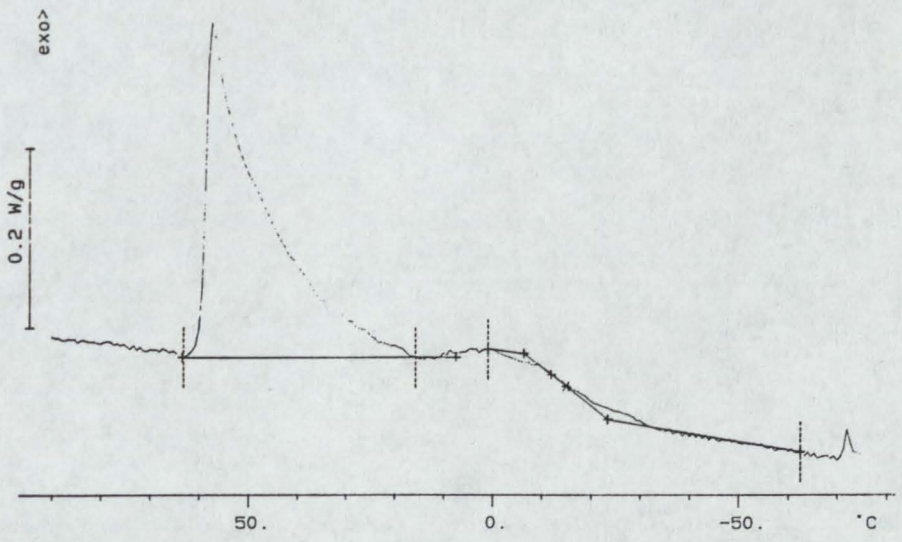

(b)

Fig 103. DSC cooling curves of adhesives containing 2 500MI ExUL EVAs. (a) ADH 14/2500NC and (b) ADH 28/2500NC.

adhesives open times, *e.g.* [151, 247], most of which are similar to each other. These generally require the drawing down of a thin film of hot melt onto a sheet of paper and then pressing smaller strips of paper into the molten film at regularly spaced time intervals. It is the opinion of the present author, and numerous colleagues in sister companies around the world [248 - 251], together with views from other well-known practitioners of hot melt adhesive formulation [252 - 254] that, whilst such methods may be suitable for longer open time products, such as those used in the hygiene, bookbinding, or labelling industries, they are manifestly unsuitable for formulations intended for use in packaging applications where a rapid bond formation is necessary as a consequence of the speed of the machinery employed. As an example, whilst adhesives used in perfect bound book production would typically be required to have an open time greater than 15 s, a packaging adhesive would be expected to have an open time no longer than 5 s on average [171]. The adhesive formulation used in the present work is more closely approximating a packaging adhesive than a bookbinding one.

There have been numerous attempts to improve the determination of the open and setting times by the use of mechanical bond-testers, *e.g.* [23a], however, certain deficiencies in the designs of these bond testers have limited their usage and acceptance. The Pira bond tester, for example, requires large (1 - 2 kg) samples to be applied through an industrial application unit whilst the Olinger bond tester is of cumbersome design and imprecise adhesive application. The bond tester used in the present work was designed and built by engineers in the author's company precisely to overcome the limitations of early designs. The Kanebo bond tester requires only 50 - 100 g of sample, and can be computer controlled to give precise and reproducible applications of adhesive by means of a metering pump through an industry standard nozzle at a precise temperature. In addition, the substrate speed and compression pressure can be accurately controlled to give a dramatic improvement in reproducibility. The choice, and conditioning, of suitable substrates is of critical importance as has been mentioned earlier (Chapter 3, p95) and care was taken in the present work to ensure that testing was performed under conditions of near constant temperature

and relative humidity. An excellent measure of the impact of such parameters was reported by Ambrosini [154].

The interpretation of open time and setting times results obtained from the Kanebo bond tester has been discussed earlier (Chapter 3, p95) where it might be recalled that two possible points of open time identification were considered *i.e.* a differentiation in the amount of fibre tear, or a reduction in the compressed bead width. The former is an obvious indicator that the open time of the adhesive is being exceeded, *i.e.* the adhesive begins to lose its ability to fully wet the surface fibres of the board. However, the second indicator relies upon other indications that the open time of the adhesive has been exceeded - in other words, a reduction in bead width due to an increasing reluctance to flow under a constant compression pressure. It is within the experience of the author and co-workers that either method may be used, and more importantly, compared. However, in the present work, such comparisons were infrequently required and the former method was able to be used for all adhesive samples with the exception of the higher melt index adhesives (MI = 2 500). The 2 500 MI adhesives were all characterised by a low viscosity and hence tended to fully wet board surfaces under the present test conditions. In these cases, fibre tear was obtained at very long open times. Bead flatness reduced at considerably shorter time intervals. For example, ADH 28/2500NC gave fibre tearing bonds upto 10 s however bead flatness started to reduce rapidly after the 7 s quoted in Table 19. It is the latter value which more accurately relates the behaviour and performance of bonds performed under industrial conditions where any slight imperfection in the performance of an adhesive bond can have consequences for the security of the application in which it was designed to perform.

In looking at the data in Table 19 it can be seen that there are definite relationships in relation to both melt indices and composition. Figure 104a illustrates the variation of open time as a function of melt index whilst Fig 104b shows the same data plotted against copolymer composition for the adhesive pairs 14/2500NC and 28/2500NC, 19/150NC and 28/145NC, and 28/420NC* and 33/400NC*. In addition the crystalline 28/400XL and 33/400XL are also shown. Figure 104a shows clearly an initial increase in open time up to a melt

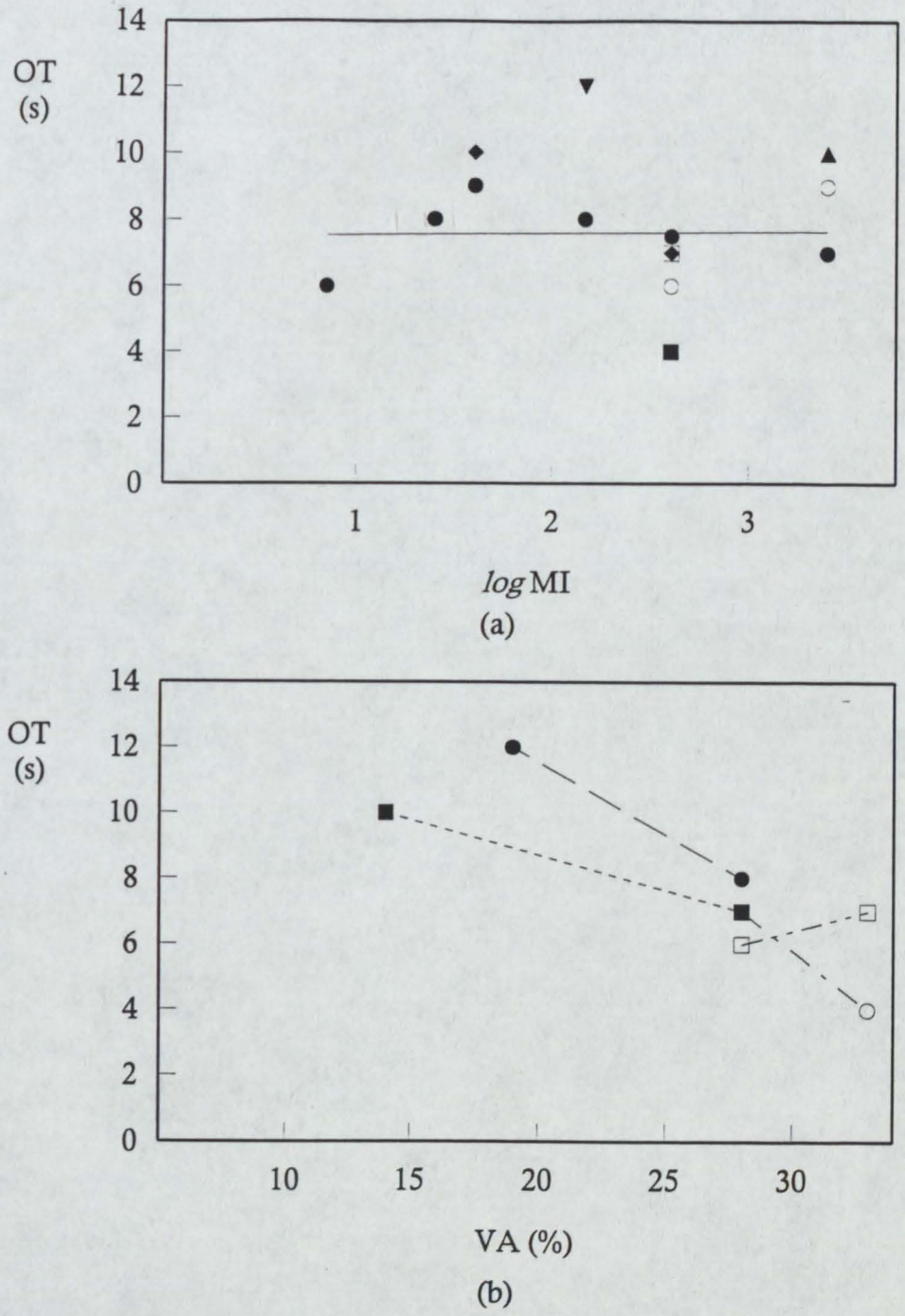

Fig 104. Graphs showing variation in open time of adhesives as a function of (a) the logarithm of the melt index MI of the polymer, and (b) the composition %VA of the polymer. Symbols: in (a) ▲ 14% VA; ▼ 19% VA; ● 28% VA NC; ○ 28% VA XL; ■ 33% VA; □ 33% VA XL; ◆ 28% VA NC*; and in (b) ■ 2 500 MI ExUL; ● 150 MI ExUL; ○ 400 MI AtEV; □ 400 MI ExAD.

index of 40, followed by a shallow decline as the molecular weight of the polymer decreases. It is probable that two mechanisms are in play with respect to molecular weight. At very high molecular weights, the viscosity is already very high even at application temperature and wetting may not easily occur in the relatively short period of time that the adhesive has before cooling. Such behaviour would result in a bond which would need to be made extremely quickly if positive wetting of the second substrate were to occur. As the molecular weight (and hence viscosity) reduces, it becomes progressively easier for the adhesive to wet the surface of the cardboard, even at lower temperatures, and hence the effective open time of the adhesive increases. Above a certain point, however, a second aspect of the viscosity becomes important. As the adhesive viscosity becomes lower, penetration of the adhesive into the surface of the substrate is increased as capillary ("wicking") forces now predominate. This wicking action allows the adhesive to cool more rapidly mainly as a function of increased surface area and more intimate contact with the cold substrate and hence the time available to form a bond is reduced. The reduction in open time is more pronounced the lower the viscosity of the adhesive. Figure 105a illustrates the variation of open time with adhesive melt viscosity at 160°C.

The viscosity hypothesis seems to apply to the narrow composition band of 28%VA, non-crystalline EVA-based adhesives but close examination of the bonds reveal that this is not the case for adhesives falling outside of these criteria. If we examine the effect of vinyl acetate content then the effects seem very clear. For adhesives comprising EVAs of similar melt indices, there is a clear reduction in open time with an increase in VA concentration. Initially, this may seem surprising on several fronts. It has already been shown and discussed that increasing the amount of VA results in a shift of the solubility of the phases, *e.g.* softening point reduces, however if we examine the earlier DSC results we can see that there is a significant decrease in the enthalpy of crystallisation with increasing comonomer content, and it is this factor which leads to the hypothesis that open time is not just a function of viscosity but is also governed by the change in heat capacity induced by compositional changes in the hot melt. If the open time of an adhesive is thus related to compositional shifts in the phases of

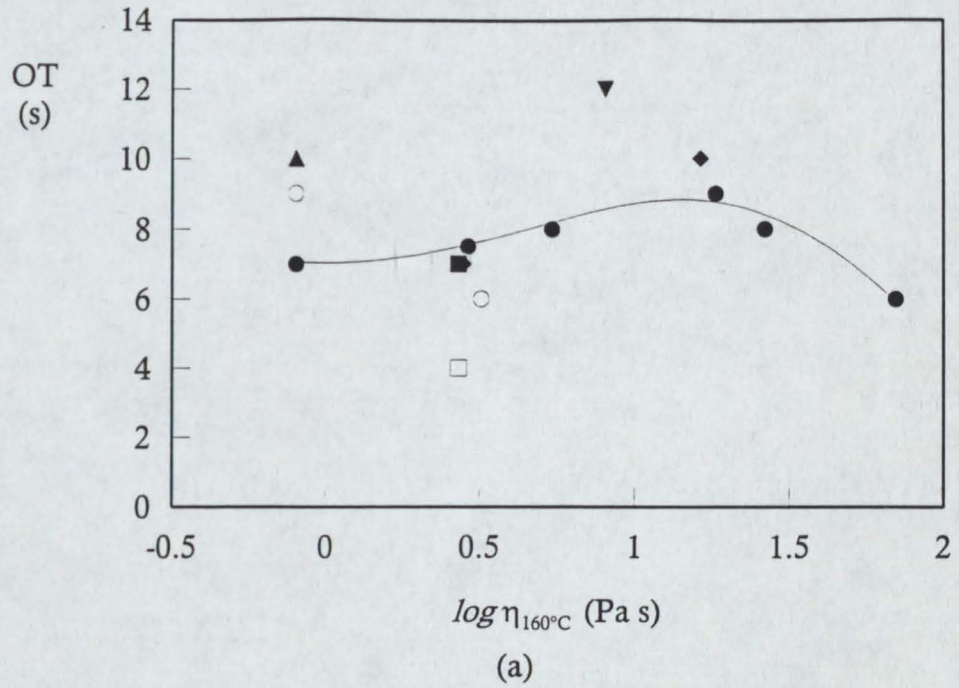

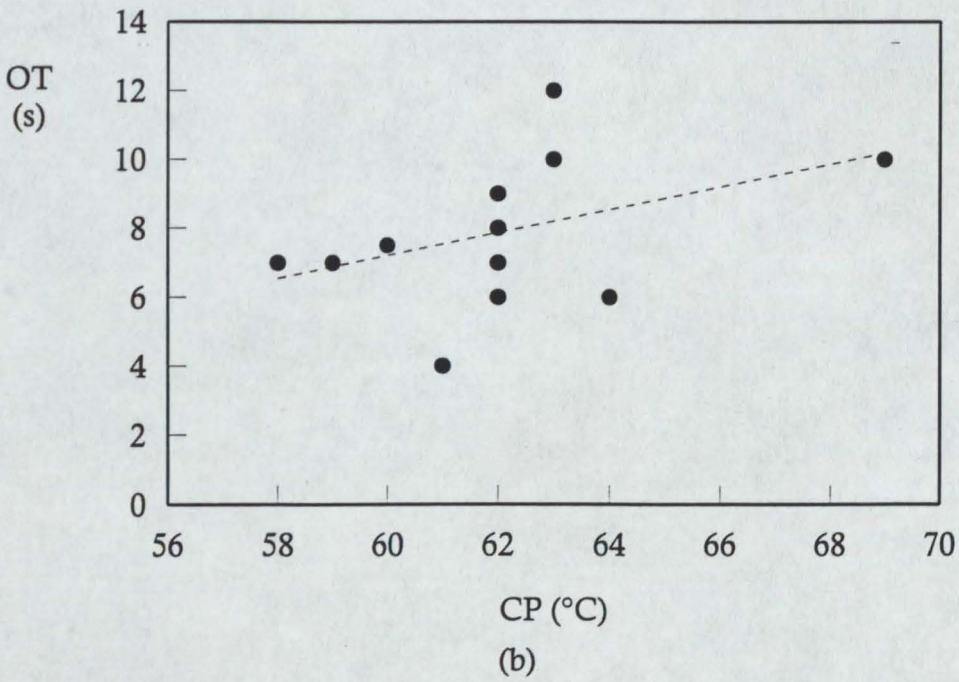

Fig 105. The variation in the open times OT of the adhesives as a function of (a) the logarithm of the adhesive melt viscosity measured at 160°C $\eta_{160°C}$, and (b) the cloud point CP. Symbols: ▲ 14% VA; ▼ 19% VA; ● 28% VA NC; ○ 28% VA XL; ■ 33% VA; □ 33% VA XL; ◆ 28% VA NC*.

hot melt adhesives as they cool, predominantly the precipitation of the wax, then it may be expected that some of the other indications of this phenomenon that have already been discussed are also applicable in determining the open time of a hot melt adhesive.

An attempt to correlate softening point with open time has already been undertaken and the conclusion was reached that the relationship is not clear. However, if open time is considered alongside the cloud point of the adhesive (Fig 105b) then a trend emerges, and although scatter is still a consideration, for the same reasons as discussed earlier, it seems that the assumption of a relationship between the two properties has some merit. The fundamental rôle that the wax plays in controlling the thermal properties is again highlighted. Although this concept is not novel [24] it is reassuring to observe these trends in the current work. Given that the wax precipitation plays a crucial part in defining the open time of a hot melt adhesive, we should see the same relationship with other analysis techniques that primarily depend upon the thermal behaviour of the wax, *e.g.* Figs 106a and 106b illustrates the relationships between open time and WPT_c and ΔH_c respectively as determined by DSC. Scatter is significant in the former case (see earlier) however clearer tends are visible when ΔH_c is considered. This is again entirely self consistent and logical. Adhesives that have large ΔH_c values must lose a larger amount of heat when cooling and hence will take longer to set. It is interesting that the two lower VA samples, ADH 14/2500NC and ADH 19/150NC both have the longer open times yet clearly have the highest crystallisation temperatures (WPT_c). A third parameter may also be thought to represent the open time of the adhesive, and this is the crossover temperature T_X which represents the point at which the adhesive changes from solid-like to liquid-like behaviour. Figure 106c illustrates the variation of open time with T_X and, whilst the regression is not particularly good ($r^2 = 0.255$) there does appear to be a slight trend. The poor regression coefficient is thought attributable to differences in the phenomenon being determined during the tests, *i.e.* open time, is determined during cooling whilst T_X is measured during heating. The relative insensitivity of the open time test (resolution is ½ s) may also be a contributary factor. This

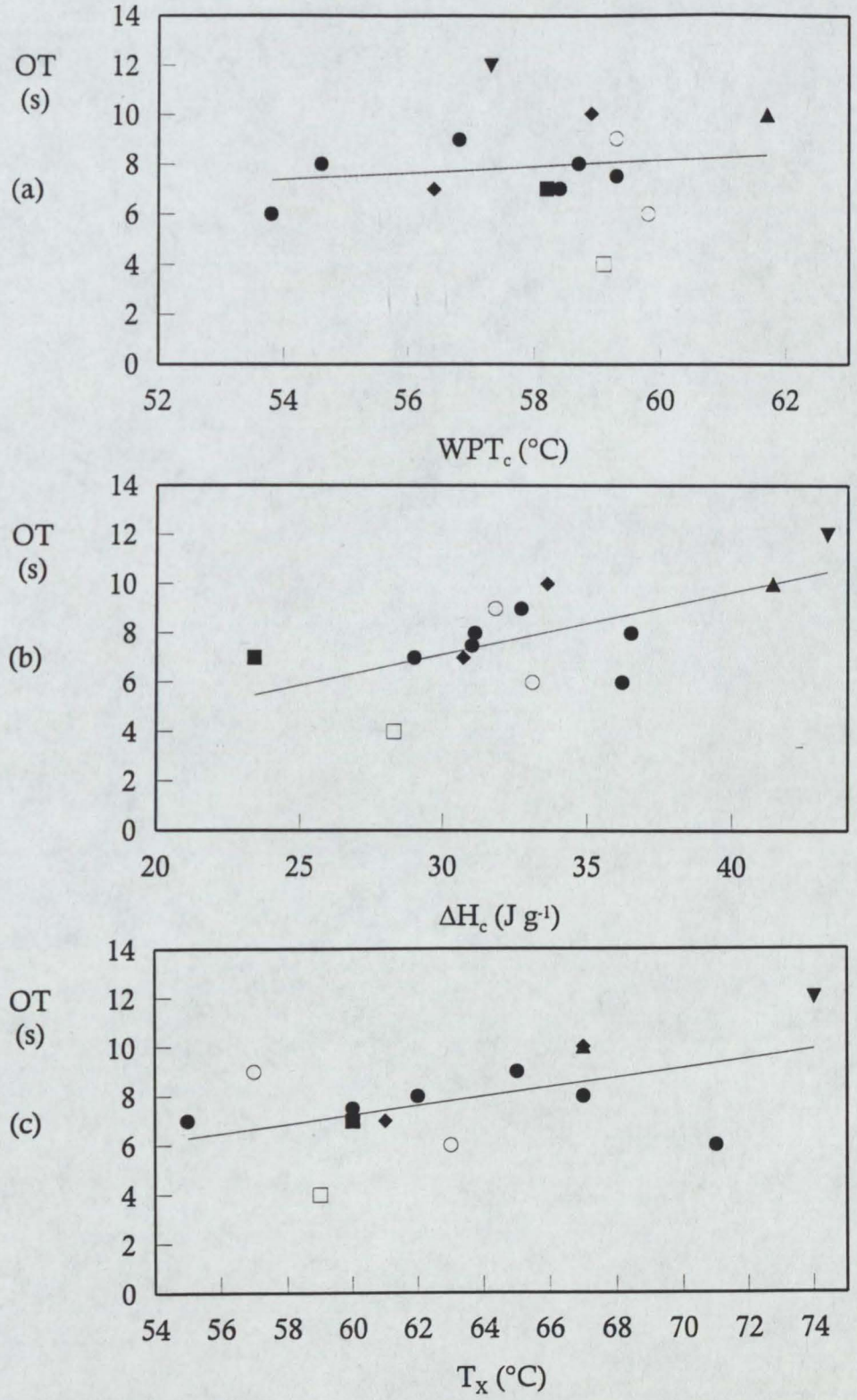

Fig 106. The variation in the open times OT of the adhesives as a function of (a) the wax peak temperature on cooling WPT_c, (b) the enthalpy on cooling ΔH_c as determined by DSC, and (c) the crossover temperature T_X as determined by oscillatory rheometry. Symbols: ▲ 14% VA; ▼ 19% VA; ● 28% VA NC; ○ 28% VA XL; ■ 33% VA; □ 33% VA XL; ◆ 28% VA NC*.

clearly demonstrates the danger of assigning a complicated adhesive phenomenon, *i.e.* open time, to a simplistic model of polymer miscibility, compatibility, or thermal behaviour in a complex system such as an adhesive.

Although attempts have been made to understand the impact that compositional changes induced by cooling can have on the properties of an adhesive [255], such attempts on determining the phase morphology associated with spinodal and binodal decomposition (as expounded by Flory) have only been seen on binary systems used in pressure sensitive adhesives. The rheological results presented in that study were strongly suggestive of the property changes but were perhaps not as conclusive as they could have been due to (acknowledged) uncertainties in film coating and preparation techniques. The phase separation on a microscopic scale seen with styrenic block copolymers have also been extensively discussed in the available literature [10, 256, 257] however there is little literature examining such phenomena in hard setting hot melts similar to those in the present work.

5.4 Strength of adhesive bonds

If the properties of the completed joint are next considered, namely their mechanical strength, then two sets of data can be examined, namely the tensile data of the neat adhesives and the peel strengths of the aluminium laminates. Tensile data for the adhesive samples was collected or described by ASTM D 638 for plastics materials, and the results are given in Table 20. As has been indicated earlier, the magnitude of the scatter obtained is variable, with some samples showing little scatter (approximately 2 - 4%) whilst other samples gave larger scatter (approximately 8 - 12% in the worst cases). The magnitude of the scatter did not appear to vary in a systematic fashion and large values of the scatter were not confined to one particular sample, test speed, or determined parameter. The scatter is thought to be attributable to a combination of factors including air inclusions into the adhesive sample, irregularities in the gauge length of the specimen, and unavoidable surface defects caused by the sample casting process. These occurred despite the precautions described in Chapter 3. Further samples were run in the most extreme cases (scatter greater than 8%)

and the results were pooled with extreme values removed to give statistically larger samples. It is appreciated that this may introduce other uncertainties but the data presented appears to be is a reasonably accurate and precise representation of the adhesives' tensile properties.

There have been previous instances where attempts have been made attempting to relate tensile data of a plastic material to viscoelastic properties, both with thermoplastic elastomers and vinyl copolymers [258, 259], and with adhesives [156]. These attempts have been both qualitative and quantitative but extreme caution must be exercised in interpreting these data. The performance of a tensile test whereby a sample undergoes extremely large elongations (typically thousands of percent of strain) performed at a constant rate of deformation and under conditions of rapidly changing sample dimensions is not analogous to the small amplitude, non-destructive oscillations used in rheometry. Indeed, the tensile test by definition does not fit into the constraints demanded by the consideration of linear viscoelasticity. As has often been stated, *e.g.* [184], such comparisons can be misleading. Given that initial premise then, it is very hard to qualitatively relate tensile data to (say) creep tests, or oscillatory rheograms. The primary aim of the present work will be to determine and assess indices of performance that can be utilised in an industrial laboratory. Firstly, relating the tensile properties of the adhesives to their molecular weight, there are no unexpected results and the same trends observed in the data presented by the polymer manufacturers for each polymer are broadly observed in the adhesive formulations (see Figs 55 to 58, Chapter 4, pp147 - 150). Linear regression was attempted on the 28% VA series data (illustrated). In general agreements were not too good (at best r^2=0.945). Nevertheless, the trends contained within the data are apparent upon visual inspection. The modulus, yield and maximum stresses, and the maximum elongation all decrease with increasing melt index. These results are as expected. It is well known that a decrease in molecular weight gives rise to inferior mechanical properties. Briefly looking at the effect of composition, it can be seen that there is a strong decrease in mechanical properties as the amount of VA in the copolymer is increased. This can be correlated with the disruptive effect that VA

has on the ability of the ethylene to crystallise. This observation is supported by the increase in yield and maximum stress with the crystalline ExAD grades, particularly at higher rates of testing. The trends in the modulus data are less clear cut where the amount of scatter is significant and the actual differences are not too great.

The data has also been examined for the effects of test rate on the mechanical properties. Examples are given, for the 28% VA series, in Fig 107. This shows the variation in Young's modulus and 1% yield stress for each melt index considered, as a function of the test speed. It is noted that significant changes in Young's modulus only occur at the highest test speeds for those polymers with the highest molecular weight. The variation of yield stress with rate is not as clear-cut as that of the modulus, although the obvious trend with a sudden and dramatic decrease in the yield stress at high rates of testing, may also be attributed to the viscoelastic response of the sample, *i.e.* a change from flexible to brittle type deformation. Again, the main exceptions to the trend are for the extremes of molecular weight: ADH 28/7NC shows the largest decrease in properties, whilst ADH 28/2500NC shows an increase. The differences probably reflect the nature of the chain morphology and differences in entanglement frequency of the polymer molecules as discussed elsewhere.

It has been shown [260] that it is possible to model, at least to a first approximation, the tensile test in terms similar to those of a creep test whereby mechanical analogues of springs and dashpots are utilised. The use of such analogues immediately allows one to see the concepts illustrated above, *i.e.* the link between molecular weight and modulus (for example) is self-evident. The use of such models provides the first tentative link between the linear viscoelastic behaviours of the adhesives and their non-linear stress/strain response, particularly with rheological data obtained in the time-domain. For example, in a cross-linked system, the stress $\sigma(t)$ at any given time during the tensile test can be described by:

$$\sigma(t) = E_e \dot{\epsilon} t + \dot{\epsilon} \int_{-\infty}^{t} H(\tau) (1 - exp(-t/\tau)) \, d \, ln \, \tau \qquad \ldots (45)$$

where E_e is the equilibrium modulus, $\dot{\epsilon}$ is the (constant) rate of strain, and $H(\tau)$ is

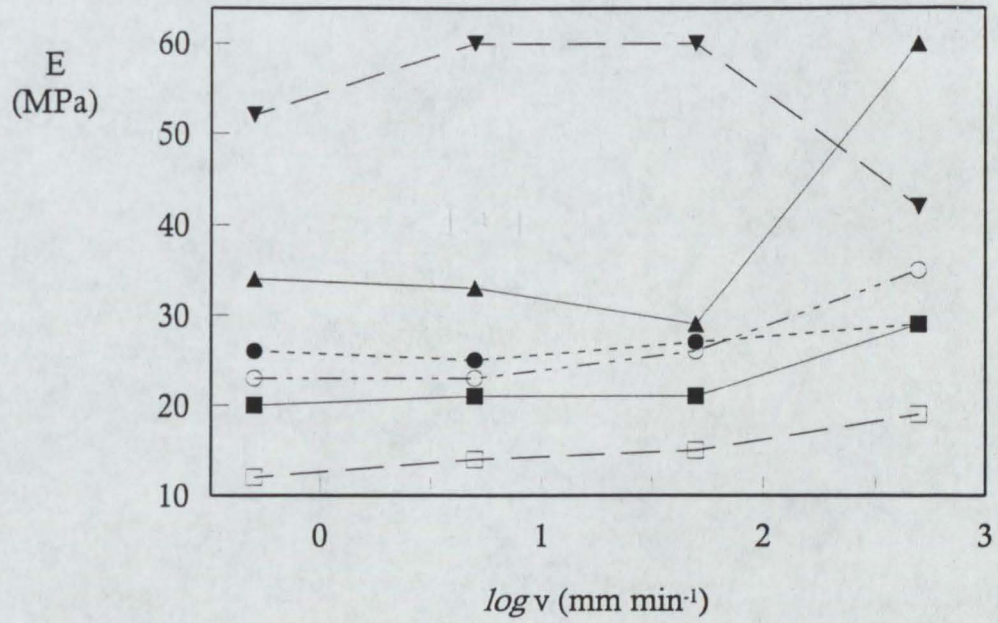

(a)

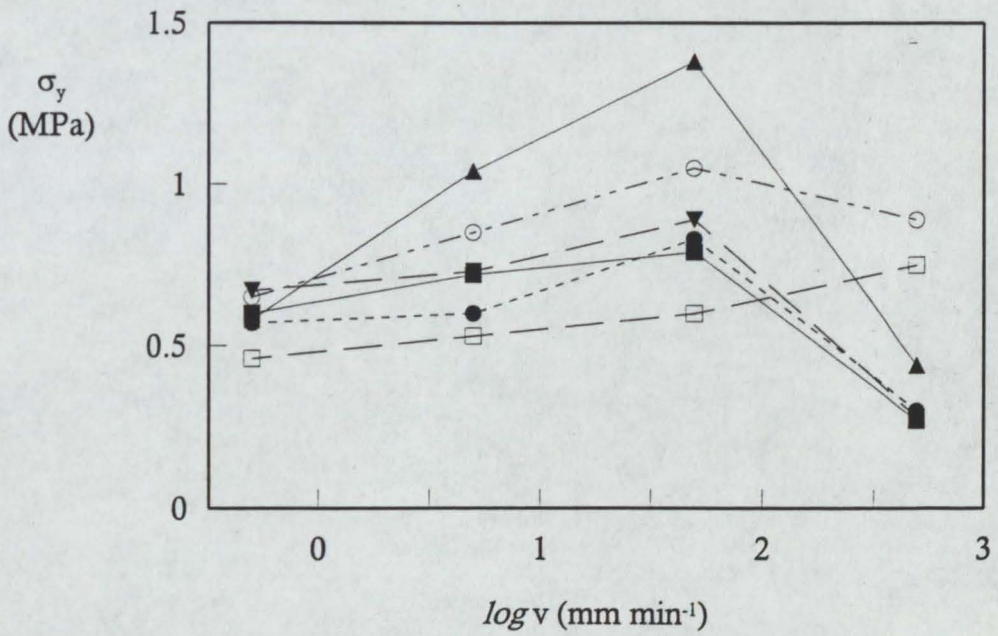

(b)

Fig 107. The variation in (a) Young's modulus E and (b) 1% yield stress σ_y of the adhesive samples containing 28%VA ExUL polymers as a function of the logarithm of the test speed v. Symbols: ▲ ADH 28/7NC; ▼ ADH 28/25NC; ● ADH 28/40NC; ○ ADH 28/145NC; ■ ADH 28/400NC; and □ ADH 28/2500NC.

the distribution function of modulus contributions of relaxation times τ of the polymer. Rewriting the above in terms of a discrete spectrum of relaxation times (rather than as a continuous spectrum) gives

$$\sigma(t) = E_e \dot{\epsilon} t + \sum E_i \, exp(-t/\tau_i)\,(1 - exp(-t/\tau_i)) \qquad \ldots (46)$$

Thus linear viscoelastic theory can give an approximation to a non-linear stress response. There are however drawbacks with this type of modelling : firstly, neither equation can be relied upon to predict the stress behaviour at large strains; secondly, neither equation can simply predict strain hardening, or softening; and thirdly, analogue models cannot predict with any degree of confidence, features on the tensile curve such as yield point or maximum strain. Attempts to model the stress/strain response of ADH 28/400NC using the parameters for J_0, J_i, and τ_i, obtained from the creep testing at 20°C are shown in Fig 108. The attempt was made using equation (46) with E_e set to be equivalent to $1/J_0$; $\dot{\epsilon}$ was taken as 8.33×10^{-6} m s^{-1} (0.5 mm min^{-1}), and E_i, τ_i were taken from the first V/K unit. The model is plotted $\sigma(t)$ against time with the tensile data being shifted to a time domain by assuming that the given crosshead speed is equivalent to the strain rate (Fig 108). This first and very approximate attempt at modelling serves to illustrate that, as before, simple assumptions cannot be made although quantitative trends maybe considered. Bamborough and Dunkley noted possible relationships between *tan* δ and elongation, and *tan* δ, G' and the tensile strength for the samples used in their paper [156]. These relationships are shown in Table 28 which shows the rheological properties at 20°C for the 28% VA adhesives together with selected tensile data. It seems to be true that G' and E_Y at slow testing rates do appear to be linearly related. The relationship

$$E=2G(1 - \nu) \qquad \ldots (47)$$

is used to relate the moduli of isotropic materials where ν is Poisson's ratio (the negative ratio of transverse to longitudinal strain). The data presented here gives $\nu = 0.44$ which, given the approximations inherent in the above example, seems reasonable for a semi-crystalline polymer. However the other relationships considered by Bamborough and Dunkley do not appear to be significant. In conclusion, the tensile data shows behaviour which is

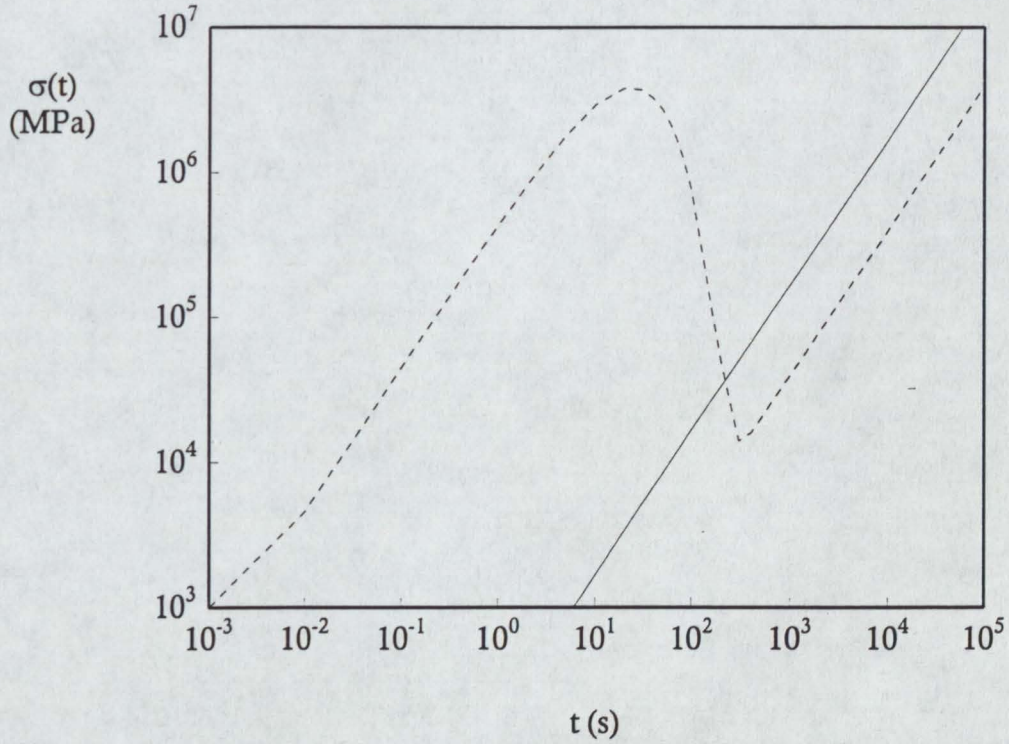

Fig 108. Graph illustrating the tensile stress σ(t) of ADH 28/400NC varying as a function of time t. (———) experimental data, (·····) model predicted utilising eqn. (46). See text for details.

Table 28 Selected tensile data (at two rates of strain) and controlled stress rheological data for 28% VA - series adhesives at a temperature of 20°C.

Adhesive	Tensile data						Rheological data	
	ϵ_f (%)		σ_y (kPa)		E_Y (MPa)		G' (MPa)	*tan* δ
v (mm min^{-1})	5	500	5	500	5	500		
28/7 NC	598	565	104	440	26	60	54	0.3
28/25NC	465	567	730	280	22	42	16	0.4
28/40NC	235	1127	600	300	25	29	20	0.37
28/145NC	558	394	850	890	23	35	18	0.36
28/400NC	526	315	720	270	21	29	15	0.34
28/2500NC	156	150	530	750	14	19	12	0.33

qualitatively related to the more precise rheological data, but the scatter is significant and the relationships postulated to exist between linear viscoelastic theory and the gross deformation do not appear to be of any immediate practical use.

The variation of peel strength of the samples is strongly dependant upon both the rate of testing and the molecular weight and composition of the polymer (Figs 109 and 110). Both effects have been extensively recorded in the literature, notably for pressure sensitive adhesives [130 - 134, 261 - 266] and, to some extent, with the work of Komormicki *et al* [88] who examined the rôle of the wax in the mechanisms of peel for hard setting hot melt adhesives. Komornicki observed that the general mode of failure varied with testing speed and wax content; the effect of the wax acting to generally lower the values of peel obtained and to shift the nature of the failure to a more interfacial mode. In the present work, the wax content of the adhesive was held constant whilst the testing speed and copolymer properties were varied. The results are given in Table 21 (in g per 25mm bond), along with the standard deviation of the results, and the observed mode of bond failure. In keeping with the nomenclature adopted by Komornicki, the adhesives were said to fail either cohesively, *i.e.* within the adhesive sample, mixed mode ('quasi-interfacial'), interfacially (rubber-like adhesive failure), or glass-like interfacial. The rapidly alternating slip-stick behaviour originally described by Kaelble was also recorded but infrequently appeared with the samples in the present study. The scatter obtained with this test is illustrated for the 28% VA series at 0.5 mm min^{-1} test speed on Fig 110. This scatter is comparable to that observed in the industrial practice of by author and that mentioned for peel testing in several of the standard test methods [267] and is inherent due to the nature of the averaging process used on a typical peel trace (Fig 59, p151).

At high rates of testing, all but the lowest molecular weight sample failed in a glassy interfacial manner with an increasing level of peel strength as the molecular weight decreased. The ADH 28/2500NC sample failed cohesively at all test rates. This may be rationalised by considering the nature of bond formation and breaking. Although the mechanical strength of the adhesives is

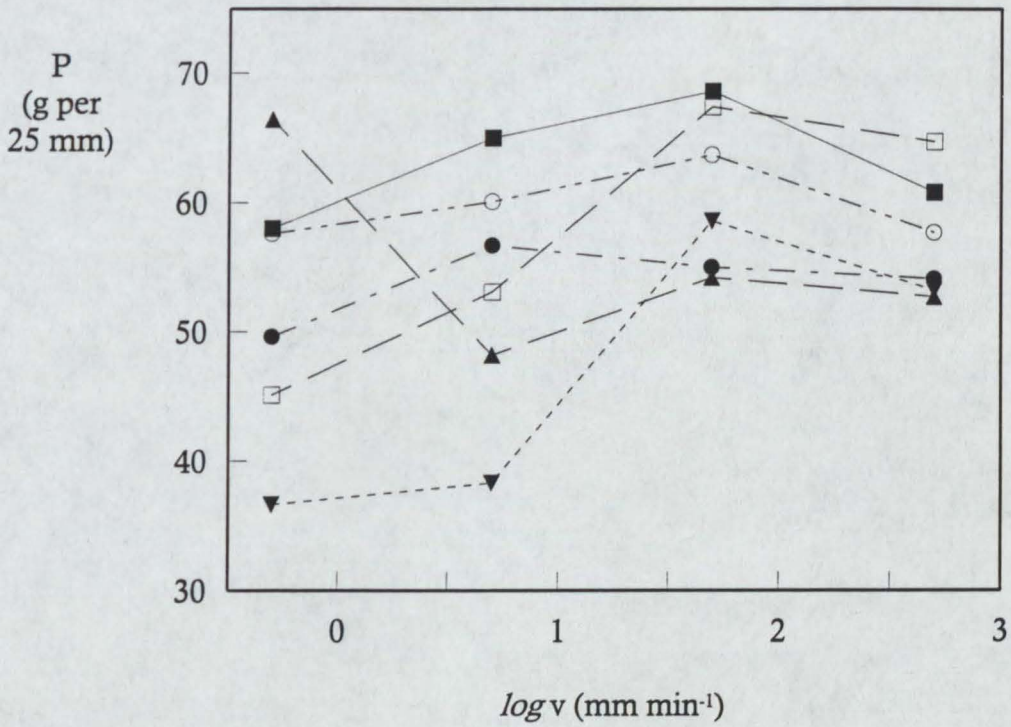

Fig 109. Peel fracture strength P as a function of the logarithm of the melt index MI. Note units of peel strength are g per 25mm width of bond. Symbols: ▲ 28/7NC; ▼ 28/25NC; ● 28/40NC; ○ 28/145NC; ■ 28/400NC; and □ 28/2500NC.

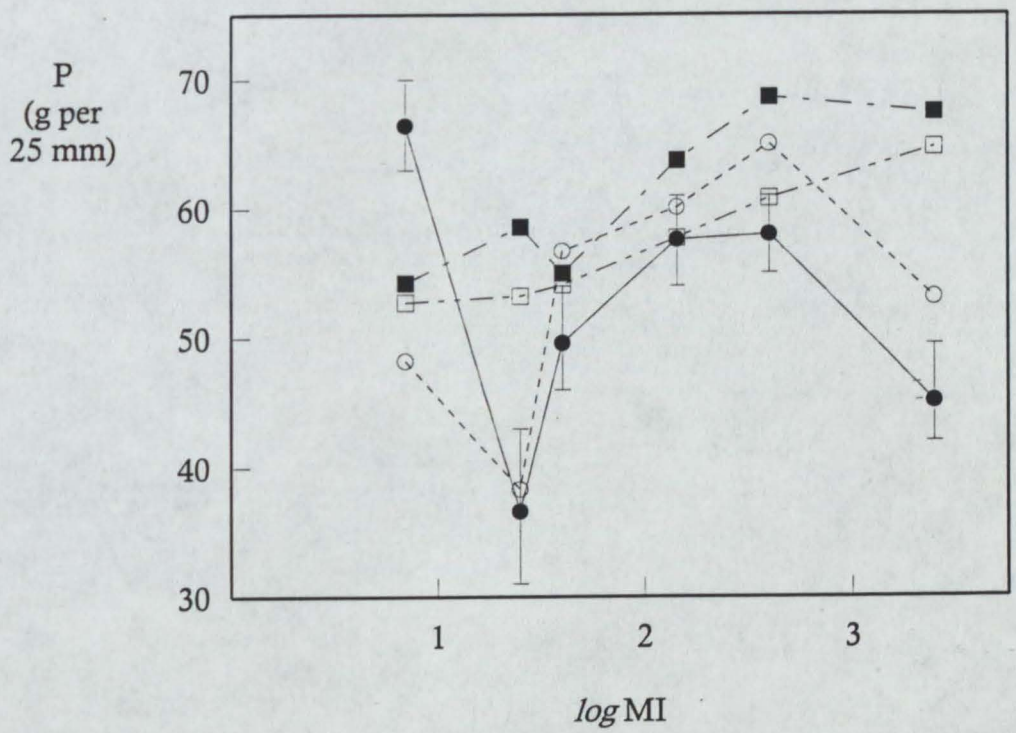

Fig 110. Graph showing the variation in adhesive peel strength P as a function of the logarithm of the melt index MI of the copolymer for 28%VA ExUL EVA-containing adhesives. Symbols: ● 0.5 mm min^{-1}; ○ 5.0 mm min^{-1}; ■ 50 mm min^{-1}; and □ 500 mm min^{-1}. Note error bars on 0.5 mm min^{-1} data are typical of scatter obtained at all test speeds, for all adhesive samples.

dependent upon the polymer molecular weight as discussed previously, there also exists a powerful influence exerted by the need to completely wet the surface of the adherend during the bonding process. Consequently, although the mechanical properties of the EVA 28/2500NC are inferior to the other samples, the low viscosity that it imparts to the adhesive permits very thorough wetting to occur. Hence, adhesion is superior to the cohesive strength of the sample under test conditions. This hypothesis on the influence of viscosity on ability to fully wet the substrate is supported by the general increase in peel strength as melt viscosity decreases. This point is discussed by Tse [268] who concluded that the bond strength to aluminium substrates was found to be independent of the application temperature, providing that the viscosity is sufficiently low, *i.e.* above a critical temperature, so that the adhesive can flow around the microscopic surface features of the aluminium.

At lower rates of peel the behaviour is less simple. The ADH 28/7NC peel values for 0.5 and 5mm min^{-1} test speeds are very high and are coupled with rubber-like adhesive failure. It could be imagined that the viscosity hypothesis mentioned above would still apply to these samples although it is evident that other mechanisms are compensating for the reduction in wetting associated with a high melt viscosity. The anomalous behaviour of the 28/7NC adhesive has been observed before with both thermal and viscoelastic measurements and it is supposed that the reasoning advanced then applies equally well here. The EVA 28/7NC is capable of forming a large number of entanglements due to its high molecular weight. This propensity to entanglement gives this polymer rubber-like properties which are not particularly observed in the other EVA polymers. The tough, rubber-like nature of EVA 28/7NC is illustrated by examining the controlled stress rheograms of the 28% EVA polymers (Fig 77) where the higher values of G' and the shifted *tan* δ peak (to higher temperatures) shows behaviour which is different to the other polymers in the series.

The variation in peel strength as a function of testing speed is illustrated in Fig 109 for selected adhesives. There is a slight increase in peel strength as testing speed increases although this is partially reversed at the highest test speeds for some adhesives. This is consistent with the results of other workers

e.g. [131] and is attributable to the viscoelastic nature of the adhesives. The reduction in peel strength is normally associated with a change in failure mode from either rubbery interfacial, cohesive, or mixed mode to the so-called glassy interfacial failure mode. This in itself causes a large drop in peel strength. However, as has already been noted, most of the adhesives in the present work were exhibiting adhesive modes of failure at even the slowest speeds. The increase in peel strength of glassy failure bonds was observed and described by Kaelble [133] who recorded that the maximum level of peel adhesion occurred during transitory regions of viscoelastic behaviour, *i.e.* glass-rubber or rubber-flow transitions. In addition the increase in peel strength was observed by Gent and Hamed [264] using rubber-based adhesives. They attributed the increase to the change in the viscoelastic behaviour of the adhesive from soft, viscoelastic liquid to elastomeric solid. The data of ADH 28/7NC indicates a different transition, from rubbery to interfacial, but this may again be attributed to the different rheological behaviour of the adhesive as discussed above. The link between rheological behaviour and peel strength is therefore well established. The data of the present work will now be critically examined to determine whether indices of peel performance can be implied from the controlled stress temperature sweeps. Numerous authors have suggested suitable ways for predicting the peel strength of, usually, pressure sensitive adhesives and these are collected in Table 29. Although this list is by no means exhaustive, it can be seen that the majority rely on the balance between storage and loss moduli, either implicitly, or by means of their ratio *tan* δ. For the present work, the latter models look appropriate, or adaptable. Table 30 summarises the data for the first of the two models of interest by presenting the residuals between the maeasured and calculated peel strengths. The model as described by Barendrecht *et al* [272] does not lend itself to direct utility with the present systems as the hot melt adhesives do not possess lower crossover temperatures, however it is felt that the *tan* δ peak temperature T_L may be reasonably substituted for the present case (as is discussed in the reference).

It can be seen that the discrepancies between the predicted and the measured values of the peel strength are extremely large (several tens of percent)

Table 29 Summary table of the determinations of peel strengths of adhesive systems by the use of rheological analysis

Method	Applicability	Ref.
Maximum peel strength (P) occurs during transitions between glassy rubber and rubber/flow regions of adhesive behaviour.	Pressure sensitive adhesives (PSAs).	131
In the frequency domain : the plateau storage modulus G'(ω) region corresponds with rubbery interfacial failure; the G'(ω) transition from glass to rubber like behaviour corresponds to the region of slip-stick.	Rubber-based PSAs.	269
Non-specific: good peel strengths are obtained when room temperature moduli G'(ω) at two frequencies (0.1 and 100 rad s^{-1}) fulfill the criteria : 2×10^4 Pa < G'(ω) = 0.1 < 4×10^4 Pa and 5 < (G'(ω=100)/G'(ω=0.1) < 300.	Rubber-based PSAs.	169
Similar to above, describes criteria for several applications.	Rubber-based PSAs.	270
Non-specific: lower values of the *tan* δ peak temperature give increased values of P.	EVA-based hot melt adhesives (HMAs).	178
Tensile properties of adhesives are linked to P, in particular the strain at break ϵ_b and various values of the stress σ.	Rubber-based PSAs	271
G'/G" crossover temperatures, G' at room temperature, and T_X can predict P and heat resistance.	Rubber-based PSAs.	272
Tan δ ∝ P at debonding frequency for interfacial failure; $(1 + \epsilon_b) \propto$ P for mixed mode failure.	EVA/ethylene copolymer HMAs.	268

Table 30 Comparison of the measured values of the peel strength at different test speeds v against calculated values from the model after Barendrecht *et al* [272]

Adhesive	Predicted peel strength using eqn. (48) (g per 25 mm) v (mm min^{-1})				% difference between measured and calculated peel strength v (mm min^{-1})				% difference for eqn. (49) v (mm min^{-1})
	0.5	5.0	50	500	0.5	5.0	50	500	50
14/2500NC	19.5	15.6	20.8	24.0	11	32	25	18	-46
19/150NC	35.6	41.3	43.2	51.1	6	-5	3	-3	16
28/7NC	65.6	53.7	54.0	56.0	1	-11	0	-6	5
28/25NC	26.9	48.0	44.7	48.7	26	-25	24	9	16
28/40NC	40.6	53.5	52.7	51.3	18	6	4	5	15
28/145NC	40.3	48.1	50.0	46.5	30	20	22	19	24
28/400NC	45.7	-3.6	31.3	11.2	21	106	54	82	26
28/2500NC	50.1	-26.5	30.8	5.4	-11	150	54	92	14
28/40NC*	29.8	37.0	40.0	38.7	-29	18	-5	17	-22
28/420NC*	55.1	-0.1	31.8	9.2	2	100	43	83	2
33/400NC*	53.0	68.2	60.0	59.5	12	-18	-14	-10	-10
28/400XL	36.4	1.1	28.1	13.2	-44	96	41	65	7
28/2500XL	29.0	-39.9	16.5	-5.8	20	201	57	114	-32
33/400XL	24.0	50.4	45.7	50.1	46	-11	11	-9	4

even after recomputation of the multiple regression with our data. In the original reference, the peel strength P was related to the *tan* δ peak temperature T_L , the crossover temperature T_X and the logarithm of the storage modulus at room temperature $log\, G'_{20}$ by:

$$P = a + bT_L + c\,log\,G'_{20} + d(log\,G'_{20})^2$$
$$+ eT_L\,log\,G'_{20} + fT_X + gT_X^2 + hT_L\,T_X + i\,T_LT_X^2 \quad \ldots (48)$$

where a...i are constants. Figure 111a illustrates the variation between measured and calculated values of the peel strength for selected adhesives at two rates of test. A further multiple linear regression of the present data was attempted with the aim of determining a simpler model:

$$P = a + bT_L + c\,log\,G'_{20} + dT_X + e(log\,G'_{20})^2 + fT_X^2 \quad \ldots (49)$$

An example of calculated values of P from eqn. (49) for 50 mm min^{-1} peel data is illustrated in Fig 111b and, as can be seen in Table 30, the residual values are much smaller, although are still significant. Note that the constants a...f are only valid for a particular rate of testing and are therefore not particularly useful in a predictive capacity if different testing rates are to be considered. The variation is small however and can be assumed constant for the present purposes.

In considering the second model [268], it can be seen Fig 112 that there is some correlation between *tan* δ at 20°C and the peel strength for the 28% VA ExUL EVA-containing adhesives. The exceptions can be explained by referring back to the modes of failure and are incorporated into the original premise of Tse's model. At 0.5 mm min^{-1} peel rate, the ADH 28/2500NC sample has a cohesive type failure whereas the others show interfacial (rubbery for 28/7NC; glassy for the rest) type failures. Similarly at 500 mm min^{-1} , 28/7NC still shows rubbery interfacial failure (with some mixed mode) whilst all other samples (including ADH 28/2500NC) experience glassy failure. It again must be emphasised that this first approach can only give indications and as it is critically dependant upon the mode of failure, which cannot be predicted, then the usefulness of this model at the present time is still limited.

The last adhesive parameter considered here is the ability of the adhesive to withstand elevated temperatures. Heat stress temperatures provide vital information on the upper limit of the service temperature range of hot melt

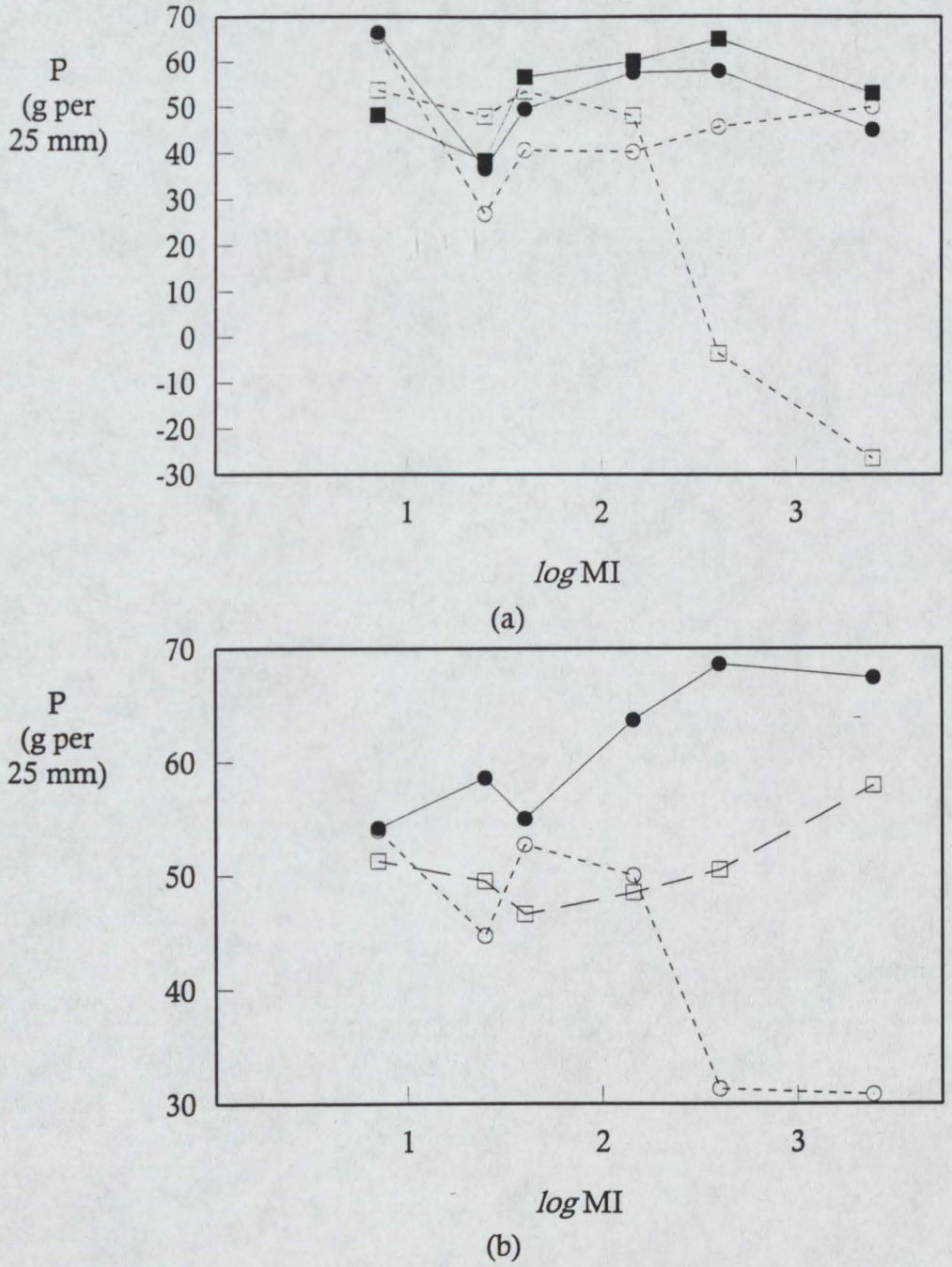

Fig 111. Graphs illustrating the peel strength P of adhesives as a function of the logarithm of the melt index MI of the polymer within them. (a) Measured and calculated peel strengths utilising eqn. (48). Symbols: ●, ○ measured, calculated peel strengths at 0.5 mm min^{-1} test speed; ■, □ measured, calculated peel strengths at 5 mm min^{-1} test speed. (b) Comparison of measured and calculated peel strengths at 50 mm min^{-1} utilising eqn. (48) and eqn. (49). Symbols: ● measured data; ○ calculated using eqn. (48); □ calculated using eqn. (49). See text for details.

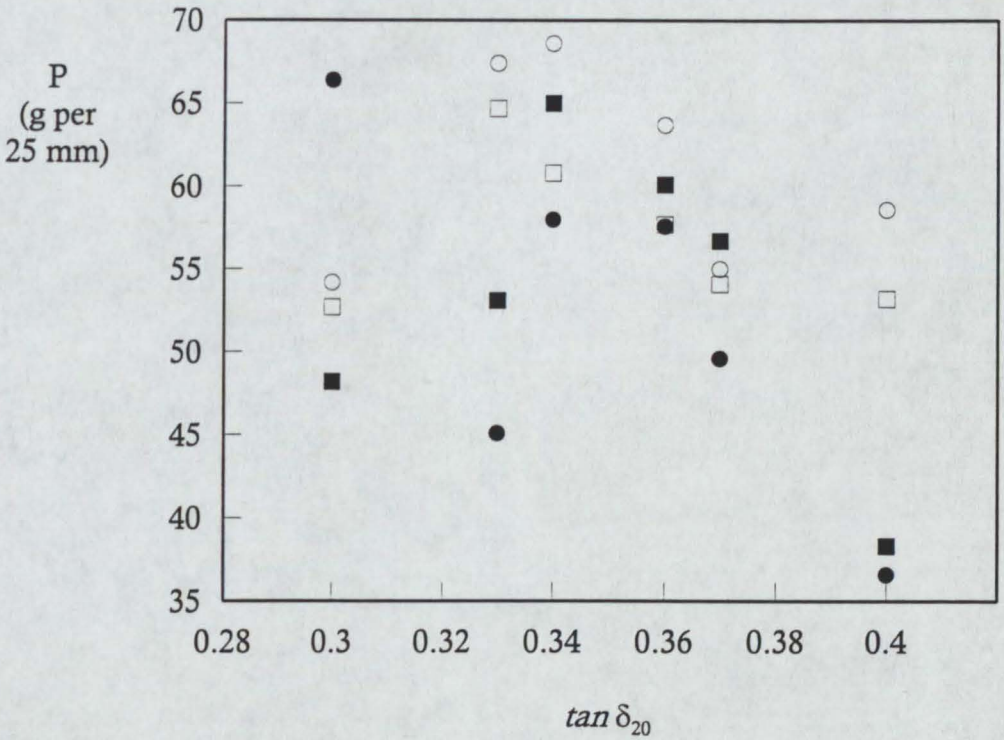

Fig 112. Graph illustrating the relationship between the value of the loss tangent at 20°C *tan* δ and the peel strength P after the model of Tse [268]. See text for details. Symbols: ● 0.5 mm min^{-1}; ○ 5.0 mm min^{-1}; ■ 50 mm min^{-1}; □ 500 mm min^{-1}.

adhesives, this upper limit typically being one of the main disadvantages of using hot melt adhesives. Depending upon the ultimate conditions of service of the hot melt, including method of applications, substrates, and applied stress levels in service, many different types of heat stress test may be selected. In the present work, the shear adhesion failure temperature (SAFT) and peel adhesion failure temperature (PAFT) test methods were selected. The author notes that these are probably not the most appropriate for a packaging adhesive-type formulation however they possess the advantages of wide industrial acceptance, historical usage, and a means by which data from other workers may be compared. Widespread industrial practice uses neither test routinely for adhesives of this type, preferring proprietary cleavage or 'box-flap' tests [150], however the conclusions that may be drawn are generally applicable to most of the heat stress tests currently used. The SAFT and PAFT tests are both described in various standard test methods which also give acceptable limits of scatter within the scope of the test [147]. On average, scatter for each point was well within the acceptable limits, with typical values of $\pm$ 2°C and $\pm$ 30 s for both test methods. The clear correlation between failure temperature and time to failure is illustrated for the SAFT test in Fig 113.

In looking at the properties of the adhesives, one can first examine the variation of SAFT and PAFT with melt index. Figure 114 illustrates both failure temperatures and times as a function of copolymer melt index. It is evident that there is a small reduction in heat resistance (both SAFT and PAFT) as the melt index increases, however differences are also observed with changes in copolymer composition, particularly for samples with higher molecular weights (corresponding to MI = 150). The correlation between SAFT/PAFT and softening point has been explored earlier (p240) however two other thermal properties are thought relevant. The first is that of the WPT_h obtained from DSC measurements (Fig 115a). The heating scan is used as it reflects more accurately the temperature history experienced by the sample undergoing the test. It reveals that SAFT shows a slight positive correlation with WPT_h whilst PAFT appears virtually independent of WPT_h. The same trends are also visible if transition enthalpies ΔH_h are also considered (Fig 115b). It has been discussed

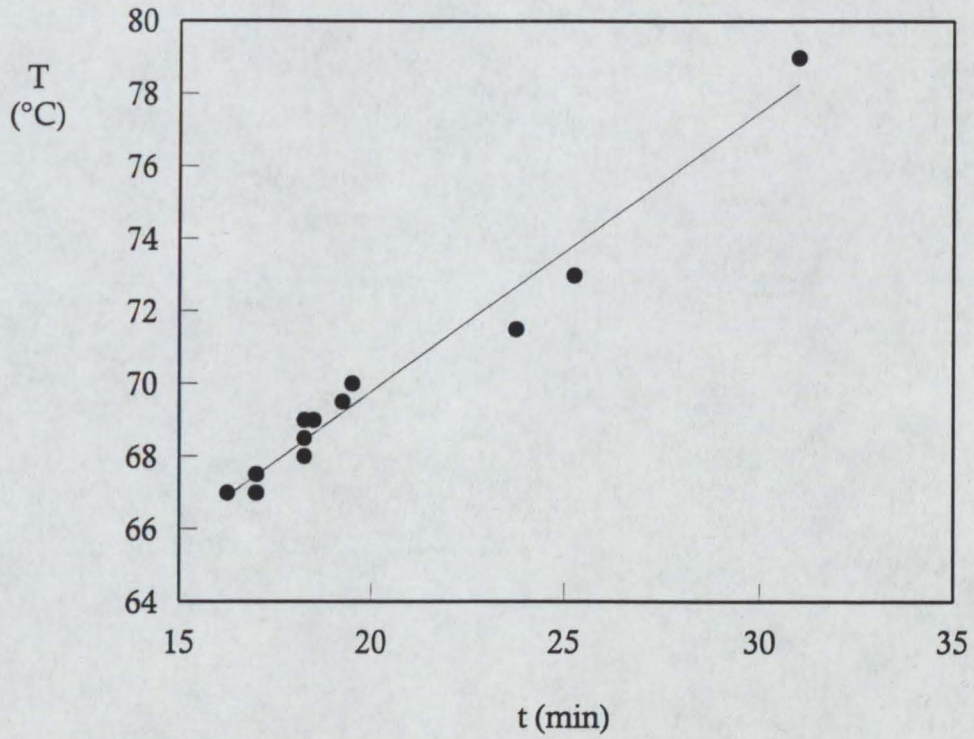

Fig 113. Graph illustrating the correlation between the temperature T and time t of failure of adhesives as determined by the shear adhesion failure test.

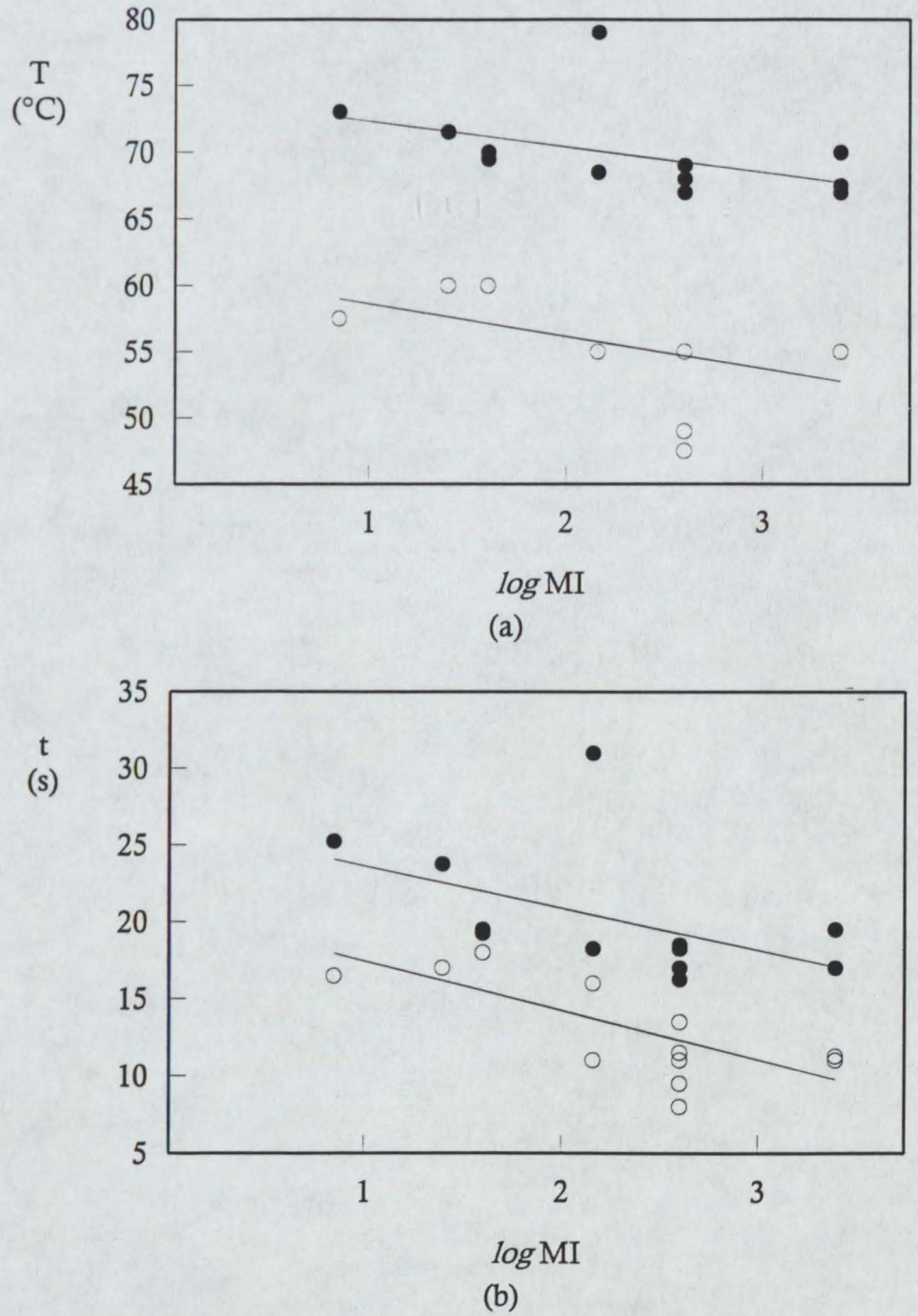

Fig 114. Graphs illustrating the relationships between (a) failure temperature T and (b) failure time t and the logarithm of the polymer melt index MI. Symbols: ● results from shear adhesion failure tests; ○ results from peel adhesion failure tests.

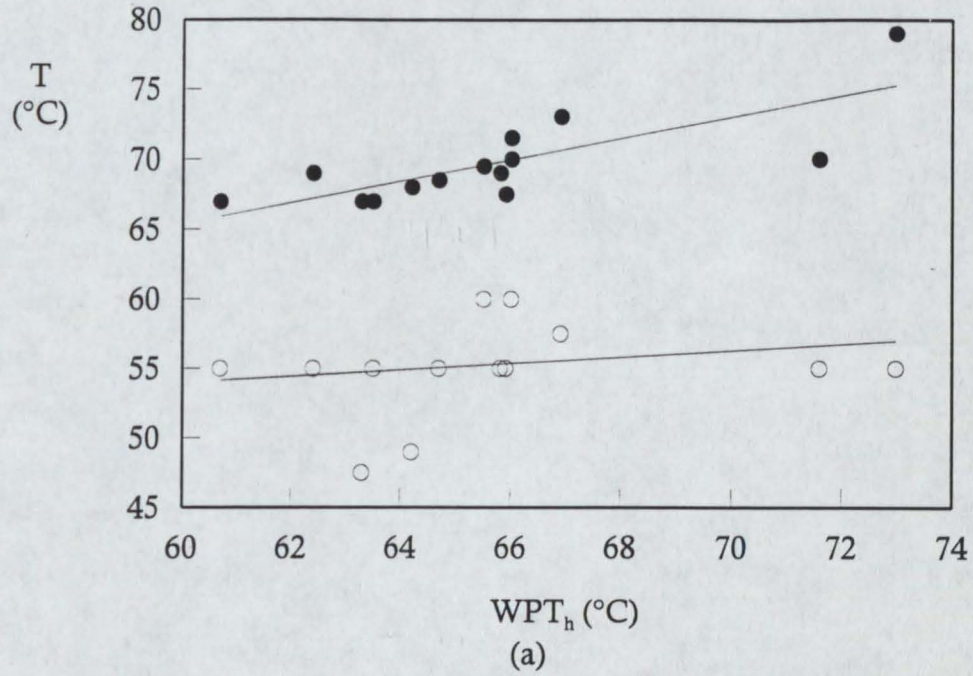

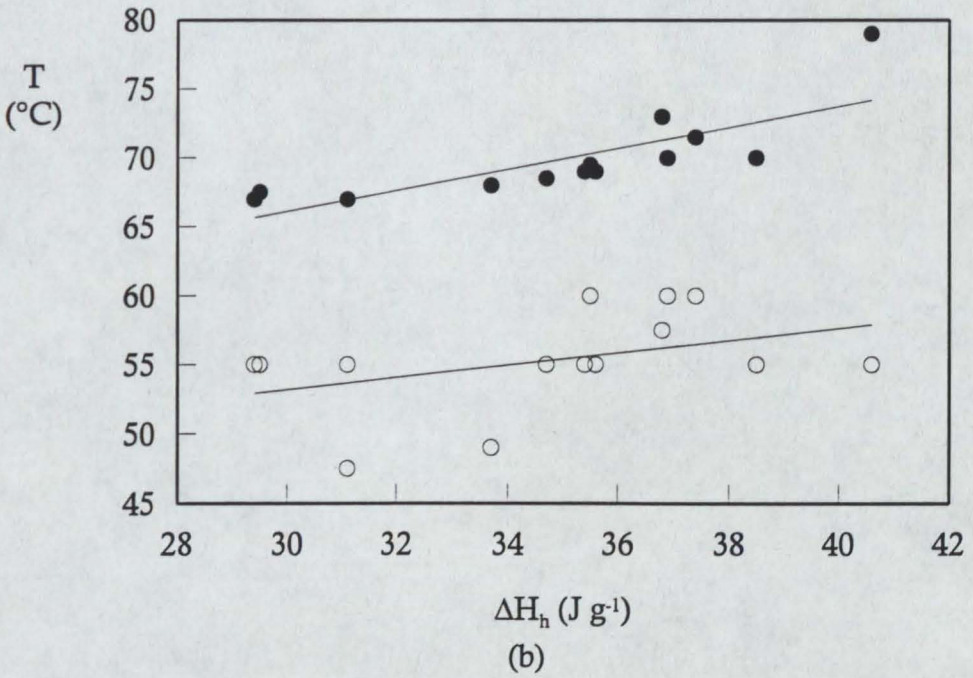

Fig 115. Graphs illustrating the relationships between the heat resistance temperature of the adhesives and (a) the WPT_h and (b) the ΔH_h as determined by DSC heating analysis. Symbols: ● SAFT; ○ PAFT.

earlier that the angle of peel strongly influences the mode of failure of the adhesive. Small angle peel tends to be dominated by shear deformation and failure, whilst peel angles above 90° fail by cleavage mechanisms. The shear dominated SAFT test, which may be considered analogous to low angle peel, is strongly temperature dependant as a result of the thermorheological properties of the adhesive. The SAFT is dominated by the adhesives resistance to flow, *i.e.* viscosity, which is strongly temperature dependant. The cleavage dominated PAFT however is governed by G_c, the adhesive fracture energy which, although it can be decomposed into a viscoelastic function and a work function representing bond formation and breaking, is less temperature dependent than the SAFT viscosity function.

In attempting to relate viscoelastic measurements to SAFT and PAFT, the same rationale described above applies, however the subtler changes in viscoelastic response, together with an accurate measurement of adhesive moduli around the relevant temperature allows additional hypotheses to be formulated. Figure 116 shows the correlation between the crossover temperature T_X from controlled stress rheological measurements and the heat resistance. The correlation is extremely good for the SAFT data ($r^2 = 0.800$). A slight temperature dependence is also observed for the PAFT data, albeit to a much lesser degree and with less confidence than with the SAFT data ($r^2 = 0.210$). The low value of r^2 is attributable to the much larger degree of scatter observed with PAFT testing The reasons behind this scatter have been discussed above. In considering the nature of rheological testing, with its emphasis on small scale, linearly viscoelastic deformations, it is hardly surprising that this more sensitive test allows the detection of adhesive viscoelastic responses that are lost on the larger scale, less precisely defined, industrial tests. These relationships allow therefore a first attempt at modelling the heat resistance temperatures from rheological data. It was found that :

$$\text{SAFT temperature} = 35.88 + 0.533\ T_X \qquad \ldots (50)$$

Other rheological relationships explored included failure temperature versus cohesion rate, *tan* δ peak temperature, and *tan* δ value at 60°C . No significant correlations were obtained, although vague trends were observed.

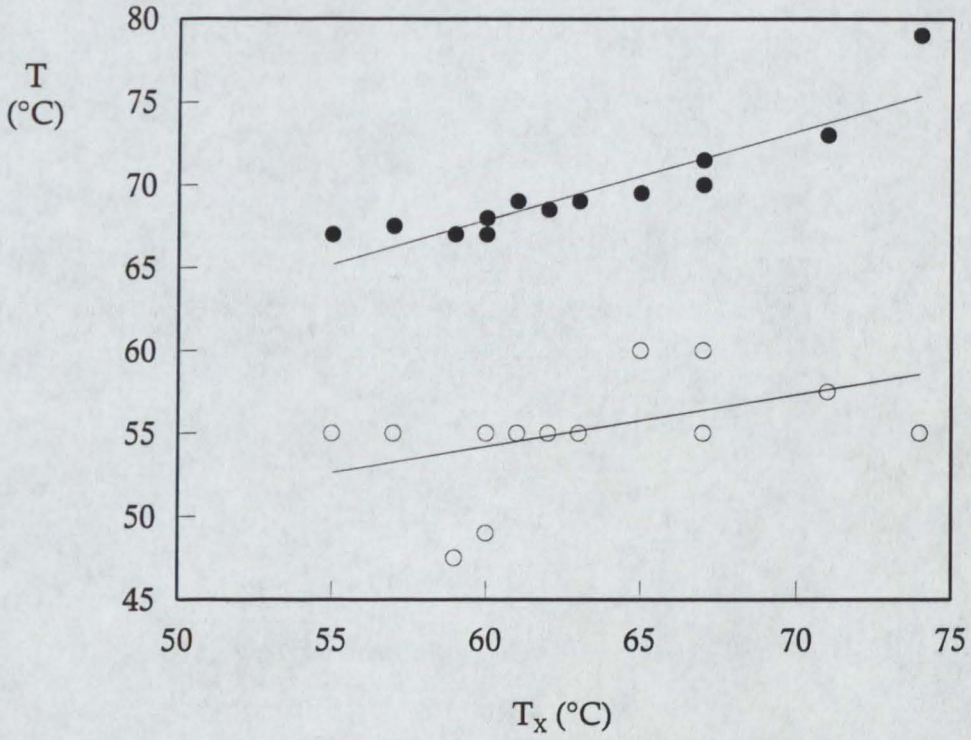

Fig 116. Graph illustrating the relationship between the SAFT and PAFT temperatures T of the adhesives and the crossover temperature T_X as determined by controlled stress rheometry. Symbols: ● SAFT; ○ PAFT.

In addition to the oscillatory rheometry as an aid to determining failure temperature, other rheological techniques such as creep have been used [178] although only as far as to relate SAFT to zero-shear viscosity and hence to melt index. Similar results to the present data were obtained in the reference although a systematic upward temperature shift was noted as a consequence of the differences in formulation of the adhesive, most notably the use a synthetic wax (softening point 100°C) and a terpene-phenolic resin of softening point 98°C. The relationship of the zero-shear viscosity and the SAFT test is self-evident. The simplistic approach adopted by Komornicki *et al* neglects the effects of copolymer composition and the way that this impacts upon the rate at which the zero-shear viscosity alters with temperature. For example, it can be seen that not all copolymers melt at the same rate by visually examining the cohesion rate data in Table 16, Chapter 4, in which cohesion rates vary from 0.229 to 0.511 $°C^{-1}$ when the amount of VA is increased from 14 to 28% in a 2 500 MI polymer.

It has been shown that the nature of the failure in a SAFT test is dominated by shear processes, however recent theories on the nature of hot melt adhesion and bonding processes [104, 268] suggest that the formation of concentration gradients of the different components in the adhesive may occur in a bonded joint. Other work has likewise described such features as the "wax boundary layer" [273] and the impact that this would have on the adhesives performance characteristics. It has been postulated that [274, 275] during the application of applied stress above ambient temperatures, as experienced during a SAFT or PAFT test, there would be a migration of the low molecular weight but essentially solid wax to the surface of the adhesive which is undergoing steady shear-induced flow. This combination would be extremely complex to model precisely. A first approach suggests that key parameters could be obtained from creep test data; mainly J_0 (from the elastic wax) and η_0 (from the flowing polymer). Table 31 shows the values of J_0 and η_0 of the adhesive at the flow point of the polymer (defined earlier as η_0 EVA = 10^6 Pa s). Two calculated values, the ratio and product of J_0 and η_0 are shown in Fig 117. There is no obvious relationship between the rheological parameters in the former case

Table 31 Creep data for 28% VA series adhesives

Adhesive	Flow point of EVA[a] (°C)	$J_{0\,ADH}$ at flow point ($m^2\,N^{-1}$)	$\eta_{0\,ADH}$ at flow point (Pa s)	Calculated data	
				J_0/η_0	$J_0.\eta_0$
28/7NC	80.0	6.3×10^{-6}	$7.2\times10^{+5}$	8.8×10^{-12}	4.5
28/25NC	77.0	7.8×10^{-6}	$5.3\times10^{+5}$	1.5×10^{-11}	4.1
28/40NC	74.0	3.9×10^{-5}	$2.6\times10^{+6}$	1.5×10^{-11}	101
28/145NC	70.5	2.0×10^{-5}	$2.1\times10^{+8}$	9.5×10^{-14}	4200
28/400NC	68.3	2.2×10^{-5}	$3.3\times10^{+7}$	7.6×10^{-13}	825
28/2500NC	63.5	9.3×10^{-5}	$5.5\times10^{+6}$	1.7×10^{-11}	512

(a) Flow point is defined as the temperature at which η_0 is equal to 10^6 Pa s. See text for details.

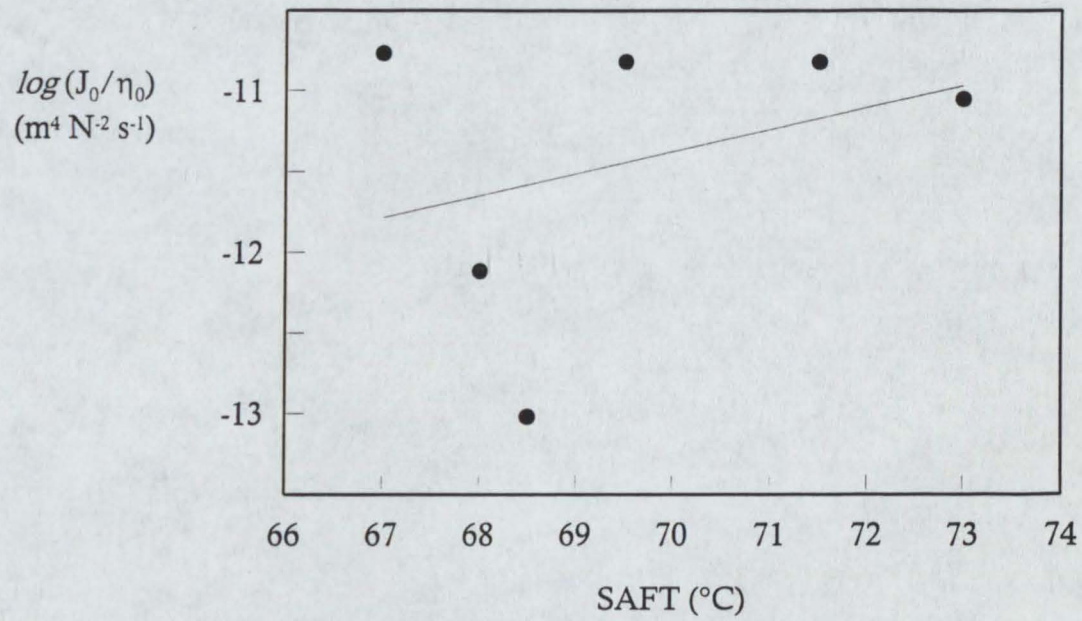

(a)

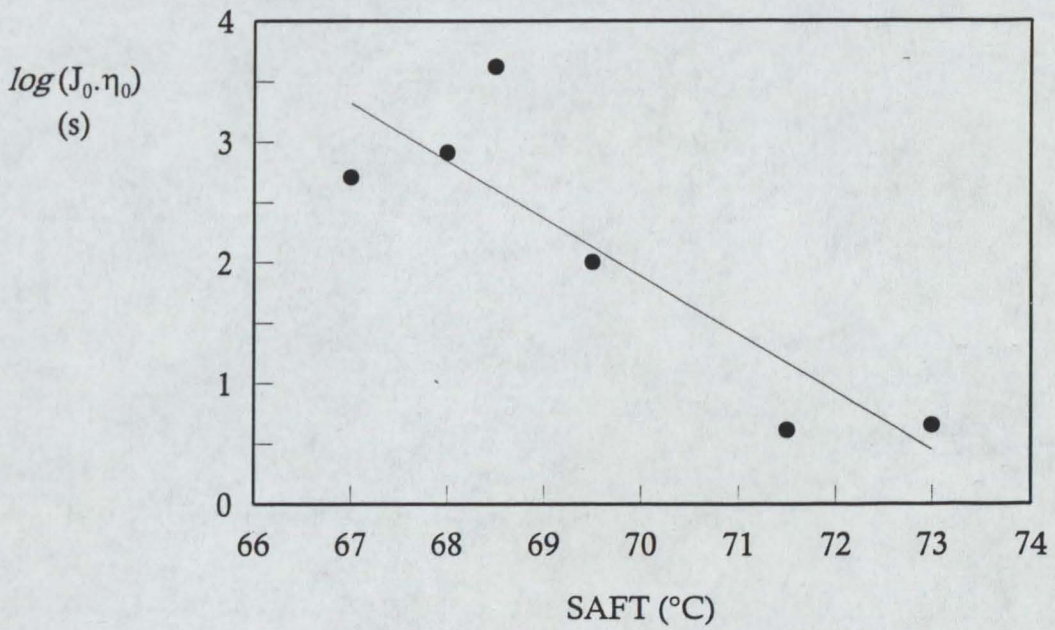

(b)

Fig 117. Graphs illustrating the correlation between the logarithms of (a) the ratio and (b) the product of the initial compliance J_0 and the zero shear viscosity η_0 of the adhesives and their shear adhesion failure temperatures SAFT. Regression lines are shown. See text for details.

and the failure temperature. Indeed the units of the ratio ($m^4 N^{-2} s^{-1}$) have no significance. Figure 117b shows however a good correlation ($r^2 = 0.78$) between the product of initial compliance and zero-shear viscosity (which has dimensions of time). It can be seen that

$$\text{SAFT temperature} = 73 - 0.7\ log(J_0.\eta_0) \quad \ldots (51)$$

The significance of the units of the product are such that there is perhaps a characteristic time for the shear failure process. There is a strong correlation (as expected given the relationship shown in Fig 113) between failure time and $J_0.\eta_0$ which has a regression coefficient of 0.83 and can be described by

$$\text{SAFT time} = 1530 - 65\ log(J_0.\eta_0) \quad \ldots (52)$$

Apart from the discussion above, the theoretical basis of using the product of $J_0.\eta_0$ is not clear.

5.5 Modelling

It is evident from the preceding discussion that hard-setting hot melt adhesives consisting of a semicrystalline thermoplastic polymer, an amorphous, low molecular weight thermoplastic resin, and a crystalline paraffinic wax clearly form complex structures upon cooling, mainly as a consequence of the different levels of crystallinity, molecular weights, and composition. These factors necessarily have a large influence on the mutual solubility of the components and hence, it is postulated that a heterogeneous solid is formed. Whilst previous workers [172, 178] have attempted to model the behaviours of hot melt systems as essentially two phase materials with limited success, it still remains that there has not yet been general success in combining the phenomenological and morphological features of a hot melt adhesive into a coherent model on which the rheology of the system can be predicted with any real accuracy.

If modelling the viscoelastic properties of an adhesive is initially attempted, specifically for G', then it is feasible, given the rheological data on the wax and polymer, that an initial attempt at estimating the adhesive modulus can be made. Consider Fig 118 which illustrates the controlled stress rheological data. It is clear that the rheological response of the adhesive over the

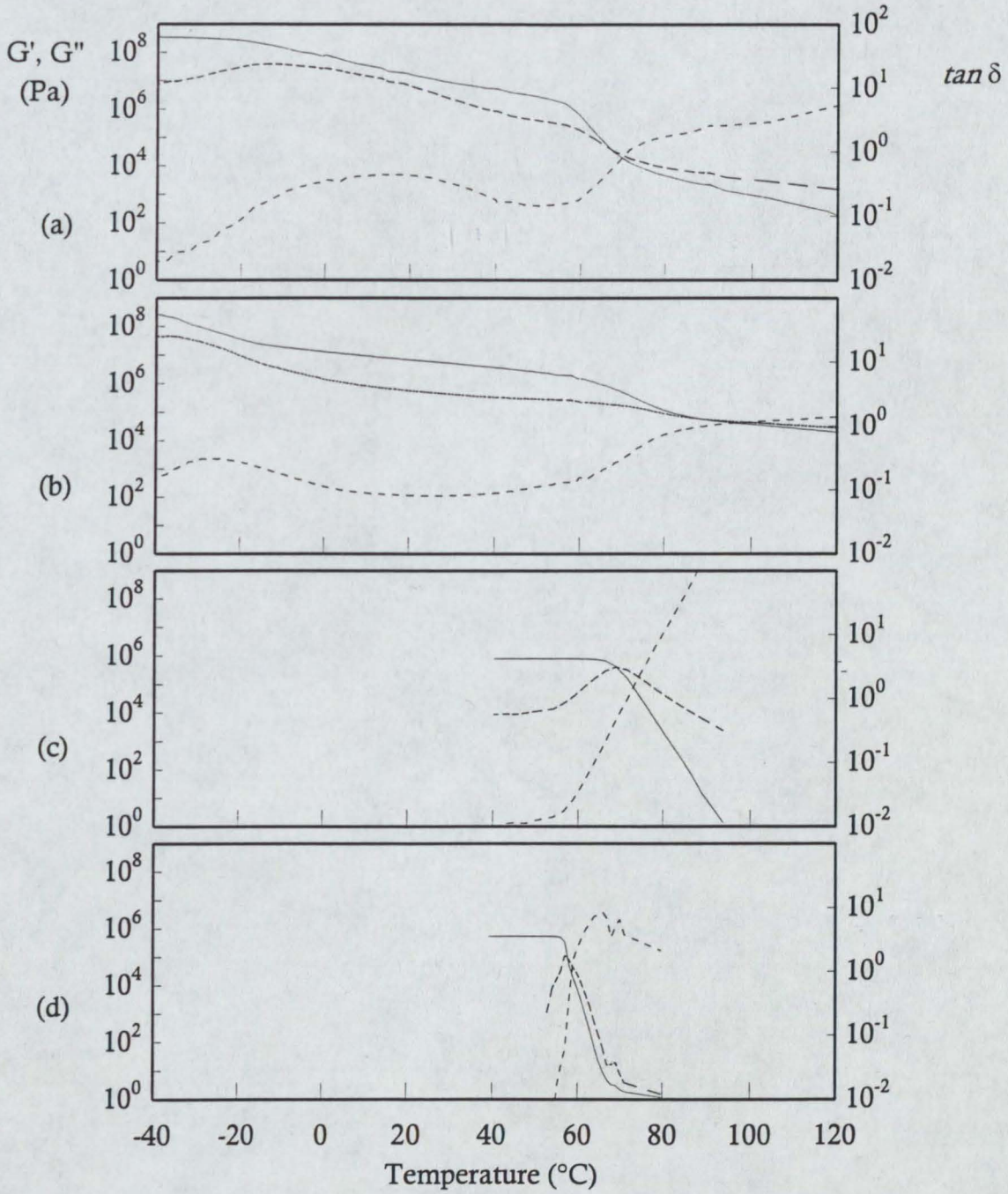

Fig 118. Rheograms of ADH 28/25NC and its components as determined by controlled stress rheometry. (a) ADH 28/25NC, (b) EVA 28/25NC, (c) Resin (Permalyn 5095), and (d) Wax (Okerin 236/H). Conditions: controlled stress; 8 mm diameter parallel plates; 1 000 μm gap; heating rate 5°C; 10 rad s^{-1}.

temperature range is not simply due to the addition of the moduli in a rule-of-mixtures type model. Figure 119 illustrates the point further for three adhesive samples; 28/7 NC, 28/25 NC and 28/400 NC. The open symbols represent the calculated elastic modulus G'_{ADH} given by a simple rule-of-mixtures:

$$G'_{ADH} = w_p G'_p + w_w G'_w + (1 - (w_p + w_w)) G'_r \quad \ldots (53)$$

where the subscripts ADH, p, w, r refer to the adhesive, polymer, wax, and resin respectively and w denotes the weight fractions of the components. The deviation of the model from the observed values is very large (1 - 1½ decades at the lowest and highest temperatures).

Given this rather simplistic approach however it is not surprising that such large differences occur. Previous attempts to model the elastic properties of heterogeneous materials have been numerous and fall into three broad categories. Two of which refer to systems based upon rigid particles suspended in either viscous fluids (a concept first introduced by Einstein [276 - 278] with further refinements [279 - 281]), or in matrices (spherical particles [282, 283] with additional refinements concentrating on particles of different shapes [284] or particulate packing [285]). The third category covers systems where discrete phases occur which may or may not be continuous within a continuous matrix phase. If the phase morphology is unknown then upper and lower limits of the elastic moduli may be predicted by considering either phase to be continuous. In this way, modulus predictions closer than the simple assumptions of the widely used parallel and series modulus addition theories can be attempted. To illustrate this, an attempt to model the material in terms of the series or parallel addition of moduli is first considered. In order to use these models, certain simplifications can be made if the following assumptions are considered: (a) the polymer and resin are completely compatible and form a single phase throughout the temperature range considered; and (b) the wax is precipitated uniformly from the polymer/resin system on cooling and behaves as an inert filler. As has already been pointed out in relation to other results, the present author does not agree with assumption (b) however this will be discussed later. If the polymer and resin are completely compatible and form an homogenous phase, then the modulus of this phase may be given by:

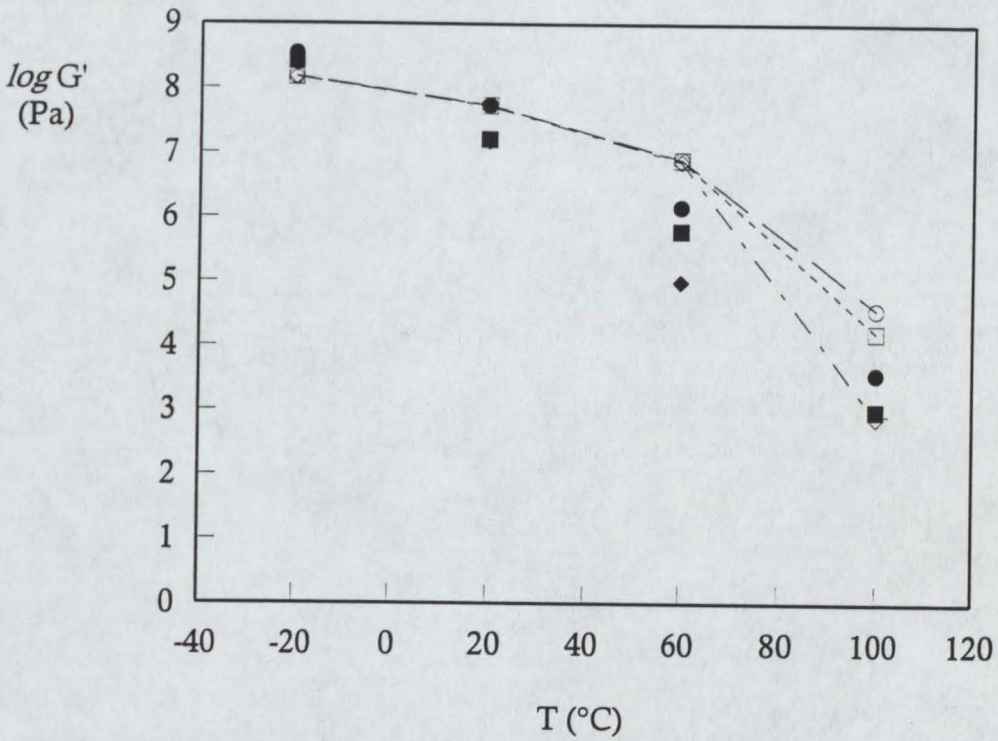

Fig 119. Graph illustrating the variation of storage modulus G' as a function of temperature T for three adhesives illustrating the measured values and the calculated values according to a simple rule of mixtures addition of the moduli of the components. Symbols: ●, ○ measured, calculated G' for ADH 28/7NC; ■, □ measured, calculated G' for ADH 28/25NC; ◆, ◇ measured, calculated G' for ADH 28/400NC. See text for details.

$$M_{pr} = \phi_p M_p + (1 - \phi_p) M_r \quad \ldots (54)$$

where M, ϕ are moduli and volume fraction, subscripts p, r refer to polymer and resin respectively. The volume fraction ϕ of a phase has been calculated by dividing the weight fraction of each component by its density ρ. Note that an additional assumption, that density is considered to be temperature invariant for the purpose of this illustration, has also been made. As the weight fractions of polymer and resin are identical this gives $\phi_p = 0.537$ and hence M_{pr} can be calculated for each polymer/temperature combination (Table 32).

The parallel model of modulus additivity gives the upper limit of the modulus of the adhesive that may be achieved when considering two different materials:

$$M_U = \phi_w M_w + \phi_r M_r + \phi_p M_p \quad \ldots (55)$$

where M_U, ϕ_w refer to upper limit of the modulus, and volume fraction of the wax component respectively. Substitution of the volume fractions of wax, polymer and resin separately for our previously calculated homogeneous polymer/resin phase gives a pseudo-binary system such that :

$$M_U = \phi_w M_w + (1 - \phi_w) M_{pr} \quad \ldots (56)$$

Calculated values for M_U are also given in Table 32 and data for ADH 28/7NC, ADH 28/25NC, and ADH 28/400NC are given as Fig 120a. It can be seen that this model (open symbols) consistently gives modulus values which are too high compared with the measured values (solid symbols), except at low temperatures when the measured data appears slightly higher. The accuracy of the data in the glassy region has already been discussed at length (Chapter 5.2 p186) and it is clear that compliance effects of the rheometer are significant.

The lower limit of the modulus M_L can be calculated using the same pseudo-binary system according to a series addition of moduli as given by the following equation:

$$1 / M_L = \phi_w / M_w + (1 - \phi_w) / M_{pr} \quad \ldots (57)$$

These data are given in the table and plotted for the same adhesive samples in Fig 120b. Note now that the model values are substantially lower than those actually measured.

It is obvious that the closest representation of the adhesive modulus lies

Table 32 Measured and calculated values of the storage modulus G' of the adhesives using several different models

Adhesive	Measured G'				Calculated modulus for polymer/resin phase M_{pr}				Calculated adhesive modulus - parallel model M_U				Calculated adhesive modulus - series model M_L			
	-20°C (10^8 Pa)	20°C (10^7 Pa)	60°C (10^5 Pa)	100°C (10^3 Pa)	-20°C (10^8 Pa)	20°C (10^7 Pa)	60°C (10^6 Pa)	100°C (10^3 Pa)	-20°C (10^8 Pa)	20°C (10^7 Pa)	60°C (10^6 Pa)	100°C (10^3 Pa)	-20°C (10^8 Pa)	20°C (10^7 Pa)	60°C (10^5 Pa)	100°C (Pa)
14/2500NC	3.0	3.5	14	ND[a]	1.5	3.3	8.7	0.54	1.5	5.7	7.8	0.48	1.5	3.7	4.9	9.4
19/150NC	2.9	3.4	19	ND	1.5	3.3	9.1	2.7	1.6	5.7	8.2	2.4	1.5	3.7	4.9	9.5
28/7NC	3.4	5.4	14	3.4	1.4	3.1	8.3	44	1.4	5.4	7.4	39	1.4	3.4	4.9	9.6
28/25NC	2.6	2.6	6.1	0.98	1.3	3.0	8.1	19	1.4	5.4	7.2	17	1.4	3.3	4.9	9.6
28/40NC	2.9	2.0	7.6	0.69	1.3	2.9	7.8	12	1.4	5.3	7.0	11	1.3	3.2	4.9	9.6
28/145NC	2.8	1.8	2.8	0.04	1.3	2.9	7.6	3.1	1.4	5.3	6.8	2.7	1.3	3.2	4.9	9.5
28/400NC	2.3	1.5	0.98	ND	1.3	2.8	7.5	0.92	1.4	5.2	6.8	0.82	1.4	3.1	4.9	9.5
28/2500NC	2.4	1.2	0.06	ND	1.2	2.7	7.3	NC[a]	1.3	5.1	6.5	NC	1.3	3.0	4.9	NC
28/40NC*	2.2	1.7	6.4	1.1	1.4	3.0	8.1	16	1.5	5.4	7.3	14	1.5	3.4	4.9	9.6
28/420NC*	2.4	1.3	2.2	ND	1.3	2.9	9.2	0.86	1.4	5.2	8.2	0.77	1.3	3.1	4.9	9.5
33/400NC*	2.5	1.4	0.47	ND	1.3	2.8	7.3	0.92	1.4	5.2	6.6	0.82	1.3	3.1	4.9	9.5
28/400XL	2.0	1.9	7.3	ND	1.4	3.0	8.0	1.0	1.5	5.4	7.2	0.92	1.4	3.3	4.9	9.5
28/2500XL	0.96	1.6	0.25	ND	1.3	2.9	7.5	NC	1.4	5.3	6.7	NC	1.4	3.3	4.9	NC
33/400XL	2.7	2.0	0.89	ND	1.3	2.9	7.5	1.4	1.4	5.2	6.7	1.3	1.3	3.1	4.9	9.5

(a) ND, NC = Not detected, not calculated.

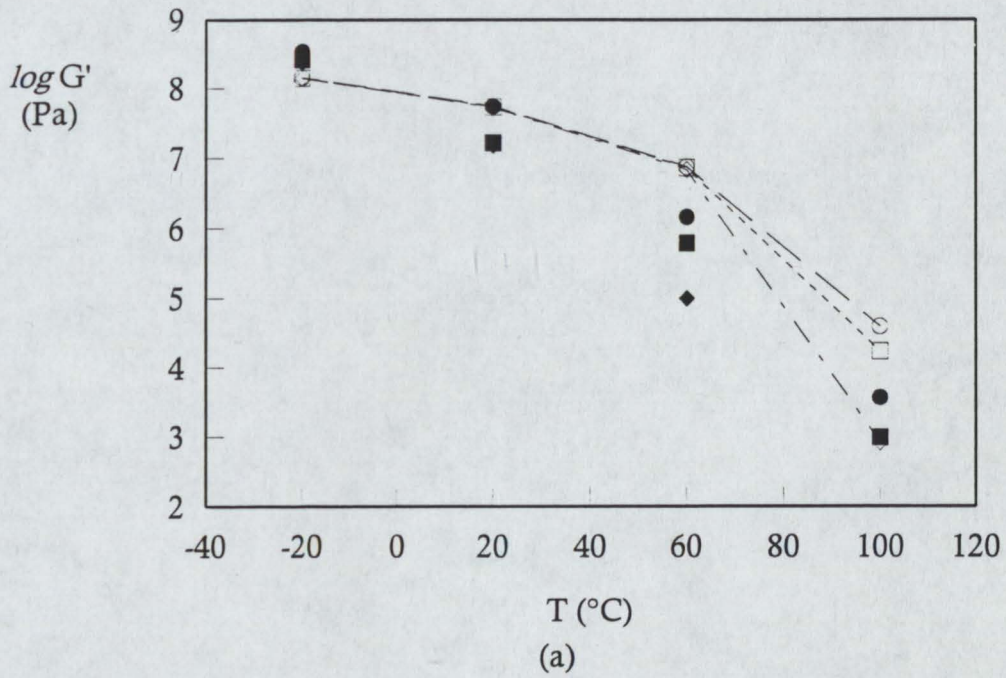

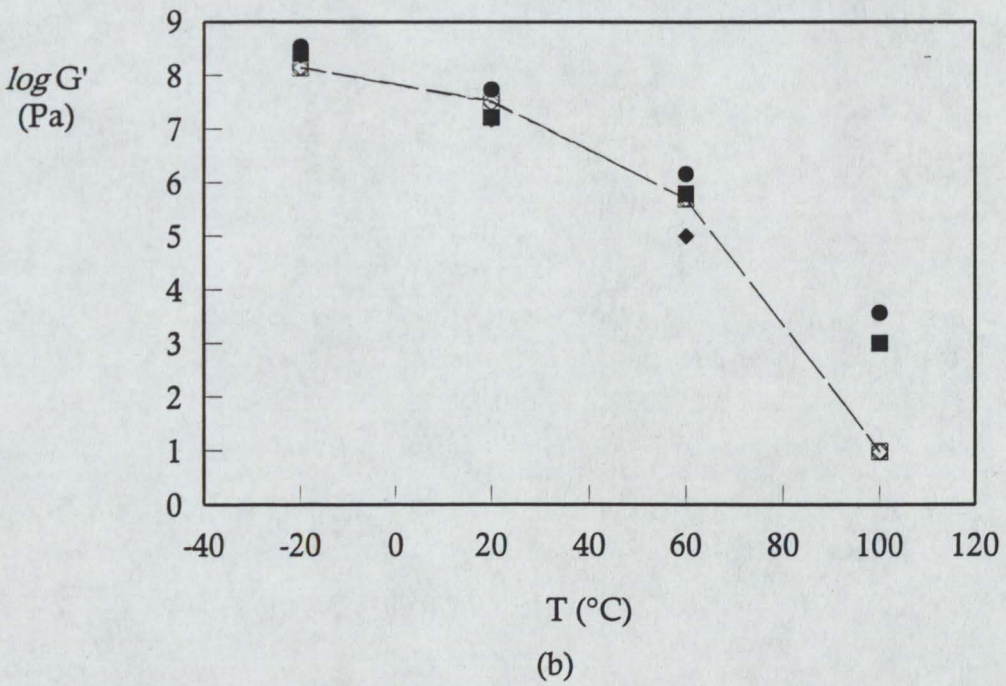

Fig 120. Graphs illustrating the variation of adhesive storage modulus M as a function of temperature T for two models (a) parallel model M_U and (b) series model M_L. Symbols: ●, ○ measured, calculated storage modulus for ADH 28/7NC; ■, □ measured, calculated storage modulus for ADH 28/25NC; and ◆, ◇ measured, calculated storage modulus for ADH 28/400NC. See text for details.

between the two extremes albeit closer to the parallel model than the series one. The composite model proposed by Coran and Patel [280] is based upon a phenomenological adjustment between the parallel and series models for upper and lower bound moduli M_U and M_L where

$$M_{ADH} = \phi_H^n (n\phi_S + 1) (M_U - M_L) + M_L \quad \ldots (58)$$

where ϕ_H, ϕ_s are the volume fractions of the hard and soft phases and n is the adjustable parameter. Although this model was originally proposed for use in mixtures where the relative proportions of the phases were changing (as a result of concentration of the hard or soft phase), it has also found utility in looking at the melt viscosities of polymer blends. Table 33 and Fig 121 illustrate the calculated values of M_{ADH} for ADH 28/7NC at each temperature for several values of n. It should be noted that, looking at the data for ADH 28/7NC, a value of n equal to 1.4 most closely fits the experimental data at temperatures greater than approximately 40°C. Values of n close to zero effectively lead to the model behaving as the simple parallel model, whilst, in this case, values of $n \geq$ 4.5 are practically identical to the earlier series model. The value of n which gives a closest fit to the data was obtained computationally by using a best fit algorithm based upon a least-squares approach. The value of n obtained for this particular sample lies in-between the reported values of a poly(propylene)/ EPDM blend (n = 2.0) and a composite material consisting of graphite flakes in an epoxy matrix (n = 0.75). A styrene-butadiene block copolymer was found to have n = 4.5. Coran and Patel stress that the value of n cannot be directly related to a particular morphology however the dispersed nature of the PP/EPDM blend contrasting with the pseudo-crystalline/flaked structure of the composite material suggests that the actual morphology of the adhesive in the present work is between the two. The large difference between the value obtained here and that obtained for the block copolymer (in which the styrene forms discrete domains) is noteworthy only in passing; EVA copolymers not forming domain-like structures.

Although qualitatively the agreement is good for ADH 28/7NC at higher temperatures, at lower temperatures the difference is much more significant,

Table 33 Calculated values of the adhesive storage modulus for ADH 28/7NC using the model of Coran and Patel [280] for different values of the adjustable parameter n[a]

	Calculated adhesive modulus M_{ADH}			
n	-20°C (10^8 Pa)	20°C (10^7 Pa)	60°C (10^6 Pa)	100°C (10^3 Pa)
0	1.4	5.4	7.4	39
0.1	1.4	5.2	6.5	34
0.25	1.4	4.8	5.3	27
0.5	1.4	4.3	3.7	18
0.75	1.4	4.0	2.6	12
1	1.4	3.8	1.9	7.7
1.25	1.4	3.6	1.4	4.9
1.4	1.4	3.6	1.2	3.7
1.5	1.4	3.5	1.0	3.1
1.75	1.4	3.5	0.8	1.9
2	1.4	3.4	0.70	1.2
5	1.4	3.4	0.49	0.01
10	1.4	3.4	0.49	0.01

(a) See text for detailed discussion of model.

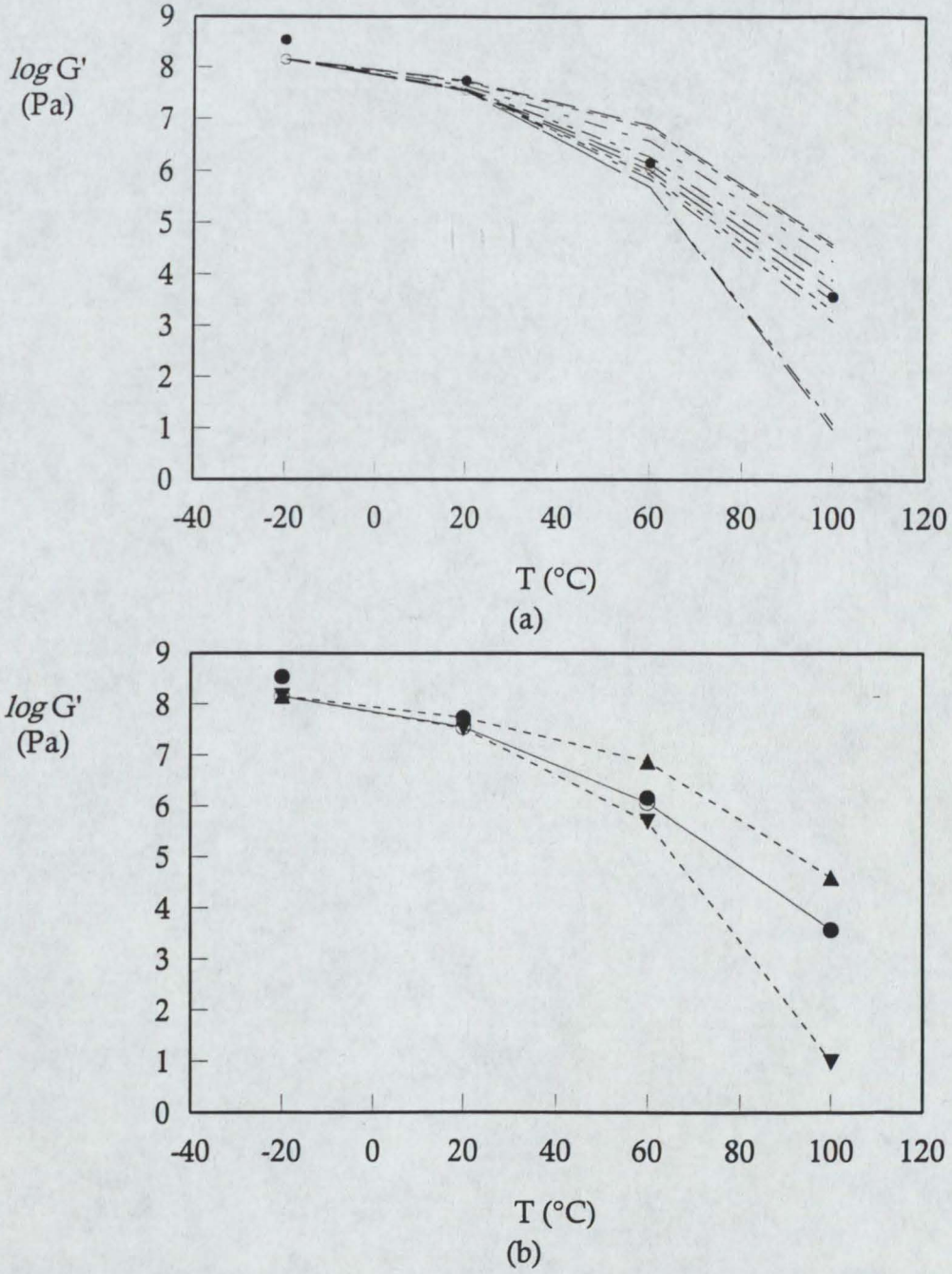

Fig 121. Graphs illustrating the modulus M of ADH 28/7NC as a function of temperature T according to the composite model of Coran and Patel [280]. (a) M_{ADH} as calculated for selected values of the adjustable parameter n as given in Table 33 and (b) a comparison of the measured modulus with the various models, including the composite model with the value of $n = 1.4$. Symbols: ● measured storage modulus of the adhesive; ○ calculated modulus with $n = 1.4$; ▲ calculated modulus for parallel model; ▼ calculated modulus for series model. See text for details.

overall leading to a coefficient of variation ~ 0.88. In examining the model proposed by Coran & Patel, it appears that it was formulated around the basis of morphology changing with composition, *i.e.* volume fraction of components, and the systems examined appear to be thermorheologically simple, for example, they did not appear to crystallise. In the complex pseudo-binary system considered here it has already been observed that the nature of the components changes significantly with temperature. These changes, such as crystallisation, obviously affect the modulus but also affect the density. Hence the volume fraction used in the calculations must necessarily be only approximate. In addition, the premise that a pseudo-binary system is formed, with little or no interaction between the phases has been shown to be open to question by the findings of other tests performed in the present work.

If the volume fractions are accepted as being approximate, we can still examine the processes which occur in the model. The lack of fit of even the best approach leads us to consider the possibility that n may change as a function of temperature. This idea has an immediate appeal as it then starts to consider the non-trivial crystallisation behaviour of both wax and EVA. If n is calculated to fit the observed data for ADH 28/7NC at each temperature it is seen (Fig 122) that it increases from 0 at -20°C to 1.25 at 60°C and 1.31 at 100°C. This implies that to fully understand the behaviour of an adhesive, account must be taken of the factors associated with the change in temperature, as indicated by the change in n value. It must be clearly emphasised however that the change in the value of n does not necessarily imply morphological changes, but can be suggestive of it. Determination of n for other adhesives containing 28%VA ExUL EVAs revealed that the value of n increases as the melt index increases. This appears to indicate that the serial modulus model is more appropriate with lower molecular weight systems (Fig 123).

Attempts to reconcile physical, rheological, and morphological properties were also attempted by Marin *et al* [172] who considered a simple binary system of EVA and resin. This approach, using a simple compatible formulation, allowed them to predict the T_g of the adhesive by considering the contribution

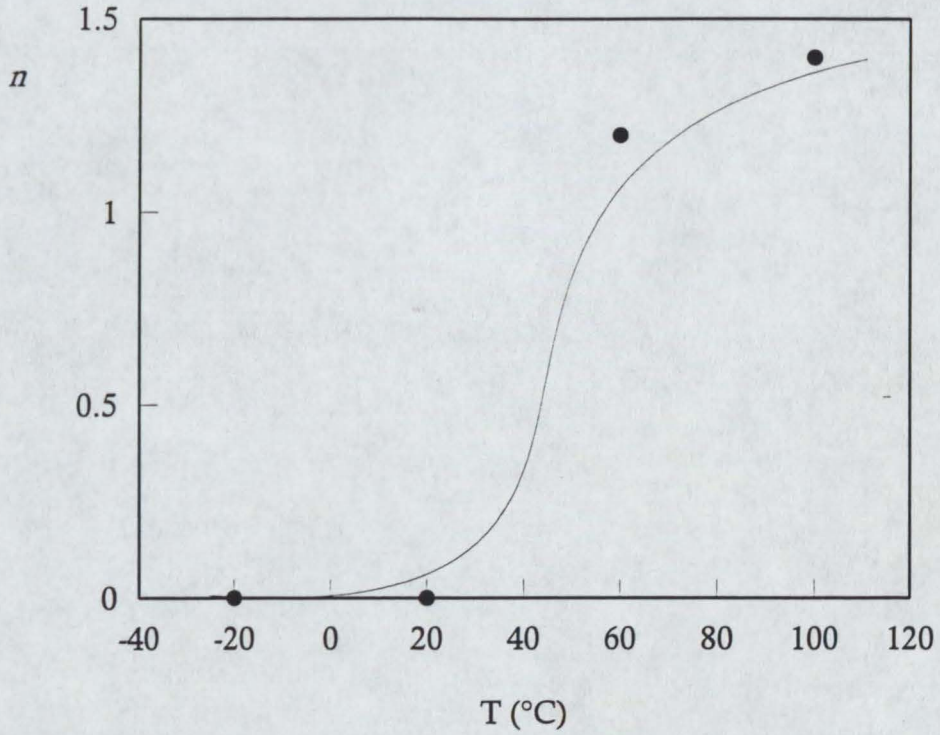

Fig 122. Graph illustrating the variation of the adjustable parameter *n* from the composite model as a function of temperature T. See text for details.

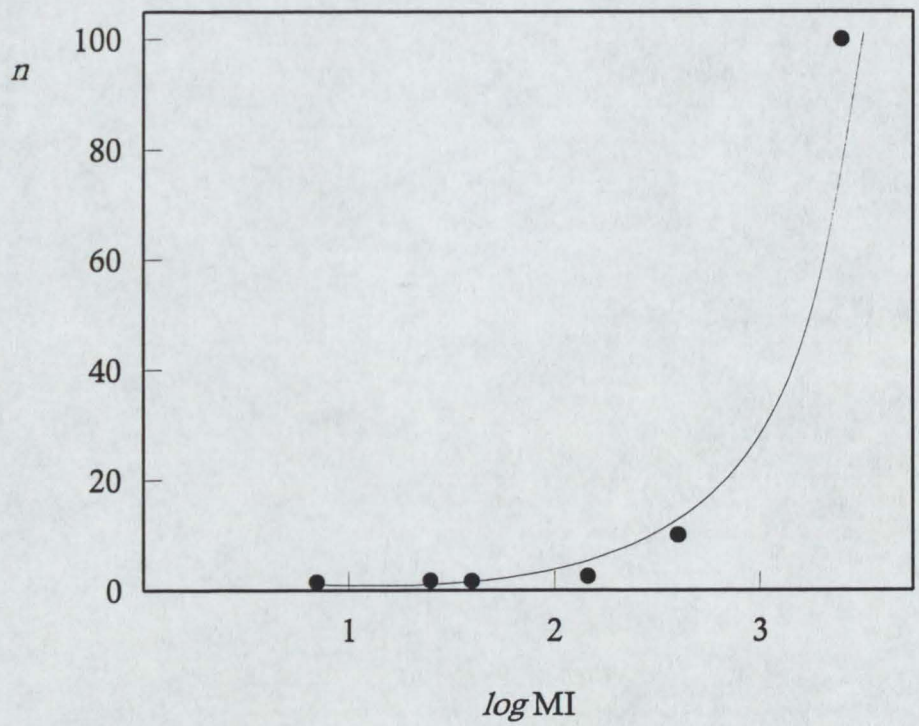

Fig 123. Graph illustrating the variation of the adjustable parameter *n* from the composite model as a function of the logarithm of the copolymer melt index MI for 28%VA ExUL EVA-containing adhesives. See text for details.

of the T_gs of resin and polymer when combined with regard to free volume expansion coefficients ($\alpha_{1f,}$ α_{2f}) and so-called coupling factors (K). Although rigorous, it is hard to quantify the additional benefits of this approach in the systems they were proposing, to that of the simpler Fox equation for compatible polymer mixtures. Indeed, the assumptions made ($\alpha_{1f} = \alpha_{2f} = \alpha_f$) reduce the equation given (eqn. 38), to a simple rule-of-mixtures as has been established above. This approach has also been applied to the prediction of modulus values (as a function of temperature) however it only showed real success with binary systems. The direct application of this approach to more complex ternary systems such as those in the present work has been clearly demonstrated to be not straightforward.

Komornicki *et al* [178] attempted to relate the peel behaviour of a ternary adhesive system by consideration of Marin's mixing law and by assuming that the wax acted as an inert filler which served to increase modulus but played no part in affecting the T_g of the system. The assumptions that were made have been proven not to be valid for the present work and evidence was found which strongly suggest that paraffinic waxes do influence the T_g, in addition to their filler effect.

In summary, attempts by the present author to link the morphology of the adhesive, *via* an admittedly phenomological equation, are seen to be successful in a limited fashion, however the complex structure and nature of the polymer and wax gives the conclusion that some simple mechanical properties of an adhesive system lie between a simple parallel and a simple series model with the closest approximation being to the simple parallel model. The properties also changed with temperature which has been quantitatively incorporated in the simple model by use of an empirical parameter.

We may finally note again that the complexity of the adhesives composition and behaviour, and that modelling has only been possible on one property to a limited extent. It is expected that significant progress in the more general modelling of these complex materials must await much further knowledge, in particular in relation to the thermodynamics and phase relationships of both the components and the systems themselves. In the

meantime, progress on an industrial and scientific basis must still be based on careful characterisation and assessment and not least upon the experience of the industrial technologist.

5.6 Conclusions

Fourteen poly(ethylene-*co*-vinyl acetate) copolymers (EVA) of varying molecular weight (represented by melt index MI), composition, and degree of crystallinity were examined both singly, and compounded into a typical hot melt adhesive formulation with a tackifying resin and a paraffin wax. The copolymers and the adhesives were examined using a large number of analytical techniques and physical tests. These included differential scanning calorimetry (DSC), several rheological techniques including simple flow, oscillatory rheometry (controlled strain and controlled stress), transient (creep) tests, and several industrial tests used mainly to simulate the more complex adhesive properties. From this work the following major conclusions can be drawn:

(1) Accurate data has been obtained on a wide range of thermal properties on a range of copolymers that vary substantially in their melt indices, composition, and crystallinity. This has enabled the influence of these parameters to be critically identified. For example, it was found that the enthalpy of fusion ΔH_h of the copolymer was constant above a certain molecular weight. Below that value of the enthalpy decreased. There was an decrease of approximately 5% as the copolymer melt index MI of the ExUL EVAs was increased from 145 to 2 500, whilst similar decreases were observed with the more crystalline grades. The EVAs from Atochem showed similar behaviour. The composition of the copolymer had a more significant effect, with the largest change in enthalpy being approximately 27% between 2 500MI copolymers of 14% and 28% VA. Detailed information on the enthalpy of crystallisation, melting and crystallisation point, and glass transition temperature were also obtained. The processes and trends were discussed with reference to the molecular behaviour such as chain branching and other sources of crystallite disruption.

(2) The thermal properties of the adhesives were influenced strongly by the copolymers however the magnitude and position of the main crystallisation or

melting peak was also altered by the presence of the paraffin wax. For example, the position of the heating peak in the adhesive showed approximately 6°C variation as a function of melt index compared with the 14°C range seen with the 28% VA copolymers. The amorphous resin had no effect on the position of the melting or crystallisation peak. The enthalpy values of the adhesives are approximately one third lower than those of the copolymers. There is also a significant decrease in the enthalpy of crystallisation of the adhesives as a function of melt index which is in contrast to the increase seen with the copolymers by themselves.

(3) In contrast to previous work using synthetic waxes it was shown that the paraffin wax in the present system exhibited limited mutual compatibility with the other components, mainly the copolymer. The T_g of the adhesive was then modelled by approximating the paraffin wax's glass transition temperature to that of a low molecular weight poly(ethylene). It was then incorporated with the familiar Fox equation in terms of a simple modification. The model gave very good agreement with the measured data and was superior to the model of Marin who treated the wax as an inert filler with respect to T_g determination.

(4) Although the melt viscosities of the adhesives were directly dependent upon the melt index of the copolymer as expected, there were no significant differences attributable to the amount of crystallinity in the copolymer, or its composition.

(5) The rheological properties of the components were determined by oscillatory (dynamic) rheometry using both controlled strain and the newer controlled stress techniques. The rheograms obtained from each technique were qualitatively similar but differences existed due to principally the nature of the temperature control on each instrument, which provided different thermal histories for the samples being evaluated. The results from the controlled stress rheometer had the distinct advantage of being produced from a more tightly controlled temperature regime.

(6) There were many interpretations on various features of the rheograms. It was found that the most useful were the storage modulus G', loss modulus G", the temperatures of the loss tangent (*tan* δ) local maximum T_L and loss modulus

local maximum $T_{L''}$, the crossover temperature at which the storage and loss moduli were equivalent T_X, and the cohesion rate at T_X, defined as $(d(log\ G')/dT)_{Tx}$. The EVA copolymers' rheological behaviour showed elements of amorphous and crystalline behaviour as defined in the literature. There was a systematic shift in modulus values as a function of the molecular weight. The range of the storage modulus at room temperature was 2 to 8 MPa, increasing as molecular weight increased, however the differences were much larger at elevated temperatures as the influence of short chain lengths exerted a greater effect. The relationship between the logarithm of melt index of the copolymer and the storage modulus was linear with extremely good correlation coefficients (0.710 to 0.999) and very small standard errors, typically less than 2%. There were also strong relationships between melt index and the crossover temperature T_X and cohesion rate. The value of the crossover modulus did not show a clear dependance upon the melt index due to the large amount of scatter inherent in its determination. It was observed that the copolymers with greater VA concentrations had higher cohesion rates than their lower VA, similar MI counterparts. It was postulated that this related to values of the monomeric friction coefficients of VA and ethylene. There was little influence of the molecular weight on the positions of T_L and $T_{L''}$. The molecular weights of all the copolymers were significantly higher than the entanglement molecular weights calculated from literature values of the plateau modulus G_N^0 of an idealised poly(ethylene) and poly(vinyl acetate) polymer blend. The composition of the copolymer also affected these properties. In particular, the positions of T_L and $T_{L''}$, which are commonly taken as glass transition temperatures, were affected in a similar way to the trends that were observed by DSC. The effect of increased crystallinity was evident by the higher moduli over a range of temperatures and by the higher maxima temperatures.

(7) The introduction of wax and resin into the formulation caused gross differences in the rheological properties of the EVA copolymers. The wax and resin affected the rheology of the formulations in several ways: (a) at elevated temperatures, the wax and resin acted as low molecular weight plasticisers and cause a reduction in viscosity as the polymer melt was diluted. This effect has

been observed in the literature for other polymer/wax/resin blends and was entirely self-consistent; (b) the addition of the wax and resin caused a shift in the *tan* δ peak position that can be attributed to the resin and wax partial compatibility. This confirmed the DSC results (conclusion (3) above) and established a link between the oscillatory rheometry and the thermal analysis results; (c) in addition there was an increase in low temperature modulus for all of the adhesives suggesting that the wax also acts as a filler. There was also a slight increase in damping which is often seen in filled polymers; (d) the addition of the wax reduces considerably the variation in the crossover temperature range (62°C for the EVA's *vs* 19°C for the adhesives) due to the sharp melting peak possessed by the wax.

(8) The adhesives showed similar rheological behaviour to the EVA copolymers however there was an increase in the plateau modulus and a shortening of its length due to the effective broadening of the polymer molecular weight distribution by the addition of the partially compatible components.

(9) The use of transient rheology (creep) supported the observations above. In addition it provided numerical parameters suitable for modelling the response of the system in terms of the Berger phenomenological model. The generation of initial compliance J_0 and zero shear viscosity data η_0 was able to be used to closely predict the shear adhesion failure temperature and time of the adhesives with regression coefficients of 0.78 and 0.83 respectively.

(10) There was no clear relationship between the softening point of an adhesive and its heat resistance, open time, or setting time. There was also significant scatter between the wax peak temperature on heating WPT_h and the softening point. There is a correlation between T_X and softening point, however this is only possible for a limited number of formulations. It is clear that the softening point cannot be taken as a clear indication of an adhesives performance.

(11) The open time was clearly influenced by both the melt index and the composition of the copolymer. At high molecular weights, the ability of the adhesive to fully wet the substrate was a major factor in controlling the open time of the adhesive whilst at lower molecular weights, the ease at which the lower viscosity adhesive penetrated the board also caused an apparent reduction

in the open time of the adhesive. The effect of copolymer composition was also found to be significant, higher concentrations of VA causing a reduced open time. This did not correlate with the expected viewpoint that increased VA gives a softer and hence longer open time adhesive, however examination of the DSC data illustrated a significant reduction in ΔH_c. This clearly illustrated that the open time was not just dependant upon viscosity but also upon the compositional shifts caused by the effect of different phase compatibilities. There was no significant correlation between WPT_c and open time. There was evidence of a slight trend between cloud point and open time and also between T_X and open time, although the scatter was quite large.

(12) The cloud points of the adhesives were not dependant upon the molecular weight of the copolymer but almost entirely on their composition and, at higher molecular weights, the degree of crystallinity. Minor differences in the start of the DSC crystallisation peak showed a slight correlation to the cloud point however the differences were small and this method would not be robust enough for widespread industrial application.

(13) The relationships between the tensile properties of the adhesives and the molecular weight of the copolymer, the effects of composition, crystallinity and testing speed, were determined. Attempts to model, on a very limited basis, the tensile properties of an adhesive utilising data obtained from creep testing demonstrated some success however the limitations of the model were significant and attention was drawn to the fact that a more fundamental examination of such complex behaviour was required.

(14) The variation of peel strength as a function of molecular weight, composition, crystallinity, and testing speed were examined and agree well with results from the established literature. The impact of the testing speed, for example, clearly demonstrates the viscoelastic nature of the adhesives and is entirely consistent with previous work. Attempts were made at modelling the peel strength as a function of several key rheological parameters as determined by oscillatory rheometry. The first model was a multiple linear regression performed on the identified parameters which was broadly successful, however large differences between calculated and measured data were obtained

(differences of up to 46%) and the regression had to be performed upon each adhesive limiting its use a predictive tool. A second model from the literature was also examined. The relationship between *tan* δ and the peel strength was also explored. Trends were clearly visble and the large deviation from the simple linear relationship were attributable to the mode of failure obtained during the test.

(15) Heat resistance tests on the adhesive in both shear and peel modes revealed that there is a slight dependency on copolymer molecular weight, however it was clearly shown that the composition of the copolymer was also significant. The shear adhesion failure temperature SAFT shows a linear correlation with the wax peak temperature obtained during heating on the DSC WPT_h, however the peel adhesion failure temperature PAFT appears independant. Similar trends are observed with the enthalpies of melting. The different dependencies of SAFT and PAFT to the thermal properties were attributed to the mechanisms involved in the failure of the joints; shear tests are dominated by the resistance to flow and the viscoelastic properties of the adhesive, whilst the peel tests are governed by mechanisms of adhesive fracture which can be decomposed into bulk viscoelastic functions (strongly temperature dependent) and a work function which represents the breaking and formation of adhesive bonds which is not strongly influenced by temperature.

(16) The T_X correlated strongly with SAFT ($r^2 = 0.800$) however a similar significant correlation with PAFT was not observed. The sensitivity of the rheological tests were such that it was found possible to model, with some degree of confidence, the SAFT temperature as a linear function of T_X for the 28% VA adhesive series. Other rheological parameters from oscillatory testing considered were cohesion rate, *tan* δ peak temperature and *tan* δ value at the temperature of failure however no significant correlations were observed. It was clearly shown that the use of parameters determined from creep testing could be successfully used to model the SAFT. Consideration of the flow point of the copolymers (defined as the point at which $\eta_{0\,EVA} = 10^6$ Pa) revealed that the product of J_0 and η_0 at that temperature correlated extremely well with the SAFT. The use of the product term was justified by consideration of failure occurring by migration of

wax within the adhesive to the boundary between adhesive and substrate, in combination with the overall flow properties of the adhesive. Strong correlation was also obtained with the shear adhesion failure time.

(17) Overall it is clear that some of the industrial tests have a strong scientific basis and it is considered that these could be exploited and developed more in the future. Nevertheless, the distinctive and idiosyncratic nature of the tests will continue to be of considerable technological use.

(18) The complexity of the systems limits considerably the development of more general models. Simple rules of mixtures applied to the elastic moduli were found not to correlate with the measured data however an extended model based upon the present thermal and rheological results enabled the compatibility to be successfully incorporated in the model as a parameter *n*. The value of *n* varied as a function of adhesive composition and temperature, *e.g.* for ADH 28/7NC, *n* is zero at -20°C but increases to 1.25 at 60°C and 1.31 at 100°C, indicating that the adhesives behaviour changed subtly as the compatibility of the phases changed. The value of the parameter could not be directly related to the morphology of the adhesive phases.

5.7 Recommendations for future work

It is seen from the present work that there are still many aspects of hot melt adhesives that need clarifying or determining. In particular: (a) The present work has used an adhesive with one standard wax and one standard resin in the formulation. In terms of relevance to current industrial practice these must be extended to more compositions and in particular the copolymers into binary, or even ternary, blends. Thus it is recommended that as a first stage, further work is directed towards the thermal and rheological properties of such systems; (b) Rheological parameters are dependant upon frequency as well as temperature, and it is thought that considerably more information could be gained from exploring the detailed rheological behaviour over a wider range of frequencies; (c) Further development of modelling must take greater account of, and hence awaits a more detailed determination of, the component solubility and detailed phase and morphological relationships in the adhesives; and (d)

From an industrial viewpoint there is still a need for the behaviour of adhesives to be examined under a wide range of environmental conditions, *e.g.* humidity, temperature.

References

1. O Lacoste, Hot Melt Adhesives - 1994/5 European Market Study, Trade literature, Exxon Chemical International Inc., Paris, France, 1996.
2. American Society for Testing and Materials, ASTM D907: Terminology of Adhesives, A.S.T.M., Philadelphia, PA., USA, 1988.
3. C Cervellati, European HMA Overview - 1991, Trade literature, Exxon Chemical International - Adhesives Industry Business Unit (A.I.B.U.), Brussels, Belgium, 1992.
4. Anon., Polymers for Adhesives and Sealants, Trade literature, Exxon Chemical International Inc., Brussels, Belgium, 1994.
5. Anon., Evatane™ - Range of EVA Copolymers, Trade literature, Elf Atochem S.A., Paris, France, 1992.
6. Anon., Elvax™ Resins, Trade literature, Du Pont de Nemours International S.A., Geneva, Switzerland, 1993.
7. Anon., Copolymers for Hot Melt, Trade literature, Neste Chemicals International N.V.-S.A., Brussels, Belgium, 1992.
8. D H Kaelble, Physical Chemistry of Adhesion, Wiley-Interscience, New York, NY., USA, 1971, Chapter 6.
9. R Shutt, Personal communication, Exxon Chemical International - Adhesives Industry Business Unit (A.I.B.U.), Machelen, Belgium, 1994.
10. J T Harlan and L A Petershagen, revised by E E Ewins, Jr. and G A Davies, Thermoplastic Rubber (A-B-A Block Copolymers) in Adhesives, in: Handbook of Adhesives, ed. I Skeist, 3rd edn., Van Nostrand Reinhold, New York, NY.,USA, 1989, Chapter 13.
11. D C Bugada and A Rudin, Eur. Polym. J., 28(3)(1992)219.
12. M Audenaert, P Borg, and I Leclère, Microstructure and Physical Properties of EVA Copolymers, in: TAPPI Symposium Notes - 1990 Hot Melt, 10-14 June 1990, Santa Barbara, CA., USA, Conference proceedings, (pub. TAPPI Press, Atlanta, GA., USA, 1990).
13. W C Wake, Adhesion and the Formulation of Adhesives, Applied

Science Publishers Ltd., London, 1976, Chapter 14.

14. J S Autenreith and K F Foley, Resins for Elastomer-Based Adhesives, in: Handbook of Adhesives, ed. I Skeist, 3rd edn., Van Nostrand Reinhold, New York, NY., USA, 1989, Chapter 13.
15. S D Sorbo, Eur. Adh. & Sealants, 6(1992)16.
16. M Morgan, Chem. & Ind., 9(1996)645.
17. Anon., Resins for Hot Melt Adhesives, Trade literature, Hercules B.V., Rijswijk, The Netherlands, 1994.
18. J A Schlademan, Tackifier Resins, in: Handbook of Pressure Sensitive Adhesive Technology, ed. D Satas, 2nd edn., Van Nostrand Reinhold, New York, NY., USA, 1989, Chapter 20.
19. R Sayers, Wax - An Introduction, Gentry Books Ltd., London, 1983, Chapter 1.
20. R T Edwards, Ind. Eng. Chem., 47(1955)2555.
21. W M Mazee, J. Inst. Pet., 35(1949)97.
22. R L Jones and G F Pace, Petroleum Wax as a Hot Melt Adhesive Modifier, in: TAPPI Notes - 1992 Hot Melt Symposium, 14-17 June 1992, Hilton Head, SC., USA, Conference proceedings, (pub. TAPPI Press, Atlanta, GA., USA, 1992).
23. T R Graves and J G McCormick, Adhesives Age, 31(1988)22.
24. M Huntley, Adhesives Age, 34(1991)28.
25. W J Honiball, Effect of a Speciality Fischer-Tropsch Wax on the Performance of EVA Hot Melt Adhesives, in: TAPPI Notes - 1993 Hot Melt Symposium, 13-16 June 1993, Santa Barbara, CA., USA, Conference proceedings, (pub. TAPPI Press, Atlanta, GA., USA, 1993).
26. A Renfrew and P Morgan, Polythene, 2nd edn., Iliffe & Sons, London, 1960.
27. T O J Kresser, Polyethylene, Reinhold, New York, NY., USA, 1961.
28. Anon., Olefin Polymers, in Kirk-Othmer Encyclopædia of Chemical Technology, 4th edn., 1991, Volume 12.
29. J J Aklonis and W J MacKnight, Introduction to Polymer Viscoelasticity, 2nd edn., Wiley-Interscience, New York, NY., USA, 1983.

30. H A Barnes, J F Hutton and K Walters, An Introduction to Rheology, Elsevier, Amsterdam, The Netherlands, 1989, Chapter 2.
31. P E Rouse, J. Chem. Phys., 21(1953)1272.
32. B H Zimm, J. Chem. Phys., 24(1956)269.
33. F Bueche, J. Chem. Phys., 20(1952)1959.
34. J D Ferry, R F Landel, and M L Williams, J. Appl. Phys., 26(1955)359.
35. F Bueche, J. Appl. Phys., 26(1955)738.
36. A J Chompf and W Prins, J. Chem. Phys., 48(1968)235.
37. R S Marvin and H Oser, J. Res. Nat. Bur. Stand., 66B(1962)171.
38. A V Tobolsky, R Schauffhauser, and R Böhme, Polym. Lett., 2(1964)103.
39. W Pechold, M Böhm, and W v Soden, Prog. Coll. Polym. Sci., 75(1987)23.
40. W Pechold, O Grassl, and W v Soden, Prog. Coll. Polym. Sci., 77(1989)368.
41. M Böhm, O Grassl, W Pechold, and W v Soden, Prog. Coll. Polym. Sci., 75(1987)62.
42. W Pechold, Coll. Polym. Sci., 258(1980)269.
43. W Pechold, Makromol. Chem. Suppl., 6(1984)163.
44. U Eisle, Introduction to Polymer Physics, Springer-Verlag, Berlin, Germany, 1990, Chapter 6.
45. S F Edwards, Proc. Phys. Soc., 92(1967)9.
46. P G de Gennes, J. Chem. Phys., 55(1971)572.
47. J D Ferry, Viscoelastic Properties of Polymers, 3rd edn., John Wiley & Sons, New York, NY, USA, 1980, Chapter 10.
48. L E Nielsen and R F Landel, Mechanical Properties of Polymers and Composites, 2nd edn., Dekker, New York, NY., USA, 1994, Chapter 1.
49. R J Seyler (ed.), Assignment of the Glass Transition, ASTM STP 1249, A.S.T.M., Philadelphia, PA., USA.
50. J D Ferry, Viscoelastic Properties of Polymers, 3rd edn., John Wiley & Sons, New York, NY, USA, 1980, Chapter 11.
51. I M Ward, Mechanical Properties of Solid Polymers, 2nd edn., Wiley-

Interscience, Chichester, England, 1983, Chapter 8.

52. U Eisle, Introduction to Polymer Physics, Springer-Verlag, Berlin, Germany, 1990, Chapter 5.
53. B Wunderlich, The nature of the glass transition and its determination by thermal analysis, in: Assignment of the Glass Transition, ed. R J Seyler, ASTM STP 1249, A.S.T.M., Philadelphia, PA., USA, 1994.
54. L Mandelkern, Crystallization of Polymers, McGraw-Hill, New York, NY., USA, 1964.
55. E W Fischer, Z. Naterforsch., 12a(1957)753.
56. A Keller, Phil. Mag., 2(1957)1171.
57. A Keller, Rep. Progr. in Phys., 31(1968)623.
58. D R Buchanan, J. Polym. Sci., A2 9(1971)645.
59. H Hendus and G Schnell, Kunststoffe, 51(1961)69.
60. E W Fischer, H Godder, and G F Schmidt, Kolloid Z. Z. Polymere, 226(1968)30.
61. G J Safford and A W Naumann, Macromol. Rev., 2(1967)1.
62. E Sauter, Z. Phys. Chem., 1318(1932)417.
63. K Hermann, O Gerngross, and W Abitz, Z. Phys. Chem., 10(1930)371.
64. O Kratky and G Porod, Form und Grösse der kristallinen Bereiche, in: Die Physik der HochPolymeren, Vol. III, ed. H Stuart, Springer-Verlag, Berlin, Germany, 1955.
65. B G Rånby and E D Ribi, Experentia, 6(1950)12.
66. K H Storks, J. Am. Chem. Soc., 60(1938)1753.
67. A P Yundt, TAPPI J., 34(1951)89.
68. A Keller and J R S Waring, J. Polym. Sci., 17(1955)447.
69. U Eisle, Introduction to Polymer Physics, Springer-Verlag, Berlin, Germany, 1990, Chapter 7.
70. B Wunderlich, Macromolecular Physics. Vol I. Crystal structure, Morphology, Defects, Academic Press, New York, NY., USA, 1973.
71. H D Keith, F J Padden, and R G Vadimsky, J. Polym. Sci., A2 4(1966)267.
72. H D Keith, F J Padden, and R G Vadimsky, J. Appl. Phys.,

37(1966)4027.

73. H D Keith, F J Padden, and R G Vadimsky, J. Appl. Phys., 42(1971)4585.
74. A Keller, J. Polym. Sci., 17(1955)291.
75. A Keller, J. Polym. Sci., 17(1955)351.
76. D G Bassett, Principles of Polymer Morphology, Cambridge University Press, Cambridge, England, 1981, Chapter 2.
77. G Nachtrab and H G Zachmann, Ber. Bunsenges. Phys. Chem., 74(1970)837.
78. V Johnsen, G Nachtrab, and H G Zachmann, Kolloid Z. Z. Polym., 240(1982)756.
79. J M Schultz, Polymer Materials Science, Prentice Hall, Englefield Cliffs, NJ., USA, 1974, pp 380-90.
80. B Wunderlich, Macromolecular Physics. Vol I. Crystal structure, Morphology, Defects, Academic Press, New York, NY., USA, 1973, Chapter 3.
81. D G Bassett, Principles of Polymer Morphology, Cambridge University Press, Cambridge, England, 1981, Chapter 7.
82. P J Flory, Principles of Polymer Chemistry, Cornell University Press, Ithaca, NY., USA, 1953, Chapter XIII.
83. U Eisle, Introduction to Polymer Physics, Springer-Verlag, Berlin, Germany, 1990, Chapter 4.
84. P Meares, Polymers: Structure and Bulk Properties.
85. M M Cross, J. Coll. Sci. 20(1965)417.
86. G Marin, Oscillatory Rheometry, in: Rheological Measurement, ed. A A Colyer and D W Clegg, Elsevier Applied Science, Barking, Essex, 1988, Chapter 10.
87. I M Ward, Mechanical Properties of Solid Polymers, 2nd edn., Wiley-Interscience, Chichester, England, 1983, Chapter 7.
88. J Komornicki, M Bourrel, G Marin, and M Brogly, J. Adhesion Sci. Technol., 6 (1992) 293.
89. L Boltzmann, Pogg. Ann. Phys., 7(1876)624.

90. I M Ward, Mechanical Properties of Solid Polymers, 2nd edn., Wiley-Interscience, Chichester, England, 1983, Chapter 5.
91. J D Ferry, Viscoelastic Properties of Polymers, 3rd edn., John Wiley & Sons, New York, NY., USA, 1980, Chapter 3.
92. H A Barnes, J F Hutton and K Walters, An Introduction to Rheology, Elsevier, Amsterdam, The Netherlands, 1989, Chapter 3.
93. J J Aklonis and W J MacKnight, Introduction to Polymer Viscoelasticity, 2nd edn., Wiley-Interscience, New York, NY., USA, 1983, Chapter 7.
94. L E Nielsen and R F Landel, Mechanical Properties of Polymers and Composites, 2nd edn., Dekker, New York, NY., USA, 1994, Chapter 3.
95. W C Wake, Adhesion and the Formulation of Adhesives, Applied Science Publishers Ltd., London, 1976, Chapter 4.
96. R N Wenzel, Ind. Chem. Eng., 28(1936)988.
97. S J Hitchcock, N T Carroll, and M G Nicholas, J. Mat. Sci., 16(1981)714.
98. E Washburn, Phys. Rev., 17(1921)374.
99. G Z Fritz, Z für Angew. Physik, 19(1965)374.
100. J J Bikerman, Ind. Eng. Chem., 59(1967)40.
101. W C Wake, Adhesion and the Formulation of Adhesives, Applied Science Publishers Ltd., London, 1976, Chapter 8.
102. T R Bullet and J L Prosser, Adhesion Problems with Paint and Powder Coatings in: Industrial Adhesion Problems, eds. D M Brewis and D Briggs, Orbital Press, Oxford, 1985, Chapter 7.
103. M F Tse, M L Hendewerk, K O McElrath, and M Faissat, Relating Polymer/Tackifier/Wax Interactions to Hot Melt Adhesive Bond Strength, in: Exxon Chemical International Adhesives Symposium, 1990, Brussels, Belgium, Conference proceedings, (pub. Exxon Chemical International, Brussels, Belgium, 1990).
104. M F Tse and M Faissat, Model of Hot Melt Adhesive Bonding, in : Eurocoat '93. Nice, France, 1993, Conference proceedings, (pub. Exxon Chemical International, Brussels, Belgium, 1993).
105. A J Kinloch, Adhesion and Adhesives - Science and Technology,

Chapman and Hall, London, 1987, Chapter 3.

106. J R Huntsberger, in: Treatise on Adhesion and Adhesives, Vol 1, ed. R L Patrick, Marcel Decker, New York, NY., USA, 1967.

107. Lian-Huang Lee (ed.), Fundamentals of Adhesion, Plenum Press, New York, NY., USA, 1991.

108. L E Perrins and K Pettett, Plastics and Polymers, 39(1971)391.

109. E H Andrews and A J Kinloch, Proc. Roy. Soc., A332(1973)385.

110. E H Andrews and A J Kinloch, Proc. Roy. Soc., A332(1973)401.

111. A N Gent, and J Schultz, J. Adhesion, 3(1972)281.

112. W C Wake, Adhesion and the Formulation of Adhesives, Applied Science Publishers Ltd., London, 1976, Chapter 5.

113. S S Voyutskii, in: Adhesion and Adhesion of High Polymers, Wiley-Interscience, New York, NY., USA, 1963.

114. S S Voyutskii, Adhesives Age, 5(1962)30.

115. S S Voyutskii, *et al.*, Adhesives Age, 8(1965)24.

116. R M Vasenin, in: Adhesion - Fundamentals and Practice, McLaren and Son, London, 1969.

117. R M Vasenin, Adhesives Age, 8(1965)21.

118. R M Vasenin, Adhesives Age, 8(1965)30.

119. J N Anand, J. Adhesion, 5(1973)265.

120. C A Dahlquist, in: Aspects of Adhesion - 5, ed. D J Alner, University of London Press, London, England, 1969.

121. D H Kaelble, J. Adhesion, 1(1969)102.

122. A J Kinloch, Adhesion and Adhesives - Science and Technology, Chapman and Hall, London, 1987, Chapter 7.

123. R S Rivlin and A G Thomas, J. Polym. Sci., 10(1953)291.

124. A N Gent and A J Kinloch, J. Polym. Sci., A2 9(1971)659.

125. C L Mahoney, Surface Preparation for Adhesive Bonding, in: Handbook of Adhesives, ed. I Skeist, 3rd edn., Van Nostrand Reinhold, New York, NY., USA, 1989, Chapter 4.

126. A J Kinloch, Adhesion and Adhesives - Science and Technology, Chapman and Hall, London, 1987, Chapter 6.

127. G J Spies, J. Aircraft Eng., 25(1953)64.
128. J J Bikerman, J. Appl. Phys., 28(1957)1484.
129. D H Kaelble, Trans. Soc. Rheol., 3(1959)161.
130. D H Kaelble, Trans. Soc. Rheol., 4(1960)45.
131. D H Kaelble, J. Coll. Sci., 19(1964)413.
132. A N Gent and R P Petrich, Proc. Roy. Soc., 310(1969)433.
133. D H Kaelble, Physical Chemistry of Adhesion, Wiley-Interscience, New York, NY., USA, 1971, Chapter 7.
134. A N Gent and G R Hamed, J. Adhesion, 7(1975)91.
135. A N Gent and G R Hamed, J. Appl. Polym. Sci., 21(1977)2817.
136. A N Gent and G R Hamed, Polym. Eng. Sci., 17(1977)462.
137. A N Gent and G R Hamed, Plast. Rub. Proc., 3(1978)17.
138. A N Gent, Int. J. Adhesion Adhesives, 1(1981)175.
139. M J Loukis and N Aravas, J. Adhesion, 35(1991)7.
140. D W Aubrey, The Effect of Adhesive Composition on the Peeling Behaviour of Adhesive Tapes, in: Adhesion 8, ed. K W Allen, Elsevier Applied Science, Barking, Essex, 1986.
141. G J Lake and A Stevenson, On the Mechanics of Peeling, in: Adhesion 6, ed. K W Allen, Elsevier Applied Science, Barking, Essex, 1984.
142. D W Aubrey, G N Welding and N T Wong, J. Appl. Polym. Sci., 13(1969)2193.
143. J T Rice, Adhesion Selection and Screening Testing, in: Handbook of Adhesives, ed. I Skeist, 3rd edn., Van Nostrand Reinhold, New York, NY., USA, 1989, Chapter 5.
144. Pressure Sensitive Tape Council, Test Methods for Pressure Sensitive Tapes, 7th edn., P.S.T.C., Glenview, IL., USA, 1976, Appendix B, Test Method No. 7.
145. C Dahlquist, Creep, in: Handbook of Pressure Sensitive Adhesive Technology, 2nd edn., ed. D Satas, Van Nostrand Reinhold, New York, NY., USA, 1989, Chapter 6.
146. W C Wake, Adhesion and the Formulation of Adhesives, Applied Science Publishers Ltd., London, 1976, Chapter 6.

147. American Society for Testing and Materials, ASTM D4498: Test Method for Heat-Fail Temperature in Shear of Hot Melt Adhesives, A.S.T.M., Philadelphia, PA., USA.

148. Fédération Internationale des Fabricants et Transformateurs d'Adhésifs et Thermocollants sur Papiers et autres Supports, Test Method FINAT FTM 8: Resistance to Shear from a Standard Surface, F.I.N.A.T., Paris, France, 1985.

149. T S Daniluk, High Modulus EVA Polymers for the Hot Melt Adhesive Industry, Trade literature, Exxon Chemical Company, Baton Rouge, LA., USA, 1989.

150. C P L C Donker, Box-Flap Test Method, Trade literature, Hercules B.V., Rijswijk, The Netherlands, 1989.

151. American Society for Testing and Materials, ASTM D4497: Test Method for Determining the Open Time of Hot Melt Adhesives (Manual Method), A.S.T.M., Philadelphia, PA., USA.

152. D J Hine, Adhesives Age, 23(1980)27.

153. Kanebo-NSC Automatic Bond-Tester, Instruction Manual, Kanebo-NSC, Osaka, Japan.

154. M J Ambrosini, Set-Time and Open-Time Properties of Hot-Melt Adhesives, in: TAPPI Symposium Notes - 1990 Hot Melt, 10-14 June 1990, Santa Barbara, CA., USA, Conference proceedings, (pub. TAPPI Press, Atlanta, GA., USA, 1990).

155. B W Foster, Measuring the Operating Window of Hot Melt Adhesives, in: TAPPI Symposium Notes - 1988 Hot Melt, June 1988, Santa Barbara, CA., USA, Conference proceedings, (pub. TAPPI Press, Atlanta, GA., USA, 1988).

156. D W Bamborough and P M Dunkley, Book-Binding Hot Melt Adhesives: Prediction of Performance using Dynamic Mechanical Analysis, in: TAPPI Symposium Notes - 1990 Hot Melt, 10-14 June 1990, Santa Barbara, CA., USA, Conference proceedings, (pub. TAPPI Press, Atlanta, GA., USA, 1990).

157. F H Wetzel, ASTM Bulletin, 221(1957)64.

158. F H Wetzel, Rubber Age, 82(1957)291.
159. F H Wetzel and B B Alexander, Adhesives Age, 7(1964)28.
160. C W Hock and A N Abbot, Rubber Age, 82(1957)471.
161. C W Hock, J. Polym. Sci., C3(1963)139.
162. C A Dahlquist, Adhesives Age, 2(1959)25.
163. C A Dahlquist, Tack, in: Adhesion Fundamentals and Practice, The Ministry of Technology, McLaren, London, 1966.
164. M Sherriff, R W Knibbs, and P G Langley, J. Appl. Polym. Sci., 17(1973)3423.
165. J B Class and S G Chu, J. Appl. Polym. Sci., 30(1985)805.
166. J B Class and S G Chu, J. Appl. Polym. Sci., 30(1985)815.
167. J B Class and S G Chu, J. Appl. Polym. Sci., 30(1985)825.
168. T G Fox, Bull. Am. Phys. Soc. (Series 2), 1(1956)123.
169. S G Chu, Viscoelastic Properties of Pressure Sensitive Adhesives, in: Handbook of Pressure Sensitive Adhesive Technology, 2nd edn., ed. D Satas, Van Nostrand Reinhold, New York, NY., USA, 1989, Chapter 8.
170. E P Chang, J. Adhesion, 34(1991)189.
171. E F Eastman and L Fullhart, Jr., Polyolefin and Ethylene Copolymer-based Hot Melt Adhesives, in: Handbook of Adhesives, ed. I Skeist, 3rd edn., Van Nostrand Reinhold, New York, NY., USA, 1989, Chapter 23.
172. G Marin, Ph. Vandermaesen, and J Komornicki, J. Adhesion, 35(1991)23.
173. M L Williams, R F Landel, and J D Ferry, J. Am. Chem. Soc., 77(1955)3701.
174. I O Salyer and A S Kenyon, J. Polym. Sci., A1 9(1971)3083.
175. L E Nielsen and R F Landel, Mechanical Properties of Polymers and Composites, 2nd edn., Dekker, New York, NY, USA, 1994, Chapter 4.
176. Ph. Vandermaesen, G Marin, and Ph. Tordjeman, J. Adhesion, 43(1993)1.
177. G Marin and W W Graessley, Rheol. Acta, 16(1977)527.
178. J Komornicki, G Marin, and I Leclère, Rheological Behaviour and Adhesion Properties of EVA Based Hot Melt Adhesives; Use of

Computation Tools, in: TAPPI Notes - 1991 Hot Melt Symposium, 15-18 June 1991, Santa Barbara, CA., USA, Conference proceedings, (pub. TAPPI Press, Atlanta, GA., USA, 1991).

179. W J Honiball, J C Simons, J Lebez, and K Rijin, Formulating Deep Freeze HMA's - A Statistical Approach to Predict Performance Properties, in: TAPPI Notes - 1996 Hot Melt Symposium, 17 - 21 June 1996, Hilton Head, SC., USA, Conference proceedings, (pub. TAPPI Press, Atlanta, GA., USA, 1996).
180. Anon., Stabilisation of Hot Melt Adhesives - Product Selection Guide, Trade literature, Ciba Additives, Basel, Switzerland, 1994.
181. G Knobloch, H Martin, A Patel, and P Rota Graziosi, Influence of the Stabilization of Raw Materials on the Quality of Adhesives, in: TAPPI Symposium Notes - 1989 Hot Melt, 9-13 June 1989, Santa Barbara, CA., USA, Conference proceedings, (pub. TAPPI Press, Atlanta, GA., USA, 1989).
182. Anon., Differential Scanning Calorimetry, Instruction Manual, Mettler-Toledo, Greifensee, Switzerland, 1990.
183. American Society for Testing and Materials, ASTM D3236: Test Method for Determining the Viscosity of Hot Melt Adhesives (Thermocel Method), A.S.T.M., Philadelphia, PA., USA.
184. K Walters, Rheometry, Chapman and Hall, London, 1975.
185. T A Luckenbach, Adhesives Age, 6(1993)28.
186. CarriMed CSL^{2}500 Controlled Stress Rheometer, Guidance for use, TA Instruments, Dorking, Surrey, England, 1994.
187. T E R Jones, Controlled stress rheometry - creep, in: Theoretical and Industrial Aspects of Rheology 15 - 18 June 1990, Loch Lomond, Scotland, Technical Seminar, Strathclyde University, Glasgow.
188. J S Huang and L J Gibson, J. Mat. Sci., 26(1991)637.
189. J J Iruín, G M Guzmán, and J Ansorena, Makromol. Chem., 182(1981)2789.
190. E F Eastman, The anatomy of hot melt adhesives by thermal analyses, Trade literature, E I DuPont de Nemours, Polymer Products,

Wilmington, DW., USA, 1986.

191. W G Harland, M M Khadr, and R H Peters, Polymer, 13(1972)13.
192. I R Harrison, Polymer, 26(1985)3.
193. H E Bair, R Salovey, and T W Huseby, Polymer 8(1967)9.
194. L Mandelkern, J G Fatou, R Denison, and J Justin, J. Polym. Sci., Polym. Lett., 3(1965)803.
195. J P Bell, P E Slade, and J H Dumbleton, J. Polym. Sci., A2 6(1968)1773.
196. J P Bell, and J H Dumbleton, J. Polym. Sci., A2 7(1969)1033.
197. H D Keith and F J Padden, J. Appl. Phys., 34(1963)2409.
198. H D Keith and F J Padden, J. Appl. Phys., 35(1964)1270.
199. H D Keith and F J Padden, J. Appl. Phys., 35(1964)1286.
200. B Wunderlich, J. Chem. Phys., 29(1958)1395.
201. P J Flory, J. Chem. Phys., 13(1947)684.
202. P J Flory, J. Chem. Phys., 17(1949)223.
203. P H Geil, Polymer Single Crystals, Interscience, New York, NY., USA, 1963.
204. R Wetton, Thermal Analysis, in: Polymer Characterisation, eds. B J Hunt and M I James, Blackie Academic & Professional, Glasgow, Scotland, 1993.
205. A H Willbourn, Trans. Faraday Soc., 54(1950)717.
206. N Alberola, J Y Cavaille, and J Perez, Eur. Polym. J., 28(1992)935.
207. I M Ward, Mechanical Properties of Solid Polymers, 2nd edn., Wiley-Interscience, Chichester, England, 1983, Chapter 12.
208. D J David & T F Sincock, Polymer, 33(1992)4505.
209. Anon., Tackifiers for Hot Melt Adhesives, Trade Literature, Arizona Chemicals, Panama City, FL., USA, 1995.
210. J F Kwiatek, Adhesives Age, 11(1988)28.
211. Brookfield RVT 1 Viscometer, Instruction Manual, Brookfield Ltd., Loughton, Essex, England.
212. P D Doody, Unpublished work, National Starch & Chemical Ltd., Slough, England, 1993.
213. E McBride, Consistent viscosity in an EVA based hot melt adhesive, in:

TAPPI Symposium Notes - 1994 Hot Melt, 19-22 June 1994, Hilton Head, SC., USA, Conference proceedings, (pub. TAPPI Press, Atlanta, GA., USA, 1994).

214. D Satas, Dynamic mechanical properties and adhesive performance, in: Advances in Pressure Sensitive Adhesive Technology - 1, ed. D Satas, Satas & Associates, Warwick, RI., USA, 1992, Chapter 6.

215. J J Aklonis and W J McKnight, Introduction to Polymer Viscoelasticity, 2nd edn., Wiley-Interscience, New York, NY., USA, 1983, Chapter 1.

216. Anon., Understanding rheological testing, Trade literature, Rheometrics, Inc., Piscataway, NY., USA, 1992, Ref: 902-00092.

217. J Ferguson and Z Kemblowski, Applied Fluid Rheology, Elsevier, Amsterdam, The Netherlands, 1991.

218. D Holland, J. Rheol., 38(6)(1994)1941.

219. L E Nielsen and R Buchdal, J. Appl. Phys., 21(1950)488.

220. S E B Petrie, J. Macromol. Sci. (Phys.), B12(1976)225.

221. J E Eldridge, J. Appl. Polym. Sci., 11(1967)1199.

222. A J Kovacs, R A Stratton, and J D Ferry, J. Phys. Chem., 67(1963)152.

223. J D Ferry, Viscoelastic Properties of Polymers, 3rd edn., John Wiley & Sons, New York, NY., USA, 1980, Chapter 2.

224. J D Ferry, Viscoelastic Properties of Polymers, 3rd edn., John Wiley & Sons, New York, NY., USA, 1980, Chapter 12.

225. L E Nielsen and R F Landel, Mechanical Properties of Polymers and Composites, 2nd edn., Dekker, New York, NY., USA, 1994, Chapter 7.

226. P Colmer-Villanova, S Montserrat-Ribas, M A Ribes-Greus, *et al.*, Polym.-Plast. Technol. Eng., 29(1989)635.

227. N Alberola, J Y Cavaille, and J Perez, J. Polym. Sci. Polym. Phys., 28(1990)569.

228. R P Charhoff, P T Weissman, and A Sircar, The application of dynamic mechanical methods to T_g determination in polymers: an overview, in: Assignment of the Glass Transition, ed. R J Seyler, ASTM STP 1249, A.S.T.M., Philadelphia, PA., USA, 1994.

229. S Newman and W P Cox, J. Polym. Sci., 46(1960)29.

230. D W Woods, Nature, 174(1954)753.

231. L E Nielsen and F D Stockton, J. Polym. Sci., A1(1963)1995.

232. A V Tobolsky, J. Chem. Phys., 37(1962)1139.

233. J J Joseph, J L Kandos, and L E Nielsen, J. Appl. Polym. Sci., 12(1968)1151.

234. J D Ferry, Viscoelastic Properties of Polymers, 3rd edn., John Wiley & Sons, New York, NY., USA, 1980, Chapter 13.

235. S Wu, Polymer,

236. G V Vinogradov, E A Dzyura, A Ya. Malkin, and V A Grechonovskii, J. Polym. Sci., A2 9 (1971)1153.

237. N E Hudson, Personal communication, University of Strathclyde, Glasgow, Scotland, 1993.

238. K Walters FRS, Personal communication, University College of Wales at Aberystwyth, Aberystwyth, Wales, 1993.

239. H A Barnes, Personal communication, Unilever Research Laboratories, Port Sunlight, Merseyside, England, 1995.

240. T C B McLeish, Personal communication, Interdisciplinary Research Centre for Polymer Science and Technology, University of Leeds, England, 1996.

241. P Hodder, Personal communication, T A Instruments Ltd., Dorking, Surrey, England, 1996.

242. P J Flory, Principles of Polymer Chemistry, Cornell University Press, Ithaca, NY., USA, 1953, Chapter XII.

243. Anon., Product Information Bulletin - Instant Lok 255, Trade literature, National Starch & Chemical BV, Zutphen, The Netherlands, 1995.

244. Anon., Product Data Sheet - Lunatack D 3708, H B Fuller, Vasta Frölunda, Sweden, 1993.

245. Anon., Product Information - H 2316-01, Findley Adhesives Incorporated, Wauwatosa, WI., USA, 1988.

246. Anon., Hercules resins for ethylene-vinyl acetate (EVA)-based hot-melts, Trade literature, Hercules BV, Rijswijk, The Netherlands, 1994.

247. British Standards Institution, BS 5350, British standard methods of test

for adhesives: part H4. Determination of maximum open time of hot-melt adhesives (oven method), B.S.I., Milton Keynes, England, 1989.

248. P Causton, Personal communication, National Starch & Chemical Ltd., Slough, England, 1994.

249. P Puletti, Personal communication, National Starch and Chemical Company, Bridgewater, NJ., USA, 1994.

250. J C Dupuis, Personal communication, National Starch & Chemical S.A., Villefranche sur Saone, France, 1994.

251. D Stauffer, Personal communication, Kanebo-NSC, Osaka, Japan, 1995.

252. M Faissat, Personal communication, Exxon Chemical International - Adhesives Industry Business Unit (A.I.B.U.), Machelen, Belgium, 1995.

253. J Tancrede, Personal communication, Exxon Chemical Inc., Baton Rouge, LA., USA, 1996.

254. C P L C Donker, Personal communication, Hercules B.V., Middelburg, The Netherlands, 1996.

255. S Kawahara, Y Kano, and S Akiyama, Int. J. Adhesion and Adhesives, 13(3)(1993)181.

256. E Debier and N de Keyzer, The use of rheometry to evaluate the compatibility of thermoplastic rubber based adhesives, Trade literature, Shell Research and Technology Centre, Ottignies-Louvaine-la-Neuve, Belgium, Ref: Shell Technical Manual TR8.22

257. Kirk-Othmer Encyclopædia of Chemical Technology, 4th edn., 1991, Volume 15.

258. T L Smith, Trans. Soc. Rheol., 6(1962)61.

259. H Leaderman, Trans. Soc. Rheol., 6(1962)361.

260. L E Nielsen and R F Landel, Mechanical Properties of Polymers and Composites, 2nd edn., Dekker, New York, NY., USA, 1994, Chapter 5.

261. D H Kaelble, Trans. Soc. Rheol., 9(2)(1965)135.

262. D H Kaelble and R S Reylek, J. Adhesion, 1(1969)124.

263. D H Kaelble and C L Ho, Trans. Soc. Rheol., 18(2)(1974)219.

264. A N Gent and G R Hamed, Rubber Chem. Tech., 55(1982)483.

265. A N Gent and G R Hamed, Fundamentals of adhesion, in: Handbook of

Adhesives, ed. I Skeist, 3rd edn., Van Nostrand Reinhold, New York, NY.,USA, 1989, Chapter 3.

266. A N Gent, Rubber Chem. Tech., 46(1973)202.

267. British Standards Institution, BS 5350, British standard methods of test for adhesives: part C12. 180° 't' peel test for a flexible-to-flexible assembly, B.S.I., Milton Keynes, England, 1989.

268. M F Tse, J. Adhesion, 48(1995)149.

269. D W Aubrey and M Sherriff, J. Polym. Sci. (Polym. Chem. Edn.), 18(1980)2597.

270. E P Chang, J. Adhesion, 34(1991)189.

271. N Nakajima, R Babrowicz, and E R Harrell, J. Appl. Polym. Sci., 44(1992)1437.

272. W Barendrecht, C P L C Donker, and G Loeber, A novel adhesive performance prediction approach for HMPSA tapes, Trade literature, Hercules B.V., Rijswijk, The Netherlands, 1991.

273. M Faissat, K McElrath, and M F Tse, Adhesive system design, Trade literature, Exxon Chemical International - Adhesives Industry Business Unit (A.I.B.U.), Machelen, Belgium, Ref: 89 PAP B 185, 1989.

274. S Tobing, Personal communication, National Starch & Chemical Company, Bridgewater, NJ., USA, 1994.

275. M Padmanabhan, Personal communication, National Starch & Chemical Company, Bridgewater, NJ., USA, 1994.

276. A Einstein, Ann. Physik, 19(1905)549.

277. A Einstein, Ann. Physik, 19(1906)289.

278. A Einstein, Ann. Physik, 34(1911)591.

279. H M Smallwood, J. Appl. Phys., 15(1944)758.

280. E J Guth, J. Appl. Phys., 16(1945)20.

281. M J Mooney, J. Colloid Sci., 6(1951)162.

282. E H Kerner, Proc. Phys. Soc., 69(1956)808.

283. Z Hashin and S J Shtrickman, Mech. Phys. Solids, 11(1963)127.

284. S W Tsai, Formulas for the elastic properties of fiber-reinforced composites, AD 834851, June 1958.

285. T B Lewis and L E Neilsen, J. Appl. Polym. Sci., 14(1970)1449.

286. A Y Coran and R Patel, J. Appl. Polym. Sci., 20(1976)3005.